



**HAL**  
open science

# Process design by optimization of superstructures for the factory of the future (PRO-FUTUR)

Christian Quintero-Masselski

## ► To cite this version:

Christian Quintero-Masselski. Process design by optimization of superstructures for the factory of the future (PRO-FUTUR). Chemical and Process Engineering. Université de Lorraine, 2022. English. NNT : 2022LORR0103 . tel-03887267

**HAL Id: tel-03887267**

**<https://hal.univ-lorraine.fr/tel-03887267>**

Submitted on 6 Dec 2022

**HAL** is a multi-disciplinary open access archive for the deposit and dissemination of scientific research documents, whether they are published or not. The documents may come from teaching and research institutions in France or abroad, or from public or private research centers.

L'archive ouverte pluridisciplinaire **HAL**, est destinée au dépôt et à la diffusion de documents scientifiques de niveau recherche, publiés ou non, émanant des établissements d'enseignement et de recherche français ou étrangers, des laboratoires publics ou privés.



**UNIVERSITÉ  
DE LORRAINE**

**BIBLIOTHÈQUES  
UNIVERSITAIRES**

## AVERTISSEMENT

Ce document est le fruit d'un long travail approuvé par le jury de soutenance et mis à disposition de l'ensemble de la communauté universitaire élargie.

Il est soumis à la propriété intellectuelle de l'auteur. Ceci implique une obligation de citation et de référencement lors de l'utilisation de ce document.

D'autre part, toute contrefaçon, plagiat, reproduction illicite encourt une poursuite pénale.

Contact bibliothèque : [ddoc-theses-contact@univ-lorraine.fr](mailto:ddoc-theses-contact@univ-lorraine.fr)  
*(Cette adresse ne permet pas de contacter les auteurs)*

## LIENS

Code de la Propriété Intellectuelle. articles L 122. 4

Code de la Propriété Intellectuelle. articles L 335.2- L 335.10

[http://www.cfcopies.com/V2/leg/leg\\_droi.php](http://www.cfcopies.com/V2/leg/leg_droi.php)

<http://www.culture.gouv.fr/culture/infos-pratiques/droits/protection.htm>

---

# THÈSE

Présentée par

**Christian Steven QUINTERO-MASSELSKI**

Ingénieur de l'École Nationale Supérieure des Industries Chimiques

pour l'obtention du grade de

**DOCTEUR DE L'UNIVERSITÉ DE LORRAINE**

**Spécialité : Génie des Procédés, des Produits et des Molécules**

**Conception des procédés par optimisation de superstructure  
pour l'usine du futur (PRO-FUTUR)**

*Process design by superstructure optimization for the industry  
of the future*

Thèse soutenue publiquement le 20 juillet 2022 devant la commission d'examen :

**Rapporteurs :**

Mme. Ilenia ROSSETTI

Professeure des Universités, Università degli Studi di Milano, Milan

Mme. Raphaële THERY-HETREUX

MDC, HDR, ENSIACET – LGC, Toulouse INP, Toulouse

**Examineurs :**

M. Jean-Marc COMMENGE

Professeur des Universités, Université de Lorraine (Président du jury)

M. Nicolas BION

Chargé de recherche CNRS, IC2MP, Poitiers

M. Laurent FALK

Directeur de recherche CNRS, LRGP, (Directeur de thèse)

M. Jean-François PORTHA

MDC, HDR, Université de Lorraine, (Co-directeur de thèse)



## Acknowledgements

The great effort to develop the work here proposed has been possible thanks to the presence of different people which were supporting this adventure.

Firstly, the sincerest gratitude is deserved by my supervising team, Dr. Laurent Falk, and Dr. Jean-François Portha, with which I was honoured to share more than 3 years of scientific and daily-life discussions. Their belief on my abilities, their valuable time even in the busiest days, and their instructive guidance and advice, allowed me to develop this work with complete independence and with the best of confidence. Their support was an essential foundation for the path that has been built.

A special word of gratitude to the evaluation committee of my thesis defence. Thanks to Professor Ilenia Rossetti and Dr. Raphaële Thery-Hetreux, for having accepted to review this manuscript and for the time you have dedicated for this purpose. As well, thanks to Professor Jean-Marc Commenge for the different discussions held around and beyond the work, and to Dr. Nicolas Bion, for having accepted to judge a dissertation mostly beyond its specialty on catalysis. To all of you, thanks for your remarks and enriching discussion. I've been honoured to present and defend my scientific contributions in front of you.

To my PhD-colleagues, Chakib, Karima and Di, and all the members of the team and the lab with whom I might have shared some words during this journey.

For the closest and most special people around me, I feel that the acknowledgements are best expressed in Spanish.

*Desde el fondo de mi corazón, este trabajo lo dedico a mamá y a papá, quienes han apoyado cada una de las decisiones que me han llevado a ser quien soy y que nunca han dudado de mis capacidades frente a todos los retos que he enfrentado. Gracias por ese apoyo, siempre incondicional. Sé que no fue fácil verme partir, pues es tiempo que dejamos de compartir al lado, pero siempre los llevo en mis pensamientos a cualquier lado que voy.*

*A mi hermanita linda, que el tiempo se ha encargado de ponernos cada vez más cerca después de estar tanto tiempo sin vernos. Ya tendremos muchos momentos para compartir y ser cada vez más unidos.*

*A las dos personas más especiales que he podido conocer en Francia, Nathalia y Mafe, con quienes he podido compartir tantos momentos y que me han dado una de las amistades más valiosas que puedo tener. Que podamos hacer muchas más randonnées, subir y bajar montañas, pero no el Dent du Chat, que podamos comer y beber como nos gusta, que nos sigamos rotando los guayabos, que podamos ir a las calacs (sic) y a la playita, o patinar e irnos de culo y, en fin, a tantos planes que hay por hacer. Gracias con todo mi cora, saben muy bien que las quiero mucho ♡.*

*A mis amigos de Nancy, el Pini, con planes que datan desde antes de la tesis y las noches post-CB, las dos Chouffe y pa' la casa, los Pinochazos, y nuestro grupo con la Tigri, donde creamos los viernes tranqui y nuestras noches en Hops para huir de la tesis. El tiempo de los tres juntos pudo ser corto, pero fue muy valioso y me daba el ánimo cuando los días eran más difíciles.*

*Y a mis amigos de siempre, con los que no es necesario hablar a diario o vernos con frecuencia, pero que siempre han estado presentes, incluso a distancia, y con los que nunca se deja de pasar buenos momentos; Nico desde la UIS, Sasha desde siempre.*

A todos, gracias ♡.



# Contents

General Introduction.....	- 17 -
Context .....	- 17 -
Objectives.....	- 18 -
Outline.....	- 19 -
I. Chapter I: Literature review on renewable energy storage and ammonia production.....	- 23 -
I.1. Introduction .....	- 23 -
I.2. Renewable energies.....	- 24 -
I.3. Energy storage systems .....	- 26 -
I.3.1. Chemical Energy Storage Systems (CESS) .....	- 27 -
I.3.2. Electrical Energy Storage Systems (EESS).....	- 27 -
I.3.3. Electrochemical Energy Storage Systems (ECESS) .....	- 27 -
I.3.4. Mechanical Energy Storage Systems (MESS) .....	- 28 -
I.3.5. Thermal Energy Storage Systems (TESS) .....	- 28 -
I.3.6. Concluding remark on the energy storage system selection.....	- 28 -
I.4. Chemical energy carriers.....	- 29 -
I.5. Non-conventional ammonia production processes.....	- 31 -
I.5.1. Electrochemical synthesis .....	- 31 -
I.5.2. Thermocyclic or chemical looping synthesis .....	- 32 -
I.5.3. Plasma synthesis.....	- 32 -
I.5.4. Photochemical synthesis.....	- 33 -
I.5.5. Concluding remark on the non-conventional ammonia production .....	- 33 -
I.6. Conventional thermochemical process: Haber-Bosch.....	- 33 -
I.6.1. Compression.....	- 35 -
I.6.2. Reaction.....	- 35 -
I.6.3. Separation.....	- 41 -
I.7. Progress towards more efficient Haber-Bosch processes.....	- 44 -
I.8. Conclusions .....	- 46 -
II. Chapter II: Literature review on superstructure optimization methods.....	- 49 -
II.1. Introduction .....	- 49 -
II.2. Process Systems Engineering .....	- 50 -
II.3. Process Synthesis .....	- 52 -
II.3.1. Hierarchical decomposition and evolutionary techniques.....	- 52 -
II.3.2. Mathematical-based optimization methods.....	- 54 -
II.4. Conclusions .....	- 62 -

III.	Chapter III: Materials and methodology for the superstructure conception.....	- 65 -
III.1.	Introduction .....	- 65 -
III.2.	Software and optimization algorithm .....	- 66 -
III.2.1.	ProSimPlus .....	- 66 -
III.2.2.	MIDACO Solver .....	- 70 -
III.2.3.	Computational capacities.....	- 73 -
III.3.	Principles for superstructure design .....	- 73 -
III.3.1.	Superstructure switches .....	- 73 -
III.3.2.	Bypassing streams and operating units.....	- 74 -
III.4.	Methodology for superstructure design.....	- 76 -
III.4.1.	Structural alternatives identification – Discrete variables .....	- 77 -
III.4.2.	Analysis of continuous decision variables .....	- 79 -
III.4.3.	Formulation of the optimization problem.....	- 79 -
III.4.4.	Communication procedure and calculation sequence .....	- 80 -
III.5.	Strategies for the reduction of the calculation time .....	- 81 -
III.5.1.	Association of common processing units .....	- 82 -
III.5.2.	Identification and elimination of inadequate or redundant switch positions .....	- 82 -
III.5.3.	Exploration and reduction of space search .....	- 83 -
III.5.4.	Dissociation of double-stream heat exchangers .....	- 84 -
III.5.5.	Limitation of operating units with internal discretization .....	- 87 -
III.5.6.	Limitation of nested recycling loops .....	- 87 -
III.5.7.	Execution of the optimization on a simplified progress window .....	- 87 -
III.6.	Conclusions .....	- 88 -
IV.	Chapter IV: Problem framework and preliminary data .....	- 91 -
IV.1.	Introduction .....	- 91 -
IV.2.	Problem framework.....	- 92 -
IV.2.1.	Local scenario.....	- 92 -
IV.2.2.	Ammonia market.....	- 94 -
IV.3.	Preliminary data .....	- 95 -
IV.3.1.	Compressors .....	- 95 -
IV.3.2.	Reactors .....	- 97 -
IV.3.3.	Catalysts .....	- 99 -
IV.3.4.	Separators .....	- 101 -
IV.4.	Key Performance Indicators (KPIs) .....	- 107 -
IV.4.1.	Levelized Cost of Ammonia (LCOA).....	- 107 -
IV.4.2.	Energy efficiency .....	- 108 -

IV.4.3.	Energy consumption.....	- 111 -
IV.5.	Conclusions .....	- 112 -
V.	Chapter V: Optimization of the Haber-Bosch process through reactor configurations and catalyst selection.....	- 115 -
V.1.	Introduction .....	- 115 -
V.2.	Superstructure I - Adiabatic reactors.....	- 116 -
V.2.1.	Structural alternatives and description of the superstructure.....	- 116 -
V.2.2.	Optimization problem formulation.....	- 118 -
V.2.3.	Algorithm parameters.....	- 119 -
V.3.	Superstructure II – Autothermal reactor.....	- 120 -
V.3.1.	Structural alternatives and description of the superstructure.....	- 120 -
V.3.2.	Optimization problem formulation.....	- 120 -
V.3.3.	Algorithm parameters.....	- 122 -
V.4.	Generalities on the analysis of results .....	- 123 -
V.5.	Analysis of results for Superstructure I.....	- 124 -
V.5.1.	Violation of constraints and numerical method for convergence calculation .....	- 124 -
V.5.2.	Fe-based case.....	- 125 -
V.5.3.	Ru-based case .....	- 132 -
V.5.4.	Comparison and conclusions between the Fe- and Ru-based optimal solutions .-	- 140 -
V.6.	Analysis of results for Superstructure II.....	- 144 -
V.6.1.	Distribution of variables across their boundaries .....	- 146 -
V.6.2.	Hydrogen conversion profiles in the reactors.....	- 146 -
V.6.3.	Influence of the structure on the economic criteria .....	- 148 -
V.6.4.	Influence of the structure on the energy criteria.....	- 149 -
V.7.	Summary of results and discussion .....	- 152 -
V.8.	Conclusions .....	- 153 -
VI.	Chapter VI: Optimization of the Haber-Bosch process through separator configurations and material selection.....	- 157 -
VI.1.	Introduction .....	- 157 -
VI.2.	Superstructure III – Membrane separation.....	- 158 -
VI.2.1.	Structural alternatives.....	- 158 -
VI.2.2.	Optimization problem formulation.....	- 161 -
VI.2.3.	Algorithm parameters.....	- 161 -
VI.3.	Superstructure IV – PSA, membranes, and condenser.....	- 162 -
VI.3.1.	Structural alternatives.....	- 162 -
VI.3.2.	Optimization problem formulation.....	- 164 -

VI.3.3.	Algorithm parameters .....	- 166 -
VI.4.	Analysis of results for Superstructure III .....	- 166 -
VI.4.1.	Constraints violation.....	- 168 -
VI.4.2.	Analysis of optimal solutions .....	- 169 -
VI.4.3.	Distribution of variables across their boundaries .....	- 171 -
VI.4.4.	Influence of the structure on the economic criteria .....	- 173 -
VI.4.5.	Influence of the structure on the energy criteria.....	- 175 -
VI.5.	Analysis of results for Superstructure IV .....	- 178 -
VI.5.1.	Analysis of optimal solutions .....	- 178 -
VI.5.2.	Separation efficiency and productivity.....	- 180 -
VI.5.3.	Influence of the structure on the economic criteria .....	- 180 -
VI.5.4.	Influence of the structure on the energy criteria.....	- 181 -
VI.6.	Summary of results and discussion .....	- 183 -
VI.7.	Improvement scenarios for competitiveness .....	- 184 -
VI.8.	Conclusions .....	- 186 -
VII.	Chapter VII: Energy balance on the process and thermal integration potential .....	- 189 -
VII.1.	Introduction .....	- 189 -
VII.2.	Thermal balance and integration potential .....	- 189 -
VII.3.	Balance of the process for energy storage .....	- 195 -
VII.4.	Conclusions .....	- 197 -
VIII.	General conclusions and perspectives .....	- 201 -
VIII.1.	Conclusions .....	- 201 -
VIII.2.	Perspectives .....	- 203 -
IX.	References .....	- 205 -
X.	Appendix .....	- 217 -
X.1.	Appendix A – Hypothesis and correlations for economic calculations.....	- 217 -
X.1.1.	Data and correlations for economic calculations.....	- 217 -
X.1.2.	Base price correlations and parameters .....	- 217 -
X.1.3.	Unassembled real price and correction factors.....	- 218 -
X.1.4.	Assembled real price, assembly, and sizing factors .....	- 220 -
X.2.	Appendix B – PSA pseudo-continuous model .....	- 220 -
X.3.	Appendix C – Results for the Fe-based adiabatic reactor configuration.....	- 223 -
X.4.	Appendix D – Results for the Ru-based adiabatic reactor configuration .....	- 225 -
X.5.	Appendix E – Flowsheet representation and material balance data for the optimal Fe-based adiabatic reactor configuration.....	- 226 -

X.6.	Appendix F - Flowsheet representation and material balance data for the Ru-based adiabatic reactor configuration .....	- 228 -
X.7.	Appendix G – Results for the autothermal reactor configuration .....	- 230 -
X.8.	Appendix H - Flowsheet representation and material balance data for the autothermal reactor configuration .....	- 232 -
X.9.	Appendix I – Results for the membrane separation configuration .....	- 234 -
X.10.	Appendix J - Flowsheet representation and material balance data for the membrane separation configuration .....	- 236 -
X.11.	Appendix K – Results for the membrane-PSA-condenser separation configuration ..	- 239 -
X.12.	Appendix L - Flowsheet representation and material balance data for the membrane-PSA-condenser separation configuration.....	- 240 -
XI.	Résumé en français des travaux menés et des résultats obtenus .....	- 245 -
XI.1.	Introduction générale.....	- 245 -
XI.1.1.	Contexte.....	- 245 -
XI.1.2.	Objectifs .....	- 246 -
XI.1.3.	Plan de la thèse .....	- 247 -
XI.2.	Principaux résultats obtenus .....	- 248 -
XI.3.	Perspectives .....	- 251 -

# Nomenclature

## Acronyms

Acronym	Description
ACCR	Annual Capital Charge Ratio
ACO	Ant Colony Optimization
AICR	Adiabatic Indirect Cooling Reactor
APS	Announced Pledges Scenarios
AQCR	Adiabatic Quench Cooling Reactor
BAT	Best Available Technology
CAES	Compressed Air Energy Storage
CAPEX	Capital Expenditures
CCSU	Carbon Capture, Storage and Utilization
CEPCI	Chemical Engineering Plant Cost Index
CES	Cryogenic Energy Storage
CESS	Chemical Energy Storage Systems
COP	Conference of Parties
CPS	Conceptual Process Synthesis
DBD	Dielectric Barrier Discharge
DEA	Diethanolamine
DO	Differential Evolution
DSR	Direct Steam Reforming
ECESS	Electro-Chemical Energy Storage Systems
ECP	Extended Cutting Plane
EESS	Electrical Energy Storage Systems
ESS	Energy Storage Systems
FCV	Fuel Cell Vehicles
FES	Flywheel Energy Storage
FMM	Functional Modules Method
GA	Genetic Algorithm
GBD	Generalized Benders Decomposition
GMF	Generalized Modular Framework
HB	Haber-Bosch
HEN	Heat Exchange Network
HEX	Heat Exchanger
HPP	High-Pressure Product
HTS	High Temperature Stage
IEA	International Energy Agency
IRENA	International Renewable Energy Agency
KAAP	Kellogg Advanced Ammonia Process
KPI	Key Performance Indicator
LAES	Liquid Air Energy Storage
LCOA	Levelized Cost of Ammonia

LCOE	Levelized Cost of Electricity
LHV	Low Heating Value
LOHC	Liquid Organic Hydrogen Carriers
LP	Linear Programming
LPP	Low-Pressure Product
LTS	Low Temperature Stage
MEA	Monoethanolamine
MESS	Mechanical Energy Storage Systems
MIDACO	Mixed-Integer Distributed Ant Colony Optimization
MILP	Mixed-Integer Linear Programming
MINLP	Mixed-Integer Nonlinear Programming
MW	Microwave
NC	Number of Compressors
NEC	Nitrogen Engineering Corporation
NLP	Nonlinear Programming
NZE	Net Zero Emissions
OA	Outer-Approximation
OPEX	Operational Expenditures
OTOE	One-Task One-Equipment
OTP	Optimal Temperature Progression
P2F	Power-to-Fuel
PBB	Phenomena Building Blocks
PDF	Probability Density Function
PEM	Proton-Exchange Membrane, Pré-Estime Method
PHES	Pumped Hydro Energy Storage
PPR78	Predictive Peng-Robinson
PROD	Annual Ammonia Production
PSA	Pressure Swing Adsorption
PSE	Process Systems Engineering
PSO	Particle Swarm Optimization
PV	Photovoltaic
RC	Reactor Configuration
RF	Radiofrequency
SA	Simulated Annealing
SEN	State-Equipment Network
SMES	Superconducting Magnetic Energy Storage
SMR	Steam Methane Reforming
SQP	Successive Quadratic Programming
SS	Scatter Search
SSN	State-Space Network
STEPS	Stated Policies Scenarios
STN	State-Task Network
TC	Type of Cooling
TCES	Thermo-Chemical Energy Storage

TESS	Thermal Energy Storage Systems
TRL	Technology Readiness Level
TS	Tabu Search
TVA	Tennessee Valley Authority
VBS	Visual Basic Script
VRE	Variable Renewable Energy
VTE	Variable Task-Equipment
WGSR	Water Gas Shift Reaction
WOE	World Energy Outlook
WS	Windows Script

## Greek symbols

Symbol	Description	Units
$\alpha$	Kinetic parameter	-
$\varepsilon$	Bed porosity	-
$\eta$	Energy efficiency, adsorption efficiency	-
$\mu$	Viscosity	Pa.s <sup>-1</sup>
$\rho$	Density	kg.m <sup>-3</sup>
$\tau$	Residence time	s
$v$	Superficial velocity	m.s <sup>-1</sup>
$\varphi$	Fugacity coefficient, permeability	mol.s <sup>-1</sup> .m <sup>-1</sup> .Pa <sup>-1</sup>
$\omega$	Kinetic parameter	-
$\Delta$	Variation	-
$\Phi$	Bed-state efficiency	-

## Latin symbols

Symbol	Description	Units
A	Exchange area	m <sup>2</sup>
a	Activity	-
C	Constraint	-
C <sub>p</sub>	Isobaric molar heat capacity	J.mol <sup>-1</sup> .K <sup>-1</sup>
D, d	Diameter	m
E	Activation energy	J.mol <sup>-1</sup>
F	Vector of objective functions	-
g	Vector of constraints	-
H	Enthalpy, Total mass hold-up (PSA)	J.mol <sup>-1</sup>
i	Compound, Stage, Discount Factor	-
k <sub>a</sub>	Equilibrium constant	-
k <sub>c</sub>	Kinetic rate constant	kmol.m <sup>-3</sup> .h <sup>-1</sup>
k	Adsorption constant	-
L	Length	m
$\bar{m}$	Normalized mass flowrate	-
$\dot{m}$	Mass flowrate	kg.h <sup>-1</sup>
n	Compression stage, year	-

$\bar{n}$	Normalized molar flowrate	-
$\dot{n}$	Molar flowrate	kmol.h <sup>-1</sup>
P	Pressure	bar, atm
$\dot{Q}$	Heat duty	kW
R	Gas constant	J.mol <sup>-1</sup> .K <sup>-1</sup>
r	Kinetic rate	kmol.m <sup>-3</sup> .h <sup>-1</sup>
R <sub>c</sub>	Gas constant	cal.mol <sup>-1</sup> .K <sup>-1</sup>
S	Selectivity	-
T	Temperature	K
U	Heat transfer coefficient	W.m <sup>-2</sup> .K <sup>-1</sup>
V	Volume	m <sup>3</sup>
$\dot{W}$	Mechanical work	kW
x	Molar fraction, Continuous variable	-
y	Molar fraction, Discrete variable	-

### Subscript and superscripts

Symbol	Description
-	Net production
+	Net consumption
°	Standard
C	Cold
COMP	Compressors
COOL	Cooling requirements
E	Energy
eq	Equality
H	Hot, high pressure
h	Hour
HEAT	Heating requirements
in	Inlet
L	Level, low pressure
l	Lower limit
LM	Mean logarithmic
Loss	Thermal losses
Min	Minimal
out	Outlet
p	Particle, pressure
pre	Preheat
r	reaction
TURB	Turbines
u	Upper limit
y	Year



# **General introduction**



## General Introduction

### Context

The latest report of the World Energy Outlook (WEO), from the International Energy Agency (IEA) and prepared for the last Conference of Parties (COP26), describes three main possible scenarios resulting from government policies and commitments on the evolution of the energy system, giving different outcomes on the search for a limitation on the world temperature rise. The Stated Policies Scenarios (STEPS) is the most conservative, as it does not consider the full achievement of actual governments goals, reaching an increase of +2.5 °C by year 2100. The Announced Pledges Scenarios (APS) does consider a full accomplishment of proposed commitments, even though projections indicate a temperature rise of +2.0 °C. The Net Zero Emissions (NZE) scenario considers that every country achieves net zero emissions by 2050, limiting the global temperature rise to +1.5 °C, with a 50% probability [1].

As depicted in Figure 1, which shows the predicted progression of the share of energy sources on the total primary energy supply, as well as the global emissions of CO<sub>2</sub>, the greatest difference between the scenarios is the strong reduction on fossil fuel-based sources (i.e., coal, oil, and natural gas), and a wider share of renewable sources of energy.

In the STEPS scenario, the fossil fuels keep a 2050 energy supply equivalent to the actual, with a small switch between coal and natural gas, meaning a similar quantity of emissions that the actual, near 33 Gt CO<sub>2</sub>. Nevertheless, the most ambitious scenario, the NZE, requires a final share of renewable sources around 60 %, with a strong transition from 2030 and beyond, allowing to reach net zero emissions.

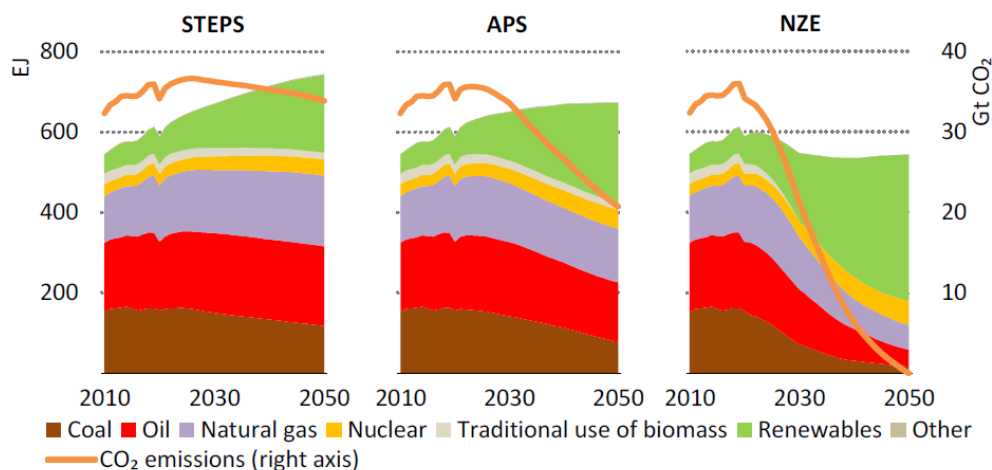


**Figure 1.** Projection from 2010 to 2050 of the energy market share and consumption (EJ) and global CO<sub>2</sub> emissions, according to STEPS: Stated Policies Scenario, APS: Announced Pledges Scenario and NZE: Net Zero Emissions Scenario. [1]

The common feature in all three scenarios is the search for sustainable solutions, with electrified, efficient, interconnected and decarbonized technologies [1]. Projections from the International Renewable Energy Agency (IRENA) support that by the year 2050, electricity will be the main energy carrier with 50 % of the share [2].

As a matter of fact, on year 2019 the renewable power generation increased more than the electricity demand, with a fossil-fuel electricity decrease, being the first time in decades that energy demand and

fossil-fuel based electricity have an inverse behaviour [3]. Among the foreseen solutions for carbon emission abatement on the NZE scenario, the renewable production of electricity shares the first place with energy conservation and efficiency, with a share of 25 % each. Other solutions are electrification in end use sectors (20 %), use of hydrogen and derivatives (10 %), and carbon capture and storage and utilization (CCSU) (20 %) [2].

The evidence of the last decade allows to affirm that political and economic measures favour the investment on the development of greener technologies and their integration on the energy market. In many markets, renewable sources of energy on newly commissioned projects have reached the minimum cost in comparison to other sources. For instance, the levelized cost of energy (LCOE) of solar photovoltaic (PV) electricity decreased from 0.381 \$/kWh in 2010 to 0.057 \$/kWh in 2020, a decrease of 85 %. Likewise, for onshore wind projects, the change from 0.089 \$/kWh in 2010 to 0.039 \$/kWh in 2020 represents a reduction of 56 %. For comparison, fossil-fuel power generation ranges between 0.055 and 0.148 \$/kWh, depending on location and fuel source [2].

Incoming years will be crucial for the flattening of the world temperature rise curve towards a maximum limit of +1.5 °C by year 2100, and the strong decrease of the global carbon emissions. The deployment of clean energy production and its integration to the energy market will play a key role towards these objectives, which goes along with the objectives proposed in this work.

## Objectives

The quest for efficient, sustainable, and economic processes is one important challenge that process engineers are constantly facing in research and industry. The more the processes are constrained by restrictive criteria, the further the engineer needs to determine optimal processes using the different technologies available for mass and energy transformation.

In order to tackle these restrictions, engineers need to determine the best structural configuration of a process, leading to the optimal arrangement of the processing units, with the respective set up of the operating conditions. As it is presented, this task could require evaluating several process designs to find the best configuration, which is a tedious and time-consuming approach to execute manually.

Therefore, this work is foreseen to enable a practical methodology for process engineers to evaluate multiple process alternatives within a unique process superstructure, to determine the best structural arrangement, the set of operating conditions and/or design parameters, leading towards the optimal process configuration regarding some economic, energetic and/or environmental criteria.

To summarize, the work that is hereafter presented intends to cover two main objectives, in the search of more efficient transformation processes and within the context of renewable energy sources:

- O1:** The proposal of a methodology for process conception through superstructure optimization, using a process simulation software as environment and an optimization algorithm as essential feature for its resolution.
- O2:** The application of the proposed methodology to a scenario of renewable energy storage in chemical compounds, specifically into ammonia, using as reference the conventional Haber-Bosch process.

---

## Outline

This manuscript is divided into eight chapters, which present the different steps carried out in this thesis for the proposal of the superstructure methodology and the evaluation of the Haber-Bosch process for ammonia synthesis. The content of each chapter is summarized as follows:

- Chapter I** Introduces the current context of renewable energy and the technologies for energy storage, describing the chemical storage of energy as potential solution for further enabling their increase in the energy market. Also, it covers the generalities on the ammonia synthesis processes found in industry, and the non-conventional routes for its production.
- Chapter II** Covers the different strategies for process synthesis available in the literature, namely the hierarchical decomposition techniques and the mathematical-based optimization. Details on the superstructure optimization methods are presented.
- Chapter III** Describes the generalities of the simulation software and the optimization algorithm used to implement the methodology. It also presents the principles for superstructure design, the methodology for its conception and the considered strategies allow to reduce the calculation time for optimization.
- Chapter IV** Presents the problem framework and the hypothetical scenario for renewable energy storage in ammonia, with the definition of the system boundaries for the study. It also presents the preliminary data required for modelling every stage of the HB process, as well as the Key Performance Indicators to minimize.
- Chapter V** Describes the first two superstructure cases of the study, related to the Haber-Bosch process optimization through the selection of the reactor configurations and the catalytic material.
- Chapter VI** Covers the third and fourth superstructure cases of the study, related to the Haber-Bosch process optimization through the selection of the separation technology for NH<sub>3</sub> recovery.
- Chapter VII** Details the analysis of the potential thermal integration between the different streams of the process, with a brief description of the HEX network and its impact on the economic KPI.
- Chapter VIII** Presents the general conclusions and perspectives for future research, highlighting the main contributions of this work, the drawbacks that need further attention and require to be handled, as well as some identified fields for improvement of the presented methodology.



# Chapter I

---

*Literature review on renewable energy storage  
and ammonia production*

---



# I. Chapter I: Literature review on renewable energy storage and ammonia production

The following chapter will cover subjects related to:

- The increase of the production of renewable energy towards a decarbonization of the energy market, as well as the challenges and solutions for their integration on the energy network.
- Details on current energy storage systems, with particular attention to solutions for delocalized, long-term, and long-capacities storage of renewable energies.
- Chemical energy carriers as alternatives to the main current energy vector, hydrogen, which can boost the integration of renewable energies due to their potential use for energy storage.
- NH<sub>3</sub> production processes, from the non-conventional to the thermochemical Haber-Bosch process, detailing on limitations encountered, equipment and technologies commonly used.
- The roadmap for storing renewable energy in chemical form as ammonia, detailing the scope of this work, the challenges, and the expected results.

## I.1. Introduction

Multiple challenges have been escalating during the last decades, affecting society due to the increase of all sorts of inequalities and uncertainties regarding the near future. As declared by the United Nations in the Sustainable Development Goals program, 17 targets are declared as guidelines for the improvement of life quality of people in the near future, without compromising the needs of the future generations [4].

Among them, the energy industry is called to embrace goal 7, *affordable and clean energy*, to “ensure the access to affordable, reliable, sustainable, and modern energy”, and goal 13, *climate action*, to “take urgent actions to combat the climate change and its impacts”. Framed within the affordable and clean energy goal, there is an urge to substantially increase the share of renewable energy in the global energy mix and to double the rate of improvement in energy efficiency, while the climate action goal encloses the climate change mitigation and impact reduction [4].

In this context, the energy industry needs to rapidly increase the share of renewable energies on the market, while keeping a continuous transformation from a strongly fossil-fuel based mix into a decarbonized energy market, in order to tackle carbon emissions to create a relief on global warming and climate change. However, the transition is strongly limited due to the availability of energy sources. Fossil-based sources can be immediately exploited from oil and gas wells, or carbon mines, while renewable energy sources have an inherent nature of intermittency and discontinuity in its production. This source shifting requires solutions to guarantee energy security in terms of availability, quality, stability and supply-demand balance [5].

Delocalized and flexible technologies for the production of renewable energy have the leverage to boost the integration of carbon-free energies, mainly in zones where grid connection is not available, promoting the deployment of seasonal storage devices to guarantee the access to a continuous supply of energy. Besides, decentralizing the energy production allows harvesting the energy surplus issued from

natural phenomena, for instance, in zones where solar radiation or wind speeds are stable during long periods of time, taking advantage of the available energy.

In this regard, the objective of this chapter is to cover the foreseen solutions for the delocalized production of energy and for its storage into chemical compounds, in particular ammonia. Following pages of this work are divided as follows. A description of renewable energy sources is carried out in section I.2, while covering the existing solutions for renewable energy storage in section I.3. On section I.4, a focus on chemical energy carriers is developed, where a description of ammonia as chemical for energy storage is introduced. Section I.5 describes the generalities of the non-conventional methods for ammonia synthesis, before giving deeper details on the thermochemical synthesis of NH<sub>3</sub> through the Haber-Bosch process in section I.6. Then, section I.7 highlights the progress towards the electrification and decarbonization of the ammonia synthesis process. Finally, section I.8 proposes the roadmap for energy storage in ammonia with concluding remarks.

## I.2. Renewable energies

A source of energy is defined as renewable if it proceeds from natural processes, with a constant replenishment, avoiding depletion during a human time scale. They are commonly associated to natural sources of stored energy, as biomass and geothermal energy, or energy produced due to natural phenomena, as sun radiation, water flow and wind flow [6]. In contrast, fossil fuels as coal, oil, and natural gas, are considered as non-renewable sources due to the great rate of consumption and low rate of replacement, leading to a complete depletion. The evolution of the share of each energy source on the last three decades is shown in Figure I-1, where an increase on wind and solar PV is evident for the last couple of years, while oil and coal have shown decreasing trend.

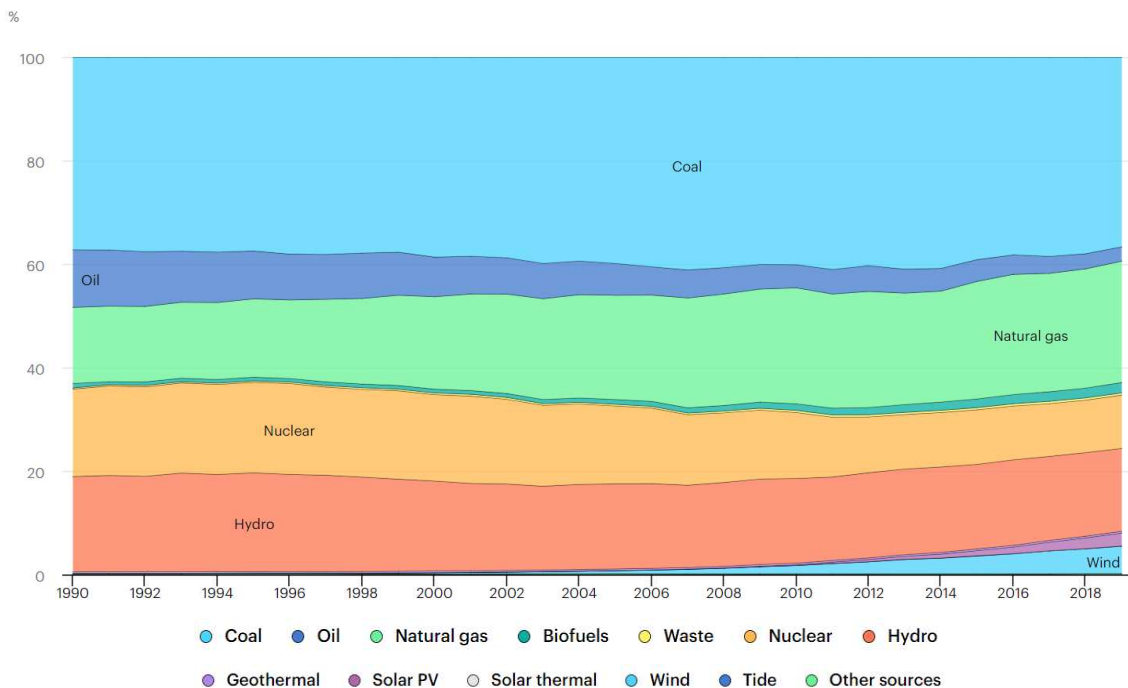


**Figure I-1.** Percentage of worldwide share for the different energy sources, according to data retrieved from the International Energy Agency data browser, online<sup>1</sup>.

<sup>1</sup> Based on IEA data from IEA 2021 Electricity Information database, [www.iea.org/statistics](http://www.iea.org/statistics), All rights reserved.

Multiple types of renewable sources can be found, which can be classified in two categories: conventional and Variable Renewable Energy (VRE). The former includes biomass, geothermal, hydropower and solar thermal, while the latter is commonly associated with solar photovoltaic (PV) and wind. Table I-1 details the global installed capacities and electricity generation of these sources and their variation on the last decade.

**Table I-1.** Installed capacities for power production and electricity generation for different sources of renewable energy, for years 2010 and 2020, with their respective variation. Sources in bold indicate principal categories. \*Data for biomass, geothermal, hydropower, and ocean electricity generation are related to year 2019. Data retrieved from [7].

Source	Installed capacity (GW)			Electricity generation (TWh)		
	2010	2020	Increase %	2010	2020*	Increase %
<b>Biomass</b>	<b>65.9</b>	<b>127.1</b>	<b>92.9</b>	<b>311.8</b>	<b>557.8</b>	<b>78.9</b>
Liquid biofuels	1.9	2.6	36.8	5.6	8.4	50.0
Renewable municipal waste	6.7	15.4	129.9	39.8	68.5	72.1
Biogas	9.5	20.1	111.6	46.2	91.8	98.7
Solid biofuels	47.8	89.0	86.2	220.2	389.1	76.7
<b>Geothermal</b>	<b>10.0</b>	<b>14.0</b>	<b>40</b>	<b>68.5</b>	<b>92.0</b>	<b>34.3</b>
<b>Hydropower</b>	<b>926.3</b>	<b>1211.7</b>	<b>30.8</b>	<b>3438.9</b>	<b>4207.1</b>	<b>22.3</b>
<b>Ocean</b>	<b>0.25</b>	<b>0.53</b>	<b>111.1</b>	<b>0.52</b>	<b>0.98</b>	<b>89.6</b>
<b>Solar</b>	<b>41.6</b>	<b>716.2</b>	<b>1621.6</b>	<b>33.8</b>	<b>693.1</b>	<b>1950.6</b>
Photovoltaic	40.3	709.7	1661.0	32.1	679.0	2015.3
Thermal	1.3	6.5	400.0	1.7	14.1	764.7
<b>Wind</b>	<b>180.9</b>	<b>732.4</b>	<b>304.9</b>	<b>342.8</b>	<b>1412.3</b>	<b>311.9</b>
Onshore	177.8	698.0	292.6	335.4	1328.0	295.9
Offshore	3.1	34.4	1009.7	7.4	84.3	1039.2

Concerning the biomass sources, the installed capacity has almost doubled in the last decade to 127.1 GW by year 2020, with an electricity generation of 557.8 TWh by year 2019. Four main types of biomass sources can be found. Liquid biofuels are used as alternative fuels for internal combustion engines in mobility, such as bioethanol and biodiesel. Renewable municipal waste, referred to the portion of biological material in municipal waste, can be valorised using either biological or thermal treatments. Biogas is the product obtained from anaerobic fermentation or the thermal treatment of biomass, mainly methane and carbon dioxide, using waste from landfill, sewage sludge, animal slurries, breweries, and agriculture industry [8]. Solid biofuels, responsible for the greatest share in biomass sources of energy, contain any organic non-fossil material from biological origin, such as charcoal, wood pellets, bagasse, and dry animal waste [9].

Geothermal energy is referred to the available energy recovered as steam or hot water from the earth crust, due to geological phenomena. It can be directly used in heating districts or transformed into electricity in steam cycles. It remains one of the sources which contributes the less to the share of renewable energy, which is reflected in low increases in installed capacities (40 %) and electricity generation (34 %) in the last decade, when compared to other sources, as it is strongly limited by the geographical location and the geological properties of land.

Hydropower uses large water reserves, mainly from natural river flow, to generate power using the stored potential energy. It demands large civil engineering structures, which strongly limits the increase of installed capacities, as seen in Table I-1, with not more than 31 % of increase in the installed capacity, and around 22 % of growth in the electricity generation. Ocean energy, also referred as tidal energy,

exploits the mechanical energy from oceanic water movement for its transformation into electricity. It represents the lowest share of installed capacity to the VRE.

Solar power is classified into PV and thermal. In the solar PV, energy radiation is transformed in solar panels into electricity using the photoelectric effect, while the solar thermal technology is used to produce heat from solar radiation. These technologies have seen a strong development, with the greatest variations in installed capacities (1621 %) and electricity generation (1950 %). In wind power technologies, the kinetic energy of wind is transformed into mechanical energy with the rotation of wind turbine blades to generate electricity. It is classified according to its location, as it can be found onshore (inland) and offshore (mainly in the ocean). Together they represent the second most developed source of VRE of the last decade.

From all above-mentioned technologies, solar PV and wind onshore have had the greatest increase in terms of installed capacity and electricity generation, as technologies have become cheaper and more developed. Nowadays, some countries have up to 30 % and more of share of VRE [3], requiring flexible power systems able to easily inject these sources of energy simultaneously with its production. The inherent nature of VRE, dependent on climate factors such as solar irradiance and wind speed, means a problem for an exclusive dependence on this type of sources. Peaks of production do not necessarily correspond to energy demand peaks, meaning a frequent offset between production and consumption.

The integration of VRE to the actual network is a challenge for the power system flexibility [10]. Four main problems are associated to the VRE integration to power grids: quality, related to the uninterrupted power supply within safe conditions of voltage and current; flow, denoting an efficient power transmission and distribution; stability, concerning the management and corrections of disturbances due to asynchrony of modular generators; balance, related the mismatch between demand and supply [5]. While these problems are the subject of grid management, regulation, and operation, a solution that emerges to add flexibility to the power system is the VRE storage. Current short- and long-term stationary energy storage capacities are estimated to 30 GWh, while projections indicate the need for up to 9 TWh energy storage capacities by year 2050 [3].

### I.3. Energy storage systems

The portfolio of Energy Storage Systems (ESS) is vast, and its classification is mainly determined by the form in which energy is stored, which defines the storage device required [11].

**Table I-2.** Classification of ESS and examples of the technologies [11]–[16].

Category	Energy storage type	Examples of technologies
Chemical	Energy carriers	Power-to-X: Hydrogen, ammonia, methane, methanol, biofuels
	Thermochemical	Reversible endothermic/exothermic reactions
Electrical	Electrostatic	Capacitors, supercapacitors
	Electromagnetic	Superconducting magnetic (SMES)
Electrochemical	Primary battery	Non-rechargeable electrolyte batteries: Zn-Cl, Li-I
	Secondary battery	Rechargeable electrolyte batteries: Ni-Cd, Ni-M hydride
	Flow battery	Vanadium redox, zinc-bromine, polysulphide bromide
	Fuel cell	PEM, alkaline, solid-oxide, reversible
Mechanical	Kinetic energy	Flywheels
	Potential energy	Pumped hydro (PHES)
	Pressurized gas	Compressed Air (CAES)
Thermal	Low temperature	Cryogenic (CES), Liquid Air (LAES)
	High temperature	Sensible heat, latent heat

While ESS classification might differ between authors, they are commonly grouped in four categories: mechanical, electrical, thermal, and chemical energy storage. Others associate electrical and chemical into electrochemical, while others include also electromagnetic technologies. Table I-2 details one classification of ESS, using several references, and some examples for each technology. To evoke the main features of the different existing ESS, a brief description is hereafter presented. A comparison between the energy storing capacities and periods of storage is then represented in Figure I-2.

### **I.3.1. Chemical Energy Storage Systems (CESS)**

In CESS, energy is stored in the chemical bonds of atoms and molecules, reason why chemical compounds are often related as energy carriers. Chemical reactions are required to store and release this type of energy within chemical bonds, involving the transformation of one or multiple chemical compounds. Any type of fuel can be considered as a chemical storage system, as it releases thermal energy, usually converted into mechanical and electrical energy. The most common energy carrier produced from VRE is hydrogen. Information about energy carriers for ESS are of interest in this thesis and will be further developed in section I.4.

Likewise, Thermochemical Storage Systems (TCES), often classified in the Thermal category, are based on reversible chemical reactions. For a given compound  $C$ , the presence of heat allows an endothermic reaction to take place, producing compounds  $A$  and  $B$  storing heat as chemical energy. When required, the reversible reaction is performed to release the stored energy. A common example of this technology is the use of inorganic hydroxides, as  $\text{Ca(OH)}_2/\text{CaO}$  and  $\text{Mg(OH)}_2/\text{MgO}$ , for dehydration and rehydration process [17].

### **I.3.2. Electrical Energy Storage Systems (EESS)**

Two categories are found in the EESS: electrostatic and electromagnetic. In the first, it is possible to find capacitors, composed of metallic layers separated by a dielectric material, and supercapacitors, a double-layer capacitor containing an electrolyte and a porous membrane with higher surface area than the capacitors [16]. They are useful due to their direct method for energy storage, having a fast-response, and supporting thousands of life cycles. However, its main drawback is the low energy density and short storage duration [18]. Concerning the second category, the Superconducting Magnetic Energy Storage (SMES) stores energy in a magnetic field created with a direct current (DC) in a superconducting coil at cryogenic temperature. The power capacity ranges between 100 kW and 10 MW, and supports tens of thousands of cycles [16].

### **I.3.3. Electrochemical Energy Storage Systems (ECESS)**

The most widespread technologies associated to this category are the batteries, with a predominant use throughout the years. It consists mainly of multiple cells in series or parallel sequence, composed of two opposite electrodes, with electrolytes as medium for electron transfer [11]. A popular classification of electrochemical energy storage systems, presented in [15], is the following:

- Primary batteries: considered to be non-rechargeable, with an electrolyte medium that can be aqueous or non-aqueous. Some examples of primary batteries are Zinc-Silver oxide, Lithium-Iodine and Lithium-Copper oxide batteries.

- Secondary batteries: can be recharged when a current is passed in the opposite direction to the discharge. They can also use aqueous and non-aqueous electrolytes, with common examples such as Lead-Acid, Nickel-Cadmium and Lithium-Ion.
- Flow batteries: are devices that store energy in the electrolyte solutions, contrary to the other type of batteries where the electrodes act as storing capacities. Electrolytes are contained in separate tanks, pumped to the electrochemical cell for the reaction to take place [16].
- Fuel cells: non properly conceived as energy storage devices, but as energy generation devices, fuel cells convert the chemical energy from a fuel into electricity through redox reactions. They function as batteries, as they are composed of two electrodes and an electrolyte membrane for electron flow. The most renamed use of fuel cells is the generation of electricity from the reaction between hydrogen and oxygen. Some of the fuel cell types found are the Proton-Exchange Membrane (PEM), Alkaline and Solid Oxide.

Batteries are commonly associated with low energy capacities in comparison with other technologies, being useful for small scale applications from some kilowatt-hours to the order of 10 MWh.

#### **I.3.4. Mechanical Energy Storage Systems (MESS)**

Based on high pressures, kinetic or potential energies, the MESS allow producing energy almost immediately at great scales and capacities. The Pumped Hydro (PHES) uses water reservoirs at different elevations, and therefore exploits its potential energy, which is converted into kinetic energy to drive a turbine and generate electricity. The Compressed Air (CAES) uses geological formation to store air at high pressures, which is then released for expansion in a set of turbines, with a possible further combustion with fuels, to increase the cycle efficiency. The Flywheel (FES) store energy in form of kinetic energy in a rotating cylinder, where the rotational speed is handled by magnetic bearing under vacuum, but are inefficient for long-term storage, reason why they are used in combination with other devices. They are also the less mature technology, when compared to batteries, making its use uncompetitive in the current market [12].

#### **I.3.5. Thermal Energy Storage Systems (TESS)**

Composed of high and low temperature technologies regarding ambient temperature, the TESS stores energy in materials in insulated conditions. The low temperature or Cryogenic (CES), in development stages, conditions a material or fluid under low temperatures, and can be used in a cryogenic heat engine [13]. High temperature energy storage is further classified in sensible or latent heat storage. In the former, energy is stored in fluids or mediums without a phase change, such in steam or hot water reservoirs, and molten salts. In the latter, a phase change occurs, as in inorganic salts or metals, involving solid-solid or solid-liquid transformations [14]. It has found applications in solar thermal energy storage. The applications of TESS are mainly industrial cooling, under -18 °C, building cooling, between 0 and 12 °C, building heating, from 25 to 50 °C, and industrial heating, at temperatures above 100 °C [12].

#### **I.3.6. Concluding remark on the energy storage system selection**

The selection of a technology for energy storage must be based under the same criteria, as it allows to classify from the most to the least adapted options according to expected results. For seasonal and delocalized VRE storage, mainly sourced from solar and wind energy, technologies must be able to store considerable high energy inputs for long periods of time. To compare some of the aforementioned

technologies, Figure I-2 shows the map of ESS according to the capacity and discharge time at rated power of stored energy.

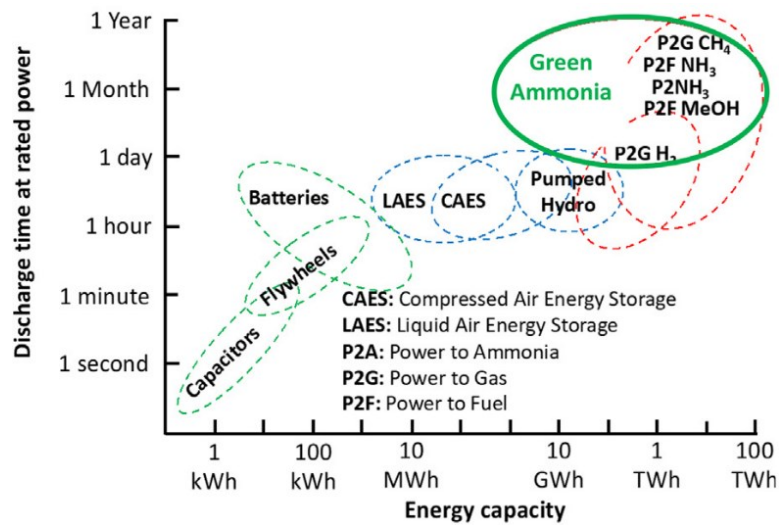


**Figure I-2.** Comparison between energy storage technologies according to the storage energy capacity and discharge time. Recovered from [19].

Higher energy capacities and longer periods of discharge are found for chemical energy storage technologies, as chemical compounds can be easily stored in great volumes in isolated reservoirs. On the contrary, electrical, and electrochemical devices are the most limited for large-scale applications. Mechanical energy storage technologies, such as PHEs and CAES are in the intermediate zone, as discharge periods at rated power are not longer than a few days.

These technologies have proven to be useful for specific energy storage requirements. For instance, when power quality, energy management and emergency back-up are required, almost only the batteries can guarantee a good response. On the other hand, MESS are effective for power peak shaving, load levelling and network expansion. Concerning the VRE integration, technologies such as the SMES, some electrochemical devices and the chemical energy storage system have demonstrated to properly respond to this need [20].

Under the considered scenario and hypothesis of requiring high energy capacities, long storage duration and discharge times higher than a day for seasonal storage applications, the CESS seem to be the most appropriate technology to consider when storing renewable energy produced from wind sources. The CESS is useful for seasonal storage of energy for several months, and due to the energy content on chemical compounds, the energy capacities for this solution are on the highest levels among the competing technologies. A deeper description of CESS and energy carriers is hereafter proposed.

#### I.4. Chemical energy carriers

The principal energy carrier used for chemical storage of energy is hydrogen. It can be produced in a zero-carbon process through the electrolysis of water with renewable electricity, to produce oxygen as by-product. Its storage can then be performed in three different routes: **physical storage**, in liquid or gas phase; **adsorption into materials**, such as metal-organic frameworks and zeolites; **chemical storage**, using hydrogen to form metal hydrides or chemical H<sub>2</sub>-based compounds, as the Liquid Organic Hydrogen Carriers (LOHC) [21]. For the interest of this work, only physical and chemical H<sub>2</sub>-based

storage will be treated. Further information about adsorption into materials is available in the following references [22]–[25].

Physical storage of hydrogen is the shortest path to store VRE in a chemical energy carrier, as no further chemical transformation is required after water electrolysis is carried out. Only a physical adaptation is needed in terms of pressure and temperature, depending on the required conditions for storage. Hydrogen has a high gravimetric energy density, around 120 MJ/kg H<sub>2</sub>, but is the lightest existing gas with a density of 0.084 kg/m<sup>3</sup> under ambient conditions [26], which translates into a low volumetric energy density, of 5.16 MJ/m<sup>3</sup>. Storing a significant amount of energy in hydrogen would require enormous gas volumes at atmospheric pressure, high pressures for compressed gas storage (> 300 bar) or cryogenic temperatures for storage in liquid phase (-253 °C) [27]. These severe conditions also have an impact on materials and insulation of storing vessels, and energy requirements to maintain constant levels of pressure and temperature, making the cost of storage an important factor to consider.

To prevent managing these storing conditions, further transformations can be performed, according to two routes of the Power-to-Fuel (P2F) strategy on the chemical H<sub>2</sub>-based compounds: **carbon-based** and **nitrogen-based compounds**. Basically, hydrogen is used to synthesize other chemicals, mainly methanol (CH<sub>3</sub>OH) and ammonia (NH<sub>3</sub>), commonly known as *e-fuels*. Additional compounds can be found, such as dimethyl ether (DME), e-gasoline or e-diesel, which have a potential use for mobility and transport applications [28].

It is important to consider a set of factors when choosing a hydrogen storage method, such as volumetric and gravimetric energy density, costs and technology maturity [27]. Energy densities are indicators of how much energy is possible to store in chemical form, normally assessed with the Low Heating Values (LHV). To compare the alternatives between *e-fuels* for energy storage, different properties of the most commonly used chemicals in the P2F route are shown in Table I-3.

**Table I-3.** Properties of chemical compounds in storage conditions. Adapted from [27], [28].

Property	Unit	H <sub>2</sub>	H <sub>2</sub>	CH <sub>3</sub> OH	NH <sub>3</sub>
Phase	-	Gas	Liquid	Liquid	Liquid
Temperature	°C	25	- 252.9	25	25
Pressure	MPa	69	0.1	0.1	0.99
Density	kg/m <sup>3</sup>	39	70.8	792	682
Gravimetric energy density (LHV)	MJ/kg	119.9	119.9	20.1	18.6
Volumetric energy density (LHV)	MJ/L	4.5	8.49	15.8	12.7
Gravimetric H <sub>2</sub> content	wt%	100	100	12.5	17.8
Volumetric H <sub>2</sub> content	kgH <sub>2</sub> /m <sup>3</sup>	42.2	70.8	99	121
Explosive limit in air	vol%	4 – 75	4 – 75	6.7 – 36	15 – 28

Regarding the H<sub>2</sub> gas storage, current applications on Fuel Cell Vehicles (FCV) use onboard storage tanks with pressures near 700 bar, even if tank volumes remain limited due to material and economic constraints. For large-scale applications, maximum pressures in storage vessels are 100 bar due to material properties and operating costs [21].

On the other hand, liquid H<sub>2</sub> storage is more challenging. It requires cryogenic temperatures and constant energy supply to maintain stable temperature conditions in the vessel, as well as excellent thermal-insulating materials. Moreover, the molecular nature of H<sub>2</sub>, composed of two spin isomers known as orthohydrogen (o-H<sub>2</sub>) and parahydrogen (p-H<sub>2</sub>), requires a catalytic reaction from o-H<sub>2</sub> to p-H<sub>2</sub> when liquefying hydrogen, as it is more stable as p-H<sub>2</sub> at cryogenic conditions. Any disturbance on temperature can induce the exothermic reversible reaction, provoking a boil-off effect in the vessel [27].

Hydrogen physical storage creates technical limitations that can be avoided when considering methanol and ammonia. As seen in Table I-3, both compounds can be stored at ambient temperatures in liquid phase, with methanol requiring atmospheric pressures, while ammonia needs around 10 bar of pressure. Methanol has slightly higher values of energy density, but hydrogen content in ammonia is higher than in methanol. Methanol can either be synthesized by hydrogenation of carbon monoxide, obtained from Steam Methane Reforming (SMR), or by hydrogenation of carbon dioxide, obtained from Water Gas Shift Reaction (WGSR), Direct Steam Reforming (DSR) or from carbon-intensive sources, as steelworks [29], [30]. Ammonia, on the other hand, can be produced by reaction of hydrogen with nitrogen recovered from air.

One of the advantages of using ammonia for VRE storage is the absence of carbon compounds in the synthesis loop, which goes along with the environmental restrictions concerning reduction and elimination of pollutants emissions. Using ammonia as energy carrier has proven to be economically viable in present and future applications in islanded regions, which can also include ammonia use as fertilizer, with a relative moderate market size [31]. Furthermore, as ammonia production, storage and transportation are mature subjects due to its long development for more than a century, and its importance in worldwide economy, carbon-based ammonia facilities can be used for carbon-free ammonia alternatives to allow the VRE integration in the energy market.

On the contrary, some drawbacks related to safety can be cited. Ammonia vapours can be toxic, corrosive to the eyes, skin and respiratory tract, life-threatening if inhaled in high concentrations, and very toxic to aquatic life. It is also a flammable gas, which can easily detonate in presence of fire [32]. Therefore, it requires extreme safety conditions for its production, handling, storage and transportation.

The following sections discuss the generalities of the ammonia production alternatives, focussing on the classical Haber-Bosch process, detailing the typical operating conditions, equipment and technical limitations encountered.

## **I.5. Non-conventional ammonia production processes**

Ammonia has been produced for more than a century at industrial scale. Currently, it is the second most produced chemical in the world, with a production around 185 Mt/y in 2020, accounting for 2% of total final energy consumption and being responsible for 1.3% of the total anthropogenic CO<sub>2</sub> emissions [33]. It finds use mainly as fertilizer in the agricultural industry, but also as precursor of other products, such as explosives, refrigerants, and cleaning agents. To achieve such great amounts of production, ammonia is mainly produced through a thermochemical route with the Haber-Bosch (HB) process.

Before focussing our attention on the HB process, it is important to draw attention to alternative processing routes that have been gaining importance in last decades, even if they remain as emerging technologies. Known as non-conventional ammonia production routes, they are briefly described hereafter, and references are included for further information.

### **I.5.1. Electrochemical synthesis**

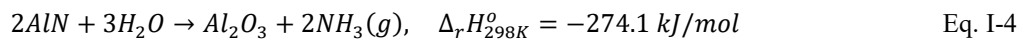
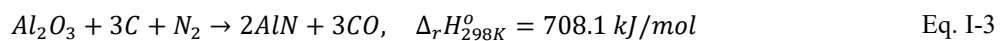
The principle of this approach consists of using two electrodes, an electrolyte, and electrical current. Hydrogen is dissociated into H<sup>+</sup> on the anode (Eq. I-1) and transported through an electrolytic medium to the cathode, where the proton reacts with nitrogen to form ammonia (Eq. I-2).



This process has a lower energy consumption and higher energy efficiency (+20%) than the HB process, but faces several issues, such as low ammonia yields and expensive electrolytes [34]. It can be further classified into two categories: high and low temperature electrochemical synthesis. In the former, different temperature ranges are found depending on the electrolyte used, such as solid electrolytes, operating at 700-800 °C, molten salt electrolytes, around 300-500 °C, and composite membrane electrolytes, at similar levels than the molten salts. Concerning low temperature synthesis, nitrogen fixation at ambient temperature employs aqueous electrolytes with a PEM, and two reactions are held: nitrogen reduction and hydrogen evolution. Further information about this synthesis approach can be found in the following references [34], [35].

### I.5.2. Thermocyclic or chemical looping synthesis

Considered also to be part of the thermochemical routes as the HB process, the thermochemical cycle synthesis consists of two circulated processes of nitrogen activation and ammonia formation. First, an endothermic reaction at high temperature (Eq. I-3) carries out a carbothermal reduction of  $Al_2O_3$  in nitrogen. Then, an exothermic reaction of AlN hydrolysis (Eq. I-4) produces ammonia.



The reduction reaction is highly endothermic, and temperatures around 1300-1500 °C are required, which can be easily achieved with concentrated solar power technology. The hydrolysis reaction is exothermic, with temperatures on the range of 950-1200 °C [36]. Studies about heat integration in thermocyclic synthesis of ammonia have been performed, to include nitrogen production and power generation, achieving energy efficiencies around 69% [37]. Even if the process does not require a catalyst and  $H_2$  production as in the HB process, it depends on a carbon source and generates carbon emissions.

### I.5.3. Plasma synthesis

In the non-thermal plasma technology, the excited species generated in the plasma state can present a higher adsorption rate than ground-state molecules. In the case of ammonia synthesis, which is limited by the  $N_2$  dissociation, plasma activation of nitrogen can create a synergetic effect with the catalyst. Multiple plasma reactor types exist, such as Dielectric Barrier Discharge (DBD) operating at atmospheric pressures, and microwave (MW) and radiofrequency reactors (RF) operating at sub-atmospheric pressures, with the DBD reactors being reported to have the lowest energy consumption [38].

Nevertheless, this technology is far from being competitive with the HB process, as the energy consumption levels are considerably high. The state-of-the-art plasma DBD reactor, operating at 300 °C and 1.5 bar, achieves only 0.16% of ammonia outlet concentration, and has an energy consumption of 197 GJ  $t^{-1}_{NH_3}$ , with a total energy consumption on the process above 235 GJ  $t^{-1}_{NH_3}$  [38]. The best case scenario for the plasma technology, with a DBD reactor, considers an energy consumption in the reactor

of  $5 \text{ GJ t}^{-1}_{\text{NH}_3}$ , and a total energy consumption in the process around  $45 \text{ GJ t}^{-1}_{\text{NH}_3}$  [38], which is even higher than the current best electric HB process of  $38 \text{ GJ t}^{-1}_{\text{NH}_3}$  [39].

#### I.5.4. Photochemical synthesis

The photocatalytic synthesis of ammonia is inspired on the natural synthesis of ammonia with nitrogenase. In this process, solar irradiance can be used to excite electrons into the conduction band of a semiconductor to reduce  $\text{N}_2$  to  $\text{NH}_3$ . Several semiconductors are used, such as titanium- and bismuth-based materials, metal sulphides, carbonaceous materials, biomimetic catalysts and biohybrid complexes. However, this synthesis technique encounters several difficulties for an industrial scale of production, as it presents low ammonia rates, poor photocatalyst stability and low solar-to-chemical conversions (10%), with an overall energy consumption of  $208.3 \text{ GJ/t}_{\text{NH}_3}$  [40].

#### I.5.5. Concluding remark on the non-conventional ammonia production

Despite being novel technologies for ammonia synthesis acting as substitutes of the Haber-Bosch process, the non-conventional routes have a low Technology Readiness Level (TRL), which indicates the phase of development of a technology, in comparison with the conventional HB process. The TRL scale varies from 1, basic idea and research, to 9, proven and commercialized technology.

*Table I-4. TRL of renewable ammonia production technologies. Adapted from [39].*

*\*Processes based on the conventional Haber-Bosch process.*

Technology	TRL
Electric HB with alkaline electrolysis*	8-9
Electric HB with high pressure proton-exchange membrane electrolysis*	6-7
Electric HB with solid oxide electrolysis*	3-5
Electrochemical	1-3
Non-thermal plasma	1-3
Photocatalytic	1-3
Biological	1-3

Novel processing routes are somewhere between 1 (basic research) and 3 (concept validation), and they suffer from low reaction rates. More research is yet to be done in order to compete with classical thermochemical routes of production [19].

The electric HB is not properly a non-conventional production route of ammonia, as it is based on the classical Haber-Bosch process, hereafter described. This is why the 3 types of electric HB have the highest TRL among the technologies. The main difference resides on the process for hydrogen recovery, as the electric HB operates with hydrogen produced by water electrolysis and not from methane through SMR. This conventional HB adapted to carbon-free sources of hydrogen depends on the type of electrolyser used.

## I.6. Conventional thermochemical process: Haber-Bosch

To introduce the HB process adapted to renewable sources of energy, it is necessary to go back to the conventional HB process, as found in many industrial facilities. A graphical comparison between the conventional and the renewable Haber-Bosch process, including hydrogen production, is depicted in Figure I-3. While the ammonia synthesis stages between the two processes can be assumed to be similar, the recovery of hydrogen and nitrogen differs between them.

On the conventional process, hydrogen is mostly recovered from natural gas (70%) and coal (26%) [33]. Considering only the  $\text{CH}_4$ -sourced hydrogen, prior steps are required to produce hydrogen under

appropriate conditions to feed the synthesis stages. The synthesis gas ( $N_2$  and  $H_2$ ) production includes feedstock pre-treatment, gas production, carbon monoxide removal and gas purification [41].

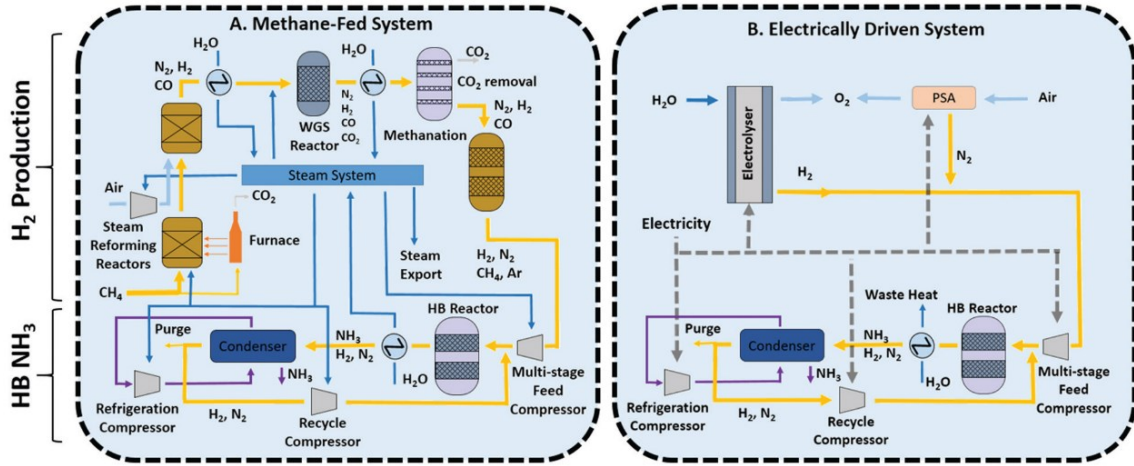
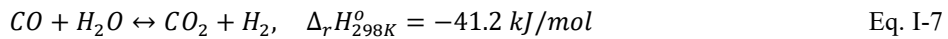
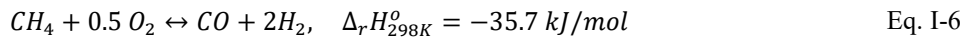


**Figure I-3.** Comparison of processing routes for ammonia synthesis. On the left, the conventional process using  $CH_4$  for hydrogen production. On the right, the electrical process using renewable energy sources. The Haber-Bosch loop remains the same in both configurations. Retrieved from [39].

Feedstock pre-treatment is referred to the removal of sulphur from the hydrocarbon mixture to prevent any damage and poisoning of the catalysts, and to break the long hydrocarbon chains into methane. Hydrogen production is carried out in multiple steps involving different chemical reactions. First, the primary SMR is done, where the endothermic reaction of methane in presence of steam and a catalyst yield towards carbon monoxide and hydrogen, as given in Eq. I-5. This reaction requires moderate pressures between 25 and 35 bar, and high temperatures between 850 and 900 °C, commonly supplied with heat duty from the combustion of natural gas. A secondary SMR, in presence of oxygen from the air and under temperature conditions between 900 and 1000 °C, partially oxidizes the remaining methane, as given by the exothermic reaction in Eq. I-6, where additional carbon monoxide is obtained as subproduct, while inert nitrogen from the air will serve for the ammonia synthesis. Following, two stages of WGSR produce more  $H_2$  from the reaction of CO with steam, as seen in Eq. I-7, with the earlier stage using high temperatures (HTS) around 310 – 450 °C, and the latter low temperatures (LTS), around 200 – 250 °C [39].



Carbon dioxide is removed from the process streams with an absorption operation. It can either be chemical adsorption, using solvents such as monoethanolamine (MEA) and diethanolamine (DEA), or physical absorption, such as in the *Selexol* process [41]. Remaining carbon monoxide is converted into methane through a methanation stage, with the reverse reaction on Eq. I-5, at similar pressures than the SMR, but lower temperatures, around 250 – 350 °C. Even if hydrogen is consumed in this stage, the reduction of methane concentration down to 10 ppm is beneficial for the HB loop [41]. The outlet stream is considered to be mainly composed of a stoichiometric ratio 3:1 of  $H_2:N_2$ , with traces of  $CH_4$  and Ar.

On the other hand, the HB process adapted to renewable sources of energy avoids the use of the reactions previously evoked. Hydrogen is produced in an electrolyser, where water molecules are decomposed into  $H_2$  and  $O_2$  by the means of an electric current, being oxygen a valuable subproduct with high purity. Nitrogen can be recovered from air using a Pressure Swing Adsorption (PSA) separation process.

Concerning the  $NH_3$  synthesis loop, it consists of four main stages: *compression*, to provide the synthesis pressure level; *reaction*, the central core of the process where  $NH_3$  is produced in multiple catalytic beds; *separation*, commonly performed through ammonia condensation; *recycle*, to re-inject unreacted gases for further conversion. Each one of these stages needs a deeper description, which covers technical limitations, typical operating conditions, and equipment configurations, as it will be the central process of study in this work. The following sections will serve to this purpose.

### I.6.1. Compression

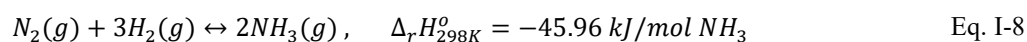
Centrifugal compressors are the standard turbomachinery used for pressure increase in ammonia synthesis plants. Independently of their use for compressing the synthesis gas, the recycle stream or the refrigerant in the cold generation loop, this type of compressor is preferred as it requires lower investment, maintenance, and power, and has higher reliability than the reciprocating compressors [41]. They are typically driven by steam turbines in the case of methane-based HB, but can also be electrically driven, as in the case of the HB using renewable energies.

Regarding the material of the compressors, they must be able to resist metal nitriding at reactor temperatures, corrosion at low temperatures in the ammonia condensed phase, and hydrogen embrittlement and attack in synthesis gas compression. Austenitic stainless steel types 304 and 316 have proven to resist these conditions [42].

On the other hand, achieving such high levels of pressure, typically above 150 bar, would require a high-pressure ratio in a single compressor. Due to mechanical limitations and material resistance, multiple stages of compression and intermediate cooling are required to avoid excessive impeller vibrations, with common pressure ratios varying from 1.8 to 3.2 [41]. Further details on the specification of pressure ratios and the number of stages will be described in Chapter III.

### I.6.2. Reaction

Ammonia synthesis occurs as described by the exothermic and reversible chemical reaction shown in Eq. I-8. Hydrogen reacts with nitrogen in presence of a catalyst, commonly an iron oxide, at high temperature (400 – 500 °C) and high pressure (100 – 300 bar).



The chemical reaction presents some drawbacks due to the trade-off between thermodynamics and kinetics. As illustrated in Figure I-4, where the  $NH_3$  mole fraction is shown as a function of temperature at 150 atm, for the thermodynamic equilibrium, higher mole fractions are favoured by high pressures and low temperatures. However, the triple bonding of nitrogen molecules inhibits the reaction at low temperatures, leading to low reaction rates. To ease  $N_2$  molecules activation and dissociation, which is the rate limiting step on the reaction, not only catalysts are required, but also high temperatures that have a counteracting effect on the extent of reaction [41]. This trade-off between thermodynamics and kinetics induces low conversions per pass in the reactors, which are typically around 20%.

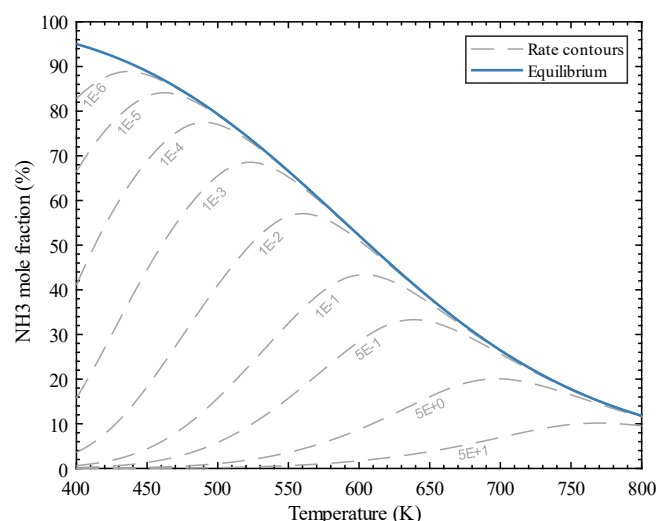


**Figure I-4.** Ammonia mole fraction as a function of temperature at 150 bar for a stoichiometric mixture of  $H_2:N_2 = 3:1$  without inert compounds. — Blue solid curve represents the thermodynamic equilibrium. — Grey dashed curves are the rate contours, expressed in  $\text{mol NH}_3/\text{m}^3/\text{s}$ . Reaction rates contours are calculated with the rate equation of Temkin-Pyzhev for an iron-oxide catalyst, which is presented and discussed in Chapter III.

Multiple technical constraints are encountered when selecting the appropriate reactor configuration. Among them, the most important limitation is related to the temperature inside the reactor. Temperature limits are often set to a maximum of 800 K, to prevent damage on the catalyst, which goes along with the maximum temperature increase per reactor, varying between 100 and 130 K. In addition, the harsh operating conditions of pressure and temperature require materials such as austenitic steels, that can resist hydrogen and nitrogen attack to the reactor structure [43].

As temperature limits are imposed due to technical restrictions, achieving high conversions in the reactors requires the use of multiple catalytic beds with intercooling stages to displace the operating conditions far from the equilibrium. Multiple reactor configurations can be suggested for this purpose, which differ according to the following design parameters:

- Synthesis gas flow direction: axial, radial or crossflow.
- Reactor orientation: vertical or horizontal.
- Number of beds per reactor envelope: single or multiple.
- Location of heat exchange regarding the reactor envelope: internal or external.
- Type of catalyst configuration:
  - Unique bed: covering all the section of the converter.
  - Multitube: with co- or counter-current flow of the cooling fluid.
- Type of heat exchange:
  - Direct: by quenching with a fraction of fresh feed.
  - Indirect: by using a surface to promote the heat exchange, which can use an external fluid as cooling media, or the reactor feed for preheating.

Among the previously cited parameters, reactors are usually classified according to the type of heat exchange involved, the type of catalyst configuration and the flow direction of the synthesis gas. Common types of reactors found in industry, are shown in Figure I-5, and described as follows:

### **I.6.2.1. Multibed converter with direct cooling**

This configuration is composed of multiple catalytic sections in the same reactor envelope, as seen in Figure I-5 a). The inlet synthesis gas (A) is pre-heated in a heat exchanger (E) at the bottom of the reactor, while cooling the hot gas effluent of the catalytic sections. The pre-heated gas flows through the catalytic beds (D) while the reaction occurs, in an adiabatic behaviour. The effluent of each catalytic section is cooled down with a fraction of fresh synthesis gas.

The quenching is carried out with distribution nozzles between the catalytic beds. While the synthesis gas enters the catalytic bed at around 673 K and increases its temperature in about 100 K, the quenching stream is commonly operated at 400 – 470 K. A classic design of this type is found in the Kellogg four-bed quench converter [44], where the internal heat exchanger is placed on top of the reactor.

### **I.6.2.2. Multibed converter with indirect cooling**

In the case of indirect cooling, as seen in Figure I-5 b), the catalytic beds operate as an adiabatic section, where temperature increases. Between beds, a heat exchanger (F) allows to remove heat from the process gas, using a cooling stream that can be another process stream, an external utility, or even the feed of the reactor for pre-heating. In comparison with the direct cooling, no dilution exists, as the heat exchanger maintains the two streams separated. The heat exchangers can be directly installed within the catalyst beds, or for large capacities, the catalytic beds are separated into individual envelopes, with heat exchangers being located outside.

This type of converter is used for revamping direct cooling converters, as it allows to convert more of the synthesis gas. In fact, the direct cooling by quenching dilutes the ammonia in fresh feed, and this fresh feed does not pass through each catalytic section, resulting in less conversion at the reactor envelope outlet. In comparison with indirect cooling, the quenching configuration is less efficient in terms of conversion [41], [45]. Some examples of this configuration can be found in the Uhde converters by Thyssenkrupp [46], where the intercooling is guaranteed by the fresh feed.

### **I.6.2.3. Multitube converter with counter-current indirect cooling**

As shown in Figure I-5 c), the multitube converter consists of multiple tubes inside the catalytic sections where the heat exchange occurs with a cooling media. In the case of the mentioned figure, synthesis gas at lower temperature acts as cooling stream, which is pre-heated until the desired temperature for the catalytic bed inlet, near 673 K. As the reaction occurs in the reactor, the heat produced is recovered by the gas feed flowing in counter-current direction, reducing the temperature within the catalytic bed.

While the heat exchange continues along the catalytic bed, the lower reaction rates are found, as the cooling becomes predominant regarding the heat released by the reaction, and the high ammonia content limits the reaction rate. Examples of this type of converter are the Tennessee Valley Authority (TVA) converter, and the ICI tube-cooled converter [41], [47].

### **I.6.2.4. Multitube converter with co-current indirect cooling**

In contrast with the counter-current design, in the co-current design shown in Figure I-5 d), the cooling stream first flow in a counter-current direction, but once it reaches the top of the catalytic beds, starts flowing in a co-current manner to recover the heat produced from the reaction. The greatest temperature difference located at the inlet of the catalytic section induces the maximum heat transfer at the top of the reactor.

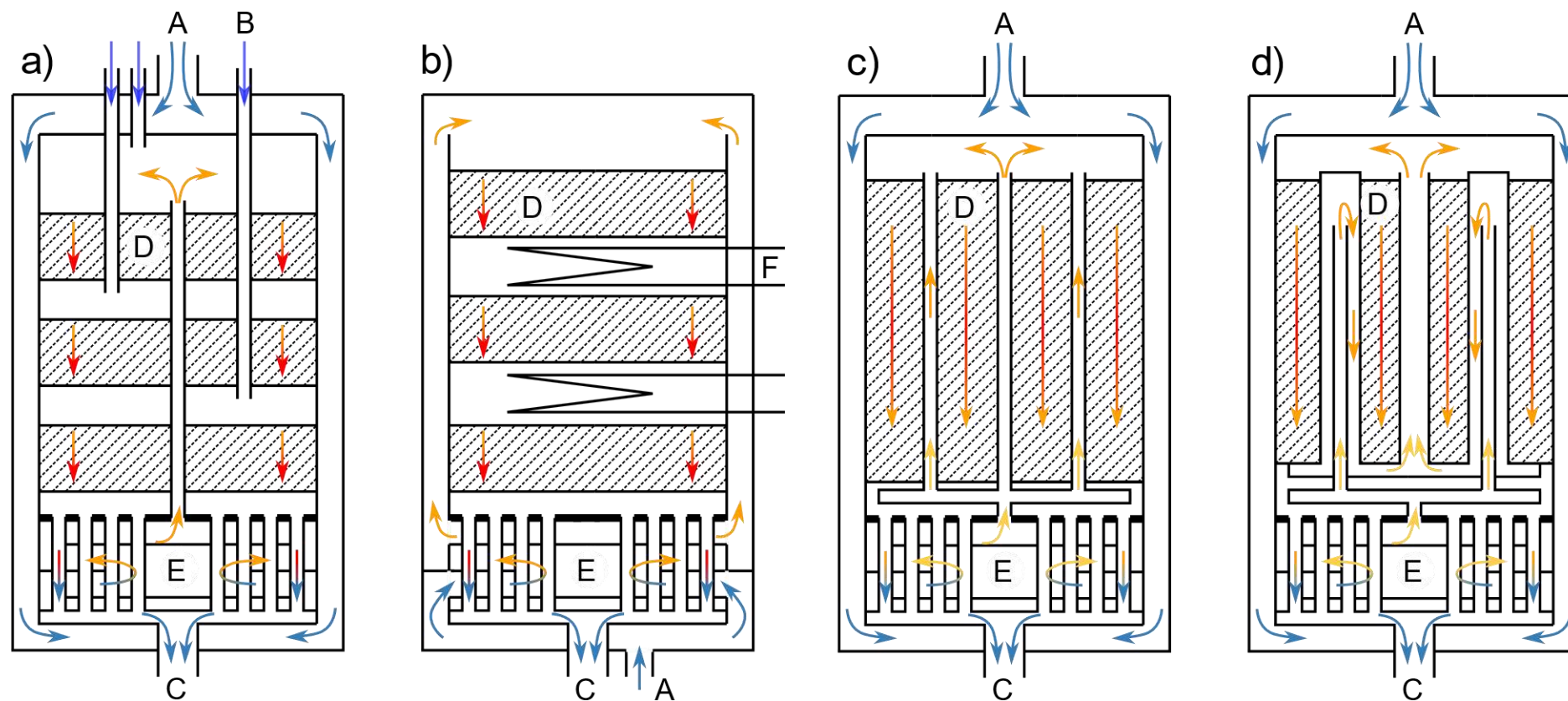


**Figure I-5.** Common reactor configurations found in industrial cases of ammonia synthesis. Adapted from [41]. a) Multitubed converter with direct cooling (quench). b) Multitubed converter with indirect cooling. c) Multitubed converter with counter-current indirect cooling. d) Multitubed converter with co-current indirect cooling. A) Synthesis gas inlet. B) Quench gas inlet. C) Gas outlet. D) Catalytic sections. E) Heat exchanger for feed pre-heating and outlet gas cooling. F) External heat exchanger for indirect cooling. In the case of indirect cooling, the multitubed converters use the heat of reaction to pre-heat the feed of the reactor, while in the multitubed converter the heat exchange occurs with an external cooling fluid. For simplicity, flow direction is considered to be axial in every configuration, even if radial configurations are also encountered. Colours are indicators of temperature, with — darker blue arrows being the coldest, and — red arrows being the hottest.

The evolution of heat transfer allows the temperature to approach the best trajectory in terms of conversion, in comparison to other configurations. Industrial applications for this configuration were used in the Nitrogen Engineering Corporation (NEC) converter [47].

Similar configurations are found with radial flow, crossflow, or a combination of radial-axial flow. The axial configuration suffers from an important pressure drop along the catalytic beds, which is increased when converters have greater depth. Radial configurations are proposed as configurations to overcome this problem, as the gas has more distribution on the catalytic beds and therefore more effective contact in less time, avoiding high pressure drops. An example of the radial flow reactors are the Topsøe S-100, S-200, and S-300 converters, by Haldor-Topsøe [48]. A mixed radial-axial flow can be found in the Ammonia Casale configuration, who first introduced this configuration [49].

For all the previously evoked configurations, the catalytic sections are usually placed within an internal reactor envelope, known as the cartridge, built with high-grade materials, in comparison to the external envelope, operating at lower temperatures.

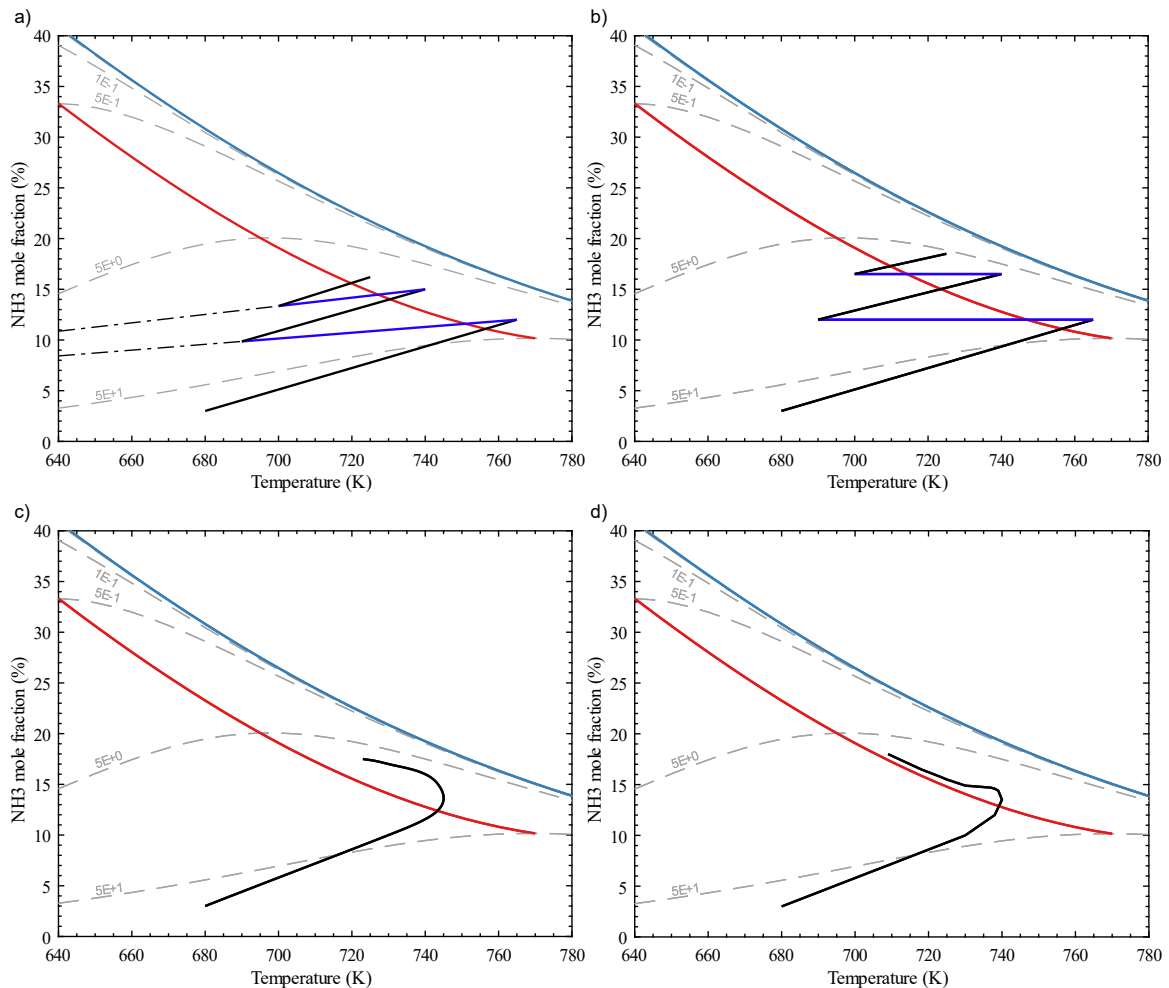


**Figure I-6.** Profiles of the mole fraction evolution in the reactor, as a function of temperature. a) Multibed converter with direct cooling. b) Multibed converter with indirect cooling. c) Multitube converter with counter-current cooling. d) Multitube converter with co-current cooling. For the multitube converters, cooling is performed with reactor feed. — Light blue solid curve represents the thermodynamic equilibrium. — Red solid curve denotes the OTP. — Black solid lines are the trajectories inside the catalytic beds. — Dark blue lines are the cooling stages. — Grey dashed curves are the rate contours, expressed in  $\text{mol NH}_3/\text{m}^3/\text{s}$ . - - Black dot-dashed curves are the projection to the quench cooling conditions. Trajectory lines are qualitative.

An important parameter to consider when designing reactors for exothermic reactions is the Optimal Temperature Progression (OTP). This indicator is the trajectory that can be found when plotting a chart of  $\text{NH}_3$  mole fraction against temperature, for different reaction rates. The OTP consists of the points for which the maximum mole fraction is found for every rate contour, as seen in Figure I-6.

As the Optimal Temperature Progression is the locus of the maximum conversions for the rate contours, higher ammonia mole fractions are expected when following the OTP trajectory. This behaviour allows also to reduce the amount of required catalyst and, therefore, the size of the reactor. Nevertheless, following the OTP requires specific converter configurations and the optimization of its parameters.

From Figure I-6, plots a) and b) are related to the multibed converter with direct and indirect cooling, respectively. As it can be seen, the use of multiple adiabatic sections and heat exchangers in between allows, in a certain way, to place the temperature profile in the vicinities of the OTP. On the other hand, in plots c) and d), the multitube converter with counter- and co-current flow, respectively, have a better approach to the OTP. In fact, as reaction heat is removed from the catalytic bed, the decrease in temperature allows to follow the OTP while increasing the  $\text{NH}_3$  mole fraction. However, once the catalytic bed has been cooled to a certain temperature, the reaction is no further occurring. Even if the temperature trajectory in multitube configuration gets closer to the OTP, multibed adiabatic reactors seem the best option to employ due to their technological simplicity, operability, and maintenance.

#### **I.6.2.5. Catalysts**

While the selection of the reactor configuration and the appropriate operating conditions is of the utmost importance, choosing an effective catalyst remains the main step before any reactor design. In effect, reactor parameters will be adapted according to the chosen catalyst. As kinetic rates and reaction extent might differ between different catalytic materials, a specific reactor design which is well-suited for a catalyst A, might not be ideal for a catalyst B.

The catalytic materials used for the synthesis of ammonia have been widely studied during the last decades, in order to improve the low conversion per pass found in the HB process. Moreover, many efforts have been made with the purpose of using milder pressure and temperature conditions, that allow reducing the energetic consumption of the ammonia synthesis loop.

For more than a century, catalysts belonging to two main categories have been used: fused iron and supported metallic catalysts.

The former includes three types of iron oxides, which are hematite ( $\text{Fe}_2\text{O}_3$ ), magnetite ( $\text{Fe}_3\text{O}_4$ ) and wüstite ( $\text{Fe}_{1-x}\text{O}$ ). Magnetite has been used in majority in the industrial synthesis of ammonia, even if wüstite has gained interest on the last decades, as it shows a greater catalyst activity than the other two types [50]. Iron oxides are usually associated with a promoter material, able of enhancing the catalytic activity. Among them, alumina, potassium, and iron alloys such as iron-cobalt and iron-nickel have been recorded among the propositions.

On the other hand, supported metallic catalysts are materials using a support, such as activated carbon or a metal oxide, with metallic elements on their surface, as ruthenium or cobalt. In fact, ruthenium-based catalysts are the second most used catalyst for ammonia synthesis after iron-based. Since the early 1980s, the Kellogg Advanced Ammonia Process (KAAP) has used Ru-based catalysts supported in graphite carbon, which has high activity at low temperatures and pressures. For instance, at pressures around 100 atm, the catalyst activity is claimed to be somewhere between 10 and 20 times the magnetite

activity, achieving outlet ammonia content around 20 – 21.7 % [51]. More recently, cobalt-based catalysts have been studied as an alternative to the Ru-based catalyst. The main interest to consider Co as substitute of Ru is the scarcity of the latter, and the high cost associated to its production. Also, nickel-based catalysts are being studied as substitute of Ru, and it has been proven in some applications the interest of Ni-based catalyst for low temperature ammonia synthesis, in comparison with Fe-based catalyst conditions. An extensive review on ammonia synthesis catalysts can be found in [50].

It is also important to remark the possible catalyst poisons that can be found in process streams, that might drastically decrease the catalytic activity. Catalysts must avoid any contact with oxygen compounds, such as CO, CO<sub>2</sub>, and H<sub>2</sub>O, and non-metallic compounds, like sulphur, phosphorous and chlorine [51]. While considering the HB process to be completely based on renewable energies, there does not exist any risk of catalyst poisoning by these compounds.

Even if plenty of catalytic materials are reported in literature with high activities and conversions, the selection of the catalyst for this work has to meet two criteria: (i) the catalyst must be associated to a properly defined kinetic rate equation issued from experimental data, able to describe the catalytic behaviour in the reactor, and (ii) an economic indicator must be available for its cost evaluation, in order to estimate the expenses related to its investment. To fulfil these requirements, an iron-based catalyst and a ruthenium-based catalyst are chosen, as they have been widely studied and all the required information can be found in literature. Further information is given in Chapter III.

### **I.6.3. Separation**

Low conversions on the reaction stage impose the need of an effective ammonia separation method, which allows not only to produce a high-purity ammonia stream, but to recycle the unreacted gases with the lowest ammonia content as possible. Historically, separation has been performed through condensation technologies, but with the search for milder synthesis conditions, other separation technologies have been placed onto the radar, such as separation by absorption, adsorption or by permeation through membrane materials. These technologies are briefly described hereafter.

#### **I.6.3.1. Condensation**

Separation by condensation is based on the use of multiple heat exchangers to cool down reactor gases until reaching the NH<sub>3</sub> condensation temperature. This method takes advantage of the non-condensable nature of H<sub>2</sub> and N<sub>2</sub>, recovered in gas phase for recycle. Condensation temperature is directly related to the pressure of the process stream and its content in ammonia. Figure I-7, shows the condensation temperature for different pressures and ammonia mole fraction, varying between 8 and 14 %. The remaining is a stoichiometric mixture of H<sub>2</sub>:N<sub>2</sub>.

It is evident that for pressures higher than 100 atm, cooling temperatures approaching ambient conditions are adequate for NH<sub>3</sub> condensation, which can be easily satisfied with cooling water and air streams. For lower pressures on the process stream, lower temperatures are encountered, which can be satisfied using a mechanical refrigeration cycle with ammonia as cooling media. Indeed, refrigerant temperatures as low as – 33 °C can be achieved in a cold cycle using high purity ammonia (> 99.5 %), which is vaporized at atmospheric pressure and recompressed at pressures around 15 – 20 atm.

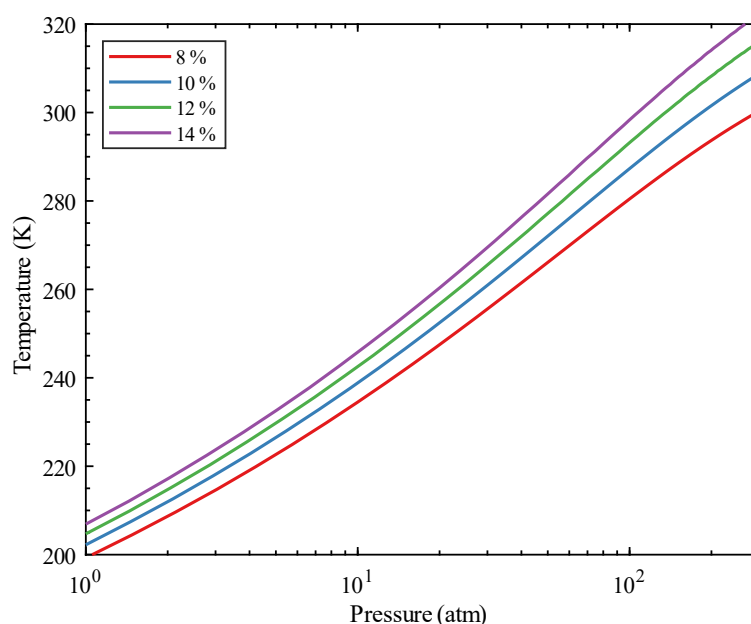


**Figure I-7.** Dew point temperatures at different synthesis pressures, for mole fractions of ammonia varying from 8 to 14 %. The remaining content is a stoichiometric mixture of  $H_2:N_2$ . Curves traced using data from ProSimPlus.

### I.6.3.2. Absorption

As a replacement of the condenser, absorption systems have emerged as potential solutions to enhance low-pressure synthesis loops. Crystalline salts are able to absorb ammonia molecules at low pressures, around 20 – 30 atm, and moderate temperatures, around 200 – 300 °C [39]. Among them, the most common metal halides found in literature are chlorides as  $MgCl_2$ ,  $CaCl_2$  and  $MnCl_2$ , and bromides like  $CaBr_2$  [52]. Silica and zeolites are frequently used as supports for scale-up applications, being the former cheaper and preferred over zeolites, even if the latter have greater absorbent capacities [53].

The main advantage of absorbents for ammonia separation is that at such reduced synthesis pressures, capital expenditures are drastically reduced in comparison to the condensation separation. However, desorption of ammonia from absorbents has been reported to require high temperatures, meaning the need for heating [54]. Therefore, even if costs are reduced, energy consumption is somehow increased, as seen in Table I-5.

### I.6.3.3. Adsorption

As for absorption technologies, adsorption has been widely studied for ammonia separation. Being a superficial phenomenon, the adsorption capacity is lower in comparison to the volume-based absorption. For instance, reports on  $NH_3$  absorption with chloride-bromide salts allow to absorb up to 32 wt.%, while  $NH_3$  adsorption on molecular sieves shows an adsorption capacity of 9 wt.% [53].

Some patents have been published for ammonia separation with zeolites 4A, 5A and 13X [55], activated carbons and Ca-X zeolites [56]. Ammonia has shown to be preferentially adsorbed on zeolites, when compared to nitrogen and hydrogen, being the latter the least adsorbed of the mixture [57]. This proven fact is important, as renewable hydrogen is the main economic driver in HB processes, and its recovery and recycle needs to be as efficient as possible, to avoid incurring in  $H_2$  losses. Works by Helminen *et al.* allowed to find that low separation temperature applications (~ 298 K) favour the adsorption in activated carbons, while zeolites are insensitive to temperature and could be used for high-temperature

cases ( $\sim 398$  K). On the other hand, silica and alumina have low adsorption capacities, which decrease with temperature increase [58].

**Table I-5.** Comparison of main indicators between condenser, absorption, and adsorption separation technologies. The desorption mechanism is considered to be by temperature increase. Adapted from [59].

Indicator	Units	Condenser	Absorption with metal halides	Adsorption with zeolites
Separation temperature	$^{\circ}\text{C}$	-20 – 30	150 – 250	20 – 100
Desorption temperature	$^{\circ}\text{C}$	-	300 – 400	200 – 250
Synthesis pressure	bar	100 – 300	10 – 30	10 – 30
Energy consumption of the separation	$\text{GJ t}^{-1}\text{NH}_3$	3 – 5	6 – 11	8 – 13
Ammonia mole fraction in recycle stream	mol. %	2 – 5	0.1 – 0.3	0.1 – 0.3
Ammonia gravimetric capacity	wt. %	100	5 – 30	5 – 15
Ammonia volumetric density	$\text{kg m}^{-3}$	680	100 – 600	30 – 90
TRL	-	9	4 – 5	4 – 5

Comparing the technologies in Table I-5, the sorption methods allow to avoid the high temperature gradient found between the reactor outlet temperatures, typically  $500^{\circ}\text{C}$ , and the required separation temperature, as well as high synthesis pressures. However, sorbents regeneration by temperature swing represents a significant increase in the energy consumption, that do not compensate energy savings when avoiding the low condenser temperatures. Besides that, it is interesting to notice the low  $\text{NH}_3$  mole fraction on the recycle stream, which goes down to 0.1 % in the best of cases, favouring the conversion in the reactors. On the other hand, sorption methods have TRLs of 4-5 at pilot-scale applications but have the advantage of being adapted for intermittent operation, being interesting for delocalized and seasonal operations [53].

Whether it is absorption or adsorption separation, the chosen sorbent material must have a high ammonia selectivity regarding the competing molecules found on the processing streams. These materials need to be easily regenerated, either by temperature or pressure swings, must be economically competitive, and should have a reasonable lifetime before replacement.

#### I.6.3.4. Membranes

The use of membranes has gained particular attention for its use as physical barriers for ammonia recovery, as it does not require any regeneration step as in the sorption separation. Membranes are usually evaluated with two counteracting parameters: permeation and selectivity. The former is referred to the ability of a compound to diffuse through the membrane, commonly measured by permeances, while the latter is seen as a relation between two compound permeances. Both parameters have a counteracting effect. While higher permeabilities involve higher diffusion through the filter medium, the selectivity might be affected as higher quantities of the different compounds pass through the membrane.

The ability of a compound to pass through the membrane filter depends on the nature of the material, the affinity of the compound with the material, the concentration of the compound, and operating conditions such as temperature, pressure, among other factors. The pressure is an important parameter, as the difference in partial pressures between the retentate and the permeate sides is the driving force which favours the diffusion.

Different types of membranes, depending on their materials, their operating conditions and their diffusion mechanisms can be found. The interest of using this separation method resides in, as for the

sorption methods, avoiding the temperature gradients across the HB process, as they can operate at intermediate temperature, closer to the synthesis conditions [60].

Multiple works on ammonia separation for different membrane materials can be found. For instance, organic membranes, such as cellulose acetate, polyvinyl ammonium thiocyanate and poly-perfluoro-sulphonates present high permeabilities and selectivities, but due to their organic nature are not commonly resistant to harsh conditions, as in the HB process [60]. Inorganic membranes, as silica and zeolites are stable at different levels of temperature and pressure [61]. Works by Pengilley allowed to find that MFI zeolite membranes are useful for ammonia separation from reactive gas mixture. The membrane performance is strongly related to temperature, increasing its ammonia selectivity up to 353 K. Higher temperatures induce greater permeabilities of nitrogen and hydrogen, following a decrease in ammonia selectivity. At 353 K, the effective (real)  $\text{NH}_3$  selectivity over  $\text{N}_2$  and  $\text{H}_2$  is found to be 46 and 15, respectively. Also, Wei *et al.* have recently studied  $\text{NH}_3$  separation with ZIF-21 membranes, another type of zeolitic material, and found ideal selectivities of ammonia over nitrogen and hydrogen equal to 35 and 12, respectively [62].

To consider membranes as mean for ammonia separation, not only the material has to be selective to ammonia, but it needs also to be adequate for high temperature and pressure operations, as well as being economically competitive. It has the potential to avoid high temperature gradients for ammonia recovery and the recycle of unreacted gases. However, as for the sorption separation technologies, the additional investment on materials needs to be considered.

## I.7. Progress towards more efficient Haber-Bosch processes

The HB process has more than a century of history, development, and improvement, resulting not only in more productive but also in more efficient processes. Mass and energy transformations have been improved and the overall energy balance has yield towards less energy losses. Figure I-8 shows the different levels of energy consumption of HB processes through the last decades, revealing how technological improvements have allowed to achieve lower energy requirements.

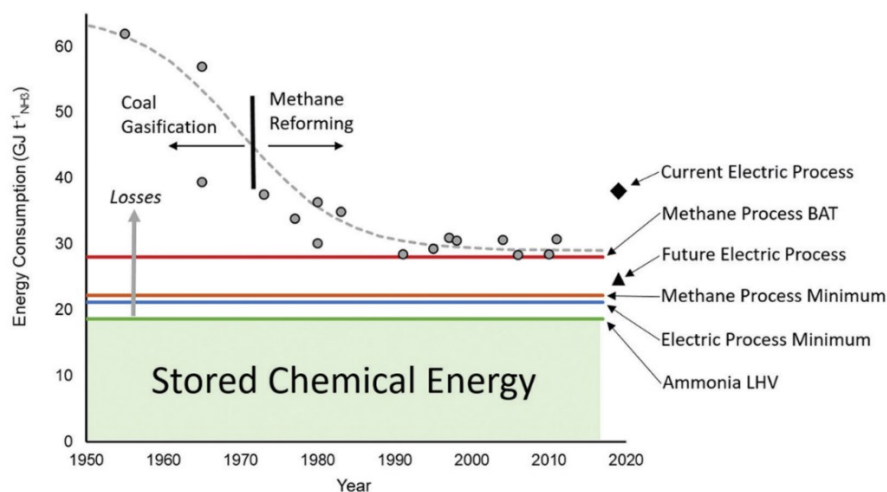


**Figure I-8.** Evolution of the energy consumption ( $\text{GJ t}^{-1}_{\text{NH}_3}$ ) for HB processes since 1950. Stored chemical energy is based on ammonia LHV. The minimum energy consumption for the electric and methane HB processes is indicated by blue and orange horizontal lines, respectively. The Best Available Technology (BAT) for methane HB is shown by the red horizontal line. Figure retrieved from [39].

The baseline for comparison between technologies is the minimum required energy for ammonia synthesis, known as the thermodynamic limit. It is based on the Low Heating Value (LHV) of  $\text{NH}_3$  equal to  $18.6 \text{ GJ/t}_{\text{NH}_3}$ , as shown by the green line. Anything above this limit is considered a loss of energy. For the electric HB process using electricity to recover  $\text{H}_2$  from water electrolysis, a minimum energy input of  $21.3 \text{ GJ/t}_{\text{NH}_3}$  is required, while for the methane-based HB it is  $22.2 \text{ GJ/t}_{\text{NH}_3}$ .

The Best Available Technology (BAT) in the methane HB requires at least  $27.4 \text{ GJ/t}_{\text{NH}_3}$ , with other processes going up to  $31.8 \text{ GJ/t}_{\text{NH}_3}$ , about half of the energy used in the mid-century HB coal-based process, with  $60 \text{ GJ/t}_{\text{NH}_3}$  [39].

A generic road map for ammonia production and storage, using renewable energy, is shown in Figure I-9. Regardless of the energy type, wind or solar sourced, it provides with electricity the air separation unit for nitrogen production, and the electrolyser for hydrogen recovery from water, while producing high-purity oxygen as a valuable by-product. Also, depending on the HB configuration, compression, recycle, and separation stages can be electrically driven, avoiding the use of steam turbines as in the conventional process.

Thermal energy produced from the intercoolers of the compressors, and the heat of reaction, can be used to heat the recycle stream, but once again, it depends on the separation technology chosen. This is an important aspect to consider, as any process involving energy transformation and storage requires to be as efficient as possible, and to avoid as much as possible any thermal losses. The analysis of the potential thermal integration will be further addressed in Chapter VII.

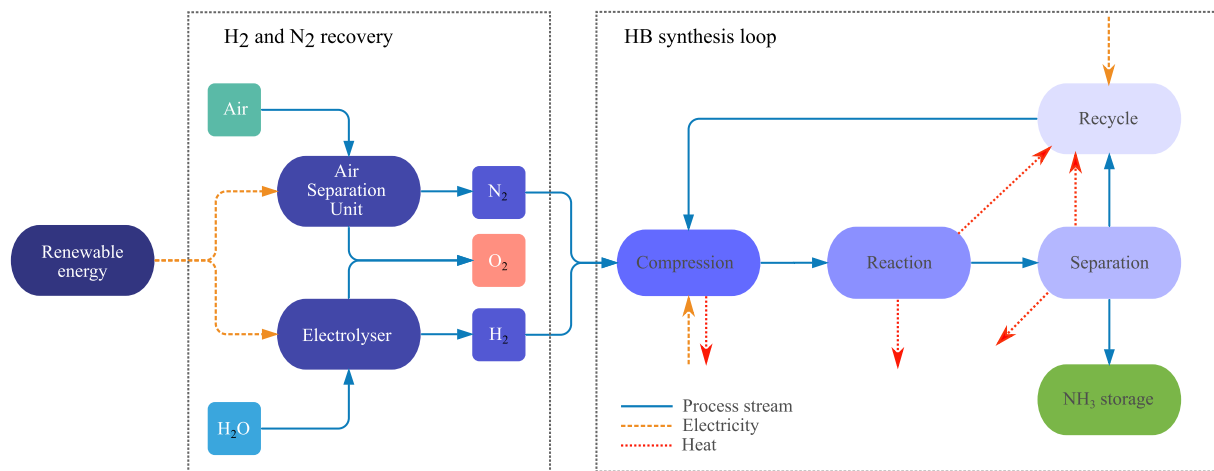


**Figure I-9.** Block diagram of the storage of renewable energy into ammonia.  $\text{H}_2$  and  $\text{N}_2$  recovery are not directly related to a specific technology, but the ammonia synthesis loop resembles the conventional Haber-Bosch process. Depending on the selected technologies, energy integration can be performed between the recovery of reactive gases zone and the synthesis loop. Heat streams are indicative of possible thermal integration, as they are dependent on the type of reactor, the type of cooling and the separation technology.

While the Best Available Technology (BAT) for ammonia production, based on a methane HB process, is equal to  $27.4 \text{ GJ/t}_{\text{NH}_3}$ , the current electrical HB process is reported to have a total energy consumption of  $38.4 \text{ GJ/t}_{\text{NH}_3}$ , with an overall energy efficiency of 65%, and total energy losses of  $13.3 \text{ GJ/t}_{\text{NH}_3}$ . Energy losses are referred not only to losses from the system to the surroundings, but to energy spent on equipment or process stages. For instance, the PEM electrolyser for  $\text{H}_2$  production is responsible for

losses of 10.8 GJ/t<sub>NH<sub>3</sub></sub>, while N<sub>2</sub> production accounts for 0.33 GJ/t<sub>NH<sub>3</sub></sub>, the HB synthesis loop spends 1.8 GJ/t<sub>NH<sub>3</sub></sub>, and additional losses are equal to 0.33 GJ/t<sub>NH<sub>3</sub></sub> [39].

The major points allowing the reduction of the energy consumption from the conventional to the electric HB process, reported in [39], are:

- The purity of H<sub>2</sub> and N<sub>2</sub> incoming to the process, which allow to avoid the purge as no inert compounds are introduced synthesis loop, reducing in 1.8 GJ/t<sub>NH<sub>3</sub></sub> the energy losses.
- The compressors being driven by electrical motors instead of steam turbines, making the energy transfer more efficient and reducing the energy losses from 6.6 to 3.5 GJ/t<sub>NH<sub>3</sub></sub>.
- The high-pressure hydrogen produced by the electrolyzers, reducing the mechanical work in compression stages. Assuming the H<sub>2</sub> to be recovered at 10 bar, from an alkaline electrolyser, energy savings account for 0.9 GJ/t<sub>NH<sub>3</sub></sub>.

Moreover, shifting from fossil-fuels to renewable energy allows to reduce in almost 80 % the CO<sub>2</sub> emissions. The remaining 20%, between 0.12 and 0.53 t<sub>CO<sub>2</sub></sub>/t<sub>NH<sub>3</sub></sub>, is associated with wind turbine carbon footprint, which varies between 9 and 13 g<sub>CO<sub>2</sub>eq</sub>/kWh for offshore wind turbines and is around 20 g<sub>CO<sub>2</sub>eq</sub>/kWh for onshore turbines [63].

It is evident that technological improvements of equipment and materials, such as more efficient electrolyzers and catalysts, are some of the solutions that can lead towards more efficient and also, more economic processes. Nevertheless, external factors have the leverage to facilitate the integration of renewable energies to the current energy market, as policies for carbon taxation and high prices on natural gas, allowing, among others, green ammonia processes to compete with conventional fossil-fuel industry.

## **I.8. Conclusions**

Having covered the current interest towards a decarbonization of the industry and the energy market, as well as the different alternatives that exist to enable this solution for the reduction of global carbon emissions, NH<sub>3</sub> stands out as an important energy carrier to be exploited in the near future, to boost the H<sub>2</sub> economy.

Beyond being one of the chemicals with higher production worldwide and having a key role on the agriculture chain for food production, current application boundaries can be expanded towards the energy sector to facilitate the integration of renewable energies in delocalized zones with seasonal energy surplus. However, it is crucial to consider the intermittent nature of energy and, therefore, the discontinuous supply of hydrogen and nitrogen. Intermediate storages of H<sub>2</sub> and N<sub>2</sub> can be proposed as buffering media, allowing the HB synthesis loop to operate in continuous conditions. Buffer capacities must be estimated from specific conditions of the project location, to guarantee a continuous supply of reactive gases during energy production shortage periods.

The main objective of this work is to propose a process flowsheet configuration, mainly of the Haber-Bosch synthesis loop, which will be the result of a superstructure optimization, as will be detailed in Chapter II. This configuration will be evaluated with performance indicators, such as the Levelized Cost of Ammonia production (LCOA), the specific energy consumption (e.g., kW/kg<sub>NH<sub>3</sub></sub>), or the energetic efficiency, in order to compare the optimal process configuration with processes from the literature, related to energy storage alternatives. The interest resides on determining how helpful the superstructure optimization methodology is when evaluating multiple process alternatives simultaneously.

# Chapter II

---

*Literature review on superstructure optimization  
methods*

---



## II. Chapter II: Literature review on superstructure optimization methods

This chapter intends to cover the following matters:

- A brief description of Process Systems Engineering field, with a special emphasis on Process Synthesis and the discussion of the dilemma of generating the optimal process structure.
- Main approaches for Process Synthesis, their classification, and principal characteristics: hierarchical decomposition and mathematical-based superstructure optimization techniques.
- Description of principal superstructure representations and details on MINLP optimization techniques, focusing on metaheuristics.

### II.1. Introduction

The quest for optimal processes remains one of the main objectives sought by process engineers. Chemical processes are often judged to be optimal according to one or multiple criteria, which tend to have a counteracting behaviour. Among the most common indicators of performance, one can find some economic, technical, and more currently, environmental criteria. Usually, more importance is given to the first one when assessing the interest of an exploitation project, as it is commonly judged according to the expected profitability. However, when evaluating processes related to energy production, it is of the utmost importance to include indicators of energetic efficiency or energy consumption, allowing to identify processing units where useful energy might be lost and to propose technical improvements. Besides, the trending urge to look up for greener processes, with low or zero emissions of pollutants, has given to the environmental criteria a key role.

Achieving optimal criteria in process optimization is frequently associated with the adjustment of a set of operating conditions or equipment design specifications, such as the temperature of the process stream in a heat exchanger or the pressure ratio in a compressor. Beyond this, when conceiving new processes or retrofitting an already established one, the optimization can also be extended to the equipment arrangement, as multiple equipment might be able to perform the same transformation to a process stream. Deciding between multiple equipment to perform a specific mass or energy transformation, for instance, cooling down a process stream using either a tube-and-shell heat exchanger or a plate-fin heat exchanger, can be considered as a discrete decision variable when optimizing the Key Performance Indicators (KPI). Thus, along with operating conditions and equipment design parameters, the process structure should also be studied.

Consequently, performing the optimization of a chemical process where multiple KPI are involved, and where the set of variables to adjust is considerably large, is a time and resource consuming mission. This requires the use of robust methodologies and computational tools to ease the search of the best set of parameters which minimize or maximize the optimality criteria.

In this context, this chapter is devoted to a literature review on superstructure optimization methods, the central objective of the work. Section II.2 proposes a brief description of Process Systems Engineering field, covering its background, and considering the main areas of study of this discipline. Next, section II.3 is committed with a deeper focus in Process Synthesis, being the area of main interest in this thesis. It covers the different methodologies for conceiving chemical processes, highlighting the principal

classifications, representations, and characteristics, emphasizing on superstructure optimization methods, and optimization techniques. Finally, a concluding discussion is held in section II.4.

## II.2. Process Systems Engineering

Process Systems Engineering (PSE) is a vast and complex field belonging to chemical and process engineering, which englobes the design, modelling, optimization, control, and evaluation of any process used to transform raw materials into value-added products [64]. It is focused on proposing systematic procedures for designing and operating chemical and biochemical processes from micro- to plant-scales, in continuous or transient behaviour [65]. The PSE terminology gained its relevance since 1982, at the 1<sup>st</sup> PSE conference in Kyoto, Japan, but it was studied since the late 60's with the pioneering works of Roger Sargent [66] and Dale Rudd [67], which described the working areas of PSE and the systematic approaches for process synthesis and optimization. The background of the PSE field, with the relevant works over the last decades, is briefly described hereafter.

PSE started to develop as a discipline due to the lack of systematic guidelines for designing processes and the use of engineering judgement based on techniques not explicitly formulated. This gave an opportunity for the Conceptual Process Synthesis (CPS) to be formally recognized. Also known as Process Design or Process Synthesis, it was first defined by Roger Sargent as the *“determination of the fixed parameters for a process such that it will deliver the required quantities of products in accordance with specifications under all foreseeable conditions, and such that the overall operation will be optimum in some sense”* [66]. In this light, CPS covers the proposal of any chemical process and the adjustment of multiple operating conditions and equipment design specifications that allow to yield towards an optimal solution. However, given the different complexities found in processes at industrial scale, which commonly present multiple intricate recycling loops, dependencies between operating conditions, and several parameters to be adjusted per operating unit, the space of alternatives tends to increase exponentially, and the search of the best solution becomes a challenge to overcome. To this effect, three central problems were identified [68]:

- Representation problem: how to represent a considerable number of alternatives, excluding the illogical or infeasible ones?
- Evaluation problem: how to evaluate a substantial number of alternatives with a good balance between speed and accuracy?
- Strategy problem: how to propose a strategy that allows finding faster the best alternatives without the need of testing each one?

Several authors have proposed plenty of methods and resources through the last decades to tackle down these difficulties. As it is the central subject of this thesis, a detailed description of Process Synthesis methods is given in section II.3, intended to overcome primarily the representation problem.

Along with the development of CPS methods, the growth of robust computing systems allowed the PSE discipline to expand towards the Process Modelling and Process Simulation fields.

Process Modelling implies representing the process structure with mathematical relations that describe the behaviour of the system. It can be handled at different levels of detail and depends also on tools used for the process conception.

One can find **high-level models**, where models are simplified into the dominant elements of the objectives and constraints, which are helpful for the first evaluations of a process but remain a simplified

approach in comparison with more detailed models. Examples on these models can be found for distillation systems [69].

As well, **shortcut models** are useful, gaining detail with more complex functions and giving better predictions on the behaviour of the system and its investment and operating costs, but keeping simple nonlinear descriptions of processing units. Works on this modelling level are found on [70]–[72].

Finally, the **rigorous models** involve more detailed descriptions of processing units behaviours and less simplifications, such as equilibrium- and rate-based mass and heat transfer [73]. Its resolution can be easily complexified, needing mathematical solving approximations, and the addition of nonconvex equations can lead to local optima. Nevertheless, more precision can be gained with a better description of the real behaviour of the system, with prejudice of requiring more computational effort.

Concerning Process Simulation, it allows representing process flowsheets in informatic tools, taking advantage of computational capacities for easily solving mass, energy, and momentum balances. Plenty of software has been created with the purpose of facilitating the calculations of complex process flowsheets. Processing unit operations are modelled and translated into computational codes, while creating simple Graphical User Interfaces (GUI), allowing engineers to effortlessly calculate processes and estimate performances through the means of imbedded mathematical solvers.

To cite some widely known tools, one can find *SPEED-UP*, which gave the first insights on the modular-sequence and equation-oriented approaches, useful for defining the best sequence for the calculation of a flowsheet [74]. *gProms*, built in an equation-oriented approach to deal with dynamic processes, including continuous and discrete variables [75]–[77]. The widespread *ASPEN* suite, a simulation software intended for broader ranges of processes, such as those treating multiphase streams including solids [78]. *ProSim*, proposed in a modular sequence approach, for testing different methods of internal recycling-simultaneous convergence [79].

These tools have evolved since their creation and their use is currently a mandatory stage in the proposal of chemical processes. They include, among other features, detailed models of unit operations at the equipment scale, extensive databases of properties of pure compounds, several thermodynamic models and parameters, diverse mathematical solvers for complex convergences, and even correlations for economic estimations. The level of development achieved throughout the years gives them the robustness and precision that ensures a proper representation of real plant projects.

Moreover, alongside with Process Modelling and Simulation, the implementation of optimization techniques has been an essential branch of PSE. Strategies to solve linear programming (LP), nonlinear programming (NLP), mixed-integer linear programming (MILP), mixed-integer nonlinear programming (MINLP), dynamic or under-uncertainty problems, can be found in the review on optimization applied to PSE carried out by Biegler and Grossmann [80]. Depending on the type of problem encountered, a specific strategy is preferred over the others, as problems can contain continuous and discrete variables, functions with or without convexities, that can be differentiable or not. Regarding design and synthesis problems involving decisions on flowsheeting arrangement, either an NLP or a MINLP procedure is required.

Finally, it must be evoked that the PSE discipline also broadens into Process Control and Process Operations. The former oversees the achievement of a high degree of consistency and stability in a process, counteracting the dynamic nature of the system or external disturbances. The latter concerns

the scheduling techniques and the optimization of supply chains. Nevertheless, both fields are beyond the scope of this thesis and will not be discussed.

### **II.3. Process Synthesis**

Recalling the first problem of CPS previously stated, and within the context of the late 60's, the idea of evaluating multiple alternatives of process arrangements was beyond the boundaries of calculation capacities due to limited optimization techniques. Until then, some specific procedures were proposed for the synthesis of heat exchanger networks (HEN), multicomponent distillation separation sequences and reactor systems [81], [82].

Two main categories of Process Synthesis techniques can be found: (i) hierarchical decomposition and evolutionary techniques, and (ii) mathematical-based optimization [70], [83], [84], the latter sometimes referred as superstructure synthesis approach [64], [85]. Reviews on Process Synthesis methodologies, perspectives and challenges can be found in the next references [68], [82]–[84], [86]. A detailed description of each one of these categories is carried out in the following subsections.

#### **II.3.1. Hierarchical decomposition and evolutionary techniques**

Chemical processes have an inherent complex nature, and its design is a challenge if treated as a unique problem. The decomposition methods and evolutionary techniques were proposed to deal with this aspect, and instead of solving the problem in its entirety, its decomposition into a set of subproblems allows to solve each section at a time. Also, hierarchical decomposition methods often include as decision-making parameters some heuristic methods based on engineers' experience [84], defined as methods of problem solving used in an empirical way, even if they have not or cannot be proven with a precise formulation [87]. Remarkable works on hierarchical decomposition and evolutionary techniques will be briefly described hereafter. The purpose of this literature review being more focused on superstructure optimization methodologies, only main features of the hierarchical and evolutionary approaches will be presented.

##### **II.3.1.1. Elementary decomposition theory and heuristic structuring**

The pioneering works of D. F. Rudd explored the global process decomposition into subproblems, until a decomposition level that can be handled using available technologies. Then, by calculating an objective function for each one of the sub problems, the global objective function will be constituted by the sum of each one of the partial objective functions. Commonly, subproblems are referred as reaction subsystems, recycle structures, separation subsystems, energy, and power networks, among others.

Nevertheless, the main disadvantage of the method is the treatment of the global problem as multiple local-independent processes, without considering the possible strong interaction and influence between subsystems [82] and without considering new potential technologies to be used in the process, leading to a struggle to estimate cost functions and use them as objective functions [67]. Following this, the heuristic structuring was proposed as a tool for learning from prior calculations, applied to a machine-learning methodology, for computers to learn how to synthesize optimal system structures [87], allowing the creation of programs able to independently select a process structure according to given heuristics and process needs [88].

### II.3.1.2. Hierarchical decisions

As identified by J. Douglas, proposing a process requires assumptions on three main aspects: fixing parts of the process flowsheet, fixing design variables and fixing connections to the environment. The first is related to the set of alternative processes found while fixing the flowsheet structure, the second concerns optimization variables and the last is related to operability and control issues. Nevertheless, fixing parts of the process at such early stage could limit the research of optimal structures, due to the exclusion of potentially optimal flowsheets. Thus, the multilevel hierarchy decision procedure was proposed, identifying five hierarchy levels for conceiving processes, as follows:

- Level 1: definition of batch or continuous process.
- Level 2: definition of input and output streams.
- Level 3: selection of recycle streams and reactor considerations.
- Level 4: vapor and liquid recovery system specification.
- Level 5: heat exchanger network.

Depending on input information, heuristics are used at each decision level to add a more detailed structure to the global process. For instance, at the definition of input streams in the second level, the presence of impurities can lead to several options, as pre-treatment of feed stream in case of reactive impurities or changing feeding stage if the impurity is also a product [89]. However, this method is limited by its sequential behaviour as the levels are studied separately, and there does not exist interaction of a level with the previous and following levels, lacking a guarantee of finding the optimal design [84].

A similar approach was proposed by Smith and Linnhoff with the renowned “onion model”, in which the process design consists of five layers, starting from the core towards the external layer. It begins with the reaction system in the core, following the separation and recycle systems, where valuable products are recovered from by-products and unreacted materials, and the last ones are recycled for further conversion. Once the reaction-separation-recycle system is defined, the heat recovery system is analysed to perform energy integration and determine the requirements of utilities, with a final balance of water and effluents from the system [90], [91].

### II.3.1.3. Means-ends analysis

As stated by J. Siirola, a process synthesis problem can be defined in terms of process states, as follows: given some raw materials as an initial state, and some desired products as the desired state, there will exist differences between properties of the initial and final states. The purpose of process synthesis is to propose corrective tasks from the initial to the final state to remove state differences, being this the principle of the general goal directed problem solving paradigm, known as Means-End Analysis [92]. The concept of state in Process Synthesis problems can be defined as the association of physicochemical properties allowing to identify a stream in a process. For instance, a material stream  $s$  with a total molar flowrate  $n$ , molar fractions  $x_i$  for each one of the  $i$  compounds, at pressure  $P$ , temperature  $T$ , enthalpy  $H$ , and so on [93], [94].

This method is applied in an opportunistic manner, starting with the initial state and successively performing state transformations until no difference exists with the final state, but with no guarantee of generating an optimal flowsheet [84]. For an identified potential transformation, associated with a specific equipment, the property difference might not be entirely eliminated, or it can even increase the

differences of other properties as a side effect. Thus, to avoid perturbations over other properties, a hierarchy on properties transformation is proposed, as follows: molecular identity, amount involved, composition of the stream, thermodynamic phase, temperature, pressure, and physical characteristics such as form and size. Starting with modifying the molecular identity, it means, performing the necessary chemical reactions to obtain the desired product, and continuing with the rest of the hierarchy until the required pressure is reached. Higher levels on the hierarchy have greater impact on the lower levels, while the contrary is less likely to occur [92]. For instance, a catalytic chemical reaction can have a great impact on the temperature of a stream, depending if it is exothermic or endothermic, but changing the temperature of a stream in a HEX will certainly not cause a change in the composition of the stream.

Certainly, the decomposition and heuristic techniques are helpful for the estimation of the performance of small-scale processes. However, the inherent characteristic of process division into smaller synthesis problems becomes a disadvantage, as the absence of interaction between the different stages or hierarchies of the methodologies, conceals possible interlocking effects, without guaranteeing of global optimality.

### II.3.2. Mathematical-based optimization methods

Optimization-based strategies emerged to overcome difficulties found in hierarchical and evolutionary methods of process synthesis, lacking interaction between the different layers of design, and being limited to alternatives close to the base case. It involves three main steps:

- Proposing a superstructure, including all the feasible alternative process structures.
- Translating the process representation into a mathematical formulation problem.
- Solving the mathematical problem through a computational optimization method.

The first signs of process synthesis involving superstructures remote to works by Umeda *et al.*, in the 70s. The principle of the method used fits properly with the definition of superstructure, as a general synthesis method is proposed for the conception of an optimal system structure, in which an enlarged system structure is represented by the interconnection of splitting units, giving place to alternative processing routes [95]. Some early applications of superstructures cover the optimization of the design of distillation columns [96], the synthesis of heat exchange networks [97] and reactor networks [98].

The following definitions, represented in Figure II-1, intend to better describe the terminology found in the superstructure-optimization approach strategy [99]. Consider the main goal of process synthesis as being the search of an optimal construction for a target process. The selection of operating units, from a set of available units, and their linking through stream interconnections is called **process structure**. Also, infinite alternatives might exist to perform the target process, thus a selection of a finite set of process structures is required, being this set known as **considered structures**. The grouping of the considered structures, with common operating units and streams, is known as **superstructure**, where each considered structure is also referred as **substructure**. A superstructure can contain non-physically feasible structures, known as **unfeasible structures**. The set of unfeasible and feasible structures not included is known as **non-considered structures**.

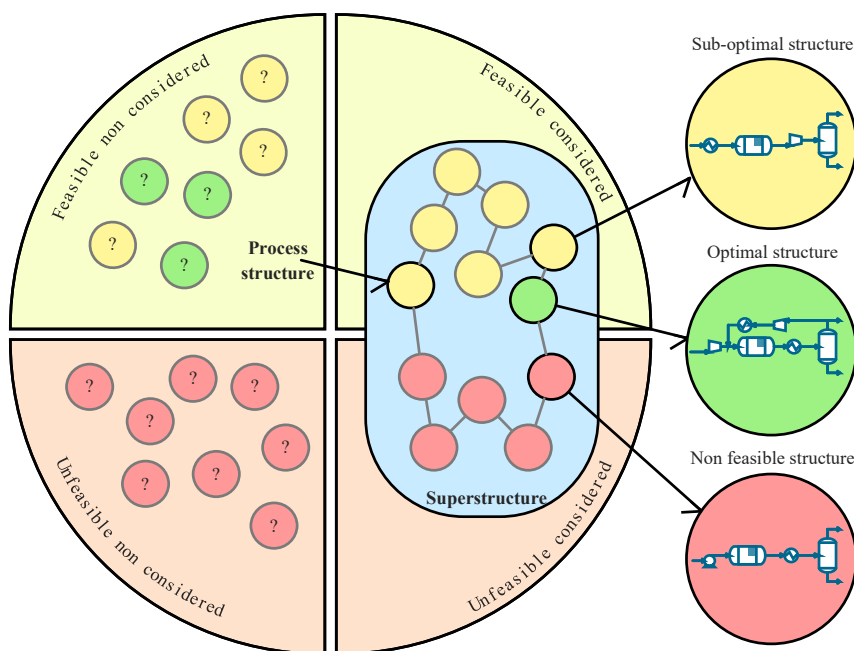


**Figure II-1.** Classification of different structures according to the terminology for superstructure conception and optimization.

One of the complex points with the superstructure approach concerns the definition of the search space of *considered structures*. The possibilities being almost illimited, all relevant processing routes must be included in the process superstructure, to avoid discarding any alternative sensible of being the optimal process architecture [82], while rejecting redundant or infeasible ones. This requires the use of a systematic method for superstructure representation that guarantees a comprehensive, but still concise space of alternatives [73], as will be presented in the next section. As will be discussed in Chapter III, the superstructure optimization approach is carried out in a software for steady-state continuous process simulation and optimization, at the macroscale level of aggregation, with equipment being the building blocks of the process. Consequently, the following section presents the main superstructure representations compatible with the application framework.

### II.3.2.1. Superstructure representations

Two approaches have been developed to tackle superstructure conception problem: the automated superstructure generation methods and the evolutionary superstructure-free methods. The former is based mainly on deterministic algorithmic procedures for superstructure construction, while the latter consists of dynamically generating different alternatives on the flowsheet during the search process [85]. To have a clear panorama of the principal methods and representations found in literature which help in the conception of process superstructures, a description is carried out hereafter. Focus is given to the automated superstructure generation, while the superstructure-free approach is briefly described at the end of the section.

#### II.3.2.1.1. State-Task Network (STN)

Introduced as a tool for process scheduling problems [100] and extended to flowsheet representations [94], it is based on a graph representation of nodes of two types: states and tasks. As stated in section II.3.1.3, state nodes represent feed, intermediate or product streams, described by a set of extensive and intensive properties. Tasks are the processing operations which transform physically and/or chemically two adjacent states, involving mass and heat transfer, as well as pressure, temperature and phase changes

[94]. An association between states and tasks allows to propose a first process architecture, free of equipment assignment. Following, tasks must be associated with available equipment capable of performing the state transformation. Two methods are identified for this purpose, as follows:

- One-task one-equipment (OTOE): each task is associated, a priori, to a single equipment if no other possibilities exist. Therefore, each equipment has a predefined task. One example of this case can be found in reference [101], where the authors propose a mass-exchange network, based on the STN approach, to study the recovery of copper in an etching process.
- Variable task-equipment (VTE): consists of associating a set of equipment to all the tasks that must be performed. A single equipment can be assigned to multiple tasks, and a single task can be assigned to multiple equipment, as seen in Figure II-2 (Right). Equipment association to tasks will be the result of an optimization.

Additionally, a useful tool for task identification and interconnection can be made using the Means-End Analysis, previously detailed. A notably characteristic of this method is the capacity of representing a very general framework for complex and arbitrary network configurations [64].

### II.3.2.1.2. State-Equipment Network (SEN)

This representation is analogous to the STN, with the main difference that task nodes are substituted by equipment nodes. These nodes can be associated to multiple tasks, but will finally perform only one, assigned through optimization calculations [102]. The main advantage in comparison to the STN representation is the reduction of nodes since a single equipment node can perform different tasks, reducing the combinatorial problem in the sense of process structure, as less equipment are to be calculated. However, as a unique equipment can perform multiple tasks, an implicit combinatorial exists, given by all the possible equipment interconnections. Furthermore, as tasks are not necessarily assigned to equipment *a priori*, intermediate states are undefined due to a dependency on the task, which can complicate the modelling stage of intermediate equipment [94]. A graphical comparison between the STN and the SEN is represented in Figure II-2, which represents the classical separation problem.

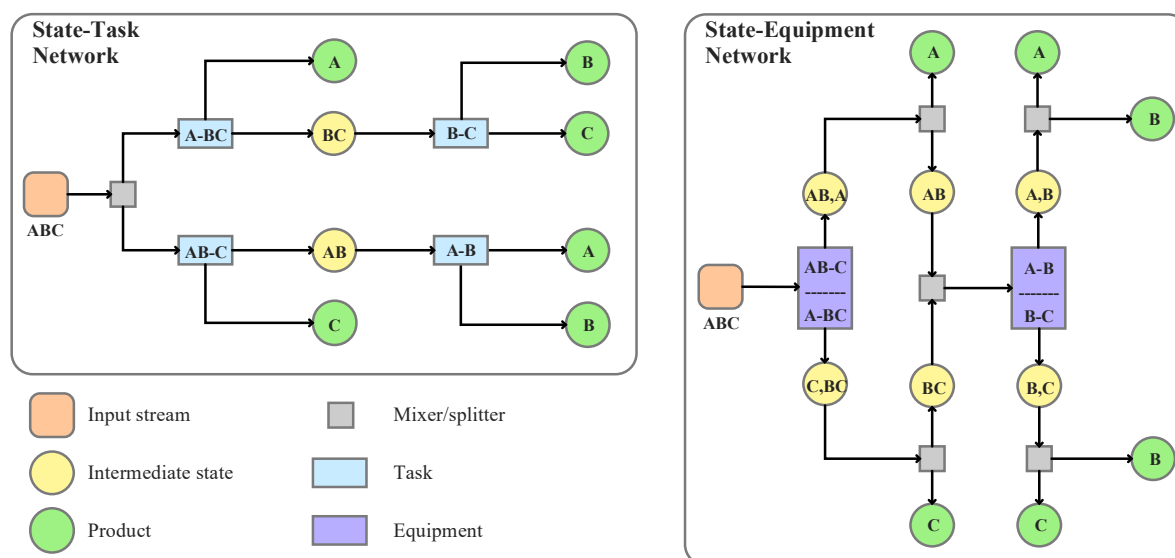


**Figure II-2.** Graphical comparison between the representations of the State-Task Network and the State-Equipment Network for the separation of a mixture of compounds ABC. Adapted from [85].

Consider a sharp separation of a mixture of 3 compounds ABC. In the case of the STN representation, two initial tasks are required, either separate A-BC or separate AB-C. If the first of the tasks is chosen, then the following task required is to separate B-C. On the contrary, the next task for the other alternative is to separate A-B. For the SEN representation, as the tasks are not directly imposed but they are the results of the optimization, the first equipment can perform two tasks: either separate AB-C or separate A-BC. Next, the second equipment performs the remaining task according to the selection on the previous equipment, meaning that it separates A-B or B-C, respectively.

The total number of task nodes in the STN representation is equal to 4, while for the SEN representation only 2 equipment nodes are required. In both cases, the same number of processing paths is obtained. For the addition of a 4<sup>th</sup> compound, the number of nodes necessary to describe all process configurations increases to 10 task nodes, while the number of equipment nodes equals 3 [73], thus being easier to describe the set of alternatives in the SEN representation than in the STN one.

### II.3.2.1.3. P-graph

The Process graph, or P-graph, is a bipartite representation composed of material nodes (M-type) and operating unit nodes (O-type), analogous to the STN representation. A simple P-graph, representing a process structure of a sharp separation of the mixture ABC into its three components, is shown in Figure II-3. Material nodes are represented by circles and operating unit nodes are horizontal bars. The operating unit nodes accept one or multiple material inputs and produce one or multiple material outputs.

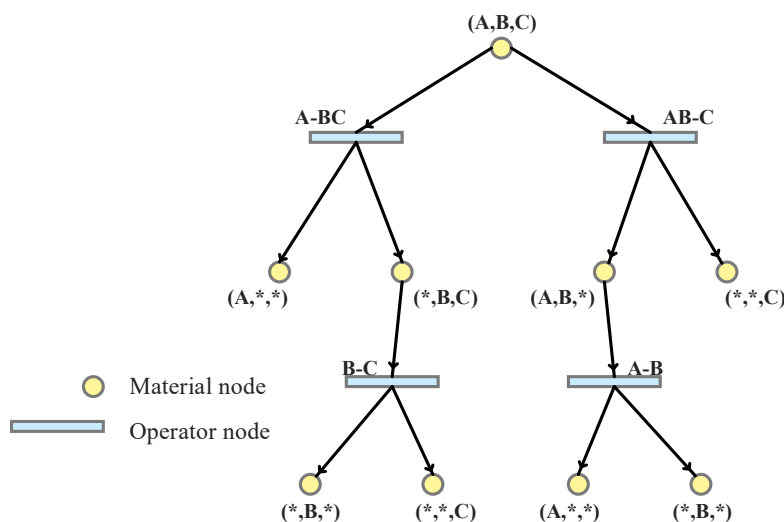


**Figure II-3.** P-graph representation for a sharp separation of a 3-compound mixture, describing every possible path. Adapted from [85], [103].

It is based on five axioms, which define the necessary and sufficient combinatorial properties for conceiving a superstructure [103], as stated:

- Axiom 1: every final product is represented in the graph by an M-type node.
- Axiom 2: an M-type node represents a raw material if, and only if, it does not have an input.
- Axiom 3: every O-type node defines an operating unit defined in the synthesis problem.
- Axiom 4: every O-type node has, at least, one path leading to an M-type node of a final product.
- Axiom 5: every M-type node should represent an input/output of at least one O-type node.

In the order as they are presented, these axioms guarantee that: (i) every product is connected to an operation unit, (ii) every raw material is included at the beginning of the process architecture, (iii) all the foreseen operating units are included for evaluation, and (iv) there does not exist either a unit operation or (v) a material irrelevant to the process.

One of the main advantages of P-graph method, is the provision of a systematic algorithm for generating the graph, and the possibility of using strategies for reducing the size of partial problems, such as the Branch and Bound method, which can restrict the search area of combinatorial feasible structures [104].

Some applications of this approach include the separation-network synthesis [105] and the optimization of energy systems [106]–[108].

#### II.3.2.1.4. R-graph

The R-graph representation is a modification of the STN-OTOE representation. The nodes are referred as input and output ports of the possible units. Streams are connected between the output port of a prior unit to the inlet port of the following unit. Feeds to the process are identified as sources, containing only an output port, while products of the process are referred as sinks, with only one input port. A simple representation of the R-graph is shown in Figure II-4.

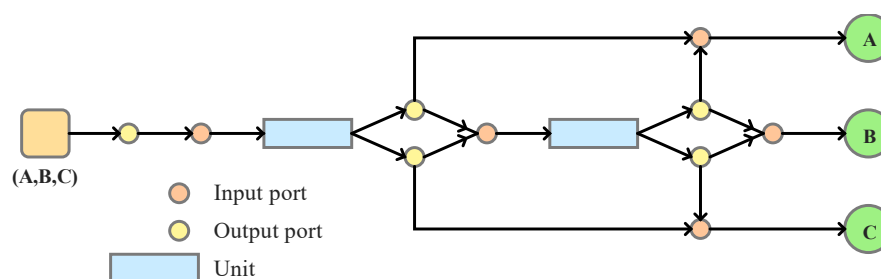


Figure II-4. R-graph representation for a sharp separation of a 3-compound mixture. Adapted from [85].

One of the main motivations for the authors to propose the R-graph representation, is to avoid the existence of multiplicity and redundancy in superstructures, and therefore, to reduce global calculation time. Structural multiplicity denotes the possibility of representing the same structure using different, but equivalent graphs. For instance, having a specific superstructure (supergraph) composed of multiple structures (subgraphs), might include two isomorphic structures with copies of the same units, meaning they are identical.

On the other hand, redundancy compares the number of subgraphs of a supergraph, and the number of substructures of the studied superstructure. There does not exist redundancy if for each substructure in study only a subgraph is assigned. A deeper explanation on graph structures can be found in next references, as well as examples on the synthesis of a distillation column [99], [109].

#### II.3.2.1.5. Generalized Modular Framework (GMF) and the State-Space Network (SSN)

Multiple methodologies differing from the equipment-level of aggregation are found. The Generalized Modular Framework (GMF) is based on fundamental mass and heat transfer modules as building blocks, combined with basic mixing, splitting and bypassing rules for superstructure synthesis.

This methodology intends to avoid the implicit assignment of processing tasks to equipment with the pre-postulation of a set of unit operations, and instead explores the possible processing routes from more elementary building blocks, completely independent of equipment. The result of the process synthesis

is a mass and heat exchange network superstructure [70]. A general representation of the approach is shown in Figure II-5.

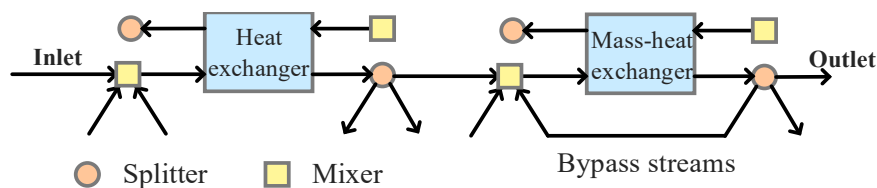


Figure II-5. Generalized Modular Framework representation. Adapter from [70].

Similarly, based on the State-Space concept in system theory, the State-Space Network representation considers the behaviour of a system as being quantitatively described by a set of variables, such as temperature, pressure, concentration, and so on, and a set of relations between these variables. While input and output variables are defined with the problem definition (i.e., inlet streams and desired outlet streams), the relations input-state-output are given by the process structure. The methodology involves the sequential application of two classes of functions: (a) mixing and splitting of streams, or (b) unit operations.

The method concept of decomposition of systems into operators such as mass and heat exchange, and their treatment as matrix operators, has gained attention in the Process Integration field, as it allows coupling different phenomena simultaneously. However, it remains a general representation method with difficulties due to the absence of tools for its implementation and its abstractness [85]. Some applications are related to process integration cases, such as hybrid membrane systems for wastewater treatment [110], energy integration systems [111] and process intensification of hydrogen production [112].

#### II.3.2.1.6. Phenomena Building Blocks (PBB)

Arizmendi-Sánchez and Sharratt [113] proposed a potential approach that could allow inclusion of Process Intensification to process synthesis stages, consisting of using a lower aggregation level in relation to unit operation paradigm: **phenomena aggregation level**. Studying process synthesis using this approach allows to identify the main limiting steps in mass and energy transformations, as well as the integration of different phenomena between the tasks, one of the purposes of Process Intensification.

In addition, this method becomes completely independent of equipment specification a priori, allowing process design to be developed without preconceived unit operations. Likewise, this method is more flexible as the PBB's are not constrained by equipment boundaries, and they can be aggregated or disaggregated according to performance criteria of identified tasks and new designed units [113]. For instance, Lutze *et al.* [114], proposed some phenomena classes used to build chemical processing, based on mass, component, energy, and momentum balances. Those are: mixing (M), two-phase mixing (2phM), phase contact (PC), phase transition (PT), phase separation (PS), reaction (R), energy transfer (H or C) and stream division (D).

As the approach goes beyond the boundaries of this work, further details of the methodologies, examples and applications for Process Intensification can be found in several references [115]–[119].

### II.3.2.1.7. Superstructure-free approach

This approach involves the construction of the superstructure using a dynamic search of process candidates, through algorithm procedures, avoiding the challenge of the proposal of an initial process architecture. Mainly based in mutation rules for replacement, insertion and deletion of structures [120], the free representations are described with initialization procedures and variation operators, which form the design search space [121]. As in the superstructure-based approach, limitations to the superstructure can be induced by the user, as mutation rules can be the result of a manual definition. However, strategies such as technology-specific mutation rules have been proposed [122], using an energy-conversion hierarchy for technology classification, regardless of the application. Some applications can be found on energy supply systems [122], [123], reaction-separation problems [124], and thermal power plants [125].

### II.3.2.2. Mathematical methods for superstructure optimization

The superstructure proposal according to one of the representations previously defined, requires its modelling and translation into a mathematical optimization problem, of the MINLP type, as follows:

$$\begin{aligned} \text{Min } Z &= f(x, y) && \text{Eq. II-1} \\ \text{s. t. } & h(x, y) = 0 \\ & g(x, y) \leq 0 \\ & x \in X \\ & y \in \{0,1\} \end{aligned}$$

Where  $Z$  is the vector of objective functions to minimize  $f(x, y)$ , while  $h(x, y)$  and  $g(x, y)$  are the equality and inequality constraints, respectively. The vector  $x$  corresponds to continuous variables, such as operating conditions or design values, and the vector  $y$  represents discrete structural variables [73].

High-level and shortcut models can often be handled with linear programming (LP), nonlinear programming (NLP) or mixed-integer linear programming (MILP). In the case of MILP problems, the variables to optimize are of two natures: continuous and discrete, reason why these type of problems are defined as Mixer-Integer. In case that no discrete variables are involved, the LP and NLP problems are defined, depending on whether they include linear or non-linear functions. For the foreseen applications and tools used in this thesis for the optimization of superstructures, MINLP techniques will be explored [126]–[128], even if other techniques can be used, such as the Generalized Disjunctive Programming (GDP), studied for optimization of STN and SEN representations in reference [94].

### II.3.2.3. MINLP optimization techniques

MINLP problems, such as the encountered in superstructure optimization, can be handled according to two main approaches: **deterministic** and **stochastic** techniques. Several works on the former can be found and are briefly described hereafter. Nevertheless, more detail is given to the latter, as the optimization algorithm used within this work fits in this classification.

Deterministic methods for superstructure optimization have been widely used in multiple applications of MINLP problems. They can handle convex and nonconvex functions. As a recall, in optimization, a convex function has no more than one minimum point, while a nonconvex can present multiple minimum points, some of them local minimums with only one global minimum.

For convex MINLP methods, several methods can be found. (i) Nonlinear Branch and Bound, where a first continuous NLP relaxation problem is solved while performing a tree search in the space of integer

variables. (ii) Outer-Approximation (OA) and (iii) Generalized Benders Decomposition (GBD), iterative methods solving a sequence of alternate NLP subproblems with the integer variables fixed while solving a master MILP problem which predicts lower bounds and new integer variables. Both methods have the same principle, but differ on the definition of the master problem, as the OA method uses accumulated linearization, while the GBD includes Lagrangian functions parametric in the integer variables. (iv) Extended Cutting Plane (ECP) which relies on successive linearization of the problem. Detailed reviews on this subject can be found in [128]–[131].

On the other hand, stochastic techniques, and more precisely metaheuristic methods are useful for mathematical optimization problems treating multi-objective formulations, with nonlinear behaviours, such as those encountered in combinatorial scenarios [132]. The main characteristics of these methods are the diversification, related to the generation of diverse solutions for a wider and global search of solutions, and the exploration, which concerns the search of local regions when considerably good improvements are made. The trade-off between these two characteristics eases the search of the global optimum [133].

A general classification of metaheuristics methods includes two categories: single-solution and population-based techniques.

In the former one can find the Simulated Annealing (SA), focused on accepting a worse solution candidate to avoid local minima, and the Tabu Search (TS), which uses a search history with the same purpose as SA. An application of SA on the synthesis of heat exchangers can be found in [134].

Concerning the second category, population-based metaheuristics are popular methods to deal with multi-objective problems, as they are able of handling multiple solutions simultaneously. The main feature is the ability of using a population of solutions to explore the search space of alternatives simultaneously. One can find the Genetic Algorithm (GA) approach, based on natural evolution, in which the population of best individuals are recombined and mutated, and the Ant Colony Optimization (ACO), inspired in the natural behaviour of ant colonies for communication through pheromones when searching for the shortest path between the colony and a food source. Applications on the synthesis of heat exchangers using GA can be found in [135], while the use of ACO for reactor system is available in [136]. Other methods include Particle Swarm Optimization (PSO), Differential Evolution (DE), and Scatter Search (SS). Comprehensive information on metaheuristics applied to PSE can be found in this book [133].

## II.4. Conclusions

The previous literature review was proposed to describe the main characteristics of PSE field, with a special focus on methodologies of Process Synthesis for the proposal of optimal process configurations, involving optimization techniques.

Heuristic and decomposition techniques, although useful, are certainly limited when confronted to problems of wide-space search of global optimal processes, due to the treatment of the global problem as a set of independent subproblems. The effect of operating conditions, design parameters and equipment specifications on performance criteria is mainly studied individually, without guarantee of global optimality.

On the other hand, mathematical-based optimization techniques using superstructures allow the study of a wider space of alternatives in terms of process architecture. Nevertheless, the difficulty around the identification of potential candidates for building the process superstructure is the main drawback. For a macroscale level of aggregation, with equipment being the building blocks of the process and modelled as predetermined operating units, some of the superstructure representations previously evoked cannot be considered at all. Namely, those whose level of aggregation go down to phenomenological interactions, such as the PBBs.

Conversely, representations such as the STN and the SEN have a potential advantage as they treat the superstructure conception in an analogous manner than carried out in software for process simulation, as will be treated in this work. As in most of the approaches reviewed, splitters and mixers with the functionality of rerouting processing streams are used, giving flexibility to the optimization algorithm to test the different alternatives in the superstructure.

Furthermore, the use of discrete variables requires the implementation of MINLP optimization techniques, capable of handling continuous and integer variables, as well as nonconvexities and nonlinearities, typical characteristics of functions found on superstructure optimization of chemical processes. Either deterministic or metaheuristic optimization algorithms can carry out the solution calculation.

In this thesis, the SEN representation is preferred as basis of superstructure conception, as it can be easily translated into an equipment-dependent process flowsheet. Regarding the optimization technique, a metaheuristic population-based method is used for the MINLP problem resolution, based on the Ant Colony Optimization approach.

The discussion on the representation used for the methodology of superstructure optimization, as well as details from the simulation software and the optimization algorithm for this purpose, are available in the next chapter.

# Chapter III

---

*Materials and methodology for the superstructure  
conception*

---



---

## III. Chapter III: Materials and methodology for the superstructure conception

The following chapter will cover subjects related to:

- The materials used for the superstructure conception and optimization, ProSimPlus and MIDACO-Solver, detailing their main characteristics.
- The principles to consider in the superstructure optimization methodology, which allow the process flowsheet to be functional and to evaluate multiple process alternatives.
- The available algorithm parameters, which can be adapted to favour the search of optimal solutions according to user-defined criteria or algorithmic internal criteria.
- The methodology used to conceive, simulate, and optimize the process superstructure, covering details on the structural alternatives, their association to discrete variables, and the communication procedure between the simulation software and the optimization algorithm.
- The strategies that can be applied within the superstructure optimization methodology to facilitate the search of optimal solutions by the reduction of the global calculation time.

### III.1. Introduction

Previous chapters explored the two main axes of this work, namely the energy storage in chemical compounds and the process synthesis methods. Having as central objective the proposal of a process for ammonia production, serving as chemical storage medium, this chapter is focussed on presenting the methodology for superstructure conception, which is further employed with this application.

As detailed in Chapter II, the superstructure boundaries limit the set of considered structures to a finite region of the domain of alternatives of feasible and non-feasible structures. The main difficulty of this approach is the exclusion of potential solutions, susceptible of being optimal, and the inclusion of non-optimal or even non-feasible process structures.

In this methodology, the superstructure definition is a manual procedure from the engineer, which reduces the universe of structure solutions to a set of process structures, according to known specifications and available processing units. For the framework in which this methodology is applied and knowing the computational resources and the calculation time required to solve a superstructure optimization problem, the superstructure must be proposed with the idea that: *“a superstructure should be as complete as necessary but as concise as possible”*.

The chapter is divided into the following sections. Section III.2 describes the materials used in this work, namely the process simulation software and the optimization algorithm. The principles for the superstructure design are then described in section III.3, which covers the basic elements that allow a superstructure to be functional. Next, section III.4 examines the superstructure proposition and optimization methodology, from the problem definition to the obtention of optimal solutions, highlighting the communication procedure between the software and the algorithm. Section III.5 illustrates the strategies used within this work to improve the superstructure optimization by reducing the calculation time through the use of some simple yet useful tricks. The chapter is closed up with conclusions in section III.6.

## III.2. Software and optimization algorithm

The work within this thesis has been developed with two computational tools, in order to model, propose, calculate, and optimize the ammonia process superstructure.

On one hand, the process engineering software ProSimPlus, a steady-state simulation and optimization software, is useful for performing rigorous mass and energy balance of operating units commonly found in chemical industry. It is a graphical user interface serving as environment for the proposal of the process superstructure, allowing to execute simulation and optimization calculations. On the other hand, an external optimization algorithm, MIDACO Solver, is integrated into ProSimPlus without any additional interface, easing the definition of the mathematical optimization problem by adjusting algorithmic parameters and defining the objective functions and constraints.

The union between these tools gives the user the capacity to propose and optimize processes based on superstructure principles, where continuous and discrete variables are encountered, requiring MINLP problem handling, guaranteed by MIDACO Solver. Further details on these tools are described in the following sections.

### III.2.1. ProSimPlus

Among the main features of ProSimPlus, it is possible to find a large set of unit operations with different levels of modelling detail, a robust thermodynamic package for the description of properties of pure compounds and mixtures, strong mathematical methods for the convergence of mass and energy balances, correlations for economic calculations, as well as user-defined scripts and modules. This last feature is essential in the superstructure optimization approach, as it allows to include structural variables to the flowsheet by the means of coding scripts in Visual Basic Script (VBS) language.

#### III.2.1.1. Modelling approach

The software is based on the **sequential modular approach**, which is one of the two main types of process simulation software, the other being the **equation-oriented approach**. The former is based on calculating unit operations one at a time, in a material flow-dependent sequence, using the results of the previous unit as input data before supplying the output results to the following unit. The latter avoids the directionality of calculations by treating the entire flowsheet as a set of equations to be solved simultaneously. The combination of the two approaches results in the simultaneous-modular approach, in which initial estimates and rigorous models are calculated by the modular approach before solving the whole flowsheet with the equation-oriented method [137].

Both methods have advantages and disadvantages. While the sequential approach is easier for inexperienced users to configure and use, the downstream directionality creates recycling loops towards the upstream sections, requiring iterative calculations for flowsheet convergence. The equation-oriented approach avoids the directionality and convergence of calculations because the entirety of the flowsheet is calculated simultaneously. However, the calculation performance is heavily dependent on the initial guesses of key variables, implying that the user requires expertise to estimate the initial points correctly.

#### III.2.1.2. Relevant operating units

A non-exhaustive list of operating units found in ProSimPlus is presented in Table III-1 with the main characteristics, possible specifications, and details to consider within this work.

**Table III-1.** Modules in ProSimPlus of interest for this work with their main characteristics and possible specifications.

<b>Module</b>	<b>Description</b>	<b>Main available specifications</b>
Simple heat exchanger	Heat exchanger with a unique stream of the process, where a utility can be specified for the calculation of the heat exchange area.	Heat duty supplied or rejected.
Cooler/heater		Outlet temperature predefined or depending on the dew or bubble points of the inlet stream.
Generalized heat exchanger	Heat exchanger with two streams of the process, where the heat exchange area can be calculated from a specified heat transfer coefficient. The T vs. Q curves can be estimated directly from the module.	Flow direction: co-current or counter current. Temperature value: outlet temperature of one of the streams, temperature difference between inlet and outlet sides of one stream, temperature difference between streams in one extreme of the module, subcooling below the dew point or superheating above the bubble point. Other specifications: vapor fraction on one of the streams, minimum temperature approach between streams, heat duty exchanged, heat exchange area, product UA (heat exchange coefficient and exchange area).
GIBBS reactor	Reactor used to represent the chemical equilibrium.	Type of reactor calculation: minimization of the Gibbs energy or equilibrium constant method at specified approach temperatures.
Simple chemical reactor	Reactor used to directly specify a conversion rate or the selectivity of compounds.	Type of reactor calculation: conversion rates of compounds or selectivities of compound for multiple reactions. Type of thermal behaviour: adiabatic, isothermal, known outlet temperature, known heat duty.
Plug flow reactor	Reactor modelled as an ideal plug flow. It can include different types of kinetic rate equations: equilibrium, controlled, complex and user defined. A variation on the mixture properties is observed on the axial direction.	Type of configuration: tubular or multi-tubular. Type of thermal behaviour: adiabatic, fixed temperature profile, fixed wall temperature, specified heat duty, radiative heating of the tubes, utility in co- or counter-current direction. Geometry of the reactor: length, number of tubes, diameter of single tube and shell, roughness, particles diameter, bed porosity. Catalyst presence
Centrifugal pump	Turbomachinery to increase the pressure of a stream, depending on its phase: pumps for liquids and compressors for vapor/gases. For the compressors, a multi-stage compression can be defined, including intercoolers between them.	Outlet pressure specification given by: outlet pressure, compression ratio, pressure at bubble or dew point at specified temperature, pressure increase, power supplied. Efficiencies: isentropic, mechanical, and electrical. Volumetric or isentropic for the pumps.
Generalized pump		Type of compressor: isentropic or polytropic.
Compressor		Two specifications to select among: pressure specification, power, outlet temperature, isentropic/polytropic efficiency.
Generalized compressor		Pressure specification is given by: outlet pressure, compression ratio, pressure at bubble or dew point at specified temperature, power supplied, calculated from manufacturer curves.
Expander	Turbomachinery to decrease the pressure of a vapor/gas stream, producing electricity.	Outlet pressure specification given by: outlet pressure, expansion ratio, pressure at bubble or dew point at specified temperature, pressure decrease, power supplied. Efficiencies: isentropic, mechanical, and electrical.
Expansion valve	Module to decrease the pressure in a liquid stream.	Outlet pressure specification given by: supplied value, pressure at bubble or dew point at specified temperature. Flow sizing coefficient
Generalized two-phase flash	Drum used to split a two-phase flowing stream into vapor and liquid streams.	Flash type defined as: constant temperature and pressure, constant temperature and vapor fraction, constant pressure and vapor fraction, constant pressure and enthalpy, or constant pressure and entropy

### Chapter III: Materials and methodology for the superstructure conception

**Table III-1.** Modules in ProSimPlus of interest for this work with their main characteristics and possible specifications.

Module	Description	Main available specifications
Membrane filter	Separation method modelled as a tube-type filter, where permeate and retentate sides have a piston flow behaviour. The driving force is given by the difference in partial pressures of the compounds between the retentate and the permeate.	Flow direction: co-current or counter current. Retentate side: tubes or shell. Geometry of the membrane: length, number of tubes, diameter of single tube and shell, tubes thickness, tubes roughness. Type of membrane: porous or dense Permeabilities as a function of the membrane temperature, given by a correlation of type: polynomial, power, exponential, logarithmic, Arrhenius.
Mixer	Adiabatic mixing of streams.	No specification required.
Splitter Three-way valve	Splitting of the inlet stream into the total number of outlet streams. The three-way valve has only two outlet streams.	The outlet streams are defined by: splitting ratios, molar flowrates, mass flowrates, volume flowrates.
Constraints and recycles	Module for recycle loop convergence and constraint handling.	Numerical method: default (selection entire by the software), successive substitution, Newton-Raphson, Broyden. Tear streams and their iterative variables: temperatures, enthalpies, pressures. Constraints association between a measured deviation and an action variable.
Measurement	Module to measure deviation of a process parameter regarding a set point, which is connected to a constraints and recycle module.	Type of measure: temperature, pressure, molar/mass/volume total/partial flowrate, molar/mass fractions, partial molar/mass flowrate ratio, molar/mass fraction ratio, NOx content, NO oxidation degree, relative/absolute humidity, molar/mass concentration, pH.
Optimization	Core of the superstructure optimization, allows to communicate ProSimPlus with the optimization algorithm. Receives the new values of the decision variables and transfers the values of the objective functions and constraints.	Algorithm for optimization: Successive Quadratic Programming (SQP) or external (e.g., MIDACO Solver). Number of inequality constraints. Maximum number of iterations. Action variable bounds and steps (if discrete variables are included). Parameters of the external algorithm.
Economic evaluation	Module for estimation of capital and operational expenditures in a project. Is based on the Functional Modules Method (FMM) and the Pré-Estime Method (PEM), as described in section III.2.1.3.	Selection of the units to include in the economic evaluation. Type of expenditure to include in the economic calculation: investment, maintenance, raw materials, utilities consumed or produced, valuable products. Economic parameters: actualization rate, tax rate, working capital, annual plant operating time, time horizon for the project.

As a remark, the PSA module is not included in the software, as it is used in transitory regime processes. Nevertheless, a pseudo-continuous approach, presented later in section IV.3.4.3, is used within this work to describe by a simplified model the performance of such an operating unit.

One of the most important modules used in the superstructure optimization is the Windows Script (WS) unit. It is a void module, where the user has the option to create its own subroutines, functions, and parameters. The module accepts material and information streams. These information streams allow to configure the optimization problem, by communication of parameters between the modules. It is useful to centralize the optimization on a few WS units, in order to communicate every decision variable with the process units via scripting codes, and to calculate the objective functions and constraints. Details on the use of WS modules is presented in section III.4.4.

To model the process, there exist two types of streams: material and information streams. The material streams are described by material quantities and thermodynamic properties, which rely the different operating units on the flowsheet. The information streams help to communicate parameters from one unit to another, to set up specifications under a predefined constraint or simply to modify the calculation sequence on the flowsheet. They are also useful to configure the optimization problem and communicate ProSimPlus with MIDACO solver.

The process is simulated using the Predictive Peng Robinson (PPR78) thermodynamic model, available in ProSimPlus thermodynamic database, which allows to predict the binary interaction parameters between compounds [138]–[140].

### III.2.1.3. Economic evaluation

One important feature of ProSimPlus is the use of an economic evaluation module, allowing to estimate the capital and operational expenditures of the current project. The economic correlations in this module are based on two different methods, retrieved from the Manual of Process Economic Evaluation [141], which are the **Functional Modules Method** (FMM) and the **Pré-Estime Method** (PEM).

The FMM is based on including not only the essential equipment, but also the peripheral or auxiliary equipment. For instance, in a distillation column costing, the method includes the column, auxiliary heat exchangers, reflux tanks, pumps, etc. This method allows to estimate the cost of the group of equipment using conventional operating parameters easy to determine, such as pressures, temperatures, or flowrates. Pricing correlations were determined from the data analysis of multiple industrial applications, and its accuracy regarding sophisticated costing procedures is around  $\pm 15\%$  [141].

The PEM is based on the available design and sizing parameters of operating units, and correction factors which consider the operating conditions and characteristics of the device. It belongs to the category of multiplying procedures, where a base price is calculated and adjusted with a series of corrective, sizing, and assembly factors. For example, a compressor base price depends on the mechanical work required and is corrected with factors related to the output pressure, the type of driver and the material of the device.

For the majority of operating modules, the PEM is preferred as it allows an easy estimation of the expenditures. Only on the case of adiabatic reactors the FMM is considered. Corrective price factors, based on the Chemical Engineering Plant Cost Index (CEPCI) and inflation are required for both modules, as the PEM gives costing values on 2000-€, while the FMM is based on 1985-FF.

Corresponding correlations used in this work and their details on calculations, correction, sizing, and assembly factors are detailed in the Appendix A, in section X.1.

### **III.2.2. MIDACO Solver**

The numerical solver MIDACO, which stands for Mixed Integer Distributed Ant Colony Optimization, is a robust and highly performant optimization algorithm that can handle mono- and multi-objective optimization problems. It is designed as a general-purpose software, based on a free-derivative evolutionary-hybrid algorithm, treating the objective functions and constraints as a black-box. It is capable of handling critical function properties, such as non-linearities, non-smoothness, non-differentiability, non-convexities, and discontinuities.

#### **III.2.2.1. Ant Colony Optimization**

MIDACO solver is based on the Ant Colony Optimization (ACO), an stochastic metaheuristic algorithm inspired by the foraging behaviour of ants [142]. The mechanism is described as the aleatory movement observed in nature when ants begin to search a source of food. Every path taken to find food and to return to the colony is marked with volatile pheromones dissipating over time. The shortest paths will then have a higher pheromone concentration because they will be preferred over time, whereas the longer paths will be less transited. After a sufficient amount of time has passed, the shortest path will remain as the only used path, serving as the optimal route between the colony and the food source.

While the biological behaviour is related to a graph path selection that can be described by discrete variables, it serves as basis for the ACO on a continuous domain of variables. For MINLP problems, it uses a multi-kernel Gaussian probability density function (PDF), where weighted one-dimensional Gaussian functions are implemented to consider multiple promising search spaces on the optimality of the objective functions.

#### **III.2.2.2. The Oracle penalty method**

The extended evolutionary ACO algorithm is combined with the Oracle penalty method for constraint handling, especially developed for metaheuristic search algorithms [143]. The method transforms the optimization problem by adding a penalty parameter to the objective function.

The method is self-adaptive and has a predictive nature, which is why the parameter is known as Oracle, and directly corresponds to the global optimal objective function value, being used as a forecasting method. The objective function is transformed into an equality constraint where the oracle parameter is included, and finding the optimal solution of the transformed problem indicates that a feasible solution of the latter is an optimal solution of the original problem. Further details on the MIDACO algorithm principles and the Oracle penalty method can be found in [142], [143].

#### **III.2.2.3. The Utopia-Nadir Balance and the Progress parameter**

In contrast to the mono-objective optimizations, where a unique solution can be found as the global optimal solution, the multi-objective optimization problem presents a set of optimal solutions, commonly referred as the Pareto front. This front is the set of non-dominated solutions that creates a trade-off curve. As multiple objective functions are intended to be optimized, they commonly have a counteracting effect, and minimizing one of them will induce an increase in the other(s). It then depends on the user to decide which objective function has greater importance over the others to select, among the Pareto Front points, the one which considers to be the best among the optimal solutions.

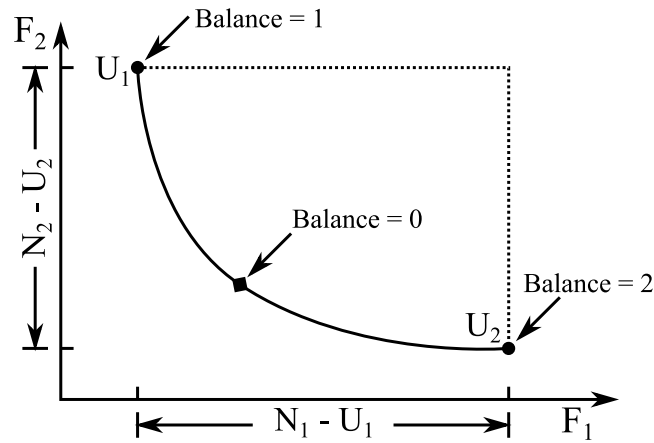


**Figure III-1.** The Utopia-Nadir Balance concept for a two-dimensional objective function optimization problem. The curve represents the Pareto front, with the Utopia parameters being described by points  $U_1$  and  $U_2$ , for the corresponding objectives  $F_1$  and  $F_2$ . In this case, the Utopia point for one function is the Nadir point for the other function. The Balance parameter equal to 0 gives the same importance to the two objectives, while a Balance equal to 1 or 2 looks for the Utopia points for objectives  $F_1$  and  $F_2$ , respectively. Adapted from [144].

As the multi-objective optimization must deal with the minimization of competing functions, the Utopia-Nadir Balance is introduced in the algorithm to favour the search direction towards a specific zone of the Pareto Front, when desired. The multi-objective problem is decomposed into multiple single-objective problems, based on Utopia and Nadir information. The Utopia parameter of an individual objective function ( $U_i$ ) represents the global optimal solution (i.e., the minimum value for the objective function), while the Nadir parameter ( $N_i$ ) is the worst objective value among all the solutions, as depicted in Figure III-1 [144].

The Balance parameter is an adjustable parameter which can aim the search of the optimal solutions to a specific zone of the Pareto front. For the example in Figure III-1 the Balance parameter equal to 0 gives equal importance to both objective functions and focuses the search of optimal points in an equidistant point of the Pareto front to the two Utopia values,  $U_1$  and  $U_2$ . Adjusting the Balance parameter to 1 means that the objective function  $F_1$  has greater importance, and the search of optimal solutions are directed towards the Utopia point  $U_1$ .

Additionally, the optimization algorithm uses the Progress parameter to indicate the improvement that has been made on the Pareto front solutions. This parameter is based on the Utopia-Nadir Balance concept. For multi-objective optimization problems, an improvement is made when the Progress parameter is lower than the previous value. The lower the value, the better the improvement on the Pareto front, which can either indicate lower values in some objective function, or a relocation of the optimal point in the Pareto Front. As a remark, MIDACO proposes a unique solution of the Pareto front as the best solution, based on the Balance parameter.

#### III.2.2.4. Algorithm parameters

Multiple parameters are available to set up the optimization problem and customize its performance and behaviour. Depending on the values chosen for each parameter, the search of the optimal solutions might differ from one calculation to another. These parameters have been classified into four different categories and are briefly described in Table III-2.

**Table III-2.** Parameters of the optimization algorithm [145].

Refers to	Parameter	Definition
Constraints	ACCURACY	Defines the tolerance for the violation of constraints. Inequality constraints are considered to be respected if they are equal or lower to the accuracy value.
Search behaviour	SEED	Parameter defining the initial seed of the internal pseudo-random number generator in the algorithm. Reproducibility of results is found at identical seeds.
	FOCUS	Allows to restrict the space search towards the most recent optimal point. It is useful for refining the optimal point.
	ANTS	Number of iterates generated in a major iteration of the algorithm. Must be defined with the Kernel parameter.
	KERNEL	Number of kernels within the algorithm gaussian probability density function. Larger kernels increase the chance of finding global optimal solutions.
	PARETOMAX	Number of optimal points (i.e., Pareto solutions) to be stored in the set of optimal solutions.
	EPSILON	Defines the precision for multi-objective solution filter, to consider one solution as a different optimal point. Small values allow closer Pareto points.
	BALANCE	Parameter to assign weights to each objective function, according to their importance, favouring the minimization of the functions with higher weights.
	CHARACTER	Internal parameter indicating the type of problem to solve. It can be for continuous, combinatorial, or all-different problem types.
Algorithmic stopping criteria	ORACLE	Parameter to indicate the search region in a constrained problem, where the optimal solutions might be placed. Requires background knowledge.
	FSTOP	Stops the optimization when the first objective function has reached an equal or lower value than the specified value.
	ALGOSTOP	Stops the optimization when the specified value equals the number of internal restarts of the algorithm without improvement of the optimal solutions.
Hard limit stopping criteria	EVALSTOP	Stops the optimization when the specified value equals the number of evaluations without improvement of the optimal solutions.
	MAXEVAL	Maximum number of iterations for the algorithm to search the best set of optimal solutions.
Results printing	MAXTIME	Maximum time in seconds for the algorithm to search the best set of optimal solutions.
	PRINTEVAL	Indicates how often the best solution should be updated in the text files of reported solutions, MIDACO_SOLUTION.TXT, MIDACO_SCREEN.TXT.
	SAVE2FILE	Indicates how many iterations should be stored in the text file of history iterations, MIDACO_HISTORY.TXT.

As seen, there exist two different types of stopping criteria to consider that the most recent set of optimal solutions is the best set of solutions found. On one hand, the hard limit stopping criteria gives the user the freedom to end the optimization after a certain number of evaluations or after an elapsed amount of time. These parameters are useful when the user needs to test the superstructure optimization, as they can be set to a few iterations or minutes.

Alternatively, the algorithmic stopping criteria are inherent to the algorithm behaviour, and they allow to stop the optimization by reaching a specified objective function value, or by a lack of improvement of the Pareto front after a certain number of evaluations. This last description, corresponding to the EVALSTOP parameter, is useful to avoid predefining a hard limit stopping criterion, as it is up to the algorithm to evaluate the optimization problem until no further improvement is obtained in the set of optimal solutions.

### III.2.3. Computational capacities

Calculations were performed in two Dell® computers. Unit 1 is a Precision 7820 Tower, with an installed RAM of 32 Gb, dual processor Intel Xeon Bronze 3106 @ 1.7 GHz and 16 cores. Unit 2 possess an installed RAM of 256 Gb, dual processor Intel Xeon Silver 4214 @ 2.2 GHz and 24 cores.

Unit 1, with lower calculation capacities, is used for the preliminary work prior to executing the optimization. It consists of several steps, such as defining the superstructure architecture, verifying the correct definition of coding scripts that handle every specification, parameter, and variable, and verifying the adequate calculation sequence, as further explained in section III.4.4. It is also useful for troubleshooting and debugging.

Unit 2 is primarily used for long optimization calculations, as it performs better in terms of time per iteration. Regarding Unit 1, it spends less time to complete the same number of evaluations.

## III.3. Principles for superstructure design

For a process superstructure to be functional it must include structural switches, working with positive integer data, capable to direct the material streams towards a specific section of the process, bypassing the rest of operating units of the other processing alternatives. These switches, hereafter defined as *opening* and *closing switches* are directly related to structural variables, and are modelled as common splitting and mixing units, which are adapted to operate according to the value of the variable. Thus, instead of using continuous data, they are dependent on integer values.

### III.3.1. Superstructure switches

The opening and closing switches englobe the section of the process where the variable has a direct influence on the choice of operating units. As an example, consider the switches in Figure III-2. The structural variable concerns the choice between the number of compressors in the compression stage, to increase the pressure of the material stream from the inlet pressure  $P_{in}$  to the outlet pressure  $P_{out}$ . Three processing routes exist, for 1, 2 and 3 compressors, and the same number of ports exist for the opening and closing switches. The selection of a position for the variable induces bypassing the other processing routes.

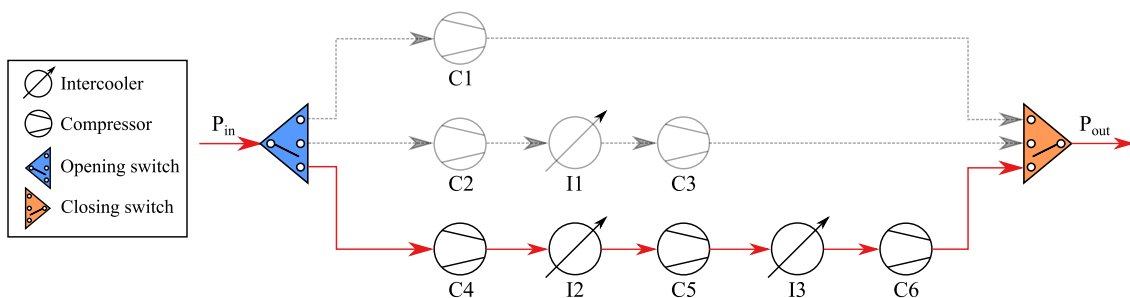


**Figure III-2.** Opening and closing switches for the selection between the number of compressors, varying from 1 to 3, including intercoolers for multistage compression. The selected process structure corresponds to the material streams and operating units in — red solid lines, while the bypassed sections are represented with — grey dotted streams and grey solid operating units.

Here, the variable denoted as  $NC$  is described as  $NC \in \{1, 2, 3\}$ , with each outlet and inlet ports of the opening and closing switches being associated to a unique position of the variable  $NC$ . The opening switch is the managing switch that conditions the outlet ports, while the closing switch does not need

any condition to be specified at all, as it is only the receiver of the selected process alternative. The conditions used in the opening switches are hereafter described.

### III.3.2. Bypassing streams and operating units

In ProSimPlus, every operating unit, except mixers, must receive a non-null flow process stream [146]. Otherwise, calculation errors are obtained due to zero flowrates. Furthermore, every operating unit of the process calculations is executed, even if it belongs to a bypassed section of the process. This occurs due to the nature of the modular sequence approach, which has a predefined calculation sequence that is implemented in the exact same order, independently of the process alternative chosen.

In this context, two approaches are used to guarantee that the bypassed zones are correctly calculated without having an influence on the results of the current structure evaluation. These are the use of residual material streams and the inactive operating units.

#### III.3.2.1. Residual material streams

The residual material streams are small fractions of the incoming flowrate of the opening switch that are sent to the bypass sections of the process. As in the example of Figure III-2, the selected processing route uses 3 compressors to increase the pressure from  $P_{in}$  to  $P_{out}$ . The outlet ports of the opening switch are defined with conditional syntax, as shown in the coding script of Figure III-3, specific to ProSimPlus.

1	If	Project.UserValues("Compressors") = 1 Then	' 1 compressor
2		.DistributionRatios(1) = 1 - 2E-15	
3		.DistributionRatios(2) = 1E-15	
4		.DistributionRatios(3) = 1E-15	
5	Elseif	Project.UserValues("Compressors") = 2 Then	' 2 compressors
6		.DistributionRatios(1) = 1E-15	
7		.DistributionRatios(2) = 1 - 2E-15	
8		.DistributionRatios(3) = 1E-15	
9	Else		' 3 compressors
10		.DistributionRatios(1) = 1E-15	
11		.DistributionRatios(2) = 1E-15	
12		.DistributionRatios(3) = 1 - 2E-15	
13	End If		

**Figure III-3.** Conditional coding script as a function of the variable "Compressors", which defines the distribution ratios of the outlet streams of the opening switch. The distribution ratio  $i$  is defined as the ratio between the flowrate of the outlet stream  $i$  and the flowrate of the inlet stream. Bypassed process sections — are given a residual distribution ratio equal to  $1 \cdot 10^{-15}$ , while the selected structural process for evaluation — is given the remaining.

As seen in Figure III-3, a conditional evaluation of the value of the user-defined variable *Compressors* allows to transmit the residual flowrates towards the bypassed sections, while the remaining of the material stream goes to the processing units of interest. The specification is based on the distribution ratios parameter, which is the ratio between the outlet stream  $i$  and the inlet stream of the switch. According to the value of the variable, the corresponding outlet stream is used, and the others are bypassed with residual flowrates of  $1 \cdot 10^{-15}$ , a value sufficiently small to avoid any impact on the calculation of the process alternative selected.

### III.3.2.2. Inactive operating units

Once the bypassed sections were assigned the residual flowrates, the operating units of these sections need to be inactive, to avoid any disturbance on the process structure evaluated. Analogously to the opening switch definition, the specification of the operating unit is set as a function of the process structure variables. Consider for instance the compressor C1 from Figure III-2. The coding script to define the compressor specification is presented in Figure III-4.

1	<code>.PressureSpecType = 1</code>
2	<code>If Project.UserValues("Compressors") = 1 Then ' 1 compressor</code>
3	<code>    .PressureSpecValue = Project.UserValues("Pout")</code>
4	<code>Elseif Project.UserValues("Compressors") = 2 Then ' 2 compressors</code>
5	<code>    .PressureSpecValue = .InputStream(1).Pressure</code>
6	<code>Else ' 3 compressors</code>
7	<code>    .PressureSpecValue = .InputStream(1).Pressure</code>
8	<code>End If</code>

**Figure III-4.** Conditional coding script of compressor C1 in Figure III-2, as a function of the variable “Compressors”. The type of the specification to supply is given by `.PressureSpecType = 1`, indicating an absolute pressure to be specified. The value, assigned by `.PressureSpecValue` can either be the desired outlet pressure  $P_{out}$ , given by the user-defined parameter “Pout” when selecting the 1-compressor structure, or the pressure of the inlet stream, `.InputStream(1).Pressure`, for the module to remain inactive when 2 or 3 compressors are used.

As seen in Figure III-4, the pressure specification type corresponds to the absolute pressure of the outlet stream, given in line 1. The value of the specification depends on the variable *Compressors*, defining the structure to evaluate in the compression section. In case that the desired evaluation is the 1-compressor structure, the pressure specification assigned is the desired outlet pressure  $P_{out}$ , given by the user-defined variable  $P_{out}$ , as shown in line 3. Otherwise, the module should remain inactive, and the outlet pressure is specified as being equal to the inlet pressure, avoiding any pressure change in the module. For the case on Figure III-2, the compressor remains inactive, as specified in line 7.

For the operating units foreseen to be included in the superstructure configuration in this work, Table III-3 includes the specifications used to inactivate the modules, and the expected results.

**Table III-3.** Specifications to inactivate the foreseen modules to be used in this work.

Module	Specification
Compressor/pump	$P_{out} = P_{in}$ . The outlet stream is identical to the inlet stream, as no pressure increase is specified.
Expander/valve	$P_{out} = P_{in}$ . The outlet stream is identical to the inlet stream, as no pressure decrease is specified.
Heat exchanger <sup>a</sup>	$T_{out} = T_{in}$ . The outlet stream is identical to the inlet stream, as no temperature change is executed.
Reactor	Stoichiometric coefficient of compounds = 0. The outlet stream is identical to the inlet stream, as no reactants are consumed.
Separation drum	Not necessary. As the previous HEX does not achieve the phase change conditions, no liquid stream is obtained from the drum.
Membranes	Permeability of compounds = 0. Outlet streams are identical to the inlet streams, as there does not exist mass transfer through the membrane.
PSA user-defined module	No separation. As it is a user-defined module, no separation is performed by definition in the scripting code.

<sup>a</sup> The heat exchanger is supposed as a one-fluid heat exchanger. Details are covered in section III.5.4

Pressure and temperature changing units specify the outlet pressure or temperature parameter as being the same as the inlet value of the parameter, which avoids any mechanical work or heat duty variation,

respectively. In modules such as the reactor and the membrane, which perform a discretized calculation along the length of the unit, stoichiometric coefficients and permeabilities are set equal to zero, to avoid any reaction to take place and any mass transfer to occur, correspondingly. The use of null or zero lengths is discouraged for the membranes, as errors might appear during the calculations. Concerning the separation drum, it is considered to be a constant temperature and pressure vessel, and no separation occurs, as the prior heat exchanger to this module is inactive and does not condition the stream to the required condensation temperatures. Finally, the Pressure Swing Adsorption (PSA) unit is a user-defined model, and no special specification is needed.

### **III.4. Methodology for superstructure design**

As in any problem in chemical engineering related to process synthesis, the engineer requires to transform some given raw materials into value added products, by identifying the most suitable process structure and operating conditions, which allow to optimize some criteria, such as economic, environmental, or energetic functions.

Beyond this general idea of process synthesis, the superstructure optimization approach is useful for its implementation in specific cases where the choice between competing technologies is required. It can be used in different types of process synthesis problems, depending on the scope and limits. The methodology is suitable for designing new processes, retrofitting an existing one, or being only focussed on a section of the process to optimize, for instance, the heat exchanger network in an industrial facility.

The procedure in Figure III-5 briefly describes the steps for the process superstructure optimization, from the problem definition, to the obtention of the optimal architecture, operating conditions, and any other optimized parameter.

The problem definition includes stating the boundaries of the problem, with the available raw materials and the expected products and/or by-products, in terms of productivity, efficiency, costing or environmental impact, among others.

Following the common procedures on process synthesis, the identification of required material and energy transformation steps is performed, using any useful source of information. Data from literature, process plant specification sheets, client information and specifications, or even knowledge on the process are valuable sources to consider. Recalling the definition from Chapter II, a transformation step is defined as the physical and/or chemical variations between two states, these ones being defined as material streams described by extensive and intensive properties. These transformations include, among others, changes in composition by chemical reactions or by separation stages, in pressure, in temperature or in flowrate quantities.

The identification of the transformation steps requires their association with the available modelling units in ProSimPlus. Multiple modules can be used to perform the same transformation step and even a single module can perform different transformations. For instance, a heat exchanger can be used for the temperature adjustment of a process stream, but depending on the value of the optimization variable, in this case the outlet temperature, it can heat or cool the stream.

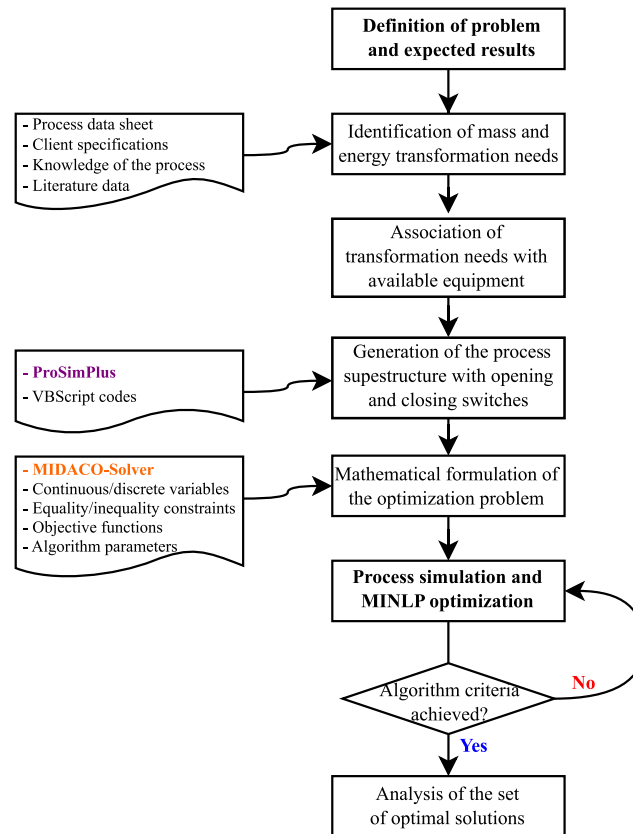
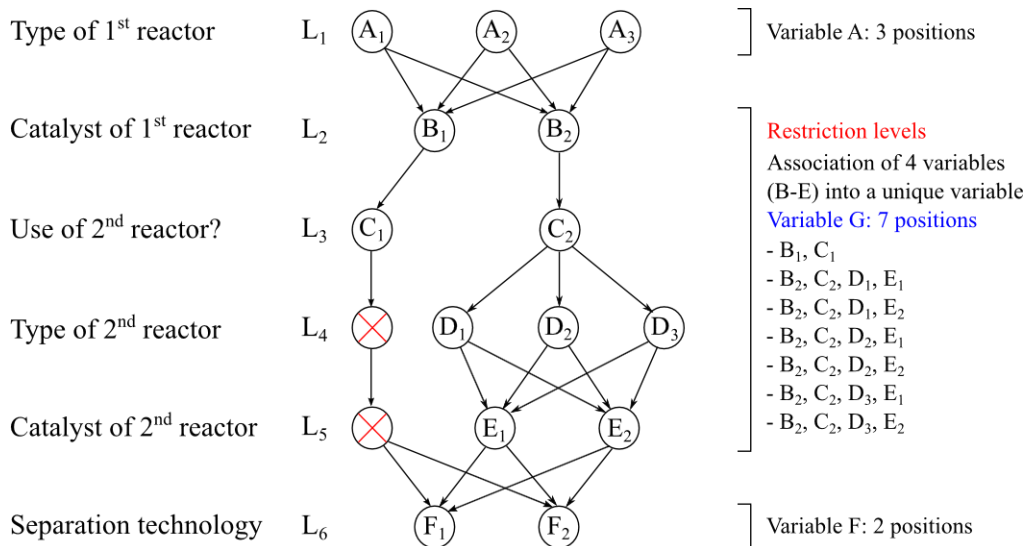


Figure III-5. Procedure for superstructure conception and optimization.

After identifying the useful operating units and the possible structural alternatives, it is necessary to identify the total number of structures within the superstructure, able to represent a different and unique processing path.

#### III.4.1. Structural alternatives identification – Discrete variables

When multiple modelling units can compete to perform the same transformation step, structural alternatives appear. It is important to identify the existing alternatives when the complete superstructure is defined, as this is related to the definition of discrete variables. The structural alternatives can be studied using graph representations, as the P-graph approach which includes combinatorial techniques, as it facilitates the graphical identification of structural variable combinations. Consider the following case of structural alternatives identification, shown in Figure III-6.



**Figure III-6.** Graph representation of the structural alternatives for a reaction stage. The graph directionality follows the process superstructure calculation sequence. Each level (L) of the graph corresponds to one discrete variable, described at the left. A total of 6 levels, two with 3 positions and four with 2 positions, give a total number of 144 alternatives ( $3^2 * 2^4$ ). However, from level 2 to level 5, there is a restriction on the combinatorial, and levels 4 and 5 do not apply to the left processing path, which reduces the total number of alternatives to 42.

Assume that each structural variable, A to F, is identified by a level on the graph representation. For the example given, the structural alternatives correspond to a reaction stage with up to 2 reactors in series. For each catalytic section, three different reactor configurations and two catalytic materials are available. The final level of the structure is associated with the separation technology.

The first two levels, L<sub>1</sub> and L<sub>2</sub>, are common to all the structural alternatives. On level L<sub>3</sub>, a decision to include a second reactor is made. In case that no additional reactor is included (i.e., left branch of Figure III-6), levels L<sub>4</sub> and L<sub>5</sub> do not apply to the configuration. Otherwise L<sub>4</sub> and L<sub>5</sub> are considered for the rest of configurations. Again, level L<sub>6</sub> is common to all the possible process structures.

The combinatorial analysis of possible alternatives, defined as the product of possible positions for each level, is given by Eq. III-1.

$$Structures = \prod_{i=1}^{n_L} P_i \quad \text{Eq. III-1}$$

Where  $n_L$  is the number of levels and  $P_i$  is the number of positions for level  $i$ . For the case in Figure III-6, the number of structures ( $3^2 * 2^4$ ), gives a total number of 144 structures. However, as seen in the graph, from level 2 to level 5, there are restrictions on the combinations, which exclude some of the 144 calculated structures. The analysis of levels on the restricted zone allows to integrate the four variables (B-E) into a single variable, denoted G and shown in the figure on the right side, which can describe the different structures with 7 positions. In this way, the final number of structures is equal to 42, ( $3 * 7 * 2$ ), eliminating 102 alternatives that are not represented by the graph.

It is important to identify the total number of structural alternatives and their uniqueness, as redundancies of processing paths might appear. In effect, two different combinations of discrete variables might describe the same process structure, which is undesired as two different sets of variables (i.e., equal

continuous and different discrete) would obtain the same values on the objective functions. Further details on this issue are covered in section III.5.2.

For sure, this analysis concerns only the structural alternatives described by discrete variables, but some of them might be infeasible due to technical constraints, associated to the continuous variables. For instance, if a specific catalyst is to be used in level  $L_4$ , but the operating temperature is beyond the range of validity, then the structural alternative becomes infeasible by violation of technical constraints. These limitations require to be analysed across the different operating units of the process, in order to define mathematical constraints in the optimization problem.

### III.4.2. Analysis of continuous decision variables

Apart from the **discrete decision variables**, specific to the structure, the choice and analysis of the **continuous decision variables** is important, as fixing the range of values for each variable defines the search space of optimal solutions. In fact, it is necessary to study the boundaries of each continuous variable, regardless of whether these are operating conditions or equipment parameters, to guarantee the feasibility of the solutions.

Consider the case of an exothermic chemical reaction which takes place in presence of a catalyst. An appropriate temperature range can ensure that the chemical reaction occurs. Placing the operating conditions in the low temperature zone inhibits the reaction due to low kinetic rates but placing them in the high temperature zone can also impede the reaction due to proximity to the thermodynamic equilibrium, or due to catalytic material limitations (deactivation, sintering, etc.).

The analysis of decision variables must be based on data retrieved from the information analysis, as depicted in the methodology proposed in Figure III-5. Following the previous example, for a given catalyst and kinetic rate equation, literature data suggest a range of values in which the reaction takes place. Nevertheless, this is not enough as other subjacent parameters should be considered. For instance, the equipment materials exposed to a domain of temperatures beyond their limits require a change on the material which can induce higher costs of investment.

In any case, values of operating conditions and equipment design parameters are commonly found in various information sources. Performing case studies on simplified process structures can give insights on the feasible regions of variables to include in the optimization. In case that a range of values is pertinent to a specific structure but not to another, constraints should be defined to guarantee respecting every technical/operational restriction on the process.

Beyond this, the analysis of optimization results can also suggest specific zones of the range of values of the variables where the optimal points are located, which allows to reduce the search space of solutions for further refinement of the optimization problem. This aspect further developed in section III.5.3.

### III.4.3. Formulation of the optimization problem

The MINLP optimization problem is defined as the minimization of a unique or a set of objective functions, subject to equality and/or inequality constraints, with continuous and discrete decision variables. The formulation is given as follows:

$$\begin{aligned}
 &\text{Minimize} && F(x, y) && (x \in \mathbb{R}^{n_{con}}, y \in \mathbb{N}^{n_{int}}, n_{con}, n_{int} \in \mathbb{N}) && \text{Eq. III-2} \\
 &\text{Subject to:} && g_i(x, y) = 0, && i = 1, \dots, m_{eq} \in \mathbb{N} \\
 &&& g_i(x, y) \geq 0, && i = m_{eq} + 1, \dots, m \in \mathbb{N} \\
 &&& x_l \leq x \leq x_u && (x_l, x_u \in \mathbb{R}^{n_{con}}) \\
 &&& y_l \leq y \leq y_u && (y_l, y_u \in \mathbb{N}^{n_{int}})
 \end{aligned}$$

Where  $F$  represents the set of objective functions, which depends on a vector  $x$  of  $n_{con}$  continuous variables and a vector  $y$  of  $n_{int}$  discrete variables. The problem is subject to a set of constraints  $g$ , that can either be  $m_{eq}$  equality and/or  $m - m_{eq}$  inequality constraints. The decision variables are bounded between lower  $x_l, y_l$  and upper  $x_u, y_u$  limits.

The inequality constraints are defined for MIDACO as positive constraints, even if the declaration in ProSimPlus is required as negative constraints. Therefore, the appropriate manner to define them is as dictated by the simulation software, which then communicates the positive value to the algorithm, if the constraint is respected.

### III.4.4. Communication procedure and calculation sequence

In order to perform an accurate optimization calculation and obtain reproducible results, there are multiple steps to be carefully performed. These include the creation of WS modules and global user parameters, the definition of decision variables, objective functions and constraints, and the definition of the algorithm parameters.

The optimization module is the core of the flowsheet calculation, as it is executed at the beginning and at the end of every full-flowsheet evaluation, as seen in Figure III-7. This module is responsible of communicating to the optimization algorithm the results of the current flowsheet evaluation and receives the updates values of the decision variables the following evaluation.

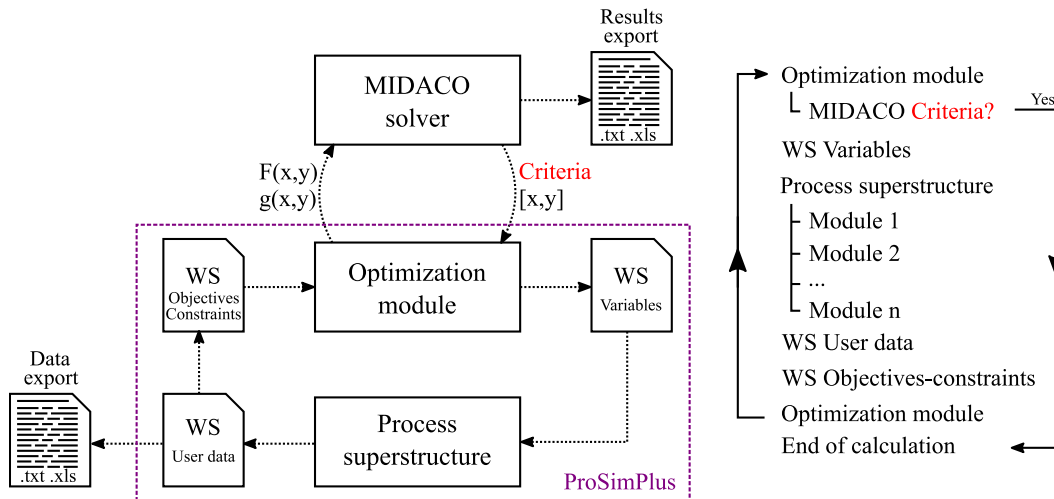


**Figure III-7.** Graphical representation of the sequence executed in ProSimPlus for the superstructure optimization, with its communication to MIDACO solver.  $F$ : objective functions.  $g$ : constraints.  $x$ : continuous variables.  $y$ : discrete variables.

In detail, the sequence is executed as follows: the optimization module updates the values of the decision variables, which are stored as global parameters in the WS module “Variables”. Every module where the decision variables are used, call the global parameters when being calculated. After the last module is calculated, the WS modules “Objectives-Constraints” and “User data” update the values of the

objective functions, constraints and any additional data required by the user, according to the results obtained. Then, these values are communicated to the optimization algorithm, which evaluates the different algorithm criteria. At each evaluation, user data and optimization intermediate results are exported to text files in case that the user requires to follow the optimal solution trends or the optimization progress.

It is important to carefully verify the correct definition of the calculation sequence, as the process architecture should be calculated after every decision variable is defined and before any optimization result has been updated. Further details on the definition, modification and validation of the calculation sequence are available in the User Guide section.

In the WS module “Variables”, the value of every decision variable communicated by the optimization module is stored. This allows to centralize all the variables in a unique module, where a global parameter is defined and associated to each one of them. Then, the modules on the process superstructure requiring the updated value of the decision variables call the global corresponding parameter through a scripting code and perform the calculation of the unit.

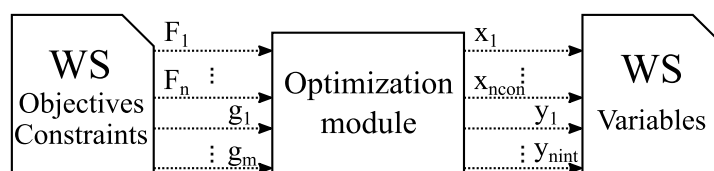


**Figure III-8.** Graphical representation of the communication of values of the objective functions and constraints from the module “WS Objectives-Constraints” to the optimization module, and the values of decision variables to the module “WS variables”.

The objective functions and the constraints are calculated at the end of the flowsheet evaluation. They involve results from the operating units, as economic calculation data from the economic evaluation module. In the WS module “Objectives-Constraints”, the user can define the scripting code for their calculation and their storage as local parameters of the module. Then, the module is connected to the optimization module via information streams, where each objective function and constraint require a unique connection, communicating each one of the parameters.

The user also has the possibility to calculate its own parameters. For instance, when optimizing the superstructure, it could be useful to recover data from the mass and energy balance of the process, punctual parameters of each module or data from the economic evaluation module. This data complements the results printed by MIDACO solver and could be useful for the analysis of the optimal solutions.

### III.5. Strategies for the reduction of the calculation time

The optimization of a process superstructure is rapidly complexified due to the number of structural alternatives that exist within the architecture. The higher the complexity, the longer the calculation time and, therefore, the longer it takes to find optimal solutions.

Considering the modular sequence approach, a unique process alternative can be complex by itself. For example, processing streams going backwards to upstream sections create recycling loops or imbrications, which require iterative calculations for their solution, increasing the total time of the optimization.

In this sense, the superstructure should be as complete as necessary, but as concise as possible. Any modification that can reduce the calculation time per iteration will have an enormous impact on the global calculation time. Thus, in principle, simplifications should be applied whenever possible, avoiding oversimplification to the point that the results are harmed.

Among the strategies for reducing the calculation time of the optimization, the following points detail the benefits of their application.

### III.5.1. Association of common processing units

It is possible to find structural alternatives that share common processing units. Recalling the example of Figure III-2, where the choice is to use between 1 and 3 compressors, the complete section can be simplified by association of common units. As seen in Figure III-9, the use of intermediate switches replacing the opening switches, allows to fusion units of competing processing paths into a unique module. The closing switch remains the same, as the number of structural alternatives remains constant. In this example, two compressors are selected for evaluation, bypassing the intercooler I2 and the compressor C3.

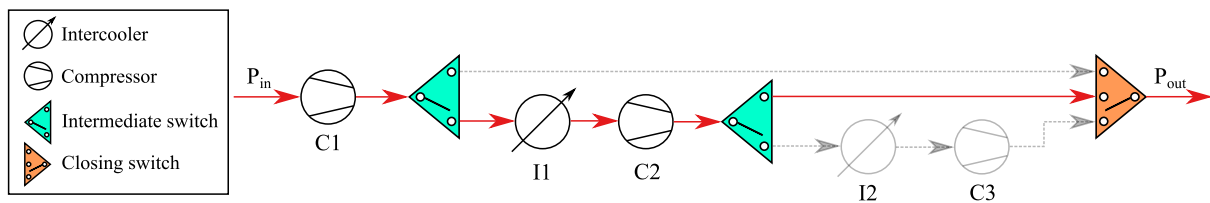


**Figure III-9.** Intermediate and closing switches for the selection between the number of compressors, varying from 1 to 3, including intercoolers for multistage compression. The selected process route corresponds to the material streams in — red solid lines, while the bypassed sections are represented with — grey dotted streams.

This association in the compression section reduces the number of units to calculate per iteration, passing from 6 compressors to 3, and reducing the number of intercoolers from 3 to 2, gaining in the overall time of calculation. Clearly, the conditional coding scripts of processing units and intermediate switches need to be adapted to respond to the structural variable position.

### III.5.2. Identification and elimination of inadequate or redundant switch positions

It is possible that multiple structural variables are found in a common section of the process, and the combination between them creates a configuration that is redundant within the superstructure evaluation, as it replicates another structural alternative. Consider the following example, which is actually a case encountered that will be covered in detail in Chapter IV.

Two structural switches are used in the reaction stage of the HB process. The first concerns the number of adiabatic catalytic sections to include, and the second, the type of cooling to use between the catalytic beds. The number of adiabatic reactors to use is defined as  $NR \in \{1, 2, 3\}$ , with the switch position being equal to the number of catalytic sections, while the type of cooling is described as  $TC \in \{1, 2\}$ , where 1 represents the indirect cooling and 2 the direct cooling. One could think that the combination of structural positions allows testing six different process structures. However, the use of a unique catalytic section does not require any intermediate cooling, as the heat exchange is only useful when a subsequent catalytic section is included. Table III-4 describes the structural alternatives found with variables NR and TC and their fusion into a unique structural variable, RC.

**Table III-4.** Transformation of two structural variables into a unique variable by analysis of redundant switch positions.

NR	TC	Configuration	Observation	RC
1	1	One catalytic section, indirect cooling - Cooling is absent	Unique structure	1
1	2	One catalytic section, direct cooling - Cooling is absent	Duplicate of {NR,TC} = {1,1}	-
2	1	Two catalytic sections, indirect cooling	Unique structure	2
2	2	Two catalytic sections, direct cooling	Unique structure	3
3	1	Three catalytic sections, indirect cooling	Unique structure	4
3	2	Three catalytic sections, direct cooling	Unique structure	5

From this analysis, five different configurations can be identified and described by a unique structural variable which regroups variables NR and TC. The variable  $RC \in \{1, \dots, 5\}$ , representing the number of reactor configurations, is described by five positions, with every position representing a unique process structure. The redundancy found with one catalytic section is eliminated.

### III.5.3. Exploration and reduction of space search

In superstructure optimization, the combinatorial of structural alternatives, plus the wide search space of the continuous variables induce large computation times to find a suitable set of optimal solutions. To accelerate finding the optimal solutions, the search space of variables can be reduced to the boundaries where the optimal solutions are possibly located, if considerable knowledge on the process allows to ascertain these bounds for each variable.

However, beyond technical constraints of the process that impose certain bounds for a variable, in the first cases of optimization there is no certainty on the appropriate bounds to be chosen, as multiple relations can be found between the optimization variables. Bounding one variable to a specific range of values might affect the selection of the values of other variables. Therefore, the boundaries should be sufficiently large to include the values leading towards the optimal points.

The exploration and reduction strategy intends to give insights on the appropriate search space of optimal solutions for the multiple optimization variables to be handled by the superstructure.

As an illustration, consider that two given objective functions,  $F_1$  and  $F_2$ , are subject to minimization with 3 discretized variables,  $V_1$ ,  $V_2$  and  $V_3$ , and assume that the optimization allowed to find 7 optimal points from the total number of solutions.

For this case, Figure III-10 shows the distribution of feasible solutions as a function of the objective functions and the optimization variables. To ease the lecture of such a plot, each subplot can be defined by its position, according to the number of rows and columns. Position  $(i, j)$  is referred to the subplot in row  $i$  and column  $j$ . The symmetrical positions on the diagonal  $(i, j) \forall i = j$ , represented by the green histograms, indicate the incidence frequency of each parameter considering all the solutions. Therefore, on the higher bars on the histogram a higher density of solutions is obtained, meaning that more feasible solutions are placed in that corresponding range of values.

On the other hand, the distribution of points in blue are referred to the results of each objective function regarding the rest of parameters, while the distribution of points in red concerns the results of the optimization variables. The framed zones in the histogram indicate the location of the optimal points for each distribution of optimization variables.

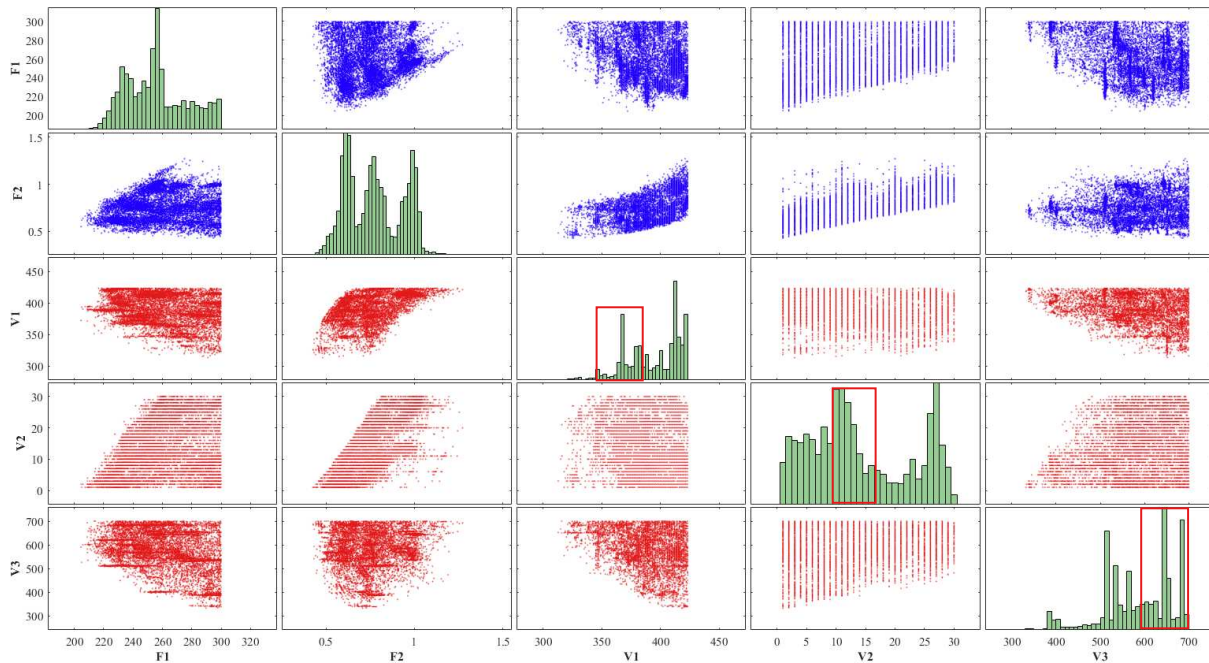


**Figure III-10.** Scatter and histogram plots for an optimization case with two objective functions,  $F_1$  and  $F_2$ , and 3 variables. Histograms show the distribution of the values for each parameter. For each discretized decision variable, the region containing the optimal points is framed in red. The total number of evaluations is 115 629 and the time elapsed is 47 924 seconds (approx. 13 hours). The algorithm stopped the optimization due to non-evolution of the optimal points after 50 000 iterations.

For the case illustrated, the optimal points are identified in the middle section of variables  $V_1$  and  $V_2$ , while they are placed on the upper region of variable  $V_3$ . Furthermore, for the variable  $V_1$ , the highest density of feasible solutions is identified in the upper limit of the variable, but the location of optimal solutions corresponds to the middle zone. Thus, special attention is required, as higher densities on the histograms do not necessarily correspond to the optimality of solutions.

This being said, the strategy of exploration of the space search of variables and the analysis of the distribution of the feasible solutions over their ranges, allows to identify the location of the optimal points on the range of values, to suggest appropriate reductions on their boundaries to ease the convergence towards the optimal solutions and a possible refinement of the Pareto front.

#### III.5.4. Dissociation of double-stream heat exchangers

To model a heat exchanger (HEX), there exists the generic method that uses a generalized heat exchanger, as seen in Figure III-11. In this module, a hot fluid transfers some heat duty to a cooling medium, commonly another stream of the process or a utility stream flowing in counter-current direction, as this configuration is more efficient for heat transfer than the co-current.

Many specifications can be used to calculate the module. Among others, the user can impose a temperature value for one of the outlet streams, a heat duty to be transferred from the hot to the cold stream, or a minimum temperature approach inside the heat exchanger. This last parameter, also known as **pinch temperature**, indicates the minimum attainable temperature in any zone of the heat exchanger, to avoid considerably large heat exchange areas. In any case, the counter-current nature of the HEX requires to perform an iterative calculation on the module, to correctly set the temperature values of the outlet streams, while respecting the temperature pinch.

To avoid this iterative approach, it is possible to dissociate the generalized HEX into two simplified units: a cooler/heater and a simple HEX, hereafter known as **decoupled heat exchanger**. There exist four possibilities to communicate the modules, depending on the specification:

- Specify a cooling temperature: use the cooler to specify the outlet temperature of the hot stream and communicate the released heat duty to the simple HEX. The example is shown in Figure III-11.
- Specify a heating temperature: use the heater to specify the outlet temperature of the cold stream and receive the required heat duty from the simple HEX.
- Specify a cooling duty: use the simple HEX to fix the cooling duty in the hot stream and communicate the rejected heat duty to the cold stream in the heater module.
- Specify a heating duty: use the simple HEX to fix the heating duty in the cold stream and communicate the required heat duty from the hot stream in the cooler module.

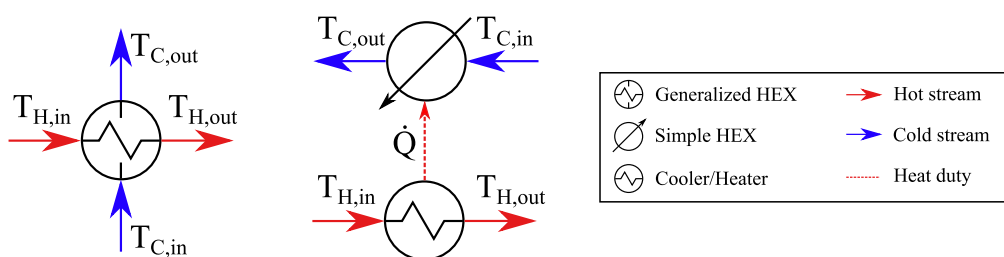


**Figure III-11.** Division of a Generalized Heat Exchanger into a Cooler/Heater and a Simplified Heat Exchanger, or decoupled HEX. The heat duty on the Cooler/Heater, which in this case is a cooler, is transferred to the Simple HEX to heat the cold stream.

The use of this decoupling approach avoids the iterative calculation in the counter-current HEX, but requires considering the possible crossing of temperature profiles, which is not directly indicated as when using the generalized HEX. The minimum temperature approach can be useful to guarantee that no profile crossing exists, but this depends on the type of streams of the heat exchanger. Three cases are found:

- No phase change occurs in any of the streams: the minimum temperature approach can be assumed to be reached in one of the two extremes of the heat exchanger.
- A phase change occurs in one of the streams: the minimum temperature approach can be presented somewhere in the body of the heat exchanger.
- A phase change occurs in both of the streams: similar to the precedent case, but special attention is required as there might exist a double temperature profile crossing.

It is important to remark that no pressure drop is considered in any HEX. Consider now the temperature profile of a counter-current heat exchanger, as seen in Figure III-12, and the equation describing the heat exchange in one of the streams, as declared in Eq. III-3.

$$\dot{Q} = \dot{m}C_p\Delta T_{LM} \quad \text{Eq. III-3}$$

$$\Delta T_{LM} = \frac{\Delta T_I - \Delta T_{II}}{\ln(\Delta T_I - \Delta T_{II})} \quad \text{Eq. III-4}$$

Where  $\dot{Q}$  is the heat duty exchanged,  $\dot{m}$  is the mass flowrate of the stream,  $C_p$  is the heat capacity at constant pressure of the stream and  $\Delta T_{LM}$  is the logarithmic mean temperature difference on the heat

exchanger, defined by the inlet and outlet temperatures of both streams. Subindexes I and II indicate each one of the extremes of the HEX.

The slope of the temperature profile is defined as the inverse of the product  $\dot{m}C_p$ . As the pressure is assumed constant in the HEX and the heat capacity is supposed independent of the temperature, no variation of the slope is expected. In real cases a small variation might occur due to temperature and pressure variations, yet the approach is conservative to consider that the pinch temperature will be reached on one extreme of the HEX, avoiding any temperature profile crossing inside the HEX.

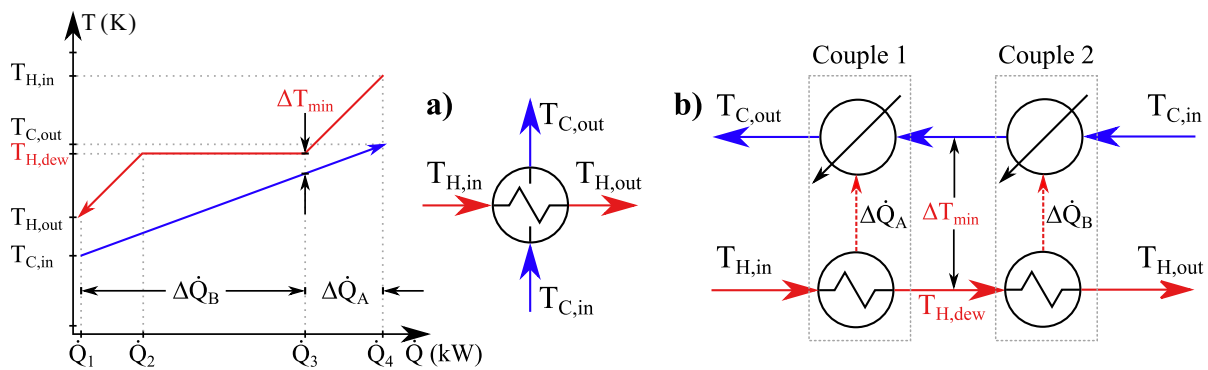


**Figure III-12.** Division of a Generalized Heat Exchanger into a double-decoupled heat exchanger.  $T$  is referred to temperature (K) and  $\dot{Q}$  to heat duty (kW). Indexes H and C describe the hot and cold streams, respectively, while indexes in and out refer to inlet and outlet streams. Refer to Figure III-11 for the description of the legend.

Furthermore, knowing the usual levels of pressure, temperature and the possible phase changes that might occur over the process is important when using the decoupled heat exchanger. This allows to impose, when required, a **double-decoupled heat exchanger**, each couple of HEX treating a phase zone of the heat transfer, having as common boundary the dew point or bubble point, depending on the direction of the phase change.

In Figure III-12, the use of a generalized heat exchanger, as shown in diagram a) allows to find a pinch temperature  $\Delta T_{min}$  inside the body of the HEX. Dividing the generalized HEX into a set of two couples of HEXs, as in the diagram b), allows to guarantee that the minimal temperature approach is found in the boundary between the two couples of HEX, as it is a specification given by the user. It means, the pinch temperature occurs between the outlet streams of the first HEX on each stream process, as seen in the diagram b).

In fact, to guarantee that the pinch temperature is found in one of the extremes of the HEX, the user specifies as desired parameter either the dew or the bubble point, depending on the phase change occurring. Then, in one couple of HEX (Couple 1), the heat duty defined as  $\Delta \dot{Q}_A$  is exchanged, while the remaining,  $\Delta \dot{Q}_B$  is transferred in the Couple 2 of HEX.

The remaining specifications to be defined are constraints of minimal temperature approach, commonly  $\Delta T_{min} \geq 10$  K, to guarantee that the decoupled HEX is correctly defined. Each couple of HEX will impose two constraints, but for a dual-decoupled HEX, the constraint in the boundary is identical, requiring three constraints for a dual-decoupled HEX.

### **III.5.5.Limitation of operating units with internal discretization**

Analogously to the counter-current HEX, other operating units are calculated by discretization of the module into a set of individual cells in series. This occurs in modules as plug-flow reactors or membranes, among others, where the molar fractions of compounds can vary through the length of the unit. Depending on the number of discretization cells, the time of calculation can increase for a larger number of cells, with the advantage of guaranteeing more precise results. On the contrary, fewer discretization cells can induce a non-smooth variation of properties alongside the module, which can result in a deviation of results.

As the calculation in these modules follows the evolution of mixture properties on the axial component of the unit, it tends to use longer calculation times than units as compressors or splitters, with punctual calculations on the specified parameter. Therefore, if possible, the reduction of the number of these units within the superstructure is required.

### **III.5.6.Limitation of nested recycling loops**

The optimization of process architectures can be more expensive in terms of computational resources when multiple recycling loops are present. This requires the resolution of every tear stream until reaching a predefined convergence within the tear stream variables (e.g., temperature, pressure, partial molar flowrates).

Even more, when these recycling loops are nested or imbricated, the calculation time of the entire flowsheet is considerably increased, as more tear streams are associated under the same recycle network, and their resolution is dependent of the appropriate calculation of the remaining tear streams in the loop. It is therefore recommended to avoid, when possible, nesting different recycling loops, in order to prevent excessive calculation time, harming the performance of the superstructure optimization.

### **III.5.7.Execution of the optimization on a simplified progress window**

ProSimPlus offers two different ways of displaying the calculation progress: a detailed and a simplified progress window. The detailed progress window, with graphical updates on the flowsheet according to the calculation sequence, shows the current unit being calculated and additional information on the convergence of constraints and recycles. This mode is useful for the first calculations of the flowsheet, as it visually indicates the modules where errors might be occurring.

The simplified window does not execute any graphical update on the flowsheet and has a reduced information display. On simple flowsheet calculations (i.e., without optimization), the difference between the detailed and the simplified window might not be perceptible. However, for optimizations with thousands of flowsheet evaluations, the graphical update induces longer calculation times, being prejudicial for the global optimization time.

The detailed calculation window should only be used for verifying the set-up of the optimization and the correct calculation of every unit. Optimizations must be executed with the simplified window mode.

### **III.6. Conclusions**

The methodology presented in this chapter for superstructure optimization of process synthesis and design has plenty of potential, as it allows to compare a set of process alternatives with a common purpose within the same mathematical optimization. It is conceived to be easy to understand and follow, based on some principles for guaranteeing its flexibility in ProSimPlus, as the use of structural switches, stream bypassing and modules inactivity. Foreseeing the large calculation times for the superstructure optimization, some strategies for time reduction are also proposed, which have been used in this work and in the case studies that are covered in the following chapters.

This chapter has presented the main points of the methodology, without giving extended details on the set-up, to have the global idea of its behaviour and the principles allowing to optimize process superstructures. The user willing to explore the details on the codes and steps for proposing a proper process superstructure, should refer to the User Guide proposed by the author as supplementary document.

# Chapter IV

---

*Problem framework and preliminary data*

---



## IV. Chapter IV: Problem framework and preliminary data

The following chapter will cover subjects related to:

- The description of the problem framework, considering the boundaries of the system as exclusively being the HB process, and giving the required renewable power in the hypothetical case of the ammonia production in a delocalized region of France.
- Highlighting the current market of ammonia from natural gas, the sharp increase in the price of production on the last couple of years and the opportunity for ammonia produced from renewable sources of energy to compete with conventional sources.
- Retrieving the preliminary data required to model the different stages of the HB process, including technical constraints and common operating conditions, as well as the detailed kinetic rates for an appropriate modelling of the chemical reaction.
- The definition of the Key Performance Indicators (KPI) that are subject to minimization or maximization in the different optimization cases that are considered: the Levelized Cost of Ammonia, the specific energy consumption, and the energy efficiency.

### IV.1. Introduction

After the description of the methodology for superstructure optimization that has been carried out in the previous chapter, this chapter describes the first elements allowing to propose the different superstructure optimization cases.

It is structured as follows: starting with the problem framework definition in section IV.2, the context and the objectives of the superstructure optimization are detailed, as well as the current trends on the ammonia market produced from natural gas.

Next, the gathering of preliminary data and the required information is described in section IV.3, and is structured for each main stage of the HB process, giving details on the required information for the correct modelling of the operating units to be included in the superstructures.

Section IV.4 gives details on the Key Performance Indicators (KPI) to be minimized within the optimization problem, namely economic and energetic criteria. Lastly, conclusions are presented in section IV.5.

## IV.2. Problem framework

Following the description of the progress towards more efficient Haber-Bosch processes, discussed in Chapter I, the boundaries defining the scope in this work are solely related to the HB synthesis loop. This includes, as raw materials, hydrogen and nitrogen produced with renewable sources of energy, which are used to synthesize ammonia, later separated, and stored. This process consumes mainly electricity for the diverse compressors found in the HB loop, and also requires utilities at high and low temperatures, as will be further detailed in the section IV.4.2.2. The reference scenario is described as follows.

Consider the diagram presented in Figure IV-1, where constant flowrates of hydrogen and nitrogen, at stoichiometric conditions, are fed to the synthesis loop. As both compounds are produced using renewable energy sources, varying through time, three scenarios are to be considered: minimal, average, and maximal levels of production. To guarantee a constant supply of  $H_2$  and  $N_2$ , a buffering storage is proposed, serving as an intermediate storage facility of gases produced during a period of energy surplus production, while supplying reactive gases during trough periods.

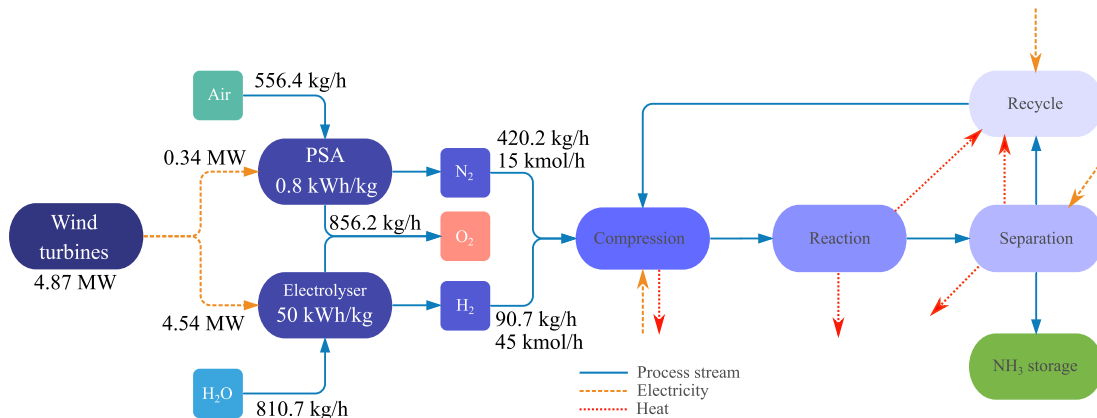


**Figure IV-1.** Schematic overview of the Power-to-Ammonia (P2A) scenario. Considering a constant molar flowrate of  $H_2$  and  $N_2$  to the ammonia synthesis loop, the required electricity output of the wind turbines is determined, as well as the mass flowrates, for an average scenario as explained in the main text. The intermediate storage is not represented.

For  $H_2$  production through water electrolysis, a specific energy consumption of  $50 \text{ kWh/kg}_{H_2}$  is required, while  $N_2$  production through a PSA unit consumes  $0.8 \text{ kWh/kg}_{N_2}$  [147]. For a molar flowrate of  $H_2$  of  $45 \text{ kmol/h}$ , a power of  $4.54 \text{ MW}$  is to be supplied. In the case of  $N_2$ , fed in a stoichiometric ratio with hydrogen, the power requirements are equal to  $0.34 \text{ MW}$ . The total power needed for raw materials production is then  $4.87 \text{ MW}$ . For this amount of material, the maximum achievable production for a complete conversion of  $H_2$ , is equal to  $4\,087 \text{ t}_{NH_3}/y$ .

### IV.2.1. Local scenario

In the context of metropolitan France and renewable electricity production, consider a location where a wind turbine capacity factor of  $54\%$  can be found. This factor indicates the ratio between the average yearly power production and the maximum power capacity, including the periods of highest and lowest or non-production of power. The map retrieved from the Global Wind Atlas, in Figure IV-2, shows that the north-western and southern regions achieve this capacity factor.

For the required power supply given above and the considered capacity factor, an installed capacity of at least  $9.02 \text{ MW}$  is necessary, only for raw materials production. Assuming the use of five generic  $3.45$

MW Class II turbines, the annual production of electricity per turbine is equal to 14 900 MWh [148], for an annual operation of 8000 h, considering the average scenario of production. This operation time considers the total operating time over the year when the wind turbine is available for operation, even if low or null production periods are observed, which is an effect included in the capacity factor.

For the example of the location highlighted with the red star in Figure IV-2, an annual mean average speed of 8.41 m/s has been recorded, with minimal and maximal average speeds of 6.7 m/s and 10.3 m/s. The total rated power production of the five wind turbines, in the lowest, the average, and the highest speed conditions (i.e., minimal, average and maximal scenarios) are 5.1, 10.5 and 16.0 MW, respectively.

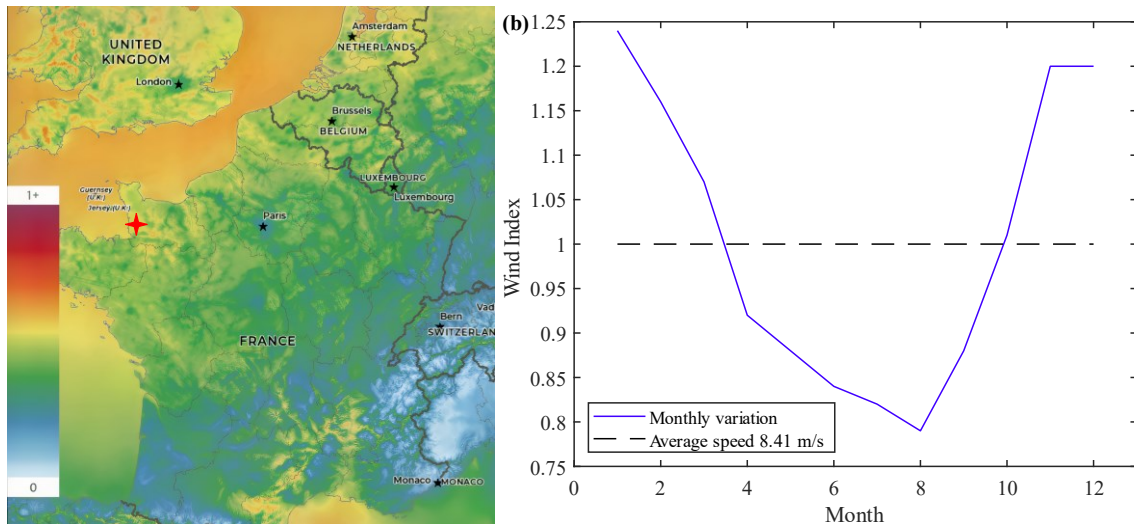


**Figure IV-2. (Left)** Capacity factor for wind turbines Class II for Metropolitan France (excluding Corse) and nearby regions, according to the norm IEC 61400 of the International Electrotechnical Commission regarding wind turbines. The capacity factor varies from 0 to 1, as indicated by the coloured scale. The red star indicates an aleatory location with a capacity factor of 54 %. Map retrieved from the Global Wind Atlas web source<sup>2</sup>. **(Right)** Monthly variation of the wind index, which is the relative change of the month average wind speed regarding the yearly average speed of 8.41 m/s (at 100 m height).

This means that for the minimal production scenario, the power output is around 44 % lower than the required power (i.e., average scenario based on 9.02 MW), and at the maximal production scenario, the power output represents 78 % more than the necessary. Moreover, for periods of maximal wind speed, even 4 wind turbines are enough to cover the low-production periods, as they are able to produce 43 % more than the average scenario.

Thus, in periods with surplus electricity production can supply the necessary power to produce the reactive gases, while storing the remaining for periods below the average power production. As seen in Figure IV-2 (Right), the period from October to March have a surplus of production, while the period from April to September has average speeds lower than the average. Other locations could be explored in regions more delocalized, where connectivity to the energy network is insufficient. However, the scenario proposed remains hypothetical and no further detailing is required.

<sup>2</sup> Map obtained from “Global Wind Atlas 3.0, a free, web-based application developed, owned, and operated by the Technical University of Denmark (DTU). The Global Wind Atlas 3.0 is released in partnership with the World Bank Group, utilizing data provided by Vortex, using funding provided by the Energy Sector Management Assistance Program (ESMAP). For additional information: <https://globalwindatlas.info>”

Assuming the stages of H<sub>2</sub> and N<sub>2</sub> recovery as established, the central work in this thesis is to propose the process superstructures for the ammonia synthesis loop. These superstructures, subject to optimization, are evaluated according to economic and energetic criteria, which intend to maximize the NH<sub>3</sub> production, boosting the quantity of energy stored in this chemical compound.

### IV.2.2. Ammonia market

Ammonia market has seen a strong increase in the last couple of years, achieving historical high prices not seen since 2008. In industrial sites of ammonia production, the natural price gas accounts for 70 – 90 % of variable production costs, suggesting that ammonia and natural gas prices move together on the same trend. However, there does not exist a direct correlation between these prices. For example, the ammonia price increased 688 \$/t from the end of 2020 to the end of October 2021, as seen in Figure IV-3, while natural gas was only responsible for 15 % of this increase on the commodity<sup>3</sup>.

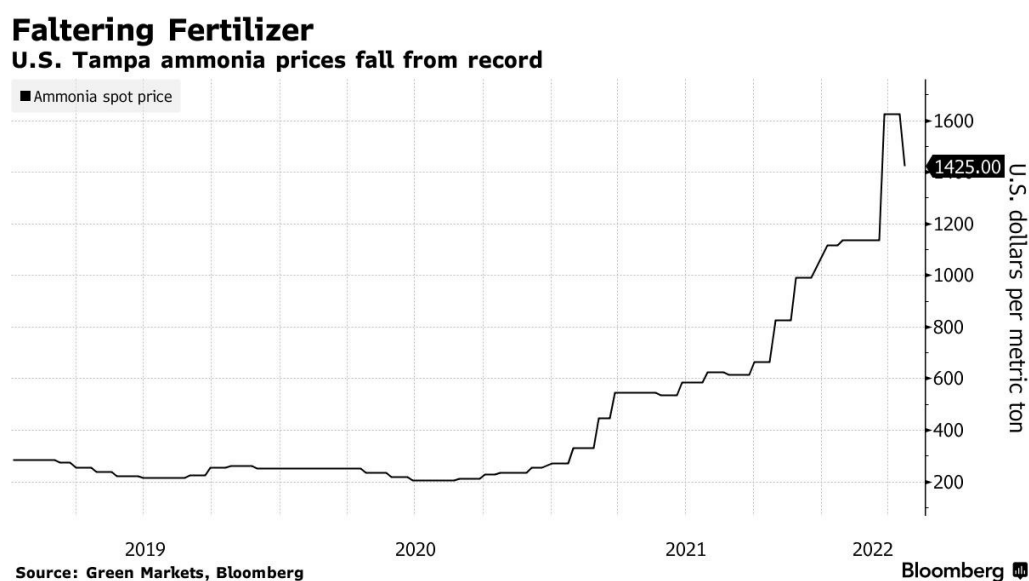


**Figure IV-3.** Evolution of ammonia price in the United States of America, according to the report carried out by Bloomberg. Chart retrieved from <sup>4</sup>.

Other reports concerning Europe suggest that the recent increases in natural gas, inflation and production cuts have impacted severely the price of ammonia, reaching 1 550 \$/t by the end of March 2022, and 1625 \$/t by the first week of April 2022 <sup>5</sup>. By the third semester of 2020, the price of this commodity was around 190 \$/t <sup>6</sup>.

<sup>3</sup> Report of the impact of natural gas on ammonia prices, according to a study carried out by Texas A&M, from January 12, 2002. Available online: <https://www.agweb.com/news/crops/corn/natural-gas-prices-only-account-15-run-anhydrous-ammonia-prices-shows-new-texas-am>

<sup>4</sup> Report by Elizabet Elkin for Bloomberg, from April 22, 2022. Available online: <https://www.bloomberg.com/news/articles/2022-04-22/ammonia-fertilizer-prices-fall-from-record-as-demand-eases>

<sup>5</sup> Report from Standard & Poor's Global (S&P Global), from April 01, 2022. Available online: <https://www.spglobal.com/commodityinsights/en/market-insights/latest-news/energy-transition/040122-higher-ammonia-prices-prompting-european-restarts-but-shortages-remain-traders>

<sup>6</sup> Market overview for ammonia prices in North America, Asia-Pacific and Europe, according to data from ChemAnalyst. Available online: <https://www.chemanalyst.com/Pricing-data/ammonia-37#market-overview>

Therefore, considering the current market of ammonia and its highest production cost on the last years, the renewable production of ammonia is a strong candidate to compete with the conventional production from natural gas. The prices of renewable energy and its related technologies have a positive scenario in the incoming years, being favoured by the policies implemented by governments regarding the energetic and ecological transition.

### IV.3. Preliminary data

The literature review regarding the HB process described in Chapter I, highlights four main stages to be considered in the superstructure. A compression stage for conditioning the reactive gases under the required pressure for reaction. The reaction stage, where gases react under a catalyst to favour the conversion towards ammonia. A separation stage, to recover ammonia from the mixture with unreacted gases. The recycle step, necessary due to low conversion per pass on the reaction stage.

In the following sections, the essential data for each one of these stages is presented and described, including technical aspects of great importance. The whole serves as basis to propose the different superstructures presented in Chapters V and VI.

#### IV.3.1. Compressors

Hydrogen and nitrogen are provided to the HB process at 10 bar and 293.15 K. The gases are compressed depending on the required pressure for the reaction stage. However, as the range of values for this pressure is considerably large, varying from 50 to 200 bar in the extreme cases, the compression stage needs to be adapted according to this operating condition. In fact, an important technical aspect of compressors is the temperature limit. The further a gas is compressed, the higher the temperature it will have at the outlet stream. Heuristic rules dictate that the outlet temperature of compressors should be limited to 463,7 K due to compressor manufacturers recommendation [149].

Also, the pressure ratio, defined as the ratio between the outlet desired pressure and the inlet pressure of the compression stage, is an indicator of the number of compression steps required to avoid this temperature limit. For pressure ratios below 4, a unique stage is recommended. For ratios between 4 and 16, at least 2 stages should be used, while for pressure ratios between 16 and 64 a third compressor must be included. Above a ratio of 64, a fourth compressor is recommended [149].

In the left diagram of Figure IV-4, the outlet temperature of compressors is shown for different outlet pressures and number of stages, for a stoichiometric mixture of  $H_2:N_2$ . The compression between stages is considered to be at constant pressure ratio, while the inlet conditions to the first compressor are 10 bar and 293.15 K. Between compression stages, intercoolers are used to cool down the mixture of gases to the inlet temperature of the first compressor.

As seen, for outlet pressures around 110 bar and above, (i.e., compression ratios of 11 and higher), the use of only two compressors is over the recommended limit of 463 K. In the case of using three or four compressors, the temperature limit is respected. As a remark, the use of a unique compressor for the lowest of the outlet pressures (50 bar), induce a temperature outlet of 530 K, far above the temperature limit. This alternative is discarded for analysis.

The temperature limit can certainly be linked to the material resistance of the compressor. However, as described in section I.6.1 in Chapter I, compressors built from austenitic stainless steels are resistant to

hydrogen and ammonia attack, and are widely used in high temperature applications [150], far beyond the highest temperatures achieved in this process, near 800 K.

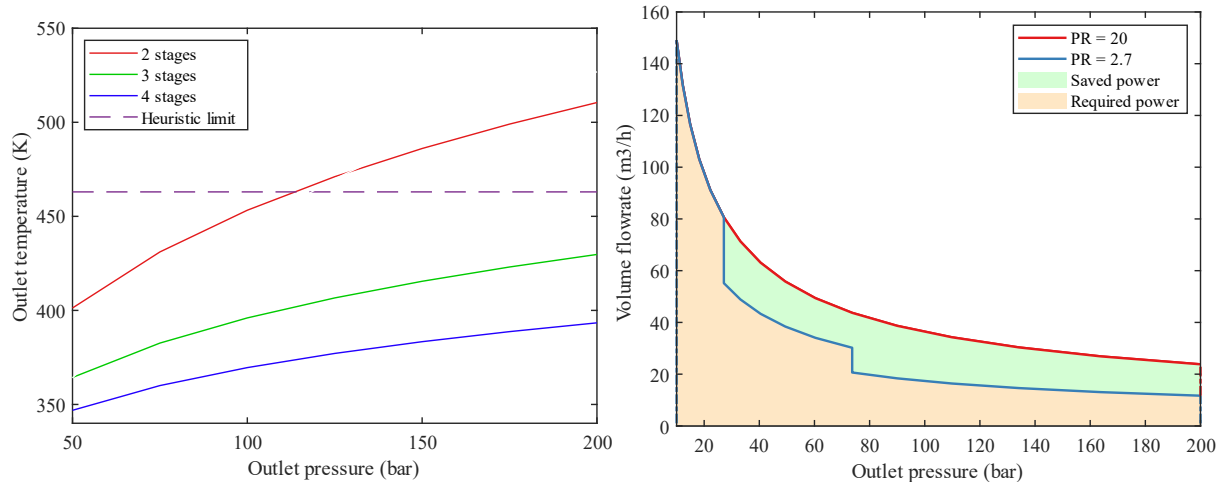


**Figure IV-4. Left:** Outlet temperature of compressors for different number of stages and pressures, for a stoichiometric mixture of  $H_2$  and  $N_2$ . The compressors are considered in series with a constant pressure ratio between stages. Intercoolers between compressors cool down the mixture of gases to the inlet temperature of the first compressor, 293.15 K. The pressure inlet on the first compressor is 10 bar. **Right:** volume flowrate of the mixture for different pressures of compression, following the trajectory from 10 bar to 200 bar, indicating the required and saved power with the surfaces under the curves. One stage (pressure ratio of 20) and three stages (pressure ratio of 2.7).

On the other hand, the temperature of the outlet stream has an important effect on the mechanical work of the compressor. Eq. IV-1 describes the mechanical work required by a compressor as a function of pressure levels and the variation of the gas volume, directly related to the gas temperature.

$$\dot{W} = \int P dV \quad \text{Eq. IV-1}$$

For a single stage of compression, between  $P_1$  as inlet and  $P_2$  as outlet pressure, the total amount of mechanical work required can be reduced with intermediate cooling stages. These cooling stages allow to reduce the temperature of the gas, and therefore its volume. For smaller volumes of gas, the total mechanical work is reduced. A graphical comparison of this fact is observed in the right diagram of Figure IV-4.

Following the same case of outlet temperatures, a stoichiometric mixture of  $H_2$  and  $N_2$ , with a molar flowrate of 60 kmol/h, at 298.15 K and 10 bar, the required work to compress the gas in a single stage up to 200 bar is equal to 280.8 kW. If three compressors are used with intercoolers in between, the required mechanical work is equal to 205.8 kW, around 27 % of power savings. The pressure specification for each compressor is given by Eq. IV-2.

$$P_{out} = P_{in} \left( \frac{P_2}{P_1} \right)^{1/n} \quad \text{Eq. IV-2}$$

Where subindexes *out* and *in* indicate the pressure in the outlet and inlet streams of the compressor,  $P_1$  is the inlet pressure of the first compressor,  $P_2$  is the desired final pressure, and  $n$  is the number of stages.

Eq. IV-2 describes a conservative pressure ratio between compression stages, which minimizes the sum of mechanical work [151]. The minimal required work is evidently obtained when the number of

compressors increases, but the economic assessment is a constraint to consider, and a trade-off between investment and required work needs to be studied. This aspect is included in the optimization problem.

### IV.3.2. Reactors

The reaction stage has multiple structural alternatives for its definition, depending on the number of catalytic sections to be included, the type of heat exchange to remove the heat produced from the exothermic reaction, and the catalyst to be considered on the reactor envelope.

As previously detailed, the thermodynamic equilibrium limitation induces low conversions and, therefore, imposes the use of multiple catalytic beds. For their modelling and calculation, each catalytic section is considered independent from the other, being isolated in a unique envelope. In contrast, industrial reactors usually include multiple catalytic sections within the same unit envelope [41].

#### IV.3.2.1. Adiabatic reactor

A maximum of three catalytic reactors in series is explored with the adiabatic configuration, including the Adiabatic Indirect Cooling Reactor (AICR) and the Adiabatic Quench Cooling Reactor (AQCR).

To recall, in the AICR a HEX is used between the reactors to cool down the outlet stream of each reactor down to the desired temperature of the following module, using other process stream of an external utility for this purpose. In the AQCR the heat exchange is carried out by mixing the outlet stream of each reactor with a fraction of a cooler process stream not used for reaction and bypassed from the previous reactors.

The geometry of the reactor is dependent on the length, an optimized variable, and the total volume flowrate at the inlet stream. To guarantee a low-pressure drop along the catalytic section, near 1 – 2 % to avoid important recompression work, a superficial velocity is fixed to 0.5 m/s. Given the superficial velocity and the volume flowrate, the diameter of the section is calculated as follows:

$$D = \left( \frac{4\dot{Q}}{\pi v} \right)^{1/2} \quad \text{Eq. IV-3}$$

Where  $D$  is the reactor diameter in m,  $\dot{Q}$  is the volume flowrate at the reactor inlet stream, in  $\text{m}^3/\text{s}$ , and  $v$  is the superficial velocity, in m/s.

The adjustment of the reactor length is important, as it allows to determine the temperature progression in the catalytic section, according to the kinetic rate equation and considering the thermodynamic equilibrium data. For considerably large reactors, the equilibrium conditions might be easily reached, resulting in a section of the reactor being unused. This is also related to the residence time  $\tau$  in the reactor. For a given superficial velocity, the residence time is equal to the quotient between the length  $L$  and the velocity, as shown in Eq. IV-4.

$$\tau = \frac{L}{v} \quad \text{Eq. IV-4}$$

For the cases that are further described, the length of the reactor varies from 1 to 7 m, giving residence times between 2 and 14 s. These limits are fixed to guarantee the reaction extent and to avoid large reactors with unused sections due to thermodynamic equilibrium limits. An analysis with the obtained

solutions from the optimization will discuss the temperature profiles on the reactor and the related geometric parameters.

#### IV.3.2.2. Autothermal reactor

For the autothermal reactor configuration only the co-current arrangement is considered due to calculation requirements, with a maximum of two catalytic reactors in series. This is due to the local convergence requirements to properly calculate the operating unit. As an illustration, consider the schematic representation of the autothermal reactor in Figure IV-5.

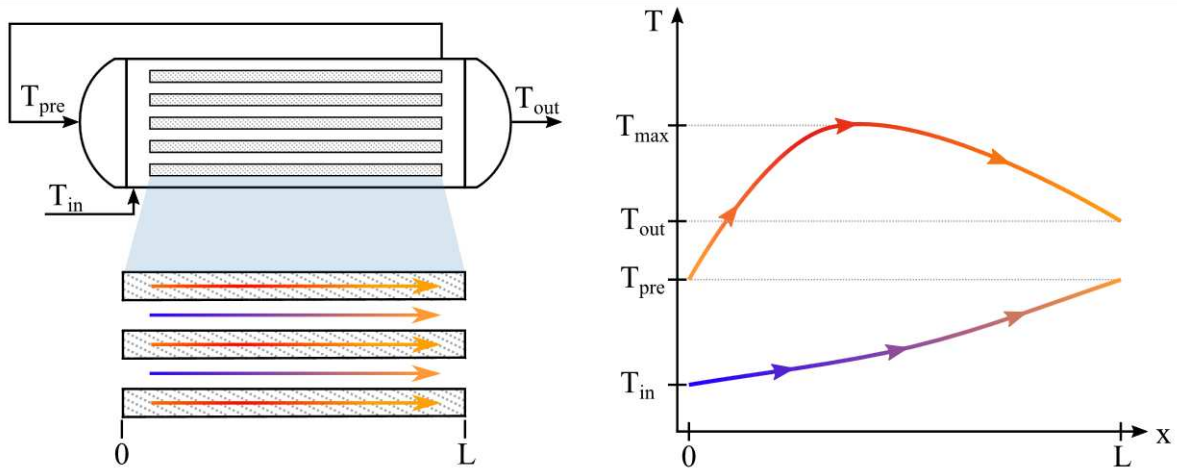


**Figure IV-5.** Representation of the autothermal reactor in co-current configuration and qualitative temperature progression along the axial dimension. In the reactor, the dotted sections represent the catalytic tubes, while the surrounding section is the shell of the module, where the feed is pre-heated.

In industrial applications, for reversible exothermic reactions as the one in study, the heat produced in the reactors needs to be recovered, not only for economic reasons and energy integration potential, but to favour the extent of reaction towards the ammonia production [152]. Using the feed of the reactor as cooling media of the catalyst tubes, induces a temperature rise in this feed (i.e., preheated feed), while cooling down the stream on the catalytic tubes. The cooling allows to approach towards the OTP line, as discussed in Chapter I.

As seen in the temperature profile of Figure IV-5, the multitube autothermal reactor uses the heat of the exothermic reaction to pre-heat the reactor inlet, from  $T_{in}$  to  $T_{pre}$ , while the reaction takes place in the catalytic tubes, varying its temperature from  $T_{pre}$  to  $T_{out}$ , passing by a maximum temperature  $T_{max}$ . As two streams flow along the reactor on the same direction, an iterative calculation is required to determine the correct temperature progression, which induces an important calculation time on the unit. Even if the autothermal reactor allows achieving higher conversions, its implementation in the superstructure is restricted by computational capacities.

As for the adiabatic reactors, the geometry parameters of the autothermal reactor are dependent of the volume flowrate and the superficial velocity. However, as the total section of the reactor is shared by the catalytic tubes and the shell side, the effective section is reduced. To avoid adding optimization variables regarding the geometry, the following relations between parameters have been used, after a sensitivity analysis on an autothermal reactor:

- The total catalytic transversal section is set as a function of the volume flowrate and a superficial velocity of 0.5 m/s.

- The catalytic section of a single tube is equal to the total catalytic cross section divided by the number of tubes, fixed to 14.
- The inner diameter of a single catalytic tube is calculated from the catalytic section of a single tube, while the outer diameter of a single tube is 10 % larger than the inner diameter.
- The catalytic section is equal to 65 % of the reactor section (including the thickness of the tubes), while the pre-heating section accounts for the remaining 35 %.
- The wall thermal conductivity is constant all along the module and fixed to 200 W/m<sup>2</sup>/K.

For both configurations, adiabatic and autothermal, the pressure drop inside the catalytic section is determined by the Ergun equation, shown in Eq. IV-5, which includes specifications regarding the catalytic material used and the geometry of the reactor.

$$\frac{\Delta P}{L} = \frac{150\mu(1-\varepsilon)^2}{d_p^2\varepsilon^3}v + \frac{1.75\rho(1-\varepsilon)}{d_p\varepsilon^3}v^2 \quad \text{Eq. IV-5}$$

Where  $\Delta P$  is the pressure drop,  $\mu$  is the fluid viscosity,  $\varepsilon$  is the bed porosity,  $d_p$  is the catalyst particle diameter,  $\rho$  is the fluid density and  $v$  is the superficial velocity. Data regarding the catalyst are shown in the following section.

### IV.3.3. Catalysts

Among the catalytic materials that have been widely used in industry, and from which extensive information exists on the literature, the iron-based and the ruthenium-based catalysts are considered in this work, from now on known as **Fe-based** and **Ru-based**. Each one of them has a proper kinetic rate describing the conversion of reactive gases to ammonia.

#### IV.3.3.1. Fe-based kinetic rate

The modified Temkin-Pyzhev equation, adapted by Nielsen *et al.* [153] and implemented by Palys *et al.* [54], is employed, as shown in Eq. IV-6.

$$r_{NH_3} = \frac{k_c \cdot (P_{N_2} \cdot k_a^2 - P_{NH_3}^2/P_{H_2}^3)}{(1 + k_{NH_3} \cdot P_{NH_3}/P_{H_2}^\omega)^{2\alpha}} \quad \text{Eq. IV-6}$$

The rate of ammonia formation is based on the partial pressures of each compound  $P_i$ , which includes the kinetic rate constant  $k_c$ , the equilibrium constant  $k_a$ , and the ammonia adsorption constant  $k_{NH_3}$ . Parameters  $\alpha$  and  $\omega$  are constant parameters. The equations for the calculation of the constants  $k_j$  are the following:

$$k_c = k_{c0} * \exp\left(-\frac{E_{A1}}{RT}\right) \quad \text{Eq. IV-7}$$

$$k_{NH_3} = k_{NH30} * \exp\left(\frac{E_{NH3}}{RT}\right) \quad \text{Eq. IV-8}$$

$$\log_{10}(k_a) = \left(k_{A1} \log_{10}(T) + k_{A2}T + k_{A3} T^2 + \frac{k_{A4}}{T} + k_{A5}\right) \quad \text{Eq. IV-9}$$

Where  $R$  is the constant of gases in J/mol/K and  $T$  is the temperature in K. The data for the proper calculation of Eq. IV-6 to Eq. IV-9 are the following.

**Table IV-1.** Fe-based kinetic rate equation parameters [54].

Parameter	Units	Value
$k_{C_0}$	kmol/m <sup>3</sup> /s	1.096*10 <sup>7</sup>
$E_{A1}$	J/mol	46 737
$k_{NH3_0}$	atm <sup>1-<math>\omega</math></sup>	2.94*10 <sup>-4</sup>
$E_{NH3}$	J/mol	100 628
$k_{A1}$	-	- 2.691122
$k_{A2}$	1/K	- 5.519265*10 <sup>-5</sup>
$k_{A3}$	1/K <sup>2</sup>	1.848863*10 <sup>-7</sup>
$k_{A4}$	K	2001.6
$k_{A5}$	-	2.6899
$\alpha$	-	0.64
$\omega$	-	1.564

### IV.3.3.2. Ru-based kinetic rate

For the Ru-based catalyst, the modified Temkin equation proposed by Rosetti *et al.* [154] which takes into account the inhibiting effect of hydrogen and ammonia on the catalyst performance, describes the rate expression for nitrogen consumption, as seen in Eq. IV-10.

$$r_{N_2} = \frac{k_f \cdot \left[ a_{N_2}^{0.5} \cdot \left( \frac{a_{H_2}^{0.375}}{a_{NH_3}^{0.25}} \right) - \frac{1}{k_a} \cdot \left( \frac{a_{NH_3}^{0.75}}{a_{H_2}^{1.125}} \right) \right]}{(1 + k_{H_2} \cdot a_{H_2}^{0.3} + k_{NH_3} \cdot a_{NH_3}^{0.2})} \quad \text{Eq. IV-10}$$

Where  $a_i$  is the activity of compound  $i$ ,  $k_f$  is the kinetic constant,  $k_a$  is the equilibrium constant, and  $k_{H_2}$  and  $k_{NH_3}$  are the hydrogen and ammonia adsorption constants, respectively. The equations for the calculation of the constants  $k_j$  are the following:

$$k_f = k_{f_0} \exp\left(-\frac{E_{A2}}{R_c T}\right) \quad \text{Eq. IV-11}$$

$$k_{H_2} = \exp\left(-\frac{k_{H_2^0}}{R} + \frac{E_{H_2}}{RT}\right) \quad \text{Eq. IV-12}$$

$$k_{NH_3} = \exp\left(-\frac{k_{NH_3^0}}{R} + \frac{E_{NH_3}}{RT}\right) \quad \text{Eq. IV-13}$$

Where  $R_c$  is the constant of gases in cal/mol/K. The calculation of the equilibrium constant,  $k_a$ , is performed as for the Fe-based case, with Eq. IV-9. The value of each parameter for the calculation of Eq. IV-10 to Eq. IV-17 is available in Table IV-2.

**Table IV-2.** Ru-based kinetic rate equation parameters [154], [155].

Parameter	Units	Value
$k_{f_0}$	kmol/m <sup>3</sup> /h	9.02*10 <sup>8</sup>
$E_{A2}$	cal/mol	23 000
$k_{NH3_0}$	atm <sup>1-<math>\omega</math></sup>	2.94*10 <sup>-4</sup>
$E_{NH3}$	J/mol	100 625
$k_{H_2^0}$	J/mol/K	56.9024
$E_{H_2}$	J/mol	37 656
$k_{NH3^0}$	J/mol/K	34.7272
$E_{NH3}$	J/mol	29 228

The activity of compound  $i$  is defined as the quotient between the fugacity  $f_i$  and the standard pressure  $P^0$ , equal to 1 atm. To calculate the fugacity, the following expression is used:

$$f_i = \Phi_i y_i P \quad \text{Eq. IV-14}$$

With  $\Phi_i$  and  $y_i$  being the fugacity coefficient and the molar fraction of compound  $i$ , respectively, and  $P$  the total pressure of the system. The correlations of the fugacity coefficients are the following:

$$\Phi_{H_2} = \exp \left\{ \exp(A_1 T^{0.125} + A_2) P - \exp(A_3 T^{0.5} + A_4) P^2 + 300 \left[ \exp(A_6 T + A_7) * \left( \exp\left(-\frac{P}{300}\right) - 1 \right) \right] \right\} \quad \text{Eq. IV-15}$$

$$\Phi_{N_2} = B_1 + B_2 T + B_3 P + B_4 T^2 + B_5 P^2 \quad \text{Eq. IV-16}$$

$$\Phi_{NH_3} = C_1 + C_2 T + C_3 P + C_4 T^2 + C_5 P^2 \quad \text{Eq. IV-17}$$

With  $P$  the pressure in atmospheres and  $T$  the temperature in Kelvin. The data to calculate the fugacity coefficient of each compound are given in Table IV-3.

**Table IV-3.** Values for the calculation of the fugacity coefficients [154], [155]. Parameter  $X$  is equivalent to the parameters of the fugacity correlations in Eq. IV-15 to Eq. IV-17.

Compound	$X_1$	$X_2$	$X_3$	$X_4$	$X_5$	$X_6$
$H_2$	-3.8402	0.541	-0.1263	-15.98	-0.011901	-5.941
$N_2$	0.9343174	$0.3101804 \cdot 10^{-3}$	$0.295896 \cdot 10^{-3}$	$-0.2707279 \cdot 10^{-6}$	$0.4775207 \cdot 10^{-6}$	-
$NH_3$	0.1438996	$0.2028538 \cdot 10^{-2}$	$-0.4487687 \cdot 10^{-3}$	$-0.1142945 \cdot 10^{-5}$	$0.2761216 \cdot 10^{-6}$	-

Regarding the properties of the catalysts, useful to determine the pressure drop in the reactors and the investment cost of the catalysts, both catalysts are considered to have a particle diameter of 0.2 mm, a constant bed porosity of 0.4, while the densities used are 3 000 kg/m<sup>3</sup> for the Fe-based and 800 kg/m<sup>3</sup> for the Ru-based [155].

#### IV.3.4. Separators

The conventional HB process at industrial scale uses a condensation system to separate and remove the produced ammonia by phase change, while the reactive compounds remain in gas phase due to their non-condensability nature at common operating conditions. However, to explore other separating alternatives, a membrane filter module is considered as well as a pseudo-continuous model adapted to the environment of ProSimPlus. For these separation methods, Figure IV-6 shows the range of temperatures where they can operate according to data found in the literature.

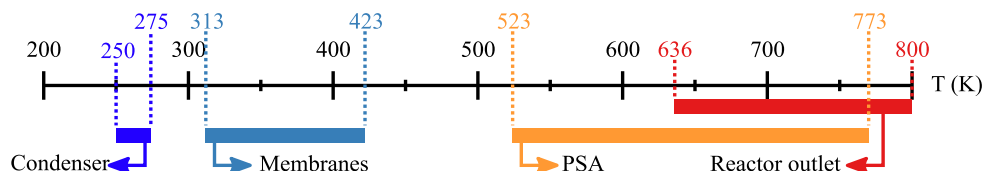


**Figure IV-6.** Range of temperatures for the separation technologies, including the common outlet temperature range obtained in the reaction stage.

The usual range of temperatures obtained at the outlet stream of the reactor stage varies from 636 K, the lowest temperature used, to 800 K, the maximal temperature fixed by the catalytic material resistance [45]. The condenser operating window varies from 250 K to 275 K, requiring the highest temperature

gradient. The membrane filter for the reported material has a larger temperature window, from 313 to 423 K [156]. Finally, the adsorbent used in the PSA system works in the vicinities of the reactor outlet temperature, with the largest range of temperature among the separation technologies, varying from 523 to 773 K [157].

#### IV.3.4.1. Condensation

Adjusting the mixture from the reactor stage outlet to its dew temperature allows to separate in liquid phase some fraction of the produced ammonia. The quantity of ammonia separated is determined by the pressure of the stream and the temperature of the HEX prior the separation drum, adjusted by optimization. This drum, an adiabatic flash at constant temperature and pressure, separates the liquid from the vapor phase. The ammonia is the major compound in liquid phase, near complete purity (i.e., 99.95 % vol.), with some small fractions of hydrogen and nitrogen.

As detailed in section I.6.3 of Chapter I, lower synthesis pressures in the HB loop requires lower separation temperatures. They are achieved by a refrigeration cycle, based on ammonia as refrigerant.

The thermodynamic chart of temperature versus molar entropy, in Figure IV-7, describes the trajectory followed in the refrigeration cycle. The evaporator stage (A) is where the refrigerant receives the heat from the process stream until full saturation in vapor phase. Following, three compressors (B) are used to increase the pressure of the refrigerant up to 15 bar. The condenser (C) serves to release the heat to the surroundings, while cooling almost to liquid saturation conditions. Next, the expansion valve (D) decreases the temperature and flashes the refrigerant to achieve colder conditions. The pressure drop in the HEXs is neglected.

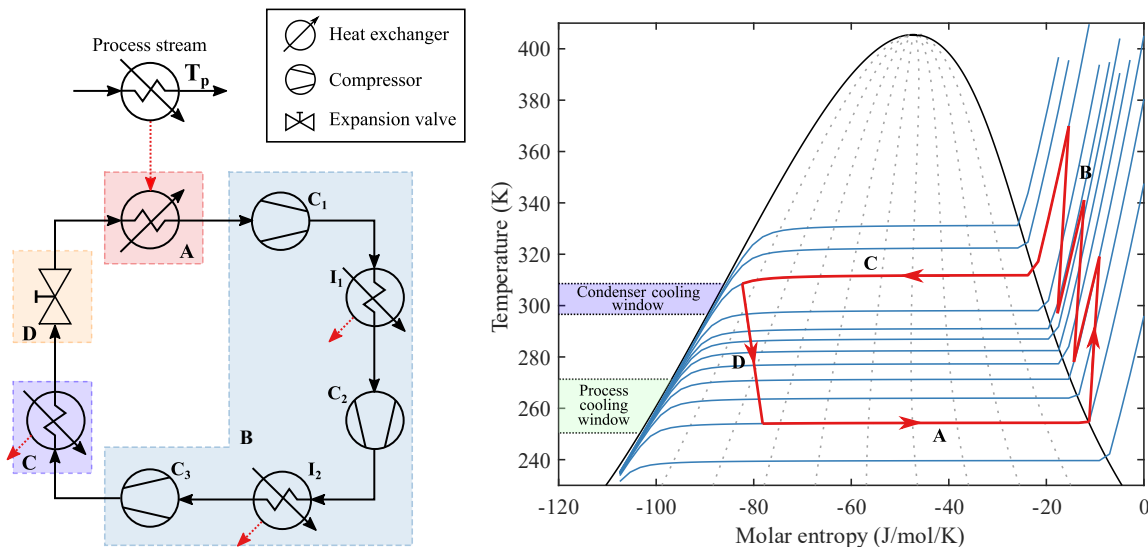


**Figure IV-7.** *Left:* Representation of the refrigeration cycle. *Right:* chart of temperature versus molar entropy for the refrigerant, with the cycle trajectory highlighted with the — dark red lines, the isobars in — light blue lines, and the dotted black lines representing the iso-vapor ratio lines. The refrigerant used in the closed cycle is mainly ammonia, with a molar fraction of 99.5 %, being the remaining a 3:1 ratio of  $H_2:N_2$ . The operating limits on the condenser are fixed between 298 and 308 K, while the cooling window for the process stream varies between 250 and 273 K.

As described in the diagram, two operating windows are available. One concerning the temperature on the process stream, 250 – 275 K, prior the separating drum, and the other related to the refrigerant temperature before the expansion valve, 298 – 308 K. The minimal attainable temperature by the refrigerant is defined by the saturation temperature at atmospheric pressure, (i.e., 240 K), to avoid sub-

atmospheric levels. A minimal temperature difference between the process and the refrigerant streams is fixed to 20 K, while the pinch in the condenser is 10 K. With this, the condensation temperature, an optimization variable, is directly related to the mechanical power consumed in the refrigeration cycle.

#### IV.3.4.2. Membranes

The membrane module available in ProSimPlus is modelled as a multitube mass filter, as seen in Figure IV-8, with an ideal plug flow in the tubes and shell sides. The flow direction can be either counter-current or co-current. The tubes side is selected for the retentate stream, while the shell side is used for the sweep gas flow, defined as the permeate side.

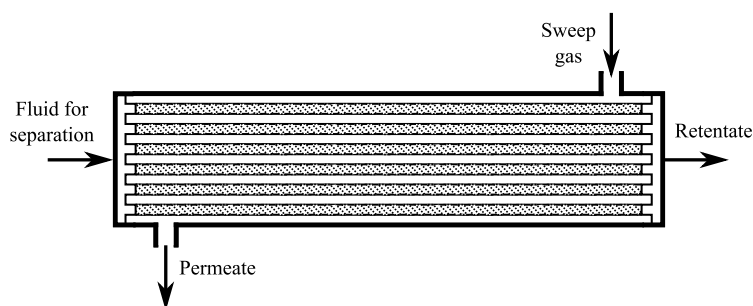


**Figure IV-8.** Membrane configuration used in ProSimPlus. The model of the membrane corresponds to an ideal plug flow behaviour in both sides of the unit, arranged as a set of hollow fibre tubes, with the fluid to be separated flowing inside the tubes and the sweep gas flowing in counter-current direction in the shell side. The membrane can also be modelled in a co-current configuration.

To describe the behaviour of the mass transfer from the retentate to the permeate side, it is possible to define the permeability of each compound as a function of the membrane temperature. To predict this property, data from the literature has been used to correlate mixed-permeabilities data to the temperature of the module, based on works by Pengilley, using nanocomposite MFI zeolite membranes [156].

The mechanism describing the favoured separation of ammonia from hydrogen and nitrogen is the preferential adsorption of  $\text{NH}_3$ , impeding the permeation of weakly adsorbed  $\text{H}_2$  and  $\text{N}_2$  molecules. Among the operating parameters studied to determine the permeance of compounds, the differential pressure across the material, the sweep flowrate, the feed flowrate and the temperature were considered, being the temperature the one with the higher effect on the performance [156].

For this configuration, the following variables are subject to optimization:

- The pressure level on the sweep gas, which allows to calculate the differential pressure between retentate and permeate sides of the membrane, while the pressure on the retentate side is defined by the pressure outlet condition from the reactor. The sweep stream is supplied to the process at 10 bar.
- The molar sweep flowrate, composed of pure nitrogen, is adjusted to determine the most suitable quantity of sweep on the permeate side. This is a compromise between enough sweep flowrate to promote the ammonia permeation, but considerably low flowrates to avoid further ammonia dilution on the permeate side. Also, as the sweep and permeate stream require pressure adjustment by compressors, this induces higher investment costs and more energy consumption that needs to be considered.

- The temperature on the membrane, which is considered as an isothermal module with equal temperature on the retentate and permeate sides. Both the feed and the sweep streams are adjusted by HEX before entering the separation module.

To determine the permeability of compounds as a function of the membrane temperature, the polynomial regression given in Eq. IV-18 is used.

$$\phi_i = A_0 + A_1T + A_2T^2 + A_3T^3 \quad \text{Eq. IV-18}$$

Where  $\phi_i$  is the permeability of compound  $i$ , in mol/s/m/Pa,  $T$  is the temperature of the membrane in K, and parameters  $A_j$  are specific to each compound, as shown in Table IV-4.

**Table IV-4.** Parameters for estimation of the permeabilities (mol/s/m/Pa), according to Eq. IV-18. Data regressed from [156].

Compound	$A_0$	$A_1$	$A_2$	$A_3$
$N_2$	$1.125 * 10^{-13}$	$-8.477 * 10^{-16}$	$2.087 * 10^{-18}$	$-1.640 * 10^{-21}$
$H_2$	$-6.978 * 10^{-14}$	$9.395 * 10^{-16}$	$-3.755 * 10^{-18}$	$4.738 * 10^{-21}$
$NH_3$	$2.168 * 10^{-12}$	$-1.808 * 10^{-14}$	$4.964 * 10^{-17}$	$-4.401 * 10^{-20}$

The correlations are applicable in the temperature range from 313 to 423 K. The ammonia selectivities, calculated as  $\phi_{NH_3}/\phi_{N_2}$  and  $\phi_{NH_3}/\phi_{H_2}$ , vary in this range between 16.6 to 30.2 regarding nitrogen, and between 4.8 to 15.2 for hydrogen.

The membrane is studied to determine the geometric parameters favouring the separation of ammonia. Membrane thickness is fixed to 15  $\mu\text{m}$  [156] and the single tube diameter is equal to 1 mm, between the typical range of diameters found in literature [150]. The diameter of the shell depends on the optimized length of the module, as it is fixed to  $L/15$ . The total section of the hollow fibres is 65 % of the total section of the shell, while the remaining is used for the sweep gas on the permeate side. The total number of tubes is then a result of the relation between the hollow fibres section and the section of a single tube.

#### IV.3.4.3. Pseudo-continuous PSA

In recent works by Sees *et al.* [158] a simple methodology for modelling a Pressure Swing Adsorption (PSA) in process simulation software under steady state regime was proposed. It is conceived as a supporting tool for engineers to study the pertinence of including such technology in their process, without the rigorous description of the real PSA units, and gives insights on its applicability without requiring the use of simulation software in transient state.

The model is based on the **virtual moving bed** approach, where the PSA unit is conceived as a black-box model in which the adsorbent is continuously regenerated by definition of streams of fresh and used adsorbent.

Two efficiencies are included to consider deviations from real systems: the adsorption efficiency and the bed-state efficiency. The former ( $\eta$ ) represents the departure from the equilibrium conditions, while the latter ( $\Phi$ ) is referred to the fraction of the bed covered by the adsorbate. In this case, both efficiencies are fixed equal to 1. In Figure IV-9, a schematic representation of the black box is presented.

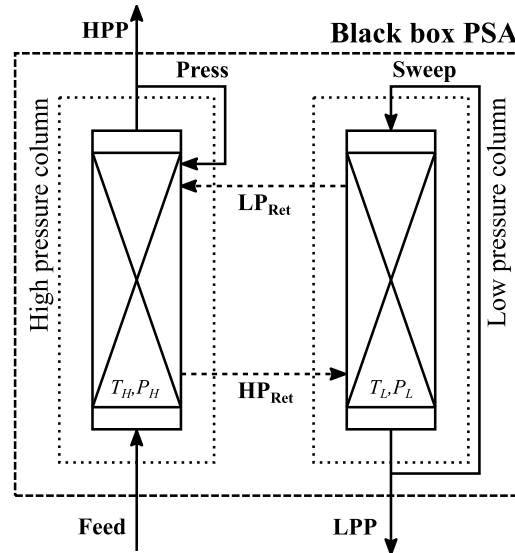


**Figure IV-9.** Representation of the black-box model for the virtual moving bed PSA. The HPP stream (High Pressure Product) is mainly hydrogen and nitrogen, not adsorbed in the column. The LPP stream (Low Pressure Product) is mostly ammonia. The pressurization of the HP column is made with a fraction of the HPP stream (Press), while the purging of the LP column is made with a fraction of the LPP stream (Sweep). Streams  $LP_{Ret}$  and  $HP_{Ret}$ , linking the two columns, are referred to the moving bed of adsorbent continuously regenerated. Adapted from [158].

The model is based on four elementary steps:

- **Feed:** the stream coming from the reactor stage, enters the HP column taking advantage of the high pressure required for ammonia synthesis. Ammonia is preferentially adsorbed, while unreacted hydrogen and nitrogen leave the column at high pressure in the HPP stream.
- **Rinse:** performed with a fraction of the LPP stream, mostly ammonia, to remove the remaining  $H_2$  and  $N_2$  in the bulk phase of the column. As the stage occurs before the blowdown, the sweep stream is compressed to high pressure conditions.
- **Blowdown:** desorption of ammonia from the adsorbent by pressure change in the column, passing from high pressure to low pressure, while producing the LPP stream.
- **Pressurization:** carried out with a fraction of the HPP stream, to pass from low to high pressure. Residual  $NH_3$  from the blowdown remains in the bulk phase of the adsorbent, but purge is not necessary as the HPP stream can contain a mole fraction of  $NH_3$  between 2 and 4 %, as usually encountered in the recycle stream of the HB process.

To specify the HPP and LPP streams, according to the feed stream compositions and operating conditions of the columns, the selectivities for each compound ( $S_i$ ) are determined based on the adsorbent characteristics, the adsorption isotherms describing the behaviour in the columns, and the normalized flowrates in the black box. For each column, the selectivity on the retentate stream (i.e., in the adsorbent phase), is defined by Eq. IV-19 and Eq. IV-20.

$$S_{i,HR} = \frac{\Phi_i^H H_i^H \bar{m}_{ads}}{y_{i,F} \bar{n}_F + y_{i,HPP} \bar{n}_{PR} + \Phi_i^L H_i^L \bar{m}_{ads}} \quad \text{Eq. IV-19}$$

$$S_{i,LR} = \frac{\Phi_i^L H_i^L \bar{m}_{ads}}{y_{i,LPP} \bar{n}_{SW} + \Phi_i^H H_i^H \bar{m}_{ads}} \quad \text{Eq. IV-20}$$

They depend on the mass-specific total hold up  $H_i$ , defined as the quantity of compound  $i$  adsorbed  $q_i^*$  and the amount of compound  $i$  in the bulk phase, as well as the molar fractions in feed  $y_{i,F}$ , pressurization  $y_{i,HPP}$ , and sweep streams  $y_{i,LPP}$ , and the normalized flowrates in feed  $\bar{n}_F$ , pressurization  $\bar{n}_{PR}$ , sweep  $\bar{n}_{SW}$ , and adsorbent  $\bar{m}_{ads}$  streams.

In fact, the real streams (i.e., Feed, HPP and LPP) are normalized depending on the selected number of columns, the defined time per step on the whole cycle duration and the amount of adsorbent used in the PSA system. A full description of the model, detailing each equation for calculation of the selectivities is available in the Appendix B, in section X.

To determine the amount of adsorbed compound in the feed stage of the PSA cycle, data from the literature allow to calculate the adsorption isotherms for the compounds, depending on the temperature of the columns and the concentration in the streams. Knaebel and Cussler worked on PSA systems for ammonia separation at high pressures and temperatures, using zeolite H-Y materials as adsorbents [157]. The authors fitted the adsorption isotherms data to a dual-mode equation for isotherm calculation, as seen in Eq. IV-21.

$$n_i^0 = \left[ K_i + \frac{A_i C_i}{1 + B_i C_i} \right] C_i \quad \text{Eq. IV-21}$$

$$S_i = S_{i,1} * \exp\left(\frac{S_{i,2}}{RT}\right) \quad \text{Eq. IV-22}$$

Where  $n_i^0$  represents the loading of compound  $i$  into the adsorbent,  $C_i$  is the concentration on the stream, and parameters  $K_i$ ,  $A_i$  and  $B_i$  are specific to each compound and calculated according to Eq. IV-22, where parameters  $S_{i,1}$  and  $S_{i,2}$  are shown in Table IV-5. The authors considered that the adsorption behaviour of nitrogen and hydrogen molecules is similar, using then the same data for both compounds.

*Table IV-5. Parameters for estimation of the adsorption isotherms for the H-Y zeolite. Data retrieved from [157].*

Compound	Parameter	Units	$S_{i,1}$	$S_{i,2}$ (cal/mol)
$NH_3$	$K_i$	-	$1.875 * 10^3$	1582.1
	$A_i$	$cm^3/mol$	$-5.114 * 10^8$	2562.0
	$B_i$	$cm^3/mol$	$2.727 * 10^5$	979.9
$N_2, H_2$	$K_i$	-	$9.500 * 10^{-4}$	6688.0
	$A_i$	$cm^3/mol$	$-2.309 * 10^{-10}$	782.4
	$B_i$	$cm^3/mol$	$1.527 * 10^{-7}$	15119.0

The operating conditions that apply for the PSA separation are pressures up to 100 atm and temperatures between 523 and 773 K.

Having covered the relevant information and necessary data to model the different stages of the HB process, the following section present the performance indicators that are included in the superstructure optimization cases. These indicators (KPI) are useful to compare the different obtained solutions according to economic and energetic parameters, to judge whether a given optimal configuration should be preferred over the other optimal solutions.

## IV.4. Key Performance Indicators (KPIs)

The evaluation of the process alternatives requires to determine performance indicators, allowing to compare a specific solution regarding the rest of structural alternatives. As usually defined in chemical engineering processes at plant scale, an economic criterion is defined, typically complemented with an energetic criterion.

In this type of processes, involving the transformation from electrical energy into chemical energy, the energy efficiency of the system is a useful and important criterion that commonly has a counteracting effect to the economic indicator. Processes which are more energetically efficient tend to have higher investment and operational expenditures.

One could also think of environmental impact criteria, such as the Life Cycle Assessment (LCA) related to emissions of pollutants to the surroundings and its equivalent related carbon emissions, usually associated to carbon-based processes [159], [160]. In this case, this type of criteria has not been considered, even if they have a relevant impact on current technological comparisons. Furthermore, exergy analysis could also be helpful to assess not only the effective use of energy across the process, but to determine the sources of energy losses to avoid process irreversibilities, allowing further improvement of energy transformation processes [161], [162]. These two aspects are included within the perspectives of this work. In this thesis, three main KPIs are proposed and described as follows.

### IV.4.1. Levelized Cost of Ammonia (LCOA)

The economic performance of the solutions is evaluated using the Levelized Cost of Ammonia (LCOA), which considers the capital and operational expenditures of the project, in order to determine the cost of a mass unit of ammonia, commonly a kilogram or tonne of produced  $\text{NH}_3$ .

The capital expenditures are associated to the required investments for the process to operate, such as the purchase of equipment and catalysts. The operational expenditures are related to maintenance of the process plant, utilities and raw materials costs, and any labour and erection costs of the plant. The LCOA is defined as follows.

$$LCOA = \frac{CAPEX * ACCR + OPEX}{PROD} \quad \text{Eq. IV-23}$$

$$ACCR = \frac{i(1+i)^n}{(1+i)^n - 1} \quad \text{Eq. IV-24}$$

Where, *CAPEX* is the sum of capital expenditures, *OPEX* is the sum of operational expenditures, and *PROD* is the annual production of ammonia. The parameter *ACCR*, known as Annual Capital Charge Ratio, represents the fraction of the initial investment to be paid each year of the plant lifetime, and is based on the interest rate *i* and the lifetime in years *n*. The LCOA is expressed in  $\text{€}/t_{\text{NH}_3}$ .

The following hypotheses are considered for the economic calculations in every superstructure optimization scenario:

- The project lifetime is 20 years, the interest rate is 8 % and the annual operating time is 8000 h.
- The considered production in Eq. IV-23 is assumed to be constant over the project lifetime.
- The maintenance cost of every equipment is fixed to 3 % of the purchased cost of the unit.

- The prices of catalysts are 15.5 \$/kg for the Fe-based [54] and 321 \$/kg for the Ru-based [155].
- Catalyst lifetime is 10 years, requiring an additional investment. They are considered as part of the CAPEX.
- The price of renewable electricity is fixed to 43 €/MWh, considering the price in the European Union, as reported by the IEA [163].
- The cost of renewable hydrogen by electrolysis of water is 3.5 €/kg [163], while the cost of nitrogen produced by PSA technology is 10.3 €/t [164].
- The Chemical Engineering Plant Cost Index (CEPCI) is used to convert investment costs from 2000 to 2021. The prices of equipment from the Pré-Estime method [141] are calculated in 2000-year euros. Indexes for conversion are 394.1 for year 2000 and 686.7 for year May 2021.

It is important to highlight the impact that the price of renewable hydrogen has on the final LCOA. According to the hypothesis of 3.5 €/kg of H<sub>2</sub>, and by the stoichiometric relation of H<sub>2</sub>:NH<sub>3</sub> given by the chemical reaction (3:2), the cost of hydrogen per kg of NH<sub>3</sub> produced, supposing a complete conversion of hydrogen is 621.86 €/t of NH<sub>3</sub>. This cost is the **minimal cost of hydrogen**, as complete conversion is supposed. Under better price scenarios, for hydrogen costing 3.0, 2.5 and 2.0 €/kg of H<sub>2</sub>, the minimal contribution of hydrogen cost to the LCOA would be 533, 444 and 355 €/kg of NH<sub>3</sub>, respectively.

As will be further discussed in Chapters V and VI, the impact of hydrogen in the total LCOA, considering the process costs, is around 75 %, which is the main obstacle for this type of technologies to be competitive against fossil-fuel based processes. Also, as the raw materials (i.e., H<sub>2</sub>, N<sub>2</sub>) are constant for every optimization case, they can be subtracted from the LCOA. For this, two different LCOA parameters are defined:

- Global LCOA: is the price of ammonia production considering every cost involved in the process. It includes the sum of the investment and operational expenditures of raw materials, electricity, and equipment.
- Process LCOA: is the portion of processing cost for ammonia production. Hydrogen and nitrogen expenditures are excluded, and only the cost of electricity, equipment investment and maintenance are counted.

#### IV.4.2. Energy efficiency

By definition, the energy efficiency indicator is the ratio between the useful produced energy and the supplied energy to the process. The chemical energy contained in hydrogen molecules can be seen as the analogous of a fuel, while the chemical energy recovered in ammonia is the useful energy, as it is the objective to produce.

Also, mechanical energy for the different compressors found in the process is a supply of energy, while the thermal energy balance allows to determine whether a thermal integration is possible, and if any cold or hot utilities are required.

Using a general definition of the energy efficiency analogous to expressions found in literature references for similar processes of energy transformation [165], [166], the expression given by Eq. IV-25 is used to evaluate the performance of the energy transformation through the process.

$$\eta_E = \frac{(\dot{m}_{NH_3} LHV_{NH_3}) + \Delta\dot{W}^- + \Delta\dot{Q}^-}{(\dot{m}_{H_2} LHV_{H_2}) + \Delta\dot{W}^+ + \Delta\dot{Q}^+} \quad \text{Eq. IV-25}$$

Where  $\eta_E$  is the overall energy efficiency,  $\dot{m}$  is the mass flowrate in kg/s,  $LHV$  is the Low Heating Value in kJ/kg,  $\Delta\dot{W}$  is the overall balance of mechanical power in kW, and  $\Delta\dot{Q}$  is the overall balance of thermal energy in kW. Subindexes + and – indicate either a net consumption or production of power. The terms of mechanical and thermal power balance require further details, as they are conditional functions.

#### IV.4.2.1. Mechanical power integration

For the case of mechanical energy, if compressors and turbines are found in the process, a mechanical integration between the turbomachinery is possible, as given by Eq. IV-26. Power produced from the turbines can be used by the compressors. In the process in study no turbines are included and, therefore, the balance of mechanical power is always positive,  $\Delta\dot{W}^+$ , requiring a mechanical power supply to the process.

$$\Delta\dot{W} = (\Delta\dot{W}_{COMP} - \Delta\dot{W}_{TURB}) \quad \text{Eq. IV-26}$$

$$\text{If } \Delta\dot{W} > 0 \text{ then } \Delta\dot{W} = \Delta\dot{W}^+ \text{ and } \Delta\dot{W}^- = 0$$

$$\text{If } \Delta\dot{W} < 0 \text{ then } \Delta\dot{W} = \Delta\dot{W}^- \text{ and } \Delta\dot{W}^+ = 0$$

For the mechanical power balance, the term  $\Delta\dot{W}^-$  is equal to zero. Then, the general balance term  $\Delta\dot{W}$  becomes equal to  $\Delta\dot{W}^+$ .

#### IV.4.2.2. Thermal power integration potential

In the case of thermal power, a simple balance between hot and cold streams is not enough. The thermal integration requires a detailed analysis, as the integration potential does not depend only on the heat duties to be exchanged but also depend on the temperature levels of the heat exchangers and the mass flowrates.

A heat exchange integration between process streams is proposed, as the heat requirement of cold streams can be satisfied with the thermal energy available in hot streams. Even if this procedure does not include a real HEX network analysis, first results of simulations allowed to justify this approach with a simple pinch analysis for an optimization case. Consider the data given in Table IV-6, being the results of a single optimal solution obtained in the very first superstructure optimizations. The hot and cold composite curves are drawn in Figure IV-10.

*Table IV-6. Data from heat exchangers for the Pinch analysis for an optimal solution.*

HEX	Stream type	Stage	$\dot{Q}$ (kW)	$T_{in}$ (K)	$T_{out}$ (K)
1	Hot	Compression	30.90	366.36	302.87
2	Hot	Compression	31.06	366.43	302.87
3	Hot	Compression	31.3	366.52	302.87
4	Cold	Reaction	134.92	366.66	639.08
6	Hot	Reaction	192.16	748.11	677.26
7	Hot	Reaction	7.79	713.25	710.35
8	Hot	Separation	1385.22	720.47	254.42
9	Cold	Recycle	848.71	258.45	639.08

All the reported optimal solutions have the same behaviour, with the cooling needs (hot curve) being greater than the heating requirements (cold curve). This allows to suggest a possible heat integration to fulfil all the heat demands, while being necessary the use of two cold utilities, one at low temperature (near ambient conditions) and the other at high temperature.

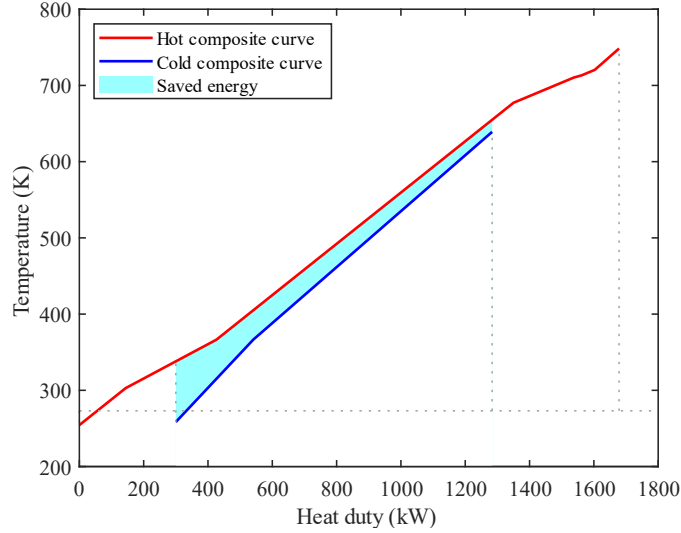


**Figure IV-10.** Hot and cold composite curves for an optimal solution, with a minimum temperature approach equal to 15 K. Saved or integrated power is represented with the coloured light blue area. Cold utilities are required at high and low temperatures. Otherwise, without any use of cold utilities, no advantage is taken of the available heat duty.

Analogously as for the mechanical power balance, the thermal energy balance in Eq. IV-27 considers that the heating requirements can be fulfilled with the hot streams of the process. As every obtained solution has the same trend, the thermal balance parameter  $\Delta\dot{Q}$  will always be greater than zero, as the cooling requirements  $\Delta\dot{Q}_{COOL}$  are higher than the heating requirements  $\Delta\dot{Q}_{HEAT}$ , and the general thermal parameter  $\Delta\dot{Q}$  transforms into  $\Delta\dot{Q}^-$ , while the contrary  $\Delta\dot{Q}^+$  is equal to zero.

$$\Delta\dot{Q} = (\Delta\dot{Q}_{COOL} - \Delta\dot{Q}_{HEAT}) \quad \text{Eq. IV-27}$$

$$\text{If } \Delta\dot{Q} < 0 \text{ then } \Delta\dot{Q} = \Delta\dot{Q}^+ \text{ and } \Delta\dot{Q}^- = 0$$

$$\text{If } \Delta\dot{Q} > 0 \text{ then } \Delta\dot{Q} = \Delta\dot{Q}^- \text{ and } \Delta\dot{Q}^+ = 0$$

Having studied this criterion for the process in study, a simplified expression that best describes the energy efficiency indicator is given by Eq. IV-28.

$$\eta_E = \frac{(\dot{m}_{NH_3} LHV_{NH_3}) - \Delta\dot{Q}_{loss}}{(\dot{m}_{H_2} LHV_{H_2}) + \Delta\dot{W}_{COMP}} \quad \text{Eq. IV-28}$$

The result of the thermal balance  $\Delta\dot{Q}^-$  is transformed into  $-\Delta\dot{Q}_{loss}$ , as the available heat duty is not utilized. It is then used as a penalty parameter included in the energy efficiency function. The best solutions, in terms of energy efficiency maximization, will be those increasing the chemical energy in ammonia (i.e.,  $NH_3$  production), while minimizing the heat duty lost to the surroundings and the consumed mechanical work.

### IV.4.3. Energy consumption

Another useful performance indicator used to compare technologies and exploitation projects is the specific energy consumption. It assesses the amount of energy in form of electricity required at the different stages of the project and is usually reported as the amount of energy required per mass unit of production, kWh/kg of  $\text{NH}_3$ .

As an illustration, the chart displayed in Figure IV-11 indicates the specific energy consumption in a separation stage by condensation, as a function of the synthesis pressure and the condensation temperature. The energy consumption is directly related to the mechanical work used by the compressors in the refrigeration cycle and the recycle stage.

The coloured points indicate the  $\text{NH}_3$  mole fraction in the recycle stage, which is an important parameter to consider in the process. Commonly, the  $\text{NH}_3$  composition in the recycle flow is around 3 – 5 %.

As it can be deduced from the chart, lower fractions of ammonia require higher synthesis pressures, as this favours the separation, but is mainly influenced by the separation temperature. Imposing a maximum mole fraction as a constraint would immediately discard an entire zone on the space of solutions, represented by green-yellow-red points in the diagram. This constraint also gives information on the minimum energy consumption to be expected for such a technology to be implemented.

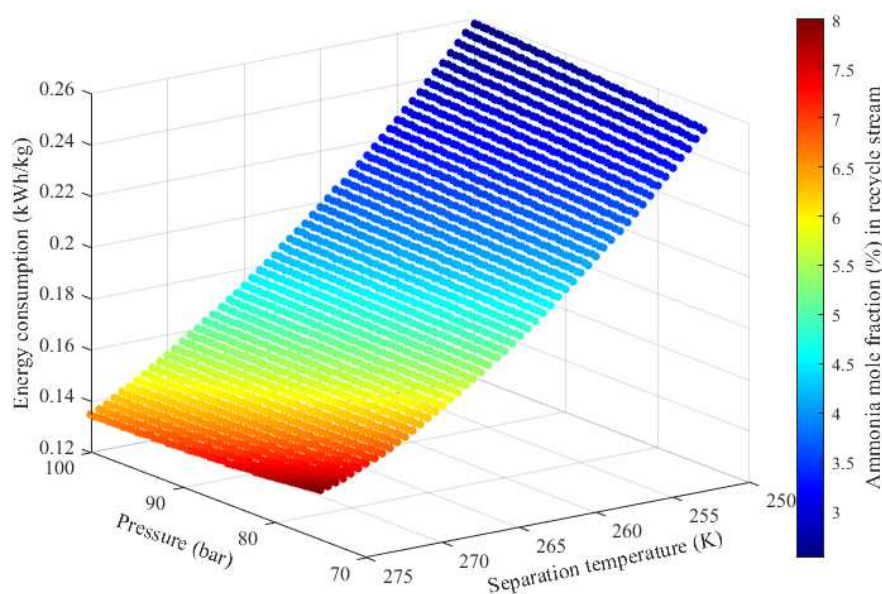


**Figure IV-11.** Relation between the specific energy consumption for compression work in separation process by condensation, for different pressures, separation temperatures and ammonia recycle compositions. The calculations consider only the separation stage, for a flowrate of 304.5 kmol/h, with molar fractions of 21.88 %, 65.64 % and 12.48 % of  $\text{N}_2$ ,  $\text{H}_2$ ,  $\text{NH}_3$ .

Depending on the superstructure case being studied, this parameter can be used as a KPI to be minimized or can be the result of the superstructure optimization searching for the maximization of the energy efficiency. In any case, the specific energy consumption should be minimized or calculated to compare the optimal solutions with the different available technologies.

## **IV.5. Conclusions**

This chapter described the first steps that are necessary for the development of the superstructure optimization cases, presented in Chapters V and VI. It covered the definition of the problem framework, describing the scenario for ammonia production from renewable energy, and the boundaries of the system to be further developed. Also, it served to describe and retrieve the required data of the different stages involved in the HB process, in order to conceive and model the superstructure cases.

The Key Parameter Indicators defined for their minimization or maximization in the optimization problems are essentially economic and efficiency criteria: the global and the process Levelized Cost of Ammonia production (LCOA), the energy efficiency of the process, and the specific energy consumption.

In the following chapter, the results of the different case studies are detailed and discussed, in order to determine the interest of such a methodology for process synthesis and optimization.

# Chapter V

---

*Optimization of the Haber-Bosch process through  
reactor configurations and catalyst selection*

---



## V. Chapter V: Optimization of the Haber-Bosch process through reactor configurations and catalyst selection

The following chapter will cover subjects related to:

- The description of the problem framework, considering the boundaries of the system as exclusively being the HB process, and giving the required renewable power in the hypothetical case of the ammonia production in a delocalized region of France.
- Retrieving the preliminary data required to model the different stages of the HB process, including technical constraints and common operating conditions, as well as the detailed kinetic rates for an appropriate modelling of the chemical reaction.
- The definition of the Key Performance Indicators (KPI) that are subject to minimization or maximization in the different optimization cases that are considered: the Levelized Cost of Ammonia, the specific energy consumption, and the energy efficiency.
- The description of each one of the four superstructure cases treated in this work, focussed mainly on the selection of the reactor configuration (I and II) and the choice of the separation technology (III and IV).

### V.1. Introduction

After the description of the methodology for superstructure optimization that has been carried out in the previous chapter, this part of the work puts into practice those steps in the ammonia synthesis process for energy storage.

This chapter is structured as follows: section V.2 describes the first superstructure optimization case, concerning the adiabatic reactor configuration, including the Fe-based and Ru-based catalysts. Next, section V.3 presents the Superstructure II, where the autothermal configuration of reactors is proposed, including the possibility of performing an intermediate separation between reactors. Following, section V.4 describes the generalities to consider for the analysis of results.

On section V.5 the results of Superstructure I are discussed, first for the Fe-based case, followed by the Ru-based case, and finishing with a comparison between the catalysts. Then, in section V.6 the results of the Superstructure II are detailed in the same manner as for Superstructure I. In section V.7 the summary of results is presented, where the optimal configurations of Superstructures I and II are compared, before presenting the conclusions in section V.8.

## V.2. Superstructure I - Adiabatic reactors

For the first proposition of the superstructure, the study is focused on determining the best configuration for the HB process, considering 3 structural variables: (i) the number of compressors; (ii) the number of adiabatic catalytic reactors; (iii) the type of cooling between reactors.

An additional feature of this case is the individual evaluation that is performed with the use of the two catalytic materials previously cited. Thus, the same superstructure is optimized twice, one for the Fe-based catalyst, and the other for the Ru-based catalyst. Ideally, both catalysts should have been included as a unique structural variable, in order to determine the best material to include in the process. However, having optimized the Fe-based case first, before including the ruthenium catalyst and its respective kinetic rate equation as an alternative, the Ru-based case has been proposed as a second case for the same process superstructure. From this, the optimizations of these superstructure cases, as well as the methodology proposition, have been published in the following paper [167].

The superstructure shown in Figure V-1 is a representation of the flowsheet proposed in ProSimPlus yet has been adapted and simplified for readability purposes.

### V.2.1. Structural alternatives and description of the superstructure

The different descriptions presented in this section are referred to the modules of Figure V-1. Hydrogen and nitrogen are supplied to mixer 1 at 10 bar, 298.15 K and in a stoichiometric ratio, with H<sub>2</sub> at a constant molar flowrate of 45 kmol/h. For the compression stage, the intermediate splitters A1 and A2 are useful for bypassing the modules when selecting the number of compressors,  $NC \in \{2, 3, 4\}$ , following the strategy of association of common processing units, defined in section III.5.1.

Concerning the reaction stage, the intermediate splitters B1, B2 and B3 are referred to the choice between the number of reactors and the type of cooling, simultaneously. In fact, this case is used as example in section III.5.2, according to the identification and elimination of inadequate/redundant switch positions. Both structural variables, the number of catalytic reactors  $NB \in \{1, 2, 3\}$  and the type of cooling  $TC \in \{1, 2\}$  are grouped into a unique structural variable, defined as the reactor configuration variable  $RC \in \{1, 2, 3, 4, 5\}$ . The configuration for each position of the variable  $RC$ , is given as follows:

*Table V-1. Position of the variable RC, according to the number of adiabatic reactors and the cooling type.*

Reactor \ Cooling	Absent	AICR	AQCR
1 reactor	1	-	-
2 reactors	-	2	4
3 reactors	-	3	5

The selection of a unique reactor immediately inactivates the cooling type choice, as the cooling variable is only included when a supplementary reactor is included. Therefore, there is no sense to use a unique reactor with either the AICR or the AQCR configuration.

The required cooling after the last reactor (or unique reactor) is performed by the HEX on the separation stage. However, in this superstructure case, the heat duty withdrawn from the HEX in module 22, before the separation drum, is not coupled to the cold cycle production, as the refrigeration cycle was modelled after this case was optimized. Therefore, the mechanical work requirements in this section are not considered. The cold cycle is considered in posterior superstructure cases.

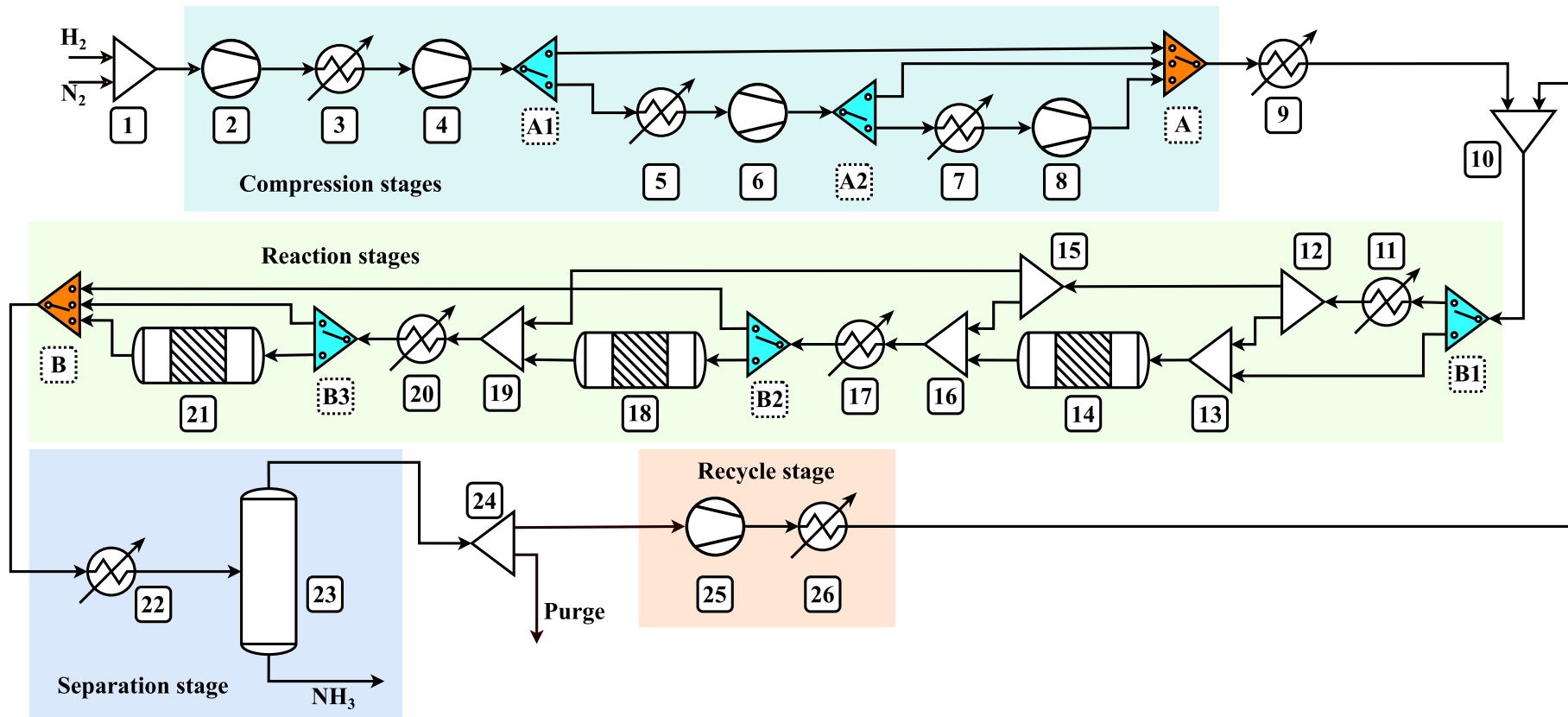


**Figure V-1.** Superstructure representation for the evaluation of the adiabatic reactor configuration. The compression stage includes the selection of the number of compressors. The reaction stage has two structural variables to determine the number of reactors and the type of cooling. Module nomenclature corresponds to: Mixers (1, 10, 13, 16, 19), Splitters (12, 15, 24), Compressors (2, 4, 6, 8, 25), HEX (3, 5, 7, 9, 11, 17, 20, 22, 26), Reactors (14, 18, 21), Separation drum (23), Intermediate switches (A1, A2, B1, B2, B3) and Closing switches (A, B).

Even if no inert compounds are included with the feed streams to the process and there does not exist any risk of inert accumulation within the process recycling loop, a purge of 1 % is fixed in module 24 to consider the usual losses found in the recycling streams. Finally, the compressor in module 25 equalizes the pressure of the recycle with the one on the feed stream, while HEX of module 26 adjusts the temperature as the HEX of module 9, to perform a mixing of streams at the same pressure and temperature.

### V.2.2. Optimization problem formulation

The LCOA and the energy efficiency of the process are the objective functions for this case. The former is minimized, while the latter is maximized by mathematical adjustment with a negative value of the energy efficiency  $-\eta_E$ , as the optimization algorithm only performs the minimization of the set of objective functions.

Concerning the variables to be optimized, they are specified in Table V-2. They involve 10 continuous and 2 discrete variables. They are common and have the same variable bounds for the Fe-based and the Ru-based cases, except for the pressure of the system. As the catalysts operate under certain pressure and temperature ranges, they are adapted depending on the catalyst chosen. The Fe-based catalyst has pressure bounds from 150 to 200 bar, and for the Ru-based it varies from 50 to 100 bar. The range of temperatures is similar in both cases.

**Table V-2.** Continuous and discrete decision variables for the optimization of the Superstructure I. The process unit is referred to the superstructure representation shown in Figure V-1.

Variable	Type	Stage	Process unit	Bounds	Units
Pressure*	Continuous	Compression	2, 4, 6, 8, 25	50 – 200	bar
Inlet temperature at 1 <sup>st</sup> reactor	Continuous	Reaction	9, 26	636 – 736	K
Inlet temperature at 2 <sup>nd</sup> reactor	Continuous	Reaction	17	636 – 736	K
Inlet temperature at 3 <sup>rd</sup> reactor	Continuous	Reaction	20	636 – 736	K
Length of 1 <sup>st</sup> reactor	Continuous	Reaction	14	0.5 – 7.0	m
Length of 2 <sup>nd</sup> reactor	Continuous	Reaction	18	0.5 – 7.0	m
Length of 3 <sup>rd</sup> reactor	Continuous	Reaction	21	0.5 – 7.0	m
Separation temperature	Continuous	Separation	22	253 - 275	K
Split ratio at first quench splitter	Continuous	Reaction	12	0.4 – 0.8	-
Split ratio at second quench splitter	Continuous	Reaction	15	0.4 – 0.8	-
Number of compressors	Discrete	Compression	A <sub>1</sub> , A <sub>2</sub>	2 – 4	-
Reactor configuration	Discrete	Reaction	B <sub>1</sub> , B <sub>2</sub> , B <sub>3</sub>	1 - 5	-

\* The pressure of the reaction stage depends on the catalyst used. The limits declared are the minimum lower and maximum upper bounds. For the Fe-based case, the pressure varies from 150 to 200 bar, while for the Ru-based case, pressure varies from 50 to 100 bar.

The pressure of the system is optimized, as it is one of the most important operating conditions for this process. It defined the pressure conditions at the inlet stream of the first reactor. For each one of the reactors of the process, the inlet temperature and the length are adjusted. However, in the case of the AQCR, no temperature adjustment is required, as the inlet stream of the reactor is the result of the quenching effect. In the AQCR case, the interest resides in adjusting the splitting ratios for the quenching streams. These ratios are adjusted in splitters 12 and 15. Also, the temperature of the HEX just before the separation drum is optimized.

Regarding the required constraints all along the process, 3 technical constraints are required, one for each reactor to avoid outlet temperatures beyond the catalyst resistance limit of 800 K. Also, 2 performance constraints are defined, one to avoid global LCOA values beyond 850 €/t, and the other to

avoid process solutions with a global hydrogen conversion below 90 %. The constraint related to the LCOA is fixed to discard solutions with high costs of production based on preliminary studies of the process, while the one regarding the H<sub>2</sub> conversion is defined to avoid configurations with low H<sub>2</sub> conversions per pass and important hydrogen losses on the purge stream.

Last but not least, the most important constraint for superstructure optimizations involving recycling loops is related to the numerical convergence of the loop in the process. Indeed, the optimization algorithm does not have the means to understand that the simulation of the process flowsheet has successfully converged. Hence, the engineer needs to declare a constraint referred to a convergence criterion, in order to communicate the status of the convergence to the algorithm. The stream in which the convergence is evaluated is the tear stream (i.e., cut stream on the process to iterate), defined between modules 26 and 10. The iterative variables correspond to the partial molar flowrates on the stream, while the temperature and the pressure are not considered, as they are imposed to be the same between the recycle and the fresh feed streams. The value used as limit for the convergence criterion to be satisfied is  $1 * 10^{-7}$ .

This, as well as the previously defined inequality constraints are declared as follows:

$$C_L = - \frac{(\text{Set point} - \text{Calculation})}{\text{Set point}} \quad \text{Eq. V-1}$$

$$C_H = - \frac{(\text{Calculation} - \text{Set point})}{\text{Set point}} \quad \text{Eq. V-2}$$

For a constraint required to be lower than a specified set point, Eq. V-1 is used as specification. On the contrary, a constraint higher than a set point is defined as in the Eq. V-2. In any case, the value of the constraint needs to be negative to avoid constraint violations.

### V.2.3. Algorithm parameters

Before executing the superstructure optimization, the algorithmic parameters need to be specified in case that the default values are not accurate. The user can apply the default values on the majority of parameters when there is no knowledge on their behaviour but needs to declare the values of the stopping criteria. For both optimizations, the Fe-based and the Ru-based cases, the following values are defined.

**Table V-3.** Values for the parameters of the optimization algorithm, in Superstructure I. Non specified parameters have the value by default.

Parameter	Values	Parameter	Values
ACCURACY	0.01	MAXTIME	1 036 800
SEED	1.0	MAXEVAL	100 010
EVALSTOP	15 000	PRINTEVAL	10
NI	2	SAVE2FILE	100 010

The maximum time for optimization is fixed to 288 h, or 12 days, to give the algorithm enough time to stop by algorithmic criteria and not by hard-limit criteria, meaning that the optimization finishes due to non-improvement of the set of optimal solutions.

### V.3. Superstructure II – Autothermal reactor

In the second superstructure, the main interest is to evaluate the performance of a couple of autothermal reactors, as they are expected to have a better performance than the adiabatic. The superstructure representation for this case is shown in Figure V-2.

This configuration benefits from the heat exchange that drives away the conditions in the catalytic section from the thermodynamic equilibrium, allowing higher conversions per pass. Along with this structural configuration, an intermediate separation by condensation is proposed, as the removal of produced ammonia allows to place the inlet conditions on the second reactor even farther from the equilibrium.

Therefore, the structural variables concern: (i) the number of compressors, and (ii) the use of the intermediate separation. For stability of the convergence calculations, it has been decided not to include a structural variable to select the number of autothermal reactors to include. Also, in both of the reactors, the catalyst selected is the ruthenium.

In this scenario, there exists an imbricated recycling loop. For each one of the reactors, due to the use of the same process stream on both sides of the reactor, a local recycling loop is created in the module for its resolution. Due to the heat exchange on the axial direction of the reactor, the calculation on the module needs to be internally discretized and iterated until convergence. This convergence problem is set between the outlet stream on the shell side and the inlet stream on the tubes side. Because of this double internal recycling loop, in addition to the global recycling loop from the separation-recycle stages, solving each flowsheet evaluation consumes important time resources.

Even though the important time for calculation, this structure is somehow explored considering the strategies presented in sections III.5.5 and III.5.6, referred to the limitation of internally discretized modules and the limitation of nested recycling loops. It remains interesting to assess and compare this alternative with the adiabatic reactor configuration.

#### V.3.1. Structural alternatives and description of the superstructure

As in the Superstructure I, the selection between the number of compression stages is included in the optimization, represented by the intermediate switches A1 and A2, and the closing switch A, in Figure V-2, allowing to select between 2, 3 and 4 compressors.

The second structural alternative is related to whether the intermediate separation stage should be included, as given by switches B1 and B. Both the intermediate and the final separation stages include the calculation of the corresponding refrigeration cycle.

#### V.3.2. Optimization problem formulation

Analogously to the Superstructure I, which evaluates the whole synthesis process, the objective functions used in this optimization scenario are the LCOA and the energy efficiency of the process. However, as the hydrogen and nitrogen flowrates are constant for every solution, their costs are constant as well, and the process LCOA is preferred as objective function instead of the global LCOA.

Nevertheless, the process LCOA is calculated for the results in Superstructure I, allowing to directly compare the optimal solutions of the autothermal configuration and the adiabatic reactors.

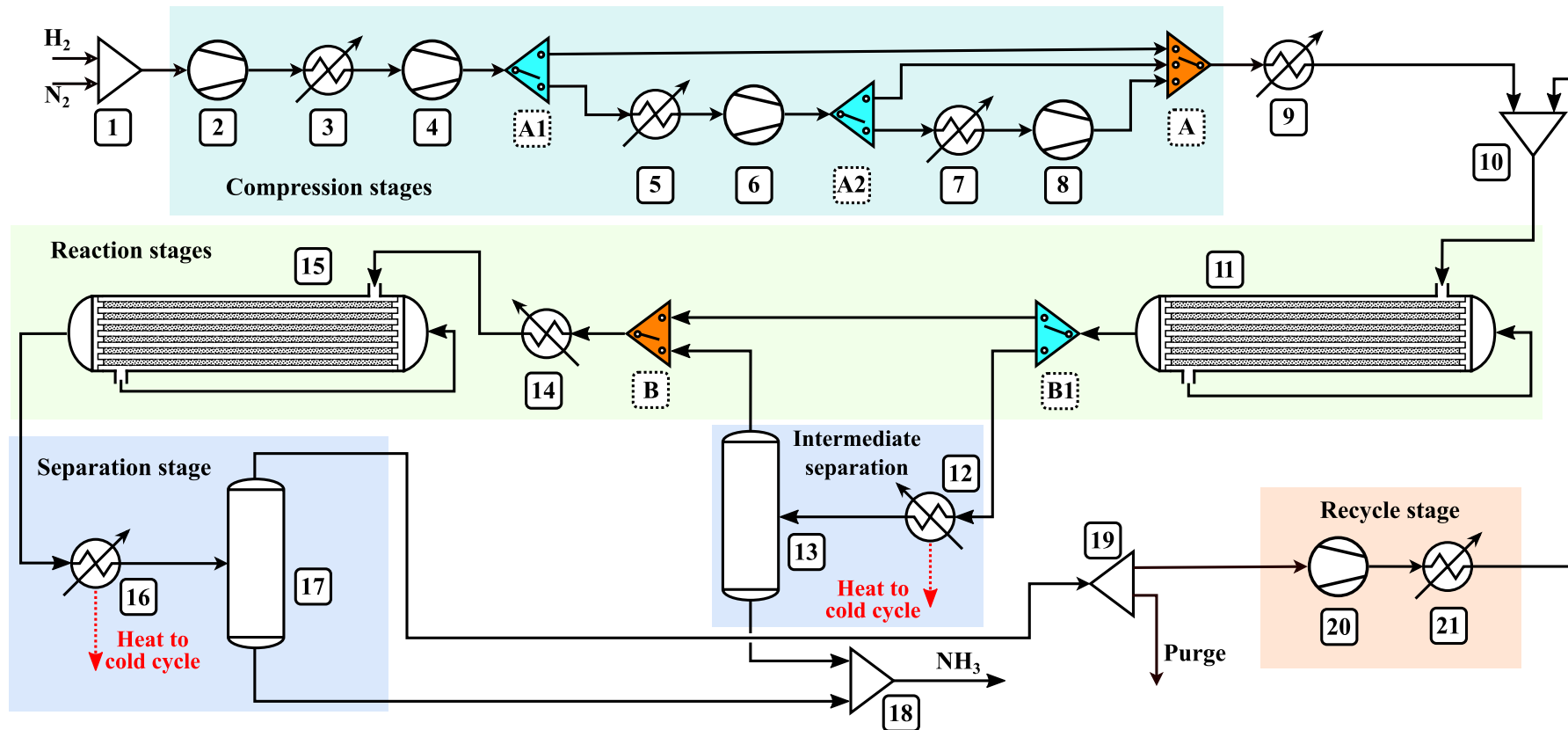


**Figure V-2.** Superstructure representation for the evaluation of the autothermal reactor configuration. The compression stage includes the selection of the number of compressors. The reaction stage includes the structural alternative to include an intermediate separation stage. Module nomenclature corresponds to: Mixers (1, 10, 18), Splitters (19), Compressors (2, 4, 6, 8, 20), HEX (3, 5, 7, 9, 12, 14, 16, 21), Reactors (11, 15), Separation drums (13, 17), Intermediate switches (A1, A2, B1) and Closing switches (A, B).

The optimization variables for this scenario include 7 continuous and 2 discrete variables. As in the Superstructure I, the pressure of the process, the temperatures and the length of each reactor are optimized. As the reactors use ruthenium as catalysts, the corresponding pressure boundaries are used.

In what concerns the temperature of each reactor, the optimized value is referred to the temperature at the inlet stream on the shell side, this means, for the feed pre-heating. Then, the temperature of inlet stream to the catalytic tubes is the result of the thermal integration in the reactor. Finally, the temperature of the intermediate and final separation modules is the same as in the previous superstructure.

**Table V-4.** Continuous and discrete decision variables for the optimization of the Superstructure II. The process unit is referred to the superstructure representation shown in Figure V-2.

Variable	Type	Stage	Process unit	Bounds	Units
Pressure	Continuous	Compression	2, 4, 6, 8, 20	50 - 100	bar
Inlet temperature at 1 <sup>st</sup> reactor	Continuous	Reaction	9, 21	643 – 733	K
Inlet temperature at 2 <sup>nd</sup> reactor	Continuous	Reaction	14	643 – 733	K
Length of 1 <sup>st</sup> reactor	Continuous	Reaction	11	1 – 7	m
Length of 2 <sup>nd</sup> reactor	Continuous	Reaction	15	1 – 7	m
Intermediate separation temperature	Continuous	Separation	12	250 – 273	K
Final separation temperature	Continuous	Separation	16	250 – 273	K
Number of compressors	Discrete	Compression	A <sub>1</sub> , A <sub>2</sub> , A	2 – 4	-
Intermediate separation	Discrete	Separation	B <sub>1</sub> , B	1 – 2	-

Even if the heat exchange between the catalytic section and the feed pre-heating occurs, a maximum level of temperature is seen in this arrangement. Therefore, to guarantee avoiding this level, one inequality constraint is defined for each reactor on the catalytic side, with the maximum value of temperature set to 800 K. The imbricated recycling loop in the process structure requires the simulation software to correctly solve the tear streams in each autothermal reactor and in the global recycle loop. The value of the convergence criterion is defined as  $1 \cdot 10^{-7}$ . The three inequality constraints are defined according to the definition of maximum value of the constraint, given by in Eq. V-1.

### V.3.3. Algorithm parameters

The following algorithm parameters have been defined for the autothermal superstructure optimization. Here, the EPSILON value has been included, which filters the optimal solutions to avoid very similar solutions to be stored, in order to explore beyond the vicinities of the optimal points.

**Table V-5.** Values for the parameters of the optimization algorithm, in Superstructure II. Non specified parameters have the value by default.

Parameter	Values	Parameter	Values
ACCURACY	0.01	MAXTIME	864 000
EPSILON	0.01	MAXEVAL	100 000
EVALSTOP	5 000	PRINTEVAL	10
NI	2	SAVE2FILE	100 000

Due to the high calculation time required by this particular superstructure, the total number of evaluations has been reduced to 5 000, in comparison with the adiabatic configuration, going up to 100 000. The maximum time for optimization is fixed to 240 h, or 10 days.

The corresponding results for the optimization of this superstructure are presented and discussed in section V.6, while a comparison with the adiabatic configuration is presented in section V.7.

## V.4. Generalities on the analysis of results

To carry out the different analyses of results of the superstructure optimization cases, it is necessary to recall the following definitions regarding the nature of the obtained solutions, as defined in Chapter II.

A solution is considered to be *feasible* if, and only if, it respects every imposed inequality and equality constraint. On the contrary, a solution is *infeasible* when at least one of the imposed constraints is violated, regardless of the nature of the constraint being violated. For a solution to be *optimal*, it needs to respect every imposed constraint, plus being a non-dominated solution, following the concept of optimality in the Pareto front.

The main interest of the analysis of results is to study the set of optimal solutions obtained in every superstructure optimization case, to understand the impact that the structural alternatives and the other optimization variables have on the objective functions. Also, it is important to consider the set of feasible dominated solutions (i.e., feasible non-optimal), as they can give insights on existing relations between the optimization variables and the KPIs, or even the infeasible solutions, as the constraints violation might give useful information for a better understanding of the process.

Optimizing process superstructures has one important drawback, as it needs several thousands of evaluations to have a solid evaluation history allowing to determine a suitable set of optimal solutions. This induces a considerable amount of time for the calculation of a single superstructure before stopping the calculations, according to the different available algorithmic parameters. Depending on the process complexity, the optimization might demand higher calculation times to obtain a significant number of evaluations that explore the vast search space defined by the bounds of the mixed variables.

Table V-6 shows a synthesis on the general information of the optimization cases of Superstructures I and II, with the main parameters regarding the consumed time and the algorithmic performances, in terms of evaluations, optimal solutions retrieved, and the number of feasible solutions obtained.

*Table V-6. General information on the results of the optimization cases of Superstructures I and II, detailing the main parameters of computational performance and time resources.*

Parameter	Case I*		Case II
	Fe-based case	Ru-based case	Autothermal
Continuous variables	10	10	7
Discrete variables	2	2	2
Number of evaluations	21 205	42 520	2 142
Total elapsed time (s)	212 857	516 060	712 343
Total elapsed time (h)	59.1	143.4	198.0
Time per evaluation (s)	10.0	12.1	332.6
Stop trigger parameter	EVALSTOP	EVALSTOP	EVALSTOP
Stop trigger value	10 000	10 000	1 000
Pareto points	17	34	13
Feasible solutions (%)	94.4	67.2	83.2

\* The Superstructure I is calculated twice for each one of the catalysts. The second calculation was carried out with a different numerical method for the calculation of the recycling loop convergence, which favours the overall performance of the optimization. This aspect is detailed in section V.5.1.

In the superstructure optimization methodology, one of the most important parameters to keep in mind is the consumed *time per calculation*. A calculation, also referred as an evaluation, is a whole flowsheet calculation where every module is calculated according to the values of the optimization variables. It is the complete cycle executed between the values of the decision variables given by the optimization

algorithm, and the communication to the algorithm of the values of the objective functions and constraints, as defined in section III.4.4.

Regarding the Case I, for the HB process optimization, the time per evaluation is around 10 – 12 s, as the recycling loop imposes the convergence of the tear stream. On the contrary, for Case II in which the autothermal reactors are evaluated, the existence of a global recycling stream and two internal recycling loops increases substantially the time per evaluation, requiring more than 5 minutes in average, which is a significant disadvantage. Nevertheless, as will be further discussed, this configuration allows to reach better solutions regarding the KPIs.

Furthermore, for all the cases the parameter triggering the optimization to end is EVALSTOP. This indicates that no improvement was made in the optimal solutions after a specified triggering value, and the algorithm decided to end the optimization. The hard limit criteria, giving the user the authority to end the calculations, were not reached.

Finally, the percentage of feasible solutions needs special attention and further analysis. Understanding why the solutions are infeasible is crucial. The infeasibility can be caused by technical/operational constraints, which cannot be neglected as they are restrictions given by the process, or by calculation constraints, as the ones specified for the convergence of the recycling loops. In solutions where a significant number of infeasible solutions are obtained, it is necessary to determine what is causing the violation of constraints.

The sections hereafter developed are committed to the analysis of results of the superstructure optimization cases.

## **V.5. Analysis of results for Superstructure I**

As previously evoked, the superstructure of the adiabatic reactors has been executed twice, once for each catalyst with its respective kinetic rate equation. The results of both optimizations are presented in this section one after the other, focussed on understanding the influence of the structural variables on the KPIs.

This section is divided into four parts: in section V.5.1 an important remark is presented, regarding the feasibility of solutions and the violation of constraints, necessary for a better understanding of the results. Section V.5.2 presents the results of the Fe-based case optimization, and section V.5.3, is dedicated for the Ru-based case. Both sections are structured in a similar way to be consistent with the analyses, but it has been decided to separate the analysis to avoid an overload of results. Of course, the results between the cases need to be compared one to another, and a final comparison between the cases is offered in section V.5.4.

### **V.5.1. Violation of constraints and numerical method for convergence calculation**

A primary analysis of results regarding the percentage of feasible solutions over the total number of evaluations, indicates that there exist constraints violations in 54.4 % of the Fe-based case evaluations and 56.5 % of the Ru-based case solutions, which is a counterproductive effect for this kind of applications. This makes imperative to determine why the constraints are being violated.

Recalling the specified inequality constraints for this superstructure, presented in section V.2.2 they are presented in Table V-7.

**Table V-7.** Percentage of violation of predefined inequality constraints in Superstructure I, for the Fe- and Ru-based cases.

ID	Constraint description	Units	Value	Fe-based	Ru-based
C1	Maximal LCOA	€/t	850	20.93 %	23.42 %
C2	Minimal H <sub>2</sub> global conversion	%	90	35.65 %	27.96 %
C3	Minimal recycle convergence criterion	-	1*10 <sup>-7</sup>	45.75 %	55.39 %
C4	Maximal temperature in reactor 1	K	800	1.54 %	1.44 %
C5	Maximal temperature in reactor 2	K	800	0.71 %	1.01 %
C6	Maximal temperature in reactor 3	K	800	0.66 %	1.00 %

According to the results, the maximal temperature constraints are responsible, in the worst of cases for 1.54 % and 1.44 % of constraints violation in the Fe-based and the Ru-based case, respectively. Surprisingly, the convergence criterion constraint leads to the highest violation of constraints, as it accounts for 45.75 % and 55.39 %, in the same order of cases. Violation of constraints C1 and C2 are a result of the non-convergence of the recycling loop, as suggested by constraint C3. This implies that, more than being infeasible solutions due to process limitations, as should be expected, it is due to a problem on the convergence of the tear stream variables on the recycle stream.

After studying the alternatives available in ProSimPlus related to the numerical resolution of the recycle convergence, it was found that changing the numerical method improved the calculations of the problem.

By default, the software selected the Broyden method over the Newton-Raphson method, but the latter allowed to easily achieve the convergence of the tear stream in quite a few iterations. This change improves the optimization, which is evident in three aspects: (i) the computational performance, as the time per evaluation is reduced to a fifth of the original time; (ii) the feasibility of solutions, as more solutions respect the inequality constraints; (iii) the optimality of solutions, as the final Pareto front has a slightly better placement. Even though, this modification is useful for this particular application, it is recommended for further process superstructures to consider the different numerical methods for resolution of the tear variables convergence.

In this regard, a second optimization with the Newton-Raphson numerical method was carried out, for which the performance results are presented in Table V-6. These results are discussed in the following section.

### V.5.2. Fe-based case

The optimization of the Superstructure I for the Fe-base case reached a total number of evaluations of 21 205, from which 20 008 (94.4 %) are feasible solutions and 17 of them are considered optimal points. For the optimal solutions, the LCOA varies from 752 to 816 €/t of NH<sub>3</sub>, while the energy efficiency is found between 54.4 and 56.4 %.

The distribution of feasible solutions of Figure V-3 shows the objective functions as a function of the structural variables. On subplot (a), the solutions are highlighted according to the corresponding number of compressors. On subplot (b), the same is made for the corresponding reactor configuration. In both figures, the optimal solutions are represented by stars ★.

From the figures it can be inferred that the reactor configuration, which is the combination of the number of reactors and the cooling type, has greater influence on the global LCOA than the number of compressors. Certainly, within each reactor configuration distribution shown in Figure V-3 (b), there

exists another distribution of solutions according to the number of compressors. Consider for instance the configuration identified as “1 – Absent” in the reactor structure, using a unique reactor without cooling. For this zone of the map of solutions, each structure of compressors is identified in Figure V-3 (a). This behaviour is also evident for the other reactor structures.

Moreover, the optimal solutions reported in the figure allow to identify that the AICR is preferred over the AQCR. For the same number of reactors, the AICR achieves higher energy efficiencies and lower LCOAs.

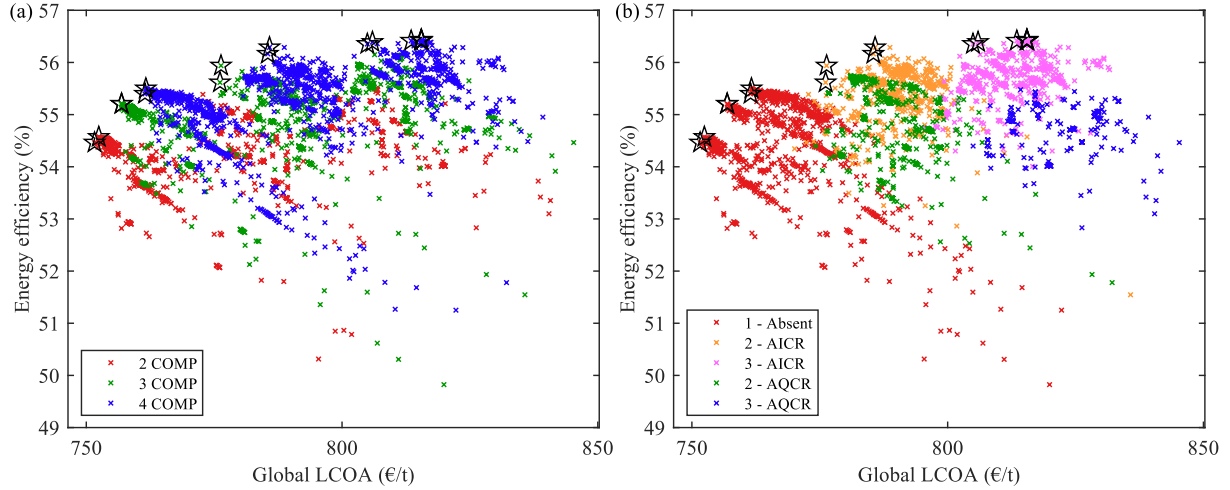


**Figure V-3.** Distribution of the objective functions for the feasible solutions in the Fe-based case, according to the structural alternatives. (a) Number of compressors, varying from 2 to 4. (b) Reactor configuration, varying from 1 to 3 reactors, with absent, indirect (AICR) or direct (AQCR) cooling configuration. The 17 optimal solutions are represented by the stars ★.

To ease the analysis of the differences between the variables of the optimal solutions, 6 optimal points have been selected from the totality, each one with a different process structure. Their corresponding values of the KPIs and the decision variables are shown in Table V-8.

**Table V-8.** Results of the KPIs and the optimization variables for the optimal solutions of the Fe-based case. The totality of the Pareto front points are presented in the Appendix C, in section X.3. \*The split ratios for the AQCR splitters are omitted, as no optimal solutions were obtained for this cooling configuration.

Key Performance Indicator	Units	Point 1	Point 2	Point 3	Point 4	Point 5	Point 6
Global LCOA	€/t	752.4	756.9	761.6	776.3	785.8	806.5
Energy efficiency	%	54.57	55.20	55.50	55.94	56.29	56.39
<b>Variables</b>							
Pressure	bar	151.74	151.79	151.79	156.76	150.37	151.30
Inlet temperature at 1 <sup>st</sup> reactor	K	636.04	636.00	636.00	636.28	672.61	712.23
Inlet temperature at 2 <sup>nd</sup> reactor	K	-	-	-	688.57	676.51	675.19
Inlet temperature at 3 <sup>rd</sup> reactor	K	-	-	-	-	-	675.19
Length of 1 <sup>st</sup> reactor	m	3.63	3.64	3.64	2.85	2.61	0.53
Length of 2 <sup>nd</sup> reactor	m	-	-	-	5.61	6.54	3.46
Length of 3 <sup>rd</sup> reactor	m	-	-	-	-	-	5.05
Separation temperature	K	265.49	254.58	254.48	253.14	265.42	261.10
<b>Structural configuration</b>							
Number of compressors	-	2	3	4	3	4	4
Number of reactors	-	1	1	1	2	2	3
Cooling configuration	-	Absent	Absent	Absent	AICR	AICR	AICR
<b>Additional data</b>							
Total volume of reactors	m <sup>3</sup>	0.239	0.239	0.239	0.388	0.481	0.440
Points with equal configuration	%	11.11	6.84	17.13	5.13	21.20	15.26

The solutions are well distributed among the possible structural alternatives, as every possibility in terms of compressors is used, and the same occurs for the reactors. Though, the AQCR does not achieve competitive results in comparison to the AICR and no optimal point concerns this configuration.

### V.5.2.1. Distribution of variables across their boundaries

One of the benefits of using the superstructure optimization methodology is the great amount of data available. After several thousands of evaluations, using the historic data of feasible solutions as a source of information allows to obtain certain knowledge on a search preference in the wide range of possible values for each optimization variable.

With this purpose, Figure V-4 represents the distribution of the incidence frequency for every variable of interest, all along the search space, for both the feasible and the optimal solutions. The structural alternatives correspond to those described by the optimal solutions in Table V-8, meaning that the direct cooling configuration is removed, as it is not represented by any optimal point.

Also, for every optimization variable, only the feasible solutions where it has an impact is included. This means, for example, that the temperature inlet in the second reactor is only considered in those solutions using at least two reactors. This is why the configuration “1 – Absent” is neither represented for temperatures in reactors 2 and 3, nor for lengths 2 and 3, as only 1 reactor is implemented. The bars represented as “Optimal” indicate the frequency for the Pareto points only.

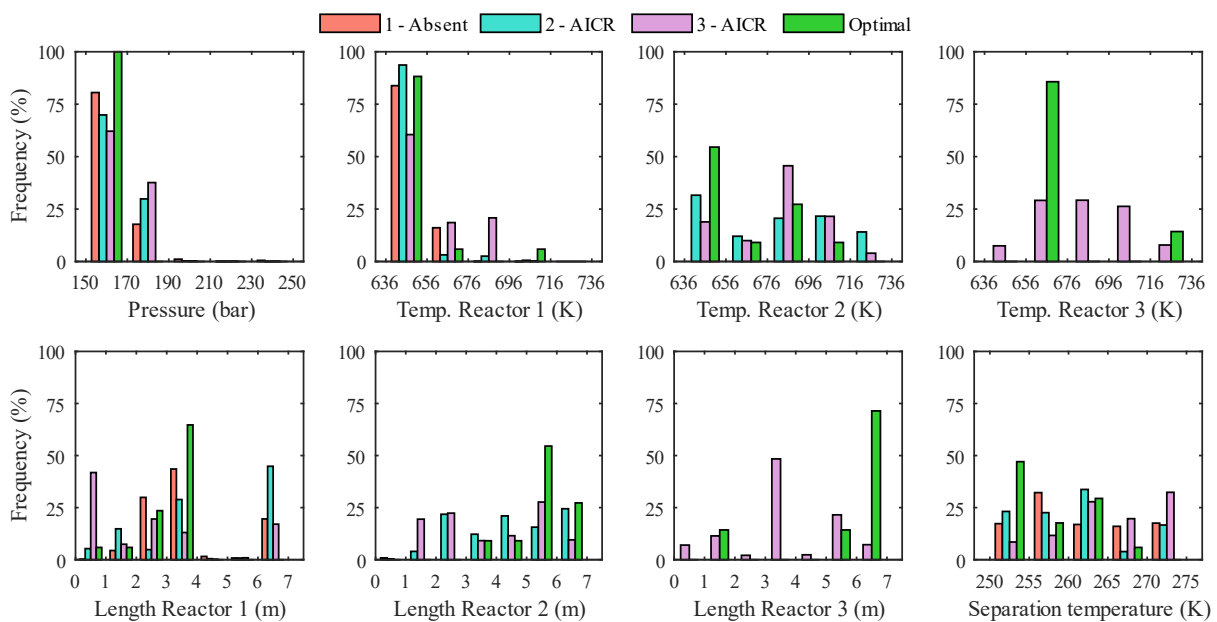


**Figure V-4.** Histogram representing the incidence frequency for every optimization variable, for the Fe-based case. Data corresponds to every reactor configuration represented by the optimal solutions (1 – Absent, 2 – AICR, 3 – AICR). The AQCR configuration and the variables of splitting ratio have not been included. The data considers only the solutions where the variable has an influence due to the structural arrangement.

From the distribution in the solutions, it can be inferred that the optimality regarding the pressure of the system tends to the lower boundary of 150 bar, as it is evident not only in the histogram, but also in Table V-8. The highest pressure in the optimal solutions is 156.76 bar. In the same trend goes the preferential selection of the lower bound for the temperature inlet at the first reactor, which is 636 K. Regarding the temperature at the second and third reactors, it gets more distributed over the range of values for all the solutions.

In what concerns the length of the reactors, the first one has a preferential selection on the middle range of values, around 3 and 4 m. For the second and the third units, the length preference is moved towards higher values. This trend is explained when analysing the H<sub>2</sub> conversion profiles in the reactors and its relationship with the thermodynamic equilibrium. In fact, the more reactors are included, the higher the length is required, as the NH<sub>3</sub> mole fraction in the process stream increases and the operating conditions are closer to the equilibrium. To achieve higher H<sub>2</sub> conversions, more catalyst and, therefore, larger reactors are needed. This aspect is further explained in the next section.

Regarding the separation temperature, there is not an evident preference over the range of values. This might be a result of the absence of the refrigeration cycle calculation, as the removed heat duty only has an effect on the energy efficiency penalty parameter of the thermal energy loss from the system. However, lower separation temperatures favour the ammonia production, allowing to reduce the LCOA.

In any case, studying the range of variables and the placement of the feasible solutions suggests possible reductions of the search space if further refinement of the optimal solutions is required, or if other optimizations including these configurations are foreseen.

### V.5.2.2. Hydrogen conversion profiles in the reactors

To explain the behaviour of the distribution of solutions it is necessary to study the conversion profiles on each catalytic section, as shown in Figure V-5.

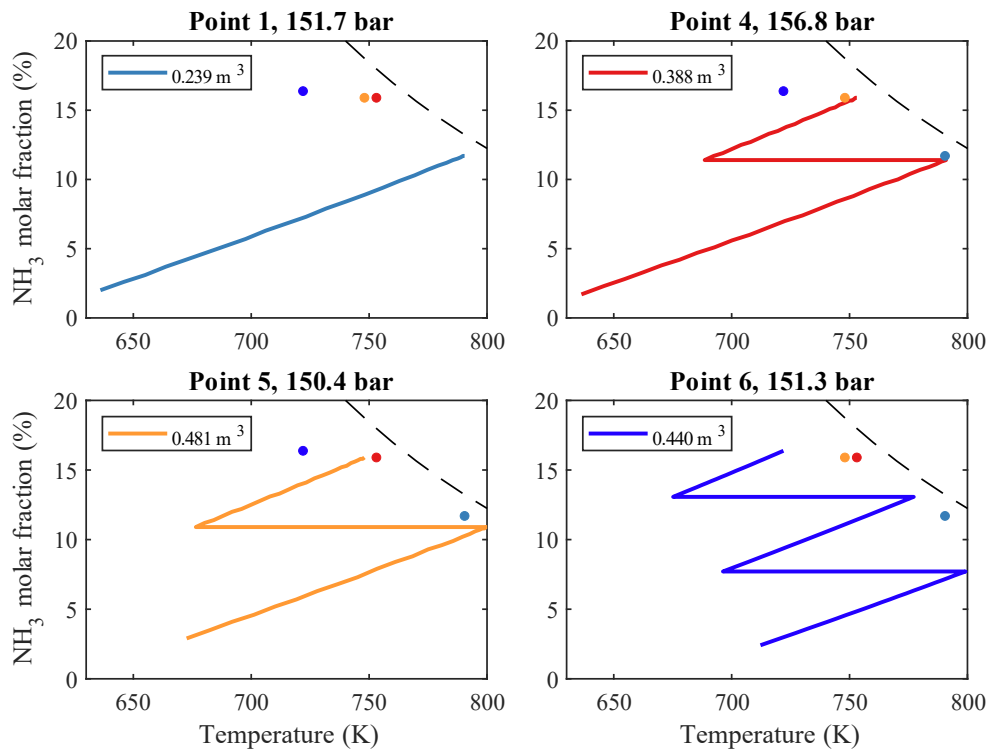


**Figure V-5.** Trajectories on the reactors for the optimal points of the Fe-Based case shown in Table V-8, representing the evolution of the ammonia molar fraction as a function of the temperature. Points 1, 2 and 3 have similar results, therefore only point 1 is represented. Data markers indicate the final conversion for the other solutions with the respective colours. The total volume of the reactors is indicated for each solution.

On the first section of the reactors, the temperature rises considerably while the H<sub>2</sub> conversion occurs and the NH<sub>3</sub> mole fraction increases. The further the reaction advances, the closer the mixture conditions

tend to the thermodynamic equilibrium, as seen in Figure V-5. For points 1, 2 and 3, which have the same reactor configuration and similar operating conditions, the profiles are identical. In fact, for these points only the number of compressors changes, but this does not affect the extent of reaction. These configurations achieve a similar final  $\text{NH}_3$  molar fraction of 11.7 %.

Following, points 4 and 5, using two reactors, have two different trajectories, but reach a similar concentration of ammonia. While point 4 has a lower temperature at the inlet stream of the first reactor than point 5 (636.3 K against 672.6 K), the cooling trajectory is more important for point 5, with a greater temperature difference. This allows for the solution of point 4 to use a higher inlet temperature on the second reactor. In the end, both configurations achieve a similar conversion, with a final ammonia composition of 15.9 %. Nevertheless, the total volume of reactors for point 4 is 20 % lower, with an increase in pressure of only 6 bar.

The last configuration, with three reactors, does not show a considerable improvement regarding the solutions using two reactors. The final  $\text{NH}_3$  molar fraction is 16.4 %, just 0.5 points above the best conversion obtained with two reactors. This suggests that a third catalytic section should be avoided, regarding only the conversion per pass. Evidently, to support this advice, a further analysis on the trade-off between economics and productivity is necessary.

### V.5.2.3. Influence of the structure on the economic criteria

Including any additional equipment or avoiding its use within the process has multiple effects across the system. An extra compressor can induce higher investment costs but favours the energy efficiency due to the decrease on the required mechanical work. In the same manner, a supplementary reactor might allow higher  $\text{H}_2$  conversion and ammonia production, although its investment and maintenance costs can hinder the economic gain observed with better productivities. In the figure depicted below, the share of every expenditure across the process is shown as a percentage to the corresponding category, either capital or operational expenses.

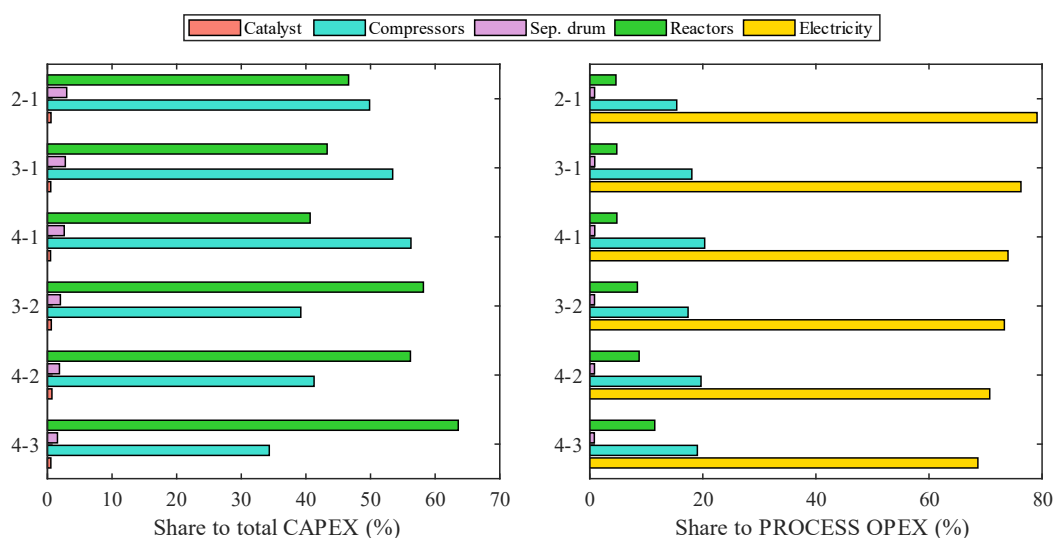


**Figure V-6.** Share of expenditures according to the equipment and materials type, to the total CAPEX and the process OPEX, for the Fe-based case. In the process OPEX, the raw materials cost is not included, which corresponds to around 95 % of the global OPEX. The cases are referred to the Compressor-Reactor configuration, as seen in Table V-8 and Table V-9.

For the CAPEX, the catalyst, compressors, separation drum and reactors are included. For the OPEX, instead of the catalyst, the expenses on electricity are shown. They correspond to every optimal solution, as shown in Table V-8, here referred according to their configuration *Compressors-Reactors*. As a remark, in the OPEX section, the cost of raw materials (H<sub>2</sub> and N<sub>2</sub>) is not included, mainly due to the high cost of hydrogen, which represents around 95 % of the OPEX. Therefore, the OPEX shown is referred as *process OPEX*.

Evidently, the compressors and reactors are the majority of the investment expenditures. The cost of the Fe-based catalyst is less than 1 % for every case, while the cost of the separation drum does not exceed 6 %. As the structural alternatives are related to the number of compressors and reactors, their cost proportion varies between the solutions.

For the configurations 2-1, 3-1 and 4-1, where only the number of compressors vary, its share to the total CAPEX goes from 50 to 57 %, while the part for the reactors decreases from 47 to 40 %. However, the impact when a supplementary reactor is used is more evident. Changing from a configuration 4-1 to a 4-2, increases the share of the reactor from 40 to 56 %. This trend explains the behaviour seen on the structure distribution maps shown in Figure V-3, where the number of reactors has a predominance over the number of compressors.

Beyond the share of every type of expenditure over the capital and operational categories, the absolute values of these indicators give further information on the impact over the KPIs. Consider the information presented in Table V-9. To compare the CAPEX and OPEX of the optimal solutions, it is necessary to determine the annualized CAPEX, as the OPEX correspond to the expenditures per year of exploitation. Here it is interesting to consider only the cost of the process to produce the ammonia, *process LCOA*, as the raw material cost is constant across the different solutions.

Point 1 is the reference case for the analysis of the impact when including additional compressors, while Point 3 is the reference in the analysis concerning the number of reactors. These points are used as references as their structural differences concern only the variable in study. To understand the impact of the number of compressors, the number of reactors remains constant, and vice versa.

**Table V-9.** Parameters for the calculation of the economic performance indicator, for the optimal solutions of the Fe-based case.

Case	Ammonia production	Annualized CAPEX	Process OPEX	Global OPEX	Process LCOA	Global LCOA
	t/y	€/y	€/y	€/y	€/t	€/t
Point 1: 2-1	3 893.7	269 694	88 680	2 663 381	92.04	753.3
Point 2: 3-1	3 894.6	290 466	85 959	2 660 659	96.65	757.8
Point 3: 4-1	3 894.6	309 254	85 688	2 660 389	101.41	762.5
Point 4: 3-2	3 953.7	404 441	91 348	2 666 049	125.40	776.6
Point 5: 4-2	3 936.8	430 586	90 603	2 665 303	132.39	786.4
Point 6: 4-3	3 947.0	515 319	93 232	2 667 933	154.18	806.5
<b>Relative variations for additional compressors regarding Point 1: 2-1</b>						
Point 2: 3-1	0.02 %	7.70 %	- 3.07 %	- 0.10 %	5.01 %	0.59 %
Point 3: 4-1	0.02 %	14.67 %	- 3.37 %	- 0.11 %	10.18 %	1.23 %
<b>Relative variations for additional reactors regarding Point 3: 4-1</b>						
Point 5: 4-2	1.08 %	39.23 %	5.74 %	0.18 %	30.55 %	3.13 %
Point 6: 4-3	1.35 %	66.63 %	8.80 %	0.28 %	52.04 %	5.77 %

Recalling the definition of the LCOA, it is the sum of the capital and operational expenditures, divided by the total ammonia production. The OPEX, also referred as *global OPEX*, can be separated into *process OPEX* and *raw materials OPEX*. Then, the LCOA depends on the share of annual CAPEX, process OPEX and raw materials OPEX to the NH<sub>3</sub> annual production.

Concerning the impact of additional compressors, Points 1, 2 and 3 have an almost identical ammonia production, while the annualized CAPEX increases up to 14.7 % due to the additional investment. On the contrary, the process OPEX decreases by 3.4 %, basically because the mechanical work is reduced, while the global OPEX has almost no variation. If only the process contribution to the LCOA is considered, the use of 3 and 4 compressors induces a final increase of 5 and 10.2 %. This repercusses on a final increase of 0.6 and 1.2 % on the global LCOA. As these variations only concern the number of compressors, its interest is more evident in the gains on the energy efficiency, which is discussed in the next subsection.

Regarding the use of additional reactors, the impact on the economic criterion is larger. Even if the productivity increases, in 1.08 and 1.35 % when using 2 and 3 reactors, the annualized CAPEX is strongly impacted, with growths of 39.2 and 66.6 %, respectively. For the process cost, the second reactor implies around 31 % of increase, while a third unit doubles this value to 52 %. Overall, the effect of the gain on the productivity is overshadowed by the increase in annualized CAPEX, resulting in an increase in the global LCOA of 3.2 and 5.8 % for the use of 2 and 3 reactors, respectively.

#### V.5.2.4. Influence of the structure on the energy criteria

Analogously as in the structural impact on the economic criteria, the effect over the energy objective function and additional parameters is analysed. It concerns the total ammonia production and its energy content, the mechanical and energy balances, and the specific consumption of energy. Table V-10 presents the relevant data for this analysis.

*Table V-10. Parameters for the calculation of the energetic performance indicator, for the optimal solutions of the Fe-based case.*

Case	NH <sub>3</sub> energy produced kW	Mechanical power kW	Thermal power lost kW	Energy efficiency %	Specific mec. power kWh/kg	Specific therm. loss kWh/kg	Power ratio NH <sub>3</sub> /H <sub>2</sub> kW/kW
Point 1: 2-1	2 514.71	203.94	755.7	54.57	0.419	1.553	0.831
Point 2: 3-1	2 515.23	190.57	743.2	55.20	0.391	1.527	0.831
Point 3: 4-1	2 515.23	184.27	737.2	55.50	0.379	1.514	0.831
Point 4: 3-2	2 553.42	194.73	755.5	55.94	0.394	1.529	0.844
Point 5: 4-2	2 542.51	186.32	738.0	56.29	0.379	1.500	0.840
Point 6: 4-3	2 549.11	186.05	741.5	56.39	0.377	1.503	0.843
<b>Relative variations for additional compressors regarding Point 1: 2-1</b>							
Point 2: 3-1	0.02 %	- 6.56 %	- 1.66 %	1.16 %	- 6.58 %	- 1.68 %	0.02 %
Point 3: 4-1	0.02 %	- 9.65 %	- 2.45 %	1.70 %	- 9.67 %	- 2.47 %	0.02 %
<b>Relative variations for additional reactors regarding Point 3: 4-1</b>							
Point 5: 4-2	1.08 %	1.11 %	0.11 %	1.42 %	0.03 %	- 0.97 %	1.08 %
Point 6: 4-3	1.35 %	0.97 %	0.58 %	1.60 %	- 0.37 %	- 0.75 %	1.35 %

The energy produced in form of ammonia is calculated from the Low Heating Value (LHV) and the mass production per hour. As before, the solutions 1, 2 and 3, present approximately the same production. However, their main difference concerns the mechanical power consumption. Adding a second compressor reduces the power needs in 6.6 %, while a third compressor allows to save up to 9.7

% of power. The thermal power losses from the process decrease mainly due to the intercooling stages on the compressors. As a result of using 2 and 3 compressors, the energy efficiency indicator increases in 1.2 and 1.7 %, respectively.

Passing to the analysis for the number of reactors, its impact is reflected in the amount of energy content in produced ammonia, which increases by at least 1 %. Even if the mechanical power and the thermal energy losses increase, the energy efficiency grows, reaching 1.6 % when 3 reactors are implemented. This suggests that the energy production in ammonia overcomes the losses associated to mechanical and thermal energy increase. Beyond these results, the lowest specific energy consumption is achieved with the use of 4 compressors, for point 6, while the lowest specific thermal loss from the system is seen for solution of point 5.

The stoichiometric chemical reaction for ammonia synthesis has a relation of 1.5 mol H<sub>2</sub> per mol of NH<sub>3</sub>. For a complete hydrogen conversion, for 363.2 MJ contained in the 1.5 mol of H<sub>2</sub>, 316.8 MJ are produced in 1 mol of NH<sub>3</sub>, according to their LHVs (i.e., 120.1 MJ/kg H<sub>2</sub> and 18.6 MJ/kg NH<sub>3</sub>). This indicates that the quotient between produced and supplied energy is 0.872.

From the amount of power supplied in form of hydrogen, 3 026.5 kW, and the ammonia production reported in Table V-10, the power ratio between NH<sub>3</sub> and H<sub>2</sub> is, at least 0.831 and in the best of cases 0.845. Regarding the theoretical complete conversion, the solutions offer at least 95.3 % of energy conversion, which is directly related to the global hydrogen conversion of the process.

Undoubtedly, the analysis of the influence of the structure on the KPIs is affected by the operating conditions across the process. As the optimal solutions present conditions relatively close for most of the cases, as the synthesis pressure or some of the temperatures for the reactors, the analysis remains conservative and gives certain notions on the effect of changing the process structure. The choice of the best structural alternative is presented in section V.5.4, in conjunction with the Ru-based case optimal.

### **V.5.3. Ru-based case**

The different analyses previously presented for the Fe-based case are also performed on the solutions for the Ru-based case. Therefore, the description is resumed to the basic details, as it is analogous to the other case.

The optimization of the Superstructure I for the Ru-base case allowed to obtain a total number of evaluations of 42 522, from which 28 580 (67.2 %) are feasible solutions and 34 of them are considered optimal solutions. Concerning the Pareto points, the LCOA varies from 754 to 804 €/t of NH<sub>3</sub>, while the energy efficiency is found between 55.3 and 58.1 %.

As can be seen in Figure V-7, the density of solutions is greater than for the Fe-based case. The total number of evaluations is around the double. This is mainly due to a longer time of calculation, as the Ru-based case reached the stopping criterion of non-evolution of the optimal solutions after a longer calculation time. While the Fe-based case spent 59 hours, the Ru-based case doubled this time, up to 143 hours, as indicated in Table V-6.

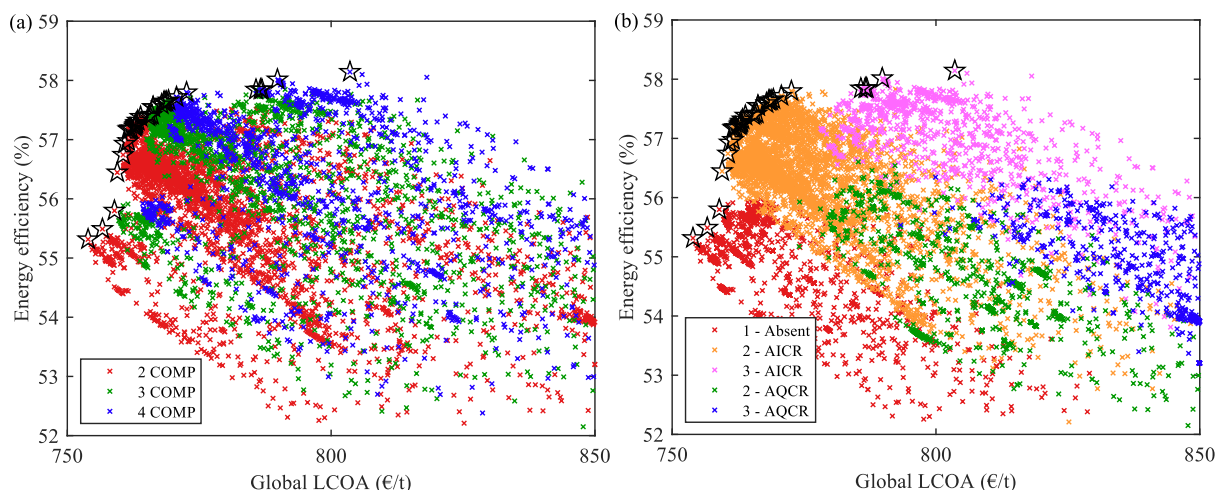


**Figure V-7.** Distribution of the objective functions for the feasible and optimal solutions for the Ru-base case, according to the structural variables position. **(Left)** Number of compressors, varying from 2 to 4. **(Right)** Reactor configuration, varying from 1 to 3 reactors, with absent, indirect (AICR) or direct (AQCR) cooling configuration. The 34 optimal solutions are represented by the  $\star$  black stars.

Similar to the Fe-based case, the dominant structural variable regarding the distribution of process alternatives is the reactor configuration. As well, the number of compressors seems to be distributed for each reactor configuration, which is more evident in the 2 – AICR zone of the Pareto Front. This indicates that the choice between the number of compressors has less effect on the global LCOA than the selection of the reactor configuration.

Furthermore, when comparing in subplot (b) the most energy-efficient optimal point of the *1-Absent* configuration (1 reactor, 4 compressors) with the least energy-efficient optimal point of the *2-AICR* configuration (2 reactors, 2 compressors), a steep difference is identified. Between them, there exists 0.6 points of difference in the energy efficiency indicator, while the LCOA changes only in 0.6 €/t. This shows an improvement on the energy efficiency for almost an equal ammonia production cost.

From the figures above one can suggest that the most prominent configuration on the Pareto front, showing a good trade-off between cost and energy efficiency, is the AICR configuration with 2 catalytic reactors. This is supported by the fact that this structural combination is obtained in 26 optimal solutions among the total of 34 (76.5 %).

Table V-11 shows the values of the KPIs, the optimization variables, and the number of feasible solutions with the corresponding structural configuration for the selected points for analysis, but the complete data for every optimal solution is available in the Appendix D, in section X.4. When multiple solutions are obtained for the same process structure, the chosen points correspond to the median among them.

**Table V-11.** Results of the KPI and the optimization variables for the optimal solutions of the Ru-based case. One point of each optimal configuration is selected. \*The split ratios for the AQCR splitters are omitted, as no optimal solutions were obtained for this cooling configuration.

Key Performance Indicator	Units	Point 1	Point 2	Point 3	Point 4	Point 5	Point 6
Global LCOA	€/t	759.1	765.8	771.0	775.8	788.9	789.8
Energy efficiency	%	55.49	57.22	57.59	57.80	57.84	57.85
<b>Variables</b>							
Pressure	bar	89.39	79.83	77.76	75.88	72.17	93.92
Inlet temperature at 1 <sup>st</sup> reactor	K	646.66	665.93	666.10	665.11	710.32	691.85
Inlet temperature at 2 <sup>nd</sup> reactor	K	-	651.57	653.96	654.92	678.00	689.95
Inlet temperature at 3 <sup>rd</sup> reactor	K	-	-	-	-	664.99	669.67
Length of 1 <sup>st</sup> reactor	m	3.54	1.86	1.82	1.87	0.60	1.10
Length of 2 <sup>nd</sup> reactor	m	-	5.25	5.20	5.23	1.97	2.23
Length of 3 <sup>rd</sup> reactor	m	-	-	-	-	3.59	5.01
Separation temperature	K	253.87	253.01	253.06	253.00	256.29	253.06
<b>Structural configuration</b>							
Number of compressors	-	2	2	3	4	3	4
Number of reactors	-	1	2	2	2	3	3
Cooling configuration	-	Absent	AICR	AICR	AICR	AICR	AICR
<b>Additional data</b>							
Total volume of reactors	m <sup>3</sup>	0.508	0.800	0.830	0.874	0.815	0.666
Total points in equal configuration	%	8.74	26.41	23.75	6.38	5.12	9.36

For the optimal solutions, the structural configurations consider every possible number of compressors and reactors, while only the AICR is obtained for multiple-reactor solutions. Regarding the values of the variables, they are more diverse than in the Fe-based case, and their distribution is studied as follows.

### V.5.3.1. Distribution of variables across their boundaries

The incidence frequency for each optimization variable is shown in Figure V-8. Again, only the solutions where the variables have an impact are considered.

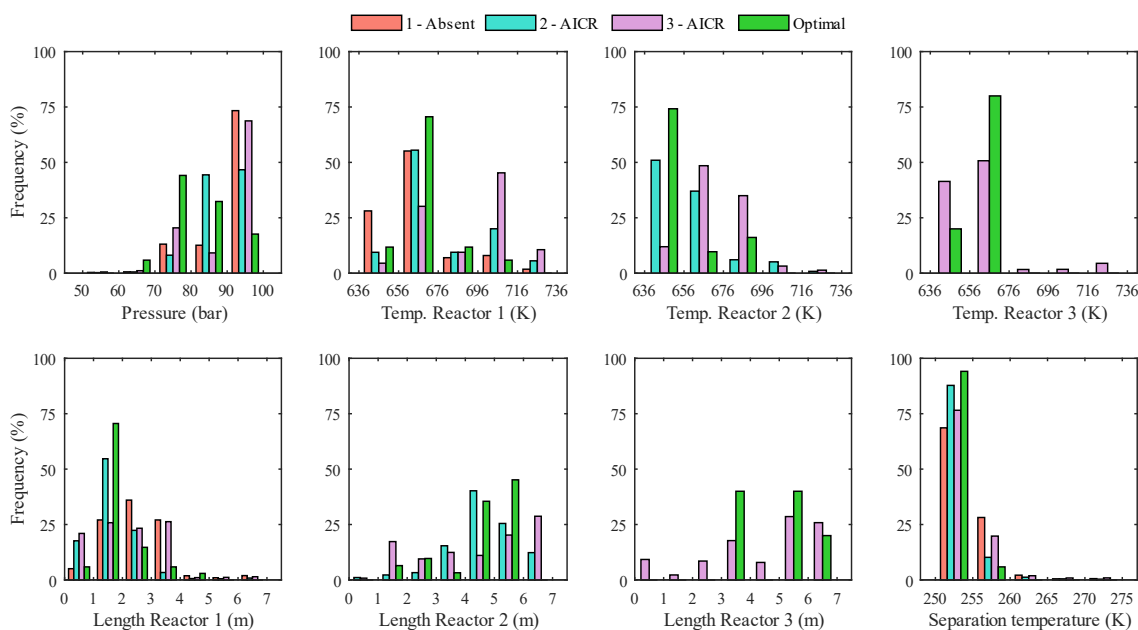


**Figure V-8.** Histogram representing the incidence frequency for every optimization variable, for the Ru-based case. Data corresponds to every reactor configuration represented by the optimal solutions (1 – Absent, 2 – AICR, 3 – AICR). The AQCR

*configuration and the variables of splitting ratio have not been included. The data considers only the solutions where the variable has an influence due to the structural arrangement.*

Regarding the trends observed for the Fe-based case in Figure V-4, the main difference concerns the synthesis pressure, as the boundaries for both cases are completely different. The ruthenium catalyst has an operating window at lower pressures, with a maximum level of 100 bar, while the iron catalyst is designed to operate at least at 150 bar. Here, the optimal solutions have a good distribution over the range of pressures, with the feasible solutions tending towards the upper boundary and being absent at pressures below 60 bar.

The temperature in the first and second reactors have a wide distribution among the solutions. For the optimal points, the majority tend to the 656 – 676 K range in the first reactor, while the preference goes towards lower temperatures on the second unit, from 636 to 656 K. The effect of the temperatures is discussed in the next section.

Concerning the length of the reactors, the first catalytic section has the majority of solutions at lengths lower than 2 m, suggesting a fast temperature increment towards the thermodynamic equilibrium. For subsequent reactors, the distribution is displaced towards higher lengths.

Finally, the separation temperature for this optimization found a preference for the lowest range of values. This is mainly due to the lower synthesis pressures in the process compared to the Fe-based case. As it is known, lower pressures require lower separation temperatures to achieve an equivalent ammonia production.

As previously evoked, for the ruthenium scenario, the 2 – AICR configuration has a substantially pronounced location in the Pareto Front compared to other structural alternatives, which hinders in some way the interest of the other optimal solutions. Special attention is given to this structural configuration for the following analyses.

#### **V.5.3.2. Hydrogen conversion profiles in the reactors**

The diagrams presented in Figure V-9 show the profiles of the NH<sub>3</sub> molar fraction and the temperature evolution in the reactors. The profiles represent the trajectories of the optimal solutions declared in Table V-11, which are shown according to the number of reactors used. For each data set, the corresponding synthesis pressure and total volume of reactor is specified.

The solution of Point 1 using a unique reactor, at 89.4 bar and 0.51 m<sup>3</sup> of volume, reaches an NH<sub>3</sub> concentration at the outlet stream of the reactor of 10.1 %, indicating the proximity to the thermodynamic equilibrium. Next, the 3 optimal solutions using two reactors, Points 2, 3 and 4, achieve nearly the same molar fraction of 13.4 %, as the pressure among them varies no more than 4 bar, and the reactor volumes are similar. Only the trajectory for Point 2 is shown, as the corresponding to points 3 and 4 are similar, according to the temperatures and volumes of reactors given in Table V-11.

In what concerns the configurations with three reactors, the solution of Point 5 has an almost similar performance than the solutions with two reactors. The final NH<sub>3</sub> molar fraction is 13.6 %, slightly higher than for points with 2 reactors. However, the pressure is at least 3.7 bar lower, for a similar volume of reactors. For this solution, the temperature decrease for the inlet streams of each reactor is more evident,

as the profiles is driven towards the left, passing from 710 to 678 and 665 K, which goes along with the expected behaviour for multiple adiabatic reactors.

On the other hand, Point 6 presents the best conversion performance as it is related to the highest pressure among the optimal points (93.9 bar). For a total volume of  $0.666 \text{ m}^3$ , it achieves a final  $\text{NH}_3$  molar fraction of 15.7 %.

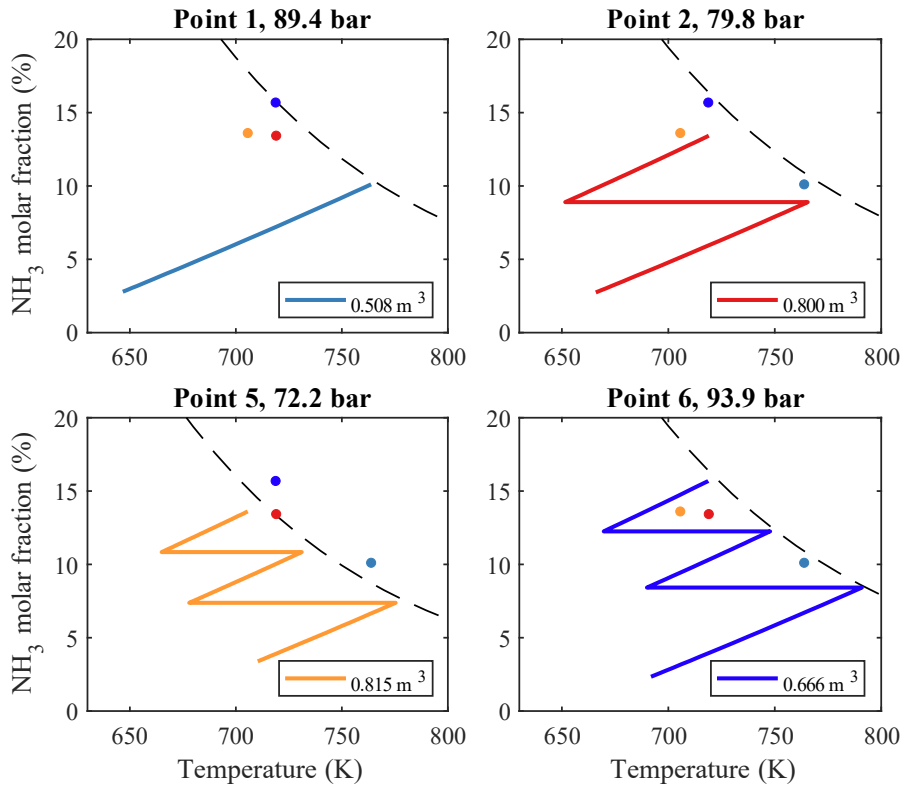


**Figure V-9.** Trajectories on the reactors for the optimal points of the Ru-Based case shown in Table V-11, representing the evolution of the ammonia molar fraction as a function of the temperature. Points 2, 3 and 4 have similar results, therefore only point 2 is represented. Data markers indicate the final conversion for the other solutions with the respective colours. The total volume of the reactors is indicated for each solution.

It is necessary to highlight the existing displacement of the inlet temperature when multiple reactors are used. It can be observed that the subsequent reactors have always a lower inlet temperature than the precedent unit. This is explained by the thermodynamic equilibrium for a given pressure. For higher  $\text{H}_2$  conversions, and therefore, for higher  $\text{NH}_3$  mole fractions in the mixture, the optimal temperature progression is displaced towards lower temperatures. Then, the inlet temperature of the following reactors should decrease, to avoid being in the vicinities of the equilibrium. Further details on this subject are covered in section V.7, where a comparison of the adiabatic and the autothermal configurations is performed.

### V.5.3.3. Influence of the structure on the economic criteria

Following the analysis of the impact of additional operating units on the economic KPI, for the Ru-based case shown in Figure V-10, the presence of the catalyst has higher impact than in the Fe-based case. Due to the cost of this material, its share on the total CAPEX increases from less than 1 % to more than 4 % and up to 7 % in some cases.

Its impact is a direct result of three parameters: the pressure of the system, the total volume of reactors, and the price of the material. Regarding the latter in comparison to the iron catalyst, it is around 20 times more expensive per kilogram. Recalling the hypothesis considered in Chapter IV, the cost of the iron catalyst is 15.5 \$/kg, while it corresponds to 321 \$/kg for the ruthenium. The pressures for the Ru-based case are considerably lower than for the iron catalyst. In the extreme of cases is less than a half, as can be observed between point 6 for the Fe-based case (150 bar) and point 5 of the Ru-based case (72.2 bar), being the latter just 48 % of the former value of pressure.

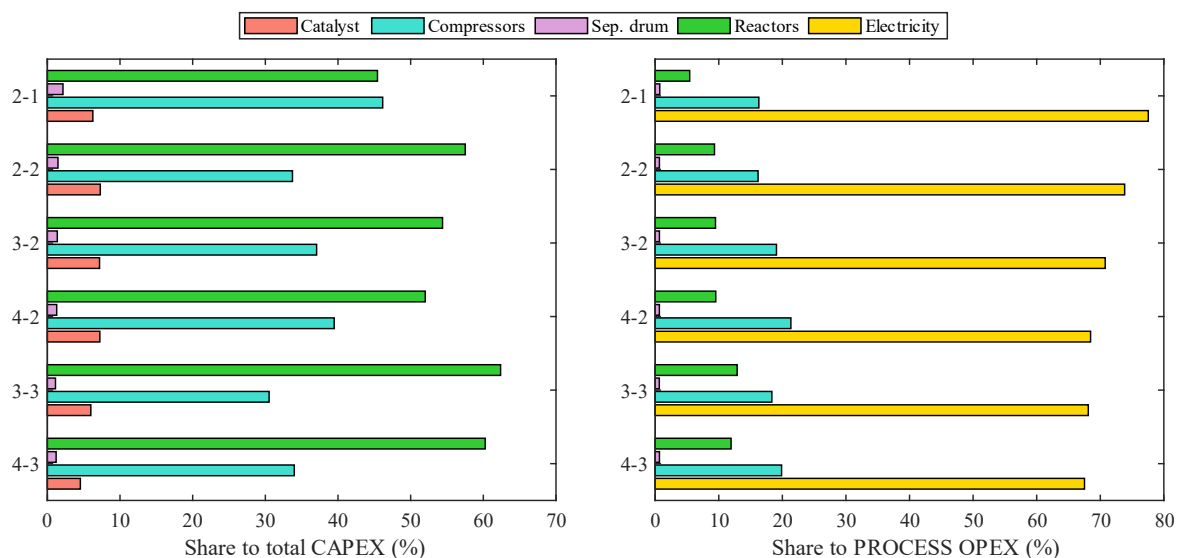


**Figure V-10.** Share of expenditures according to the equipment and materials type, to the total CAPEX and the process OPEX, for the Ru-based case. In the process OPEX, the raw materials cost is not included, which corresponds to around 97 % of the global OPEX. The cases are referred to the Compressor-Reactor configuration, as seen in Table V-11 and Table V-13.

To achieve competitive levels of H<sub>2</sub> conversion at such pressures, the volume of the reactors is significantly higher for the ruthenium catalyst, which in the majority of cases doubles the volume of the corresponding Fe-based cases with the same number of reactors. Nevertheless, the total catalytic mass remains lower for the Ru-based case due to the lower density of the material, which is around a fourth of the density of the iron catalyst (800 kg/m<sup>3</sup> for the Ru-based and 3 000 kg/m<sup>3</sup> for the Fe-based catalyst).

In this regard, in Table V-12 the main parameters for every retained optimal solution of both optimizations are presented and discussed next.

**Table V-12.** Comparison of the pressures and total volume of reactors, amount of catalyst and annualized expenditure. The densities of the catalysts are 3 000 and 800 kg/m<sup>3</sup> for the Fe- and the Ru-based, respectively.

Parameter	Units	Fe-based case					
		Point 1	Point 2	Point 3	Point 4	Point 5	Point 6
Pressure	bar	151.7	151.8	151.8	156.8	150.4	150.0
Number of reactors	-	1	1	1	2	2	3
Volume of reactors	m <sup>3</sup>	0.239	0.239	0.239	0.388	0.481	0.697
H <sub>2</sub> conversion per pass	%	17.7	17.7	17.8	24.9	23.1	25.8
Mass of catalyst	kg	717.2	717.2	716.7	1 164.7	1 444.1	2 090.4
Annual cost of catalyst	€/y	1 496.8	1 497.5	1 497.5	2 429.8	3 013.2	4 364.3
Share of catalyst to CAPEX	%	0.56	0.52	0.48	0.60	0.70	0.78
Parameter	Units	Ru-based case					
		Point 1	Point 2	Point 3	Point 4	Point 5	Point 6
Pressure	bar	89.4	79.8	77.8	75.9	72.2	93.9
Number of reactors	-	1	2	2	2	3	3

## Chapter V: Optimization of the Haber-Bosch process through reactor configurations and catalyst selection

Volume of reactors	m <sup>3</sup>	0.508	0.800	0.830	0.874	0.815	0.666
H <sub>2</sub> conversion per pass	%	13.7	19.4	19.0	18.7	18.6	23.6
Mass of catalyst	kg	406.2	639.7	664.1	699.3	652.0	532.8
Annual cost of catalyst	€/y	16 070.7	25 361.1	26 328.8	27 735.5	25 860.9	21 124.3
Share of catalyst to CAPEX	%	6.26	7.29	7.18	7.22	5.99	4.54

When comparing the solutions between the optimization cases, the low pressures on the Ru-based case are not enough to reach the same level of H<sub>2</sub> conversion as in the Fe-based cases. Moreover, the relation between the mass of catalyst in the two scenarios is inverse to the annual cost of the material. For lower mass of catalysts in the Ru-based case, the cost is higher than in the Fe-based case, due to the price per kilogram. In the end, for annual costs of catalyst around 10 times higher in the Ru-based case, the total share of the catalyst to the CAPEX is at least 4.5 %.

One could think that the Fe-based case is preferred in terms of productivity, which is indeed true, as higher hydrogen conversions are obtained. However, the economic and energetic gain obtained in the Ru-based case with slight lower productivities overcomes the losses in ammonia production. This point is developed in the next sections.

For this case, due to the lower pressures on the process, the share of compressors in the CAPEX is smaller, as seen in Figure V-10. As previously discussed for the Fe-based case, compressors and reactors were predominant depending on the configuration. In this scenario, the only case where the compressors share is above the share of reactors is for the configuration 2-1. In the rest of cases, the cost of the reactors is predominant. The contrary behaviour occurs in the share of OPEX. The compressors have higher maintenance costs than the reactors. The electricity remains prevalent for all the scenarios.

**Table V-13.** Parameters for the calculation of the economic performance indicator, for the optimal solutions of the Ru-based case.

Case	Ammonia production	Annualized CAPEX	Process OPEX	Global OPEX	Process LCOA	Global LCOA
	t/y	€/y	€/y	€/y	€/t	€/t
Point 1: 2-1	3 822.3	256 676	70 331	2 645 032	85.55	759.1
Point 2: 2-2	3 908.2	348 048	70 255	2 644 956	107.03	765.8
Point 3: 3-2	3 904.0	366 480	68 780	2 643 480	111.49	771.0
Point 4: 4-2	3 901.9	383 896	68 587	2 643 288	115.96	775.8
Point 5: 3-3	3 898.0	432 044	68 415	2 643 115	128.39	788.9
Point 6: 4-3	3 946.1	464 921	76 828	2 651 530	137.29	789.8
<b>Relative variations for additional compressors regarding Point 2: 2-2</b>						
Point 3: 3-2	- 0.11 %	5.30 %	- 2.10 %	- 0.06 %	4.17 %	0.68 %
Point 4: 4-2	- 0.16 %	10.30 %	- 2.37 %	- 0.06 %	8.34 %	1.30 %
<b>Relative variation for an additional reactor regarding Point 3: 3-2</b>						
Point 5: 3-3	- 0.15 %	17.89 %	- 0.53 %	- 0.01 %	15.16 %	2.32 %

In what concerns the impact of the process structure on the entirety of the economic balance, two points are used as reference for comparison. Point 2, with two compressors and two reactors is the basis to compare the influence of the compressors with Points 3 and 4, both with two reactors, but with 3 and 4 compressors, respectively. For the reactor influence on the economic parameters, Point 3 is used as reference, with 3 compressors and 2 reactors, and is compared with solution 5.

Regarding the number of compressors, the ammonia production remains practically unchanged, while the annualized CAPEX increases up to 10.3 %. The impact on the process LCOA is seen as growths of

4.2 and 8.3 % for 2 and 3 compressors, respectively, but the final impact on the global LCOA is less than 1.3 %. The relevance of the number of compressors is more representative in the energy balance of the next section.

For the number of reactors, the relative variation needs to be analysed with care. In fact, among the optimal solutions selected for a constant number of compressors, the pressure and the temperatures on the reactors vary considerably, which can bias the analysis. A proper comparison should be carried out for similar operating conditions. What can be seen from the addition of a third reactor is the strong increase in the annualized CAPEX and the process LCOA, with more than 15 percent points of growth, while the ammonia production is reduced in 0.15 %. These results are not conclusive, as it should be expected that an additional reactor favours the increase on the NH<sub>3</sub> production.

#### V.5.3.4. Influence of the structure on the energy criteria

The structural impact over the economic criteria is evaluated on the basis of the NH<sub>3</sub> yearly production and its energy content, the mechanical and thermal energy balances, as well as their specific consumption. Table V-14 presents the relevant data for this analysis.

*Table V-14. Parameters for the calculation of the energetic performance indicator, for the optimal solutions of the Ru-based case.*

Case	NH <sub>3</sub> energy produced kW	Mechanical power kW	Thermal power lost kW	Energy efficiency %	Specific mec. power kWh/kg	Specific therm. loss kWh/kg	Power ratio NH <sub>3</sub> /H <sub>2</sub> kW/kW
Point 1: 2-1	2 468.60	158.56	704.5	55.49	0.332	1.475	0.816
Point 2: 2-2	2 524.03	150.79	709.3	57.22	0.309	1.452	0.834
Point 3: 3-2	2 521.31	141.52	699.9	57.59	0.290	1.434	0.833
Point 4: 4-2	2 519.99	136.53	695.1	57.80	0.280	1.425	0.833
Point 5: 3-3	2 517.43	135.47	691.7	57.84	0.278	1.419	0.832
Point 6: 4-3	2 548.49	150.80	713.9	57.85	0.306	1.447	0.842
<b>Relative variations for additional compressors regarding Point 2: 2-2</b>							
Point 3: 3-2	- 0.11 %	- 6.15 %	- 1.32 %	0.66 %	- 6.05 %	- 1.21 %	- 0.11 %
Point 4: 4-2	- 0.16 %	- 9.46 %	- 2.01 %	1.01 %	- 9.32 %	- 1.85 %	- 0.16 %
<b>Relative variation for additional reactor regarding Point 3: 3-2</b>							
Point 5: 3-3	- 0.15 %	- 4.27 %	- 1.17 %	0.43 %	- 4.13 %	- 1.02 %	- 0.15 %

The highest ammonia production is observed for Point 6, the configuration with 3 reactors and operating at 93.9 bar. In decreasing order, the solution of Point 2 which has 2 reactors, achieves a production around 1 % lower, even if the process operates at 79.7 bar, 15.1 % lower. The compensation related to the pressure decrease is given by the increase in the reactor volume, which is 20 % higher than point 2.

The principal effect of the increase in the compressors, seen between Point 2 to 4, is the reduction in the total mechanical power and the thermal power losses, which influence the increase in the energy efficiency up to 1 %. Still, the pressure across these points is also reduced in 4 bar, reason why the ammonia production decreases in a minor proportion.

As for the analysis on the economic criteria, the influence of an additional reactor cannot be directly established due to the differences in the operating conditions. A more general conclusion is presented in the following section, where a comparison between the Fe-based and the Ru-based cases is given. As well, a further comparison with the autothermal configuration is given at the end of this chapter, in section V.7.

### V.5.4. Comparison and conclusions between the Fe- and Ru-based optimal solutions

The results that have been presented until now seek to interpret the influence of the structural alternatives on the economic and energetic objective functions, according to the considered hypothesis. Ultimately, the main goal of the methodology is to determine, in conjunction with the continuous variables, the optimal structure allowing the best trade-off between the objective functions.

In sections V.5.2 and V.5.3, the results for the optimization of the identical superstructure for each catalyst were detailed. However, the results between them are far from being similar. Consider the optimal solutions obtained for the two optimizations, as seen in Figure V-11.

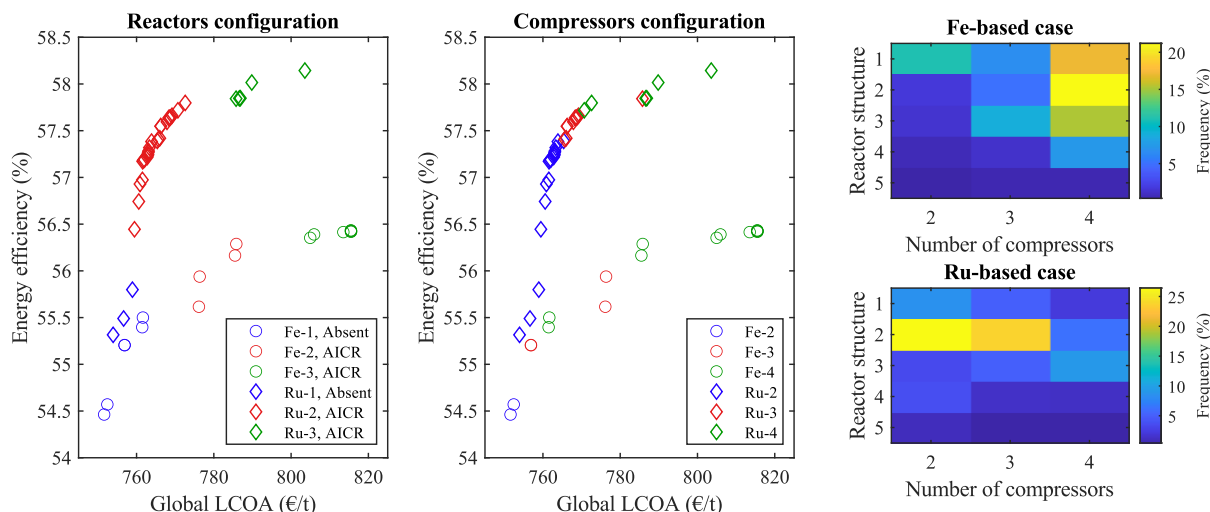


**Figure V-11.** Summary of the KPIs for the optimal solutions of the Fe-based and the Ru-based cases. The scatter plots indicate the optimal solutions for each case, while the colormaps on the right represent the frequency of the feasible solutions for each optimization case, according to the structural alternatives. As a recall, in the reactor configuration the values are specified as; 1: 1 reactor without cooling; 2: 2 reactors, AICR; 3: 3 reactors, AICR; 4: 2 reactors, AQCR; 5: 3 reactors, AQCR.

It can be observed that the Ru catalyst optimization achieves higher energy efficiencies on the process in a range of values of the global LCOA which competes with the Fe catalyst. Even more, for an identical process structure, the use of Ru shows a better performance than the Fe catalyst.

This goes along with the analysis made in section V.5.3.3, regarding the required mass of catalyst and the volume of reactors. As seen in Table V-12, even if the  $H_2$  conversion per pass is higher in the Fe-based case than in the Ru-based case (for the same number of reactors), this parameter is not a conclusive indicator to suggest that the use of Fe is better than the use of Ru. In the scenario with Ru, the results have shown that the  $NH_3$  production is slightly lower, but the lower pressure on the system provokes a lower CAPEX which overcomes the reduction of the production. Therefore, in the calculation of the LCOA, the reduction of the CAPEX parameter is higher than in the production parameter, allowing to reduce the global LCOA even for lower ammonia productions.

Concerning the energy efficiency of the process, the reduced pressure in the Ru-based case favours the obtention of higher values on this KPI. This operating condition has a great impact on the selection of the number of compressors. As seen in the colormaps in Figure V-11, for the Fe-based case, the minimal pressure of 150 bars makes that the majority of feasible solutions uses 4 compressors, with more than

60 % of them with this structural choice. On the contrary, the lower pressures in the Ru-based case allow to reduce the number of compressors, mainly to two units (44 %), as seen in Table V-15.

**Table V-15.** Frequency of structural alternatives for the solutions of the Fe- and the Ru-based cases.

	Fe-based case	Number of compressors				Ru-based case	Number of compressors			
		2	3	4	Total		2	3	4	Total
Reactor configuration	1	11.11	6.84	17.13	35.07	1	8.74	5.19	2.44	16.37
	2	1.79	5.13	21.20	28.11	2	26.41	23.75	6.38	56.54
	3	1.45	9.01	15.26	25.74	3	3.53	5.12	9.36	18.01
	4	0.77	1.36	7.42	9.55	4	3.95	1.56	1.52	7.03
	5	0.32	0.56	0.64	1.52	5	1.16	0.45	0.44	2.05
	<b>Total</b>	15.45	22.90	61.65		<b>Total</b>	43.79	36.07	20.14	

The data presented above indicates the frequency of the structural alternatives on all the feasible solutions obtained from the optimizations. There are some preferential choices that differ between the catalysts being used, mainly due to the performance of the catalyst and the pressure level of the process. While these frequencies show some trends on the preferred solutions, they do not necessarily imply that the most frequent solutions offers the best trade-off between the KPIs.

For the reactor configuration, the case with ruthenium has a strong preference for the use of two modules with indirect cooling, with more than 56 % of the feasible solutions. The direct cooling (AQCR) groups only 9 % of the feasible solutions, which gives an idea of the lower performance of the configuration. In the case of the Fe-based case, in 35 % of the solutions a unique reactor is considered, while the use of two modules is seen in 28 % of cases.

From this data and observing the Pareto front in Figure V-11, the selection of the optimal solution offering the best trade-off between the KPIs considers the best balance between both indicators. In fact, both objective functions are considered to have the same importance.

The preferred reactor configuration for the Ru catalyst is undoubtedly the *2-AICR*, as it is not only more frequent among the feasible solutions (56 %), but also has a better placement on the Pareto front, which is more prominent than the other configurations. For the Fe catalyst, there exists a flattening of the Pareto front. Here the *2-AICR* configuration is not as prominent as in the Ru case, and some solutions with the *1-Absent* configuration have an equivalent level of energy efficiency with a more marked reduction on the LCOA. As seen in Table V-15 and in the colormaps of Figure V-11, the preference of points for the reactor configuration is not as evident as for the Ru. Thus, selecting the *1-Absent* configuration allows to find a similar LCOA than in the Ru-based case, with a reduced energy efficiency.

In any case, regardless of the catalyst being used, a third reactor is not advisable, as the gain on energy efficiency and ammonia production does not justify the prejudice caused to the LCOA.

For the Fe case, it is recommended to include at least three compressors, or four, if possible, due to the high-pressure level on the process, as shown in Figure V-12 for the selected optimal configuration (Point 3 of Table V-8, with 1 reactor and 4 compressors). For the Ru case, solutions with 3 compressors are more efficient and as economic as points with 2 compressors. The optimal configuration represented in Figure V-13, is indicated by Point 3 in Table V-11 (2 reactors and 3 compressors). The full flowsheet representations, including the modules for management of the optimization parameters, and the material balances for the chosen optimal solutions are available in the Appendix E, in section X.5 and Appendix F, in section X.6.

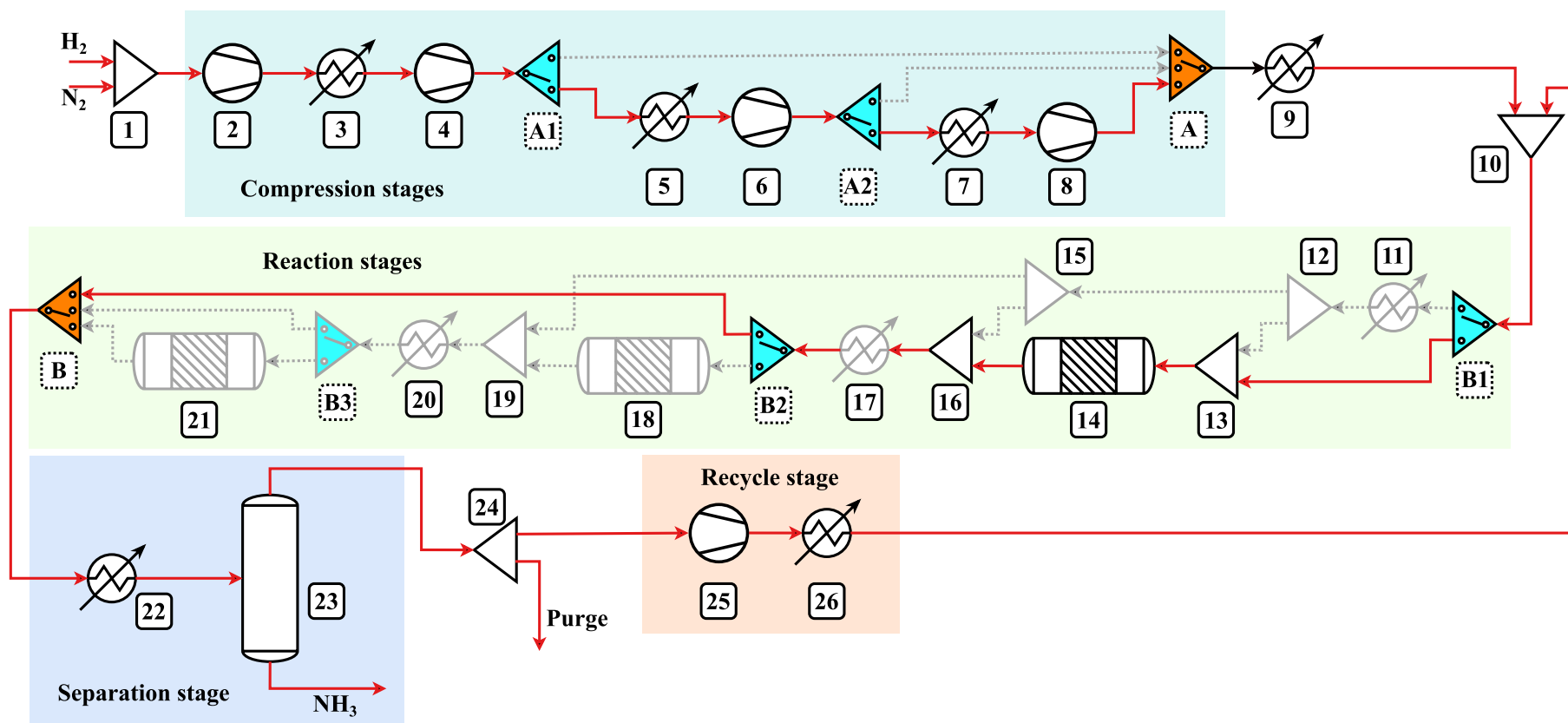


**Figure V-12.** Superstructure representation of the optimal solution for the Fe-based case, using 4 compressors and 1 adiabatic reactor. The structure is defined by the red solid process streams  $\rightarrow$ , and the black unit operations. The bypassed streams are the grey dotted streams  $\dashrightarrow$ , while the inactive modules are the grey modules. Note that the HEX in module 17 remains inactive.

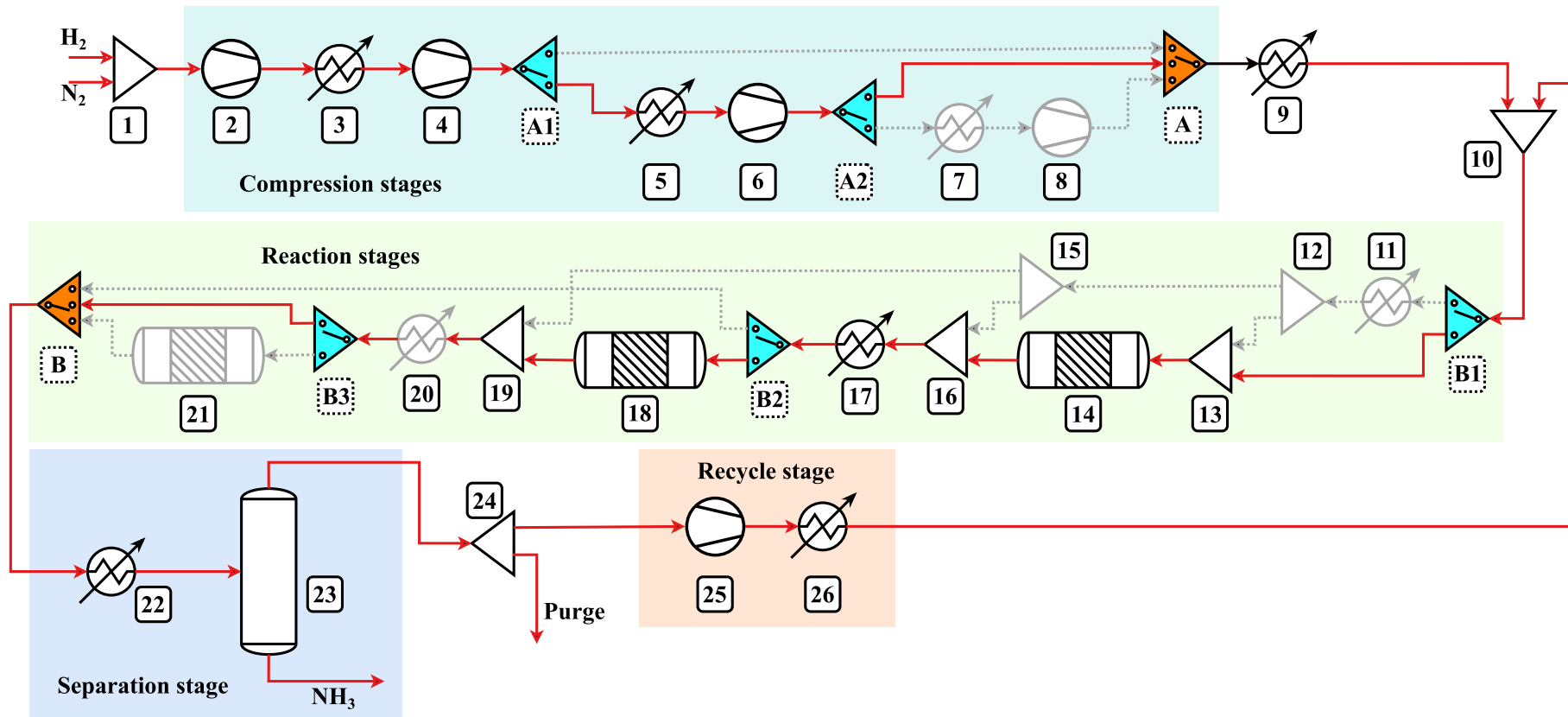


**Figure V-13.** Superstructure representation of the optimal solution for the Ru-based case, using 3 compressors and 2 adiabatic reactors. The structure is defined by the red solid process streams —, and the black unit operations. The bypassed streams are the grey dotted streams —, while the inactive modules are the grey modules.

As previously described, the two optimal solutions selected for each optimization case, are described in Table V-16, all along with the extreme cases obtained within the optimizations, which are shown for comparison.

*Table V-16. Summary of the minimal, optimal, and maximal productivities for set of Pareto points in Superstructure I.*

Case	Configuration		NH <sub>3</sub> mass production	NH <sub>3</sub> energy content	Energy efficiency	Specific mec. power	Specific therm. loss	Process LCOA
			t/y	kW	%	kWh/kg	kWh/kg	€/t
Fe	Minimal	2-1	3 892.7	2 514.7	54.57	0.419	1.553	92.04
	Optimal	4-1	3 894.6	2 515.2	55.50	0.379	1.514	101.41
	Maximal	4-3	3 959.4	2 557.1	56.43	0.382	1.508	164.72
Ru	Minimal	2-1	3 822.3	2 468.6	55.49	0.332	1.475	85.55
	Optimal	3-2	3 904.0	2 521.3	57.59	0.290	1.434	111.49
	Maximal	4-3	3 946.1	2 548.5	57.85	0.306	1.447	137.29

In regards of the NH<sub>3</sub> produced, the optimal solution of the Fe-based case is only 10 t/y lower than the one of the Ru-based case, with a total power content 6 kW. Grossly, both cases allow the same yearly production of ammonia, having into account the reduction of 48.8 % in the pressure of the process (151.8 bar for Fe, to 77.8 bar in Ru). This translates into a gain of more than 2 percent points in the energy efficiency indicator, while reducing the specific mechanical power consumption in 24 %, and the thermal losses from the system in 5.3 %. Overall, the process LCOA increases in 10 €/t, which is finally reflected in an increase in 6.3 €/t in the global LCOA.

Remarkably, the strong reduction on the pressure of the process is the most significant difference between the operating conditions of the optimal solutions. In the end, the gain on the energy efficiency due to this pressure difference compensates the minor increase in the economic indicator, suggesting that the Ru catalyst should be selected as catalyst in the process and for further calculations.

## V.6. Analysis of results for Superstructure II

The superstructure II is studied to determine the performance of two autothermal reactors in series, using the catalyst based on Ruthenium, with possible separation by condensation between the reactors, and with the selection of the number of compressors, as seen in the previous superstructure.

This case requires special attention, as the use of autothermal reactors requires to solve two local recycling loops, one for each reactor, and one global recycling loop, concerning the recycle of unreacted gases. To guarantee a stability on the convergence of solutions and the correct calculation of the two reactors, it has been decided not to set as structural alternative the number of reactors. Moreover, for the intermediate and the final separation, the corresponding refrigeration cycles were modelled to include the influence of the separation technology over the KPIs.

The optimization of this case allowed to obtain a total of 2 142 evaluations, from which 1 782 (83.2 %) are feasible solutions and 13 of them are considered optimal points. For the optimal solutions, the process LCOA varies from 130 to 146 €/t of NH<sub>3</sub>, while the energy efficiency is found between 64 and 67.1 %. The reduced number of evaluations in comparison with the optimization of the Superstructure I is related with the imbricated recycling loops, which increase substantially the calculation time per evaluation. The final average time per calculation is around 5.5 minutes, more than 30 times the average time on the previous superstructure.

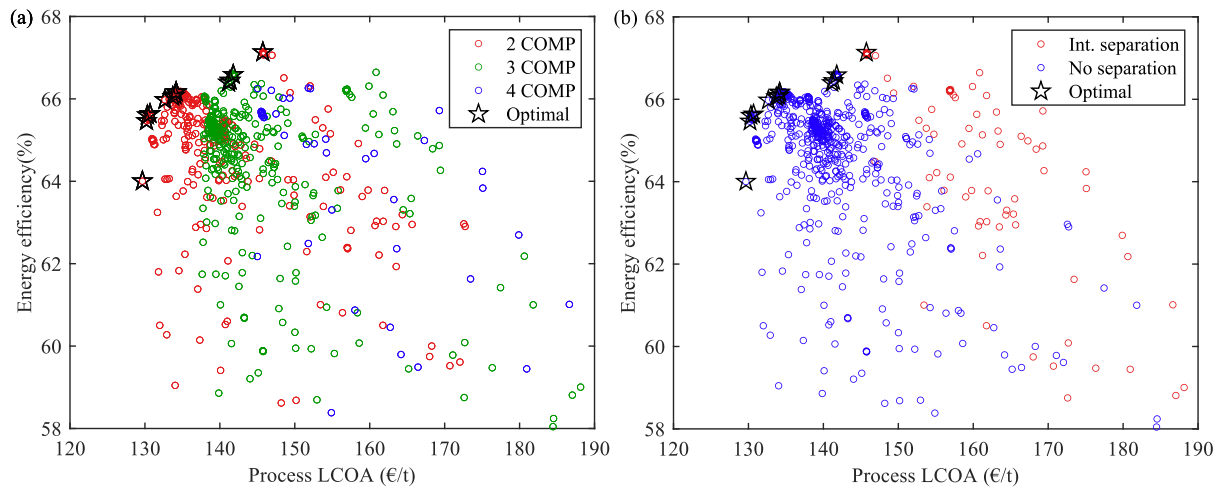


**Figure V-14.** Distribution of feasible and optimal solutions (Pareto) for both objective functions, as function of the structural variables. (a) Solutions highlighted for the number of compressor. (b) Solutions highlighted for the choice of the intermediate separation.

The previous figure shows the distribution of the structural alternatives for the two objective functions in study, the process LCOA and the energy efficiency. In Figure V-14 (a), the number of compressors is indicated, while in (b) the choice for an additional separation between the reactors is presented. Regarding the number of compressors, the optimal solutions have 10 points using 2 compressors, 3 points with 3 compressors and no optimal point with 4 compressors. For the intermediate separation choice, only one optimal point uses the separation between reactors, the one with the highest energy efficiency among and process LCOA.

Table V-17 shows the values of the KPIs, the optimization variables, and the number of feasible solutions with the corresponding structural configuration for the selected points for analysis. Data for all the optimal solutions is available in the Appendix G, in section X.7.

**Table V-17.** Results of the KPI and the optimization variables for the optimal solutions of the autothermal superstructure. Each point corresponds to a different structure.

Key Performance Indicator	Units	Point 1	Point 2	Point 3
Process LCOA	€/t	129.7	141.8	145.7
Energy efficiency	%	64.00	66.59	67.13
<b>Variables</b>				
Pressure	bar	99.34	100	100
Inlet temperature at 1 <sup>st</sup> reactor	K	703.24	699.19	699.19
Inlet temperature at 2 <sup>nd</sup> reactor	K	695.27	691.09	691.09
Length of 1 <sup>st</sup> reactor	m	3.69	7.00	7.00
Length of 2 <sup>nd</sup> reactor	m	2.28	6.23	6.23
Intermediate separation temperature	K	-	-	273.15
Final separation temperature	K	251.81	250.15	250.15
<b>Structural configuration</b>				
Number of compressors	-	2	3	2
Additional separation	-	No	No	Yes
<b>Additional data</b>				
Total volume of reactors (catalytic section)	m <sup>3</sup>	0.599	1.052	0.795
Hydrogen conversion per pass	%	19.23	23.89	30.83
Total points in equal configuration	%	57.13	34.12	2.30

As stated, no optimal solution uses four compressors and the unique solution with intermediate separation uses 2 compressors. Then, only 3 different structural alternatives are found for the optimal

points. Their values for the continuous optimization variables, as well as for all the feasible solutions as presented as follows.

### V.6.1. Distribution of variables across their boundaries

In figure hereafter, the incidence frequency of each optimization variable is highlighted according to the structural alternative of the feasible and optimal solutions.

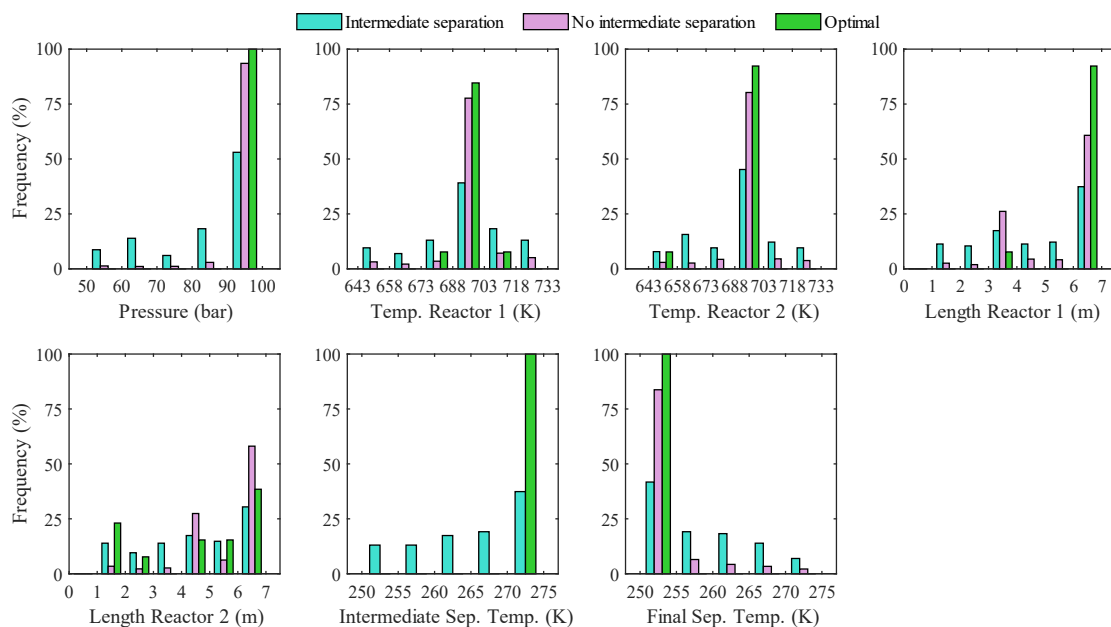


**Figure V-15.** Histogram representing the incidence frequency for every optimization variable, for the autothermal case. Data corresponds to every reactor configuration represented by the optimal solutions. The data considers only the solutions where the variable has an influence due to the structural arrangement.

Interestingly, the pressure on the process reaches the higher bound that has been defined, 100 bar, according to the kinetic rate equation limits on pressure. All the optimal solutions are found towards this limit, even if all the range of pressures has been explored by the feasible solutions. Recalling the pressures on the optimal points for the adiabatic configuration, most of the values were found between 70 and 90 bar.

Concerning the temperatures on both reactors, the most frequent range of values used for both cases is the one varying from 688 to 703 K. For the Fe-based adiabatic reactors, the most frequent range found is 636 – 656 K, while for the Ru-based adiabatic case is 656 – 676 K. In this case of the autothermal arrangement, higher temperatures on the inlet stream are the result of the pre-heating occurring on the shell side of the reactor,

### V.6.2. Hydrogen conversion profiles in the reactors

According to the distribution of feasible and optimal solutions given in Figure V-14, the energy efficiency for the Pareto front solutions is, at least, 6 points higher than the values found for the adiabatic reactor structures.

This can be explained by two main reasons: on one hand, the thermal integration occurring in the reactors allows to avoid the high outlet temperatures on the reaction zone. For this configuration, the outlet temperatures are far from the limit of 800 K, and the thermal losses at high temperatures are reduced. On the other hand, the thermal exchange in the reactors favour the extent of reaction in such a way that

the temperature on the catalytic side is reduced, and therefore, the mixture conditions are distant from the equilibrium, achieving higher H<sub>2</sub> conversions.

To better understand this behaviour, the temperature profiles for the chosen optimal configurations are represented in Figure V-16, describing the trajectory evolution and the molar fraction of NH<sub>3</sub>.

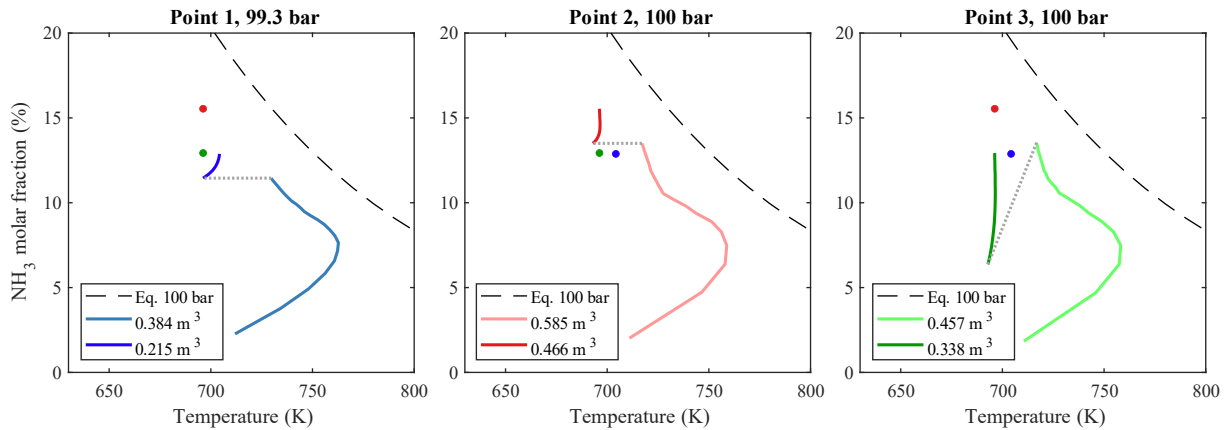


**Figure V-16.** Trajectories on the co-current multitube reactors for the optimal points of the autothermal case shown in Table V-17. The subplots indicate the temperature trajectory and the ammonia molar fraction in the catalytic (tubes) of the reactor, specifying the volume of each catalytic section for each reactor. Note that the solution of Point 3 includes an intermediate separation stage.

On the subplots the temperature profiles on the catalytic side of the reactor are shown. As seen, the temperature on the catalytic section passes through a maximum level, around 760 K, and continues with a decreasing behaviour until the end of the first reactor. The thermal exchange, cooling the mixture on the catalytic side and pre-heating the feed on the shell side, creates a synergetic effect that promotes the reaction, as the temperature trajectory bends and moves away from the equilibrium.

The three solutions for analysis have similar levels of pressure and almost the same temperature at the inlet stream of the first reactor. The difference between the first set of reactors is the volume and, therefore, the NH<sub>3</sub> mole fraction at the outlet streams, as seen hereafter:

- Point 1: the first reactor has a volume of 0.384 m<sup>3</sup> on the catalytic side, an inlet fraction of NH<sub>3</sub> of 2.3 %, reaches 16.9 % of H<sub>2</sub> conversion and an outlet fraction of NH<sub>3</sub> equal to 11.5 %.
- Point 2: the first reactor has a volume of 0.585 m<sup>3</sup> on the catalytic side, an inlet fraction of NH<sub>3</sub> of 2.0 %, reaches 20.6 % of H<sub>2</sub> conversion and an outlet fraction of NH<sub>3</sub> equal to 13.5 %.
- Point 3: the first reactor has a volume of 0.457 m<sup>3</sup> on the catalytic side, an inlet fraction of NH<sub>3</sub> of 1.8 %, reaches 21.0 % of H<sub>2</sub> conversion and an outlet fraction of NH<sub>3</sub> equal to 13.5 %.

The solution of Point 1, with the smallest volume on the catalytic tubes, achieves the lowest H<sub>2</sub> conversion and final NH<sub>3</sub> molar fraction. But, when comparing points 2 and 3, both solutions reach an equivalent content on NH<sub>3</sub>, and almost the same H<sub>2</sub> conversion, (which is different due to the initial content on ammonia), even if the reactor of point 3 has a volume 20 % smaller. This is explained by the effect of the intermediate separation. Even if this step is proposed after the first reactor, the global recycle flowrate is affected. For Point 2, with no intermediate separation, the molar flowrate in the inlet stream of the first reactor is 22% higher than for Point 3. Thus, the volume of the reactor increases as a direct result of the volume flowrate increase.

Following, the second autothermal reactor has a lower inlet temperature in the three cases. For Points 1 and 2, without intermediate separation, the performance in the second reactor is not as evident as in the solution of Point 3. In fact, the decrease in temperature is not enough to guarantee a further conversion of H<sub>2</sub>, as the presence of NH<sub>3</sub> in the mixture places the stream closer to the equilibrium conditions. On the contrary, the intermediate separation used in Point 3 improves the conversion, as seen in ammonia mole fraction increase. The difference between the solutions are resumed as follows:

- Point 1: the second reactor has a volume of 0.215 m<sup>3</sup> on the catalytic side, an inlet fraction of NH<sub>3</sub> of 11.5 %, reaches 2.8 % of H<sub>2</sub> conversion and an outlet fraction of NH<sub>3</sub> equal to 12.9 %.
- Point 2: the second reactor has a volume of 0.466 m<sup>3</sup> on the catalytic side, an inlet fraction of NH<sub>3</sub> of 13.5 %, reaches 4.1 % of H<sub>2</sub> conversion and an outlet fraction of NH<sub>3</sub> equal to 15.5 %.
- Point 3: the second reactor has a volume of 0.338 m<sup>3</sup> on the catalytic side, an inlet fraction of NH<sub>3</sub> of 0.64 %, reaches 12.4 % of H<sub>2</sub> conversion and an outlet fraction of NH<sub>3</sub> equal to 12.9 %.

There is no doubt that the benefits of the intermediate separation are important. While solutions of Point 1 and 2 have hydrogen conversion below 5 %, the removal of ammonia favours the conversion on the second reactor of Point 3, reaching a further conversion above 12 %. Considering both reactors, the H<sub>2</sub> conversions per pass through the reaction stage for Points 1, 2 and 3 are equal to 19.2, 23.9 and 30.8 %, respectively. These results are compared with the results of the adiabatic cases at the end of this chapter.

### V.6.3. Influence of the structure on the economic criteria

For the autothermal configuration, the intermediate and final separations by condensation have an important influence on both performance indicators. The refrigeration cycles in both cases consist of an ammonia flowrate at 99.5 %, which allows cooling down the process stream down to the desired separation temperature before each separation drum. Due to the properties of the refrigerant, its sole compression from near ambient pressure to 15 bar provokes an important temperature rise, reason why three compressors are included to perform a multistage compression.

These compressors induce, on one hand, an increase in the annualized CAPEX that repercussions on the economic indicator, and on the other hand, represents a fraction of mechanical power that was not considered in Superstructure I, impacting the energy efficiency of the process. Data in Table V-18 include the main values from the chosen optimal solutions, allowing to calculate the KPIs.

**Table V-18.** Parameters for the calculation of the economic performance indicator, for the optimal solutions of the autothermal case. The configuration is indicated as Compressors-Separation, where the separation value is given by 1: use of separation; 2: no separation.

Case	Ammonia production	Annualized CAPEX	Process OPEX	Global OPEX	Process LCOA	Global LCOA
	t/y	€/y	€/y	€/y	€/t	€/t
Point 1: 2-2	3 913.5	381 283	126 708	2 701 109	129.7	787.6
Point 2: 3-2	3 955.4	434 225	126 716	2 701 417	141.8	792.7
Point 3: 2-1	3 994.8	448 662	133 662	2 708 363	145.7	790.3
Relative variations according to Point 1: 2-2						
Point 2: 3-2	1.07 %	13.89 %	0.24 %	0.01 %	9.32 %	0.65 %
Point 3: 2-1	2.08 %	17.67 %	5.74 %	0.27 %	12.36 %	0.34 %

According to the data reported in Table V-17, the optimal points have similar operating conditions, allowing to compare without any bias the influence of the structure on the parameters reported for the economic indicator calculation.

The ammonia yearly production has an increase of 1.07 % in the solution of Point 2, as the total volume of the catalytic sections is increased in 75 %, allowing to increase the H<sub>2</sub> conversion per pass in 4.6 absolute points. In the same sense, the configuration of Point 3, including the intermediate separation, has a volume 33 % higher, but an increase in the H<sub>2</sub> conversion per pass of 11.6 absolute points. This suggests that, more than including larger catalytic sections, the NH<sub>3</sub> production is largely favoured by the intermediate separation.

Regarding the use of the condenser between the reactors, the annualized CAPEX is affected by an increase in 17.67 %, which translates into a final increase in 12.36 % in the process LCOA. Nevertheless, the benefits of the intermediate separation reflect a minor growth of 0.34 % in the global LCOA, which can be justified by the important improvement in the energy efficiency indicator, hereafter analysed.

#### V.6.4. Influence of the structure on the energy criteria

As previously highlighted, one of the main effects of the autothermal configuration for ammonia synthesis is the thermal integration existing in the reactors. The outlet temperature of each catalytic section is drastically reduced in comparison to the adiabatic arrangement, reaching around 80 K of difference between both configurations. This is then reflected in a decrease in the thermal energy losses, as no further refrigeration is required at high temperatures (c.f. Chapter VII).

The following data presented in Table V-19, allows to understand the impact of the structural choice in the energy efficiency indicator.

*Table V-19. Parameters for the calculation of the energetic performance indicator, for the optimal solutions of the autothermal case. The configuration is indicated as Compressors-Separation, where the Separation value is given by 1: use of separation; 2: no separation.*

Case	NH <sub>3</sub> energy produced	Mechanical power	Thermal power lost	Energy efficiency	Specific mec. power	Specific therm. loss	Power ratio NH <sub>3</sub> /H <sub>2</sub>
	kW	kW	kW	%	kWh/kg	kWh/kg	kW/kW
Point 1: 2-2	2 527.46	230.6	447.0	64.00	0.471	0.914	0.835
Point 2: 3-2	2 554.55	220.2	397.3	66.59	0.445	0.803	0.844
Point 3: 2-1	2 580.01	229.7	397.9	67.13	0.460	0.797	0.853
Relative variations according to Point 1: 2-2							
Point 2: 3-2	1.07 %	- 4.50 %	- 11.13 %	4.04 %	- 5.51 %	- 12.07 %	1.07 %
Point 3: 2-1	2.08 %	- 0.40 %	- 11.00 %	4.89 %	- 2.43 %	- 12.81 %	2.08 %

The differences between Points 1 and 2 are the number of compressors and the volume of the reactors. This is reflected in the increase in the energy produced in ammonia by 1.07 %, and the decrease in the mechanical power in 4.50 %. Moreover, thermal power savings of at least 11 % are seen in solutions 2 and 3.

On the overall balance, the energy efficiency is strongly impacted by this reactor arrangement, as this indicator increases in at least 6 points regarding the adiabatic cases. When comparing the optimal solutions with the highest energy efficiencies between the adiabatic and the autothermal cases, the improvement of the latter is almost of 10 percent points. This is reflected in less thermal energy losses to the environment and higher power ratios between the produced ammonia and the supplied hydrogen.

These results are confronted to those obtained for the adiabatic configuration in section V.7. On one hand, the mechanical power consumption is higher than in cases of Superstructure I, as the refrigeration cycles have been included for the autothermal case. On the other hand, the thermal power losses are decreased due to the thermal integration in the reactor.

For this configuration, the intermediate separation has an important effect on the KPIs. Even if the process LCOA increase is at least of 10 %, compared to the solution without separation, the final increase in the global LCOA is just 0.34 %. This growth is minor when compared to the gain in the energy efficiency and the reduction of the thermal losses. Therefore, for this specific superstructure optimization, the solution of Point 3, including 2 compressors and intermediate separation by condensation, is chosen as the optimal structure, hereafter represented in Figure V-17. The complete superstructure flowsheet, as seen in ProSimPlus, is shown in the Appendix H, in section X.8.

The results presented until this section, concerning the optimization of Superstructure I and II, were proposed to analyse the choice of the structural configuration in the number of compressors, number of reactors, type of reactors, type of cooling, and catalysts. A summary that centralizes the main indicators for the selected optimal configurations is presented in section V.7, which serves to compare and select the best structural arrangement by crossing the data from the superstructure optimizations.

Ideally, a unique superstructure containing all the previous presented structural alternatives and optimization variables should have been conceived, to allow the optimization algorithm to search for the best structure by itself. However, as the superstructures were progressively studied, modelled, and optimized, the final – centralizing – superstructure could not be presented due to time limitation. Insights on further developments to this application case are presented in Chapter VIII.

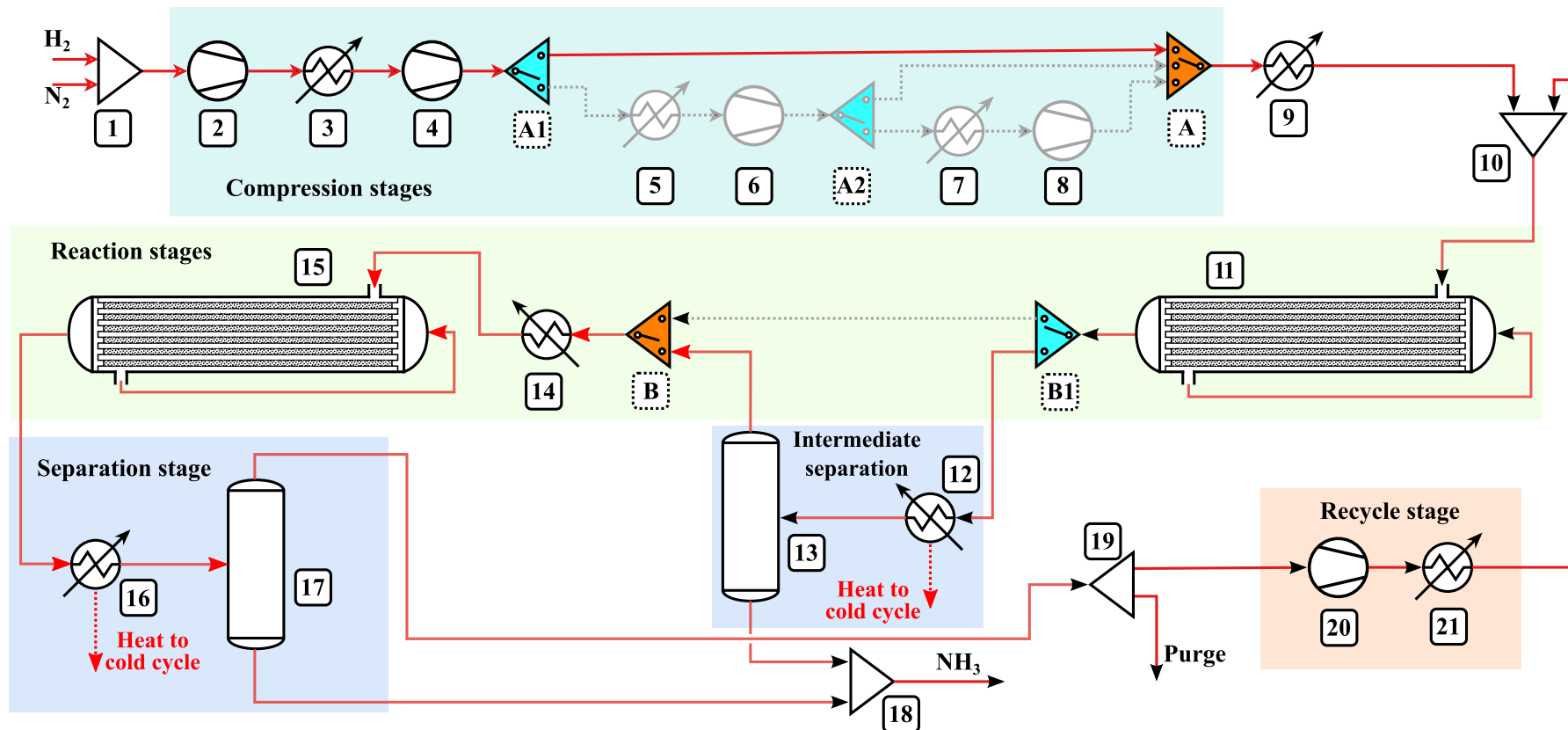


Figure V-17. Superstructure representation of the optimal solution for the autothermal case, using 2 compressors and the intermediate separation. The structure is defined by the red solid process streams  $\rightarrow$ , and the black unit operations. The bypassed streams are the grey dotted streams  $\dashrightarrow$ , while the inactive modules are the grey modules.

## V.7. Summary of results and discussion

Having studied the Superstructures I and II, the analyses of results presented in this chapter were focused on determining how the structural alternatives of the superstructure in study affect the KPIs. This permits to select, among the optimal solutions obtained, the structure that offers the best trade-off between the performance indicators.

In this last section, a summary of the optimal solutions retained for each superstructure are presented and compared between to finally determine the best structural arrangement for the ammonia synthesis application, regarding the reactor configuration.

Consider the data presented in Table V-20, where the optimal results of the adiabatic and autothermal configurations are given.

**Table V-20.** Summary of optimal solutions for the reactor configuration, according to the results of the superstructure optimization of cases I and II. \*The specific mechanical power and thermal losses of the Adiabatic cases do not include the cold cycle envelope.

Key Performance Indicator	Units	Adiabatic Fe	Adiabatic Ru	Autothermal Ru
Global LCOA	€/t	761.6	767.9	790.3
Energy efficiency	%	55.50	57.59	67.13
<b>Additional data</b>				
Number of compressors	-	4	3	2
Number of reactors	-	1	2	2
Reactor cooling type	-	Absent	AICR	Integration/AICR
Intermediate separation	-	-	-	Yes
Process LCOA	€/t	101.41	111.49	145.7
Separation cost to Process LCOA	€/t	-	-	50.30
Ammonia yearly production	t/y	3 894.6	3 904.0	3 994.8
Synthesis pressure	bar	151.8	77.8	100
Specific mechanical power*	kWh/kg	0.379	0.290	0.460
Specific thermal losses*	kWh/kg	1.541	1.434	0.797
Energy converted ( $H_2 \rightarrow NH_3$ )	kW/kW	0.831	0.833	0.853

In the adiabatic configurations, the cold cycle cost is not included, as this section of the process was developed after these optimization results were obtained. For the autothermal case, both the intermediate and the final separation stages include the calculation of the refrigeration cycles.

A direct comparison on the KPIs allows to determine that, in terms of ammonia production economy, the adiabatic case using Ru and the autothermal case (with the same catalyst) are 1 % and 3.8 % higher, regarding the adiabatic case using the Fe catalyst, respectively. A greater impact is seen on the energy efficiency of the solutions, as they are 3.8 % and 21 % higher, in the same order, than the adiabatic Fe-based case.

Between the adiabatic cases, the difference in the cost is not as evident as for the autothermal case. This is mainly due to the inclusion of the cost of the refrigeration cycles for the latter. However, when exploring the real impact of the two separation stages on the process LCOA for the autothermal case, its total cost is 50.3 €/t of  $NH_3$ . Deducing this value from the process LCOA gives 95.4 €/t which can be directly compared to the process LCOA of the adiabatic cases. In the end, the cost of the autothermal process excluding the separation costs is lower than in the adiabatic cases.

The lower cost is explained by the higher  $\text{NH}_3$  yearly production. Between the adiabatic cases, a difference of 10 t/y is found, but the autothermal configuration and the intermediate separation allows further conversion of  $\text{H}_2$  and therefore a greater  $\text{NH}_3$  production, 100 t/y higher than in the Adiabatic Fe case. The higher cumulate  $\text{H}_2$  conversion per pass observed for the autothermal reactor (30.8 %) is a result of the heat exchange in the reaction module, favouring a further extent of reaction as the conditions in the envelope move away from the equilibrium, and the intermediate separation between reactors, which reduce the content of  $\text{NH}_3$  in the process stream.

On the other hand, when considering the power conversion ratio of hydrogen to ammonia, it can be seen that the autothermal case has the best performance. The theoretical power ratio given by the LHV of the compounds and the reaction stoichiometry is 0.872. The autothermal case reaches 0.853 (97.82 %), while the adiabatic cases reach a similar value of 0.833 (95.53 %). This indicator is analogous to the global hydrogen conversion on the process.

Under the considered hypothesis for the optimization of superstructures I and II, the autothermal configuration with intermediate separation favours not only the reduction of the thermal losses to the environment, but also offers the best process structure in terms of ammonia production, and therefore, of energy storage in ammonia. This point is further developed when discussing the overall scenario for ammonia production, in Chapter VII.

## V.8. Conclusions

This chapter described the different steps from the superstructure optimization methodology that have been applied to propose and optimize the superstructure cases in the HB process. The structural alternatives cover the different steps on the synthesis system, such as the selection between the number of compressors, the number of reactors, the type of reactor configurations, the catalytic material, and even the use of an intermediate separation step.

The Key Parameter Indicators included in the multi-objective optimization problem are essentially economic and efficiency criteria: the global and the process Levelized Cost of Ammonia production, the energy efficiency of the process. Among the optimization variables, there exists operating conditions, such as pressures, temperatures, and flowrates, but also design parameters, as the length of the different modules. Additionally, inequality constraints are included to respect technical and performance limits.

In the following chapter, Superstructures III and IV are presented, which concerns the evaluation of multiple separation technologies, in order to determine their performance and potential use as substitute of the condenser.



# Chapter VI

---

*Optimization of the Haber-Bosch process through  
separator configurations and material selection*

---



## VI. Chapter VI: Optimization of the Haber-Bosch process through separator configurations and material selection

The following chapter will cover subjects related to:

- The description of the superstructure cases related to the evaluation of alternative separation methods to the separation by condensation.
- The evaluation of the impact of the membrane filters, the PSA model, and the classic condenser on the KPIs, uniquely for the separation stage of the process.
- The comparison between the performance of the separation alternatives, in terms of its cost to the LCOA and the specific energy consumption for ammonia separation.

### VI.1. Introduction

As discussed in Chapter I for the different separation technologies available for ammonia recovery from the reactor outlet mixture, the separation by condensation offers an easy and practical way to separate  $\text{NH}_3$ . Due to its condensable nature at high pressures and temperatures near or below ambient temperature, and the non-condensability of  $\text{H}_2$  and  $\text{N}_2$  at such conditions, this separation offers a good productivity with adequate purity of ammonia in the product stream.

Though, the required level of temperature for separation, regarding the outlet temperature of the reaction stage, imposes a huge temperature cooling across the process, of around 500 K, as it passes from almost 800 K in the case of the adiabatic reactors, to nearly 273 K, depending on the pressure of the system. According to the literature, the separation-recycle stages for a HB process using the separation by condensation consumes between 3 and 5  $\text{GJ}/\text{t}_{\text{NH}_3}$  [59] (i.e., 0.83 – 1.39  $\text{kWh}/\text{kg}_{\text{NH}_3}$ ).

The idea to evaluate other separation technologies, as previously described, is to determine if they offer:

- Favourable temperature gradients, allowing to reduce the thermal requirements on the separation-recycle stages, which are associated with thermal needs for cold production, and with mechanical work on the cold cycle and the recycle stage.
- Comparable levels of ammonia productivity and purities to the separation by condensation, without prejudice of the economic indicator.

The main question that rises is what alternative methods for separation could be considered, and which could be used as replacement or in association with condensation to reduce the global energy consumption?

One can base its choice in engineering intuitions and in pure heuristic rules [149] which dictate the following points:

- “Attempt to condense or partially condense vapor mixtures with cooling water or a refrigerant”, which guides the use of the separation by condensation
- “Separate vapor mixtures using partial condensation, cryogenic distillation, absorption, adsorption, membrane separation, and/or sublimation”, which suggests, as alternative methods, the separation by membranes and PSA, hereafter considered.

The first alternative technology being evaluated as substitute to the condensation method is the membrane separation. At this point of the work, the PSA system was not included, as it came as an option after modelling and optimizing the membrane superstructure. For both technologies, the required data for their modelling have been presented in Chapter IV.

Therefore, this chapter that focusses on evaluating these alternative separation methods is structured as follows: section VI.2 presents the first superstructure optimization case, devoted solely to the membrane separation, in which the condensation method is proposed as a rehearsal of the first one. In section VI.3 the condenser, the membranes and the PSA methods are integrated into a unique superstructure, in which the former can be used as a sole method for separation, or as a supplementary technique after the membranes and the PSA separations. Next, sections VI.4 and VI.5 present, respectively, the results of both superstructure optimizations, which are lately compared in section VI.6, prior to the conclusions presented in section VI.8.

## **VI.2. Superstructure III – Membrane separation**

To study the HB process, multiple superstructures have been proposed in the course of this work, as the different structural alternatives were gradually studied and developed at different stages of this work. The process for methodology development and application, as well as for the software appropriation and expertise, allowed to propose the superstructure hereafter exposed, shown in Figure VI-1.

It consists of a main separation step performed by multiple membrane modules in series, modelled as a counter-current module with ideal plug flow on both sides, using pure nitrogen as sweep gas on the permeate side. Each membrane has its specific sweep gas flowrate and pressure, which do not necessarily match between them. Nevertheless, the membranes operate at the same temperature.

As previously described, the membrane is composed of a nanocomposite MFI zeolite material, favouring the preferential adsorption and permeation of ammonia molecules, while obstructing the permeation of  $H_2$  and  $N_2$ . The geometric parameters and the permeabilities of the compounds are those described in section IV.3.4.2.

The mixture to be processed is defined by a molar flowrate of 304.1 kmol/h, with compositions of 21.8 % of  $N_2$ , 65.6 % of  $H_2$  and 12.4 % of  $NH_3$ , at 724.3 K and 96.6 bar.

### **VI.2.1. Structural alternatives**

The structural alternatives concern three discrete variables: (1) the number of membranes, (2) the choice of the pressure equalization on the permeate sides, (3) the use of an additional separation by condensation to improve the purity on the production stream.

The process alternatives that have been included are more a decision from engineering insights than from a rigorous analysis on superstructure alternative by some pre-screening method. It has been decided to include up to 3 membranes for the separation of  $NH_3$ , represented by modules 8, 9 and 10, and bypassed by the opening switches A1 and A2.

Compressors 2, 4 and 6 adjust the pressure on the sweep streams 1, 2 and 3, respectively, while the HEX 1, 3, 5 and 7 set the temperature to the specified value for the membrane operation, which is isothermal. Next, if only the first membrane is used, the second and third membranes are bypassed, while the modules on the sweep streams of these membranes remain inactive.

On the permeate side, as the sweep gas flows at different pressures, an equalization of pressures can be carried out to avoid pressure losses when mixing the permeate streams. The final pressure for equalization is dictated by the highest pressure of the permeate streams. This structural choice concerns the opening switches B1, B2 and B3. As well, a temperature adjustment is performed by modules 12, 14 and 15, to mix the permeate streams at isothermal conditions.

A complementary condensation stage can be used to enhance the ammonia purity in the product stream, if necessary, which is handled by the opening switch C1. In case that this option is included, a two-stage compression is carried out in the process stream, to equal the recycle pressure. If the compression ratio between the known recycle pressure and the outlet stream pressure of the opening switch C1 is greater than 4, as given by heuristics, two compression stages are used, otherwise only modules 19 and 20 are used, while modules 17 and 18 remain inactive.

This pressure increase also favours the ammonia separation in the drum. Next, the top stream of the separation drum is mixed with the retentate streams of the membranes, which are mainly composed of hydrogen and nitrogen, the less favoured compounds for permeation in the membranes. Again, an isothermal mixing is carried out between these streams.

As seen in the HEX given in module 20, the withdrawn heat duty from the process stream is guaranteed by the refrigeration cycle.

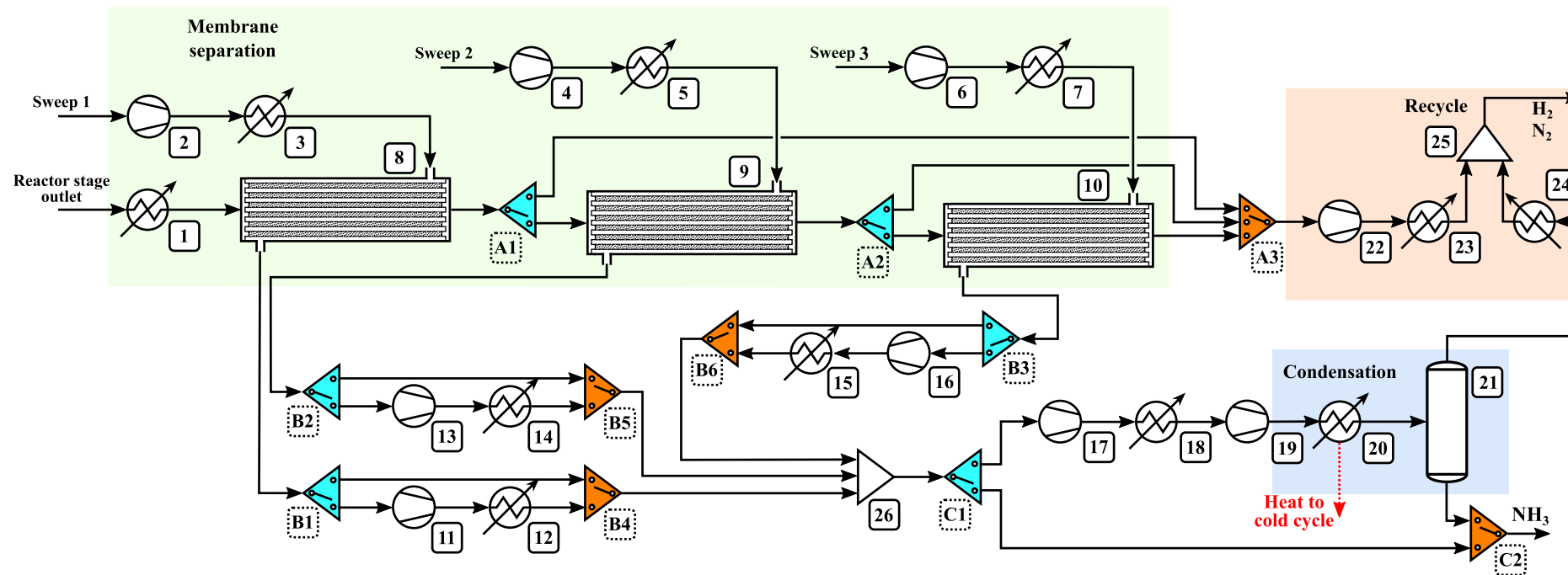


**Figure VI-1.** Superstructure representation for the evaluation of the membrane separation technology. The inlet stream to the system is a constant flowrate from one of the optimal solutions obtained from the optimization of Superstructure I, at 304.05 kmol/h, 724.3 K, 96.6 bar, with mole fractions of 65.64 % for H<sub>2</sub>, 21.88 % for N<sub>2</sub> and 12.48 % for NH<sub>3</sub>. Unit nomenclature corresponds to: HEX (1, 3, 5, 7, 12, 14, 15, 18, 20, 23, 24), Compressors (2, 4, 6, 11, 13, 16, 17; 19, 22), Membranes (8, 9, 10), Mixers (25, 26), Separation drum (21), Opening switch (A1, A2, B1, B2, B3, C1), Closing switch (A3, B4, B5, B6, C2).

### VI.2.2. Optimization problem formulation

The process LCOA and the specific energy consumption are used as objective functions. This last one is for direct comparison with the specific energy consumption chart of Figure IV-11, in order to determine if the membrane separation allows to gain any advantage in energy savings regarding the single condenser system. Also, as there are no reactors in this superstructure and no chemical transformation occurs, it has been decided to assess the energetic performance according to the consumption of energy for ammonia separation.

The optimization problem contains 11 continuous and 3 structural decision variables, as shown in Table VI-1. The 3 membranes operate at the same temperature, but the sweep flowrate, the sweep pressure and the module length can vary between them. The condensation temperature is the last continuous variable. The structural variables have been previously described.

*Table VI-1. Continuous and discrete decision variables for the optimization of the membrane superstructure. The process unit is referred to the superstructure representation shown in Figure VI-1.*

Variable	Type	Stage	Process unit	Bounds	Units
Membrane temperature	Continuous	Membranes	1, 3, 5, 7	313 – 423	K
Length of 1 <sup>st</sup> membrane	Continuous	Sweep	8	0.5 – 10	m
Length of 2 <sup>nd</sup> membrane	Continuous	Sweep	9	0.5 – 10	m
Length of 3 <sup>rd</sup> membrane	Continuous	Sweep	10	0.5 – 10	m
Sweep pressure for 1 <sup>st</sup> membrane	Continuous	Sweep	2	10 – 40	bar
Sweep pressure for 2 <sup>nd</sup> membrane	Continuous	Sweep	4	10 – 40	bar
Sweep pressure for 3 <sup>rd</sup> membrane	Continuous	Sweep	6	10 – 40	bar
Sweep flowrate for 1 <sup>st</sup> membrane	Continuous	Membranes	Sweep 1	0.1 – 20	kmol/h
Sweep flowrate for 2 <sup>nd</sup> membrane	Continuous	Membranes	Sweep 2	0.1 – 20	kmol/h
Sweep flowrate for 3 <sup>rd</sup> membrane	Continuous	Membranes	Sweep 3	0.1 – 20	kmol/h
Condenser temperature	Continuous	Condenser	20	250 – 273	K
Number of membranes	Discrete	Membranes	A1, A2	1 – 3	-
Permeate pressure equalization	Discrete	Permeate	B1, B2, B3	1 – 2	-
Additional separation by condensation	Discrete	Condenser	C1	1 – 2	-

For this superstructure optimization, three inequality constraints are considered. The first one concerns the convergence of the refrigeration cycle, set up to a convergence criterion as in the recycle loop constraints, equal to  $1 \cdot 10^{-7}$ . The other two constraints are referred as technical restrictions of the process. In fact, for the membranes to be a competitive technology, it requires to achieve similar separation performance as the condenser. These constraints are set to a maximum  $\text{NH}_3$  mole fraction in the recycling stream of the HB process, fixed to 5 %, and a minimum  $\text{NH}_3$  mole fraction in the product stream, set to 95 %.

### VI.2.3. Algorithm parameters

The following algorithm parameters have been defined for the membrane superstructure optimization. The ACCURACY (i.e., the tolerance for the constraints violation) is reduced, as the calculations in this superstructure are way faster than in the previous cases.

*Table VI-2. Values for the parameters of the optimization algorithm, in Superstructure III. Non specified parameters have the value by default.*

Parameter	Values	Parameter	Values
ACCURACY	0.001	MAXTIME	144 000
EVALSTOP	75 000	MAXEVAL	100 000
NI	3	PRINTEVAL	10
-	-	SAVE2FILE	100 000

Due to the fast calculations and the low time required by this particular superstructure, the EVALSTOP parameter has been increased to 75 000 evaluations and the MAXEVAL goes up to 100 000. The maximum time for optimization is fixed to 40 h, or 1.67 days.

The corresponding results for the optimization of this superstructure are presented and discussed in section VI.4.

### **VI.3. Superstructure IV – PSA, membranes, and condenser**

In this case, the black-box model for the PSA separation is included to the superstructure III, to evaluate three different separation technologies. As in the previous superstructure, constant conditions of the reaction stage are used as the stream to separate. The flowrate specifications to treat in this separation process are equal to those in the previous superstructure, which are equal to a molar flowrate of 304.1 kmol/h, with compositions of 21.8 % of N<sub>2</sub>, 65.6 % of H<sub>2</sub> and 12.4 % of NH<sub>3</sub>, at 724.3 K and 96.6 bar.

The interest of this superstructure optimization is to compare the three separation methods as unique alternatives, but they can also be tested as hybrid methods in the form of a couple membranes-condenser or PSA-condenser.

Furthermore, in case that the alternative methods are not as effective or economic as the separation by condensation, the information obtained from the thousands of evaluations can give insights on the improvements that are required to implement in these technologies, to compete with the classical separation method.

#### **VI.3.1. Structural alternatives**

The superstructure representation is shown in Figure VI-2. The superstructure can be described according to each one of the three main sections, corresponding to each separation technology:

- The membrane separation consists of three separate membrane units, 8, 9 and 10, modelled as counter-current units. The sweep gas streams are flow streams of nitrogen compressed up to the sweep pressures in compressors 2, 4 and 6, and adjusted to the membrane temperature in the HEXs 3, 5 and 7. The reactor outlet stream is cooled down to the membrane temperature in the HEX 1. The retentate streams, mainly nitrogen and hydrogen, are sent to the closing switch A3 for recycle, while the permeate stream is directed to either the condensation section in case a further separation is required, or out of the process as product. Here, the pressure equalization in the permeate streams is also included as alternative.
- The separation by PSA, modelled as a black-box system, receives the reactor outlet stream at the temperature fixed in the HEX 27. The high-pressure column, separates the mixture into a rich stream in H<sub>2</sub> and N<sub>2</sub>, known as the high-pressure product (HPP) obtained at the top stream, while the NH<sub>3</sub> is recovered on the bottom of the low-pressure column, in module 29, known as the low-pressure product (LPP). The HPP stream is sent to module A3, while the LPP stream goes to the module 26, where is possible to decide whether further separation is needed.

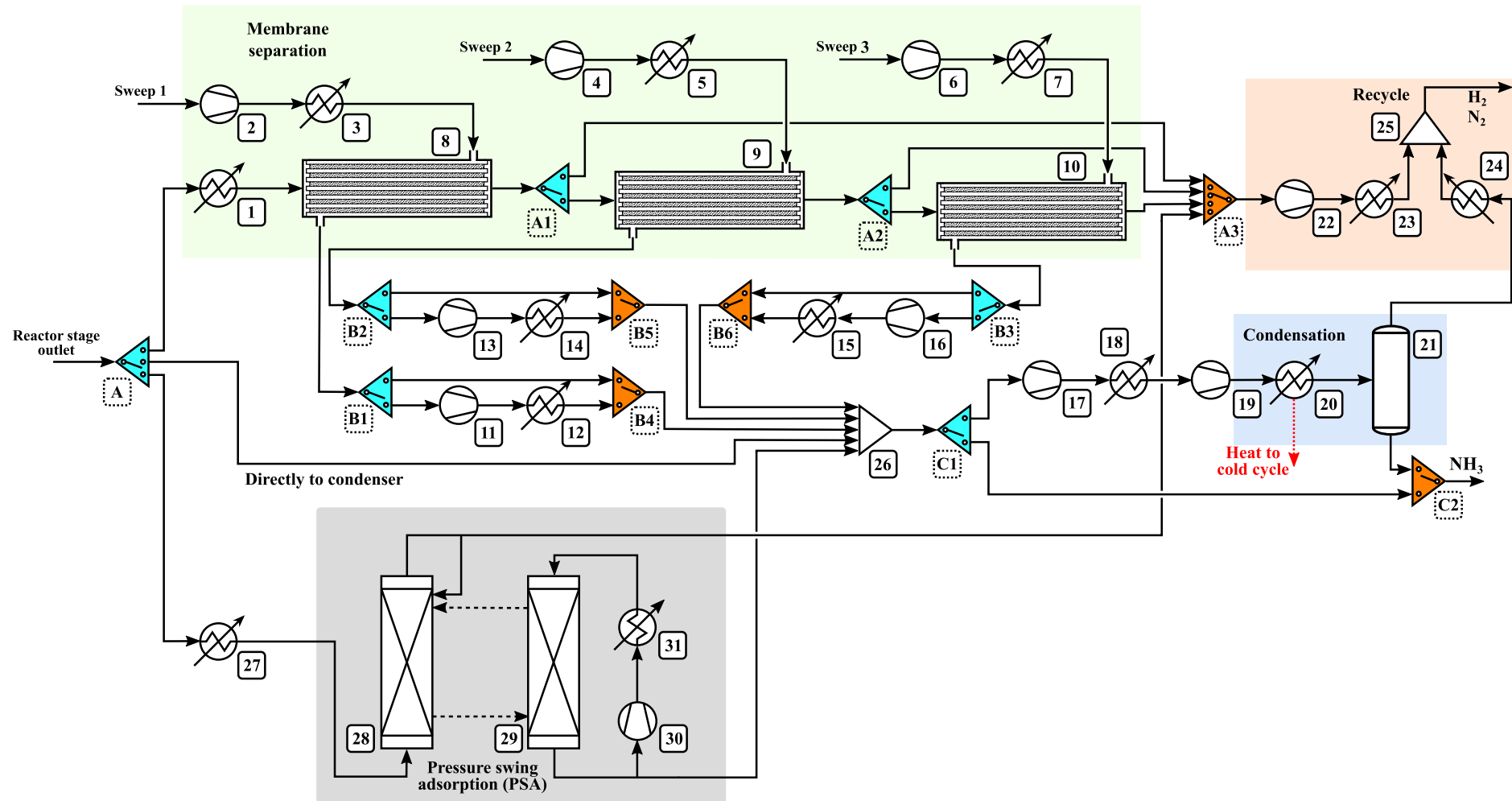


**Figure VI-2.** Superstructure representation for the evaluation of the separation technologies. The adsorption columns are part of the black-box model and are not independent units. The inlet stream to the system is a constant flowrate from one of the optimal solutions obtained from the optimization of Superstructure I, at 304.05 kmol/h, 724.3 K, 96.6 bar, with mole fractions of 65.64 % for H<sub>2</sub>, 21.88 % for N<sub>2</sub> and 12.48 % for NH<sub>3</sub>. Unit nomenclature corresponds to: Mixers (25, 26), Compressors (2, 4, 6, 11, 13, 16, 17, 19, 22, 30), HEX (1, 3, 5, 7, 12, 14, 15, 18, 20, 23, 24, 27, 31), Membranes (8, 9, 10), Separation drum (21), Adsorption columns (28, 29), Intermediate switches (A, A1, A2, B1, B2, B3, C1) and Closing switches (A3, B4, B5, B6, C2).

- The separation by condensation stage, where the reactor outlet stream is conditioned to the adjusted temperature in module 20, while the heat duty withdrawn is associated to the refrigeration cycle detailed in section IV.3.4.1. The heat exchange with the refrigeration cycle is modelled following the strategy proposed in section III.5.4, concerning the dissociation of double-stream heat exchangers. This separation can also be included as a supplementary mean for further separation of ammonia, after the membrane and the PSA separation.

The alternative separation methods are somehow interesting to avoid the low temperatures needed by the condensation stage, as the cooling requirements are in majority used to cool down the non-condensable compounds, (i.e., H<sub>2</sub> and N<sub>2</sub>). If either the membranes or the PSA allow to separate a significant amount of ammonia, the final interest resides in the purity of the product, to decide if a complementary separation by conventional condensation needs to be added. For any one of the separation techniques, the specific energy consumption is a useful indicator which can give insights on the interest to integrate the technology to the HB process superstructure.

### VI.3.2. Optimization problem formulation

Following the mathematical problem formulation in Superstructure III, as this case also concerns the separation of ammonia from the reactor outlet stream, the selected objective functions for minimization are the process LCOA and the specific energy consumption. The optimization variables concern 15 continuous variables and 5 structural variables, presented in Table VI-3 with the respective boundaries.

*Table VI-3. Continuous and discrete decision variables for the optimization of the superstructure IV. The process unit is referred to the superstructure representation shown in Figure VI-2.*

Variable	Type	Stage	Process unit	Bounds	Units
Adsorbent mass	Continuous	PSA	PSA black box	500 – 4000	kg
Temperature of the PSA columns	Continuous	PSA	27	523 – 773	K
Pressure in the low-pressure column	Continuous	PSA	PSA black box	10 – 40	bar
Total cycle time	Continuous	PSA	PSA black box	1200 - 14400	s
Membrane temperature	Continuous	Membrane	1, 3, 5, 7	313 – 423	K
Length of 1 <sup>st</sup> membrane	Continuous	Membrane	8	0.5 – 10	m
Length of 2 <sup>nd</sup> membrane	Continuous	Membrane	9	0.5 – 10	m
Length of 3 <sup>rd</sup> membrane	Continuous	Membrane	10	0.5 – 10	m
Sweep pressure for 1 <sup>st</sup> membrane	Continuous	Membrane	2	10 – 40	bar
Sweep pressure for 2 <sup>nd</sup> membrane	Continuous	Membrane	4	10 – 40	bar
Sweep pressure for 3 <sup>rd</sup> membrane	Continuous	Membrane	6	10 – 40	bar
Sweep flowrate for 1 <sup>st</sup> membrane	Continuous	Membrane	Sweep 1	0.1 – 20	kmol/h
Sweep flowrate for 2 <sup>nd</sup> membrane	Continuous	Membrane	Sweep 2	0.1 – 20	kmol/h
Sweep flowrate for 3 <sup>rd</sup> membrane	Continuous	Membrane	Sweep 3	0.1 – 20	kmol/h
Condenser temperature	Continuous	Condenser	20	250 – 273	K
Separation technology	Discrete	Structure	A	1 – 3	-
Number of PSA paired columns	Discrete	PSA	PSA black box	1 – 5	-
Number of membranes	Discrete	Membranes	A1, A2	1 – 3	-
Additional condenser separation	Discrete	Structure	C1	1 – 2	-
Pressure equalization in permeates	Discrete	Membranes	B1, B2, B3	1 – 2	-

The PSA section in the process involves the optimization of 5 variables, 4 continuous and 1 discrete. The total mass of adsorbent in all the columns, the temperature in the black box, the pressure in the LP column and the total cycle time, are declared as continuous variables. The fifth variable corresponds to the number of columns to be used in the PSA, which is declared as an integer variable. The pressure in the HP column is considered to be the same as the inlet pressure to the superstructure.

As the molar flowrates involved in the PSA model are normalized flowrates, the number of columns is used to calculate the flowrate per column. Also, this variable corresponds to one couple of columns, in order to use an even number of adsorbent beds. For instance, if the position of the variable is 3, it corresponds to 6 adsorption columns.

Next, the variables related to the membrane separation technology are similar to those used in Superstructure III, as well as the condenser temperature to be used as a supplementary separation or as an exclusive use of this technology, without considering the PSA nor the membranes.

Regarding the structural alternatives, they are represented by five discrete variables which allow to describe 22 different separation structures by combination of the positions. Evidently, some positions are exclusionary and do not affect certain alternatives. These alternatives can be represented by the following graph.

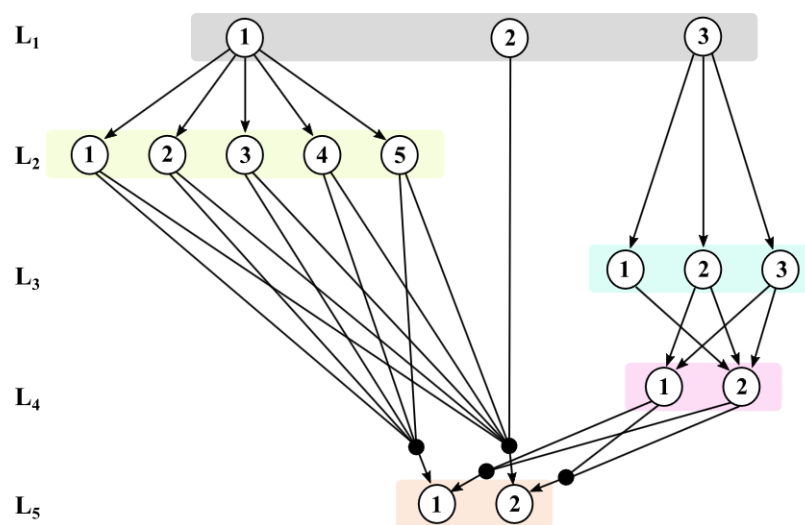


**Figure VI-3.** Graph diagram highlighting the structural alternatives for the superstructure of the separation technologies. The levels are the following, L<sub>1</sub>: separation technology, L<sub>2</sub>: number of couples of PSA columns, L<sub>3</sub>: number of membranes, L<sub>4</sub>: pressure equalization in the permeate streams, L<sub>5</sub>: additional separation by condensation.

The first variable represented in Figure VI-3 by level L<sub>1</sub> corresponds to the technology choice, having the positions 1: PSA, 2: Condenser, and 3: Membranes. In the second level, the number of column couples for the PSA allows to select between 2 and 10 columns. Note that this level is exclusive for the PSA. Next, in L<sub>3</sub>, the number of membranes vary between 1 and 3, excluding the paths from the PSA and the condenser. Following, the switch in L<sub>4</sub> represents the pressure equalization in the permeate streams for the membrane separation, being 1: Equalization and 2: Not equalization. Finally, in level L<sub>5</sub>, the additional separation is available in position 1, while the position 2 corresponds to no further separation. From the total of 22 different structures, 10 correspond to the PSA technology, 11 to the membrane separation and only 1 to the condensation method.

Concerning the inequality constraints defined for this optimization case, they include constraints for the global performance of the separation and others for the PSA model. In fact, as this black box model is based on ideal separation efficiencies, maximum limits of recovery for each one of the compounds are fixed. As described by the authors that proposed the pseudo-continuous model approach, the efficiencies of the model can be above 1, as it is based on ideal separation [158]. The 7 used constraints are the following:

- Minimum product flowrate, fixed to 10 kmol/h, to avoid null flowrates on the product stream.
- Maximum convergence criterion on the refrigeration cycle, fixed to  $1 \cdot 10^{-7}$ .
- Maximum  $N_2$  recovery on the High-Pressure Product stream of the PSA, fixed to 99.99 %.
- Maximum  $H_2$  recovery on the High-Pressure Product stream of the PSA, fixed to 99.99 %.
- Maximum  $NH_3$  recovery on the Low-Pressure Product stream of the PSA, fixed to 99.99 %.
- Maximum  $NH_3$  mole fraction in the recycle stream of the HB process, fixed to 6 %.
- Minimum  $NH_3$  purity in the product stream of the process, fixed to 95 %.

### VI.3.3. Algorithm parameters

The following algorithm parameters have been defined for the separation technologies superstructure optimization.

*Table VI-4. Values for the parameters of the optimization algorithm, in Superstructure IV. Non specified parameters have the value by default.*

Parameter	Values	Parameter	Values
ACCURACY	0.001	MAXTIME	216 000
EVALSTOP	50 000	MAXEVAL	100 000
NI	5	PRINTEVAL	10
-	-	SAVE2FILE	100 000

Due to the fast calculations and the low time required by this particular superstructure, the EVALSTOP parameter has been fixed to 50 000 evaluations and the MAXEVAL goes up to 100 000. The maximum time for optimization is fixed to 60 h, or 2.5 days.

The corresponding results for the optimization of this superstructure are presented and discussed in section VI.5, and complemented with those obtained in the optimization of Superstructure III in section VI.6.

## VI.4. Analysis of results for Superstructure III

For this case of study, the first alternative separation method is tested. The main interest of this superstructure optimization is to assess the membrane separation as method for the preferential concentration of ammonia from the reactor stage outlet mixture.

As exposed previously, the superstructures regarding the separation technologies are evaluated considering a constant mixture flowrate with known properties. Therefore, the compression and reaction stages of the HB are omitted, as a comparison between separation technologies is the purpose of this case, which includes the energy requirements on the recycle stage.

The optimization of Superstructure III allowed to achieve a total number of 137 283 evaluations, from which 57 668 (42 %) are feasible solutions and 67 are optimal points in the Pareto front. The separation cost to the LCOA varies between 128.7 and 150.4 €/t of  $NH_3$ , while the specific energy consumption of this process stage is found between 0.458 and 0.483 kWh/kg of  $NH_3$ .

It is necessary to highlight that every result here presented needs to be compared with the reference case for ammonia separation, it means the condenser. As a reference, the separation cost by condensation to the LCOA is equal to 82 €/t of  $NH_3$ , while the specific energy consumption represents 0.255 kWh/kg of  $NH_3$ , which are values obtained and detailed in the analysis of Superstructure IV. Therefore, the comparison of the competing separation technologies is carried out in section VI.6.

Recalling the structural alternatives there exists 3 discrete variables. The number of membranes, the pressure equalization in the permeate streams, and the additional separation by condensation. Figure VI-4 highlights these different structures according to the economic and energetic objective functions.

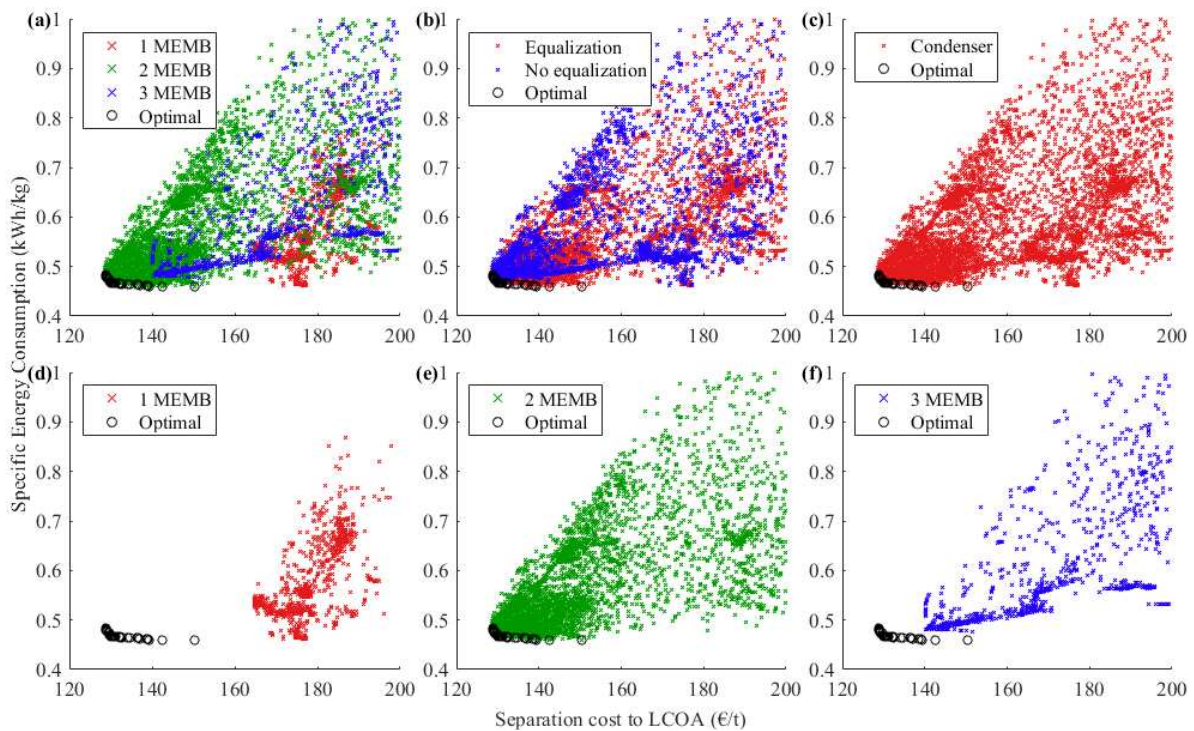


**Figure VI-4.** Distribution of the feasible solutions in the membrane superstructure optimization, according to the structural alternatives, highlighting the optimal solutions with black circles. Distribution of solutions according to (a) the number of membranes, (b) the pressure equalization in the permeate streams, and (c) the use of an additional condenser in the permeate stream. Subplots (d) to (f) are equivalent to (a) but have been separated to easily distinguish each structural alternative.

As seen in the summarizing subplot (a) for the number of membranes used, a denser and preferential population of feasible solutions is observed for the cases using 2 membranes. This is more evident when comparing the distribution of solutions in subplots (d) to (f), where the use of two membranes allows to achieve the lowest cost of separation, followed by the configurations with 3 membranes, and being the most expensive the case for only 1 membrane.

This permits to suggest that the solutions with 2 membranes achieve a good trade-off between productivity (i.e., ammonia separation) and investment. Conversely, the gain on the separation cost with a third module is hindered by the investment (more investment without a real gain in the productivity), and the use of a unique membrane does not allow to have a sufficient productivity to compete with the solutions with 2 membranes, even if the investment expenditures are lower for the solutions with 1 membrane.

In what concerns the use of the pressure equalization of the permeate streams, there does not exist an evident trend among the solutions, as seen in subplot (b). This is supported by the fact that, from the total of 67 optimal solutions, 33 of them use the pressure equalization and 34 do not include it, which is fairly distributed to suggest a preference. This point is further developed when comparing the optimal solutions.

Regarding the last structural variable, including an additional condenser on the permeate streams of the membranes is mandatory. As seen in subplot (c) not even a single feasible point avoids using the condenser. This suggests that the membrane as single separation technology does not fulfil the expected results in terms of ammonia purity in the product stream and ammonia content in the recycle stream.

Before continuing with the analyses of the feasible and optimal solutions, it is necessary to understand why such an important number of evaluations are infeasible (58 %) and which constraint is being responsible of the non-feasibility of these solutions.

#### VI.4.1. Constraints violation

This superstructure is subject to three inequality constraints. They concern the convergence of the refrigeration cycle, the maximum limit of 5 % on the  $\text{NH}_3$  content in the recycle stream, and the minimum  $\text{NH}_3$  purity in the product stream, fixed to 95 %.

In the following plots of Figure VI-5 are represented the infeasible solutions according to the constraint being violated. The constraint of the refrigeration cycle has not been included, as it is violated in less than a thousand cases, and its violation forces the separation cost to be equal to 1 000 €/t of  $\text{NH}_3$  by default.

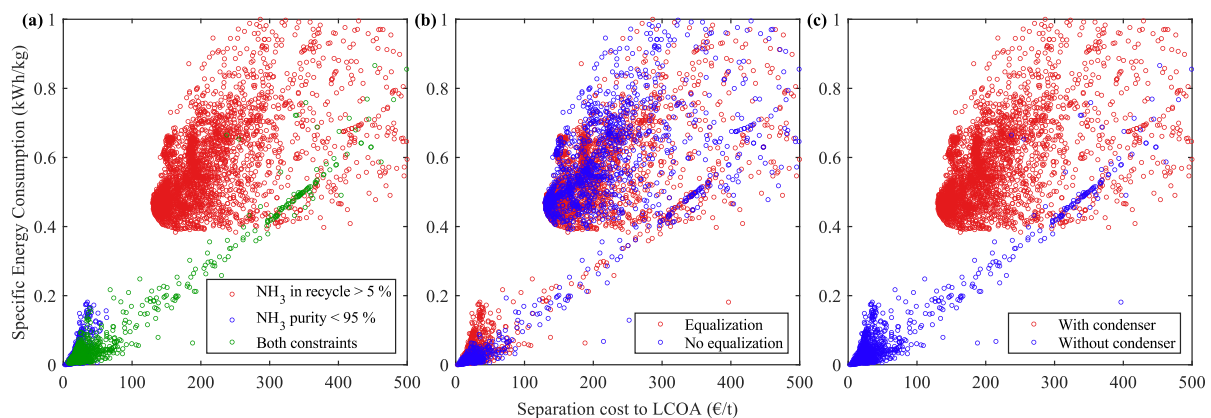


**Figure VI-5.** Maps for the identification of the constraint violation for the infeasible solution in the membrane superstructure. (a) Distribution of infeasible solutions according to the type of constraint violation, which can be due to higher mole fraction of  $\text{NH}_3$  in the recycle stream, lower  $\text{NH}_3$  purities in the product stream, or both.

In subplot (a) every infeasible solution is classified according to the constraint that has been violated, and also in the cases that both constraints are not respected simultaneously. A total of 32 341 solutions (23.6 % of all the solutions) violates only the constraint related to the  $\text{NH}_3$  mole fraction in the recycle given by the red points  $\circ$ , while 38 836 (28.3 % of all the solutions) do not respect the ammonia purity constraint, represented by blue points  $\circ$ . Also, 8 149 points (5.9 % of all the points) violate both constraints, as seen by the green points  $\circ$ .

When comparing the constraint violation type in subplot (a) and their relationship with the structural alternatives in subplots (b) and (c), there does not seem to be a direct relation with the pressure equalization in the permeate streams. Whether there exists or not pressure equalization, its main impact is reflected on the energy consumption of the separation process. Mixing two streams at different pressures in the process flowsheet induces a final pressure equal to the lowest of the mixing streams, requiring further mechanical work for compression in the subsequent compressors.

However, as seen for the use of an additional condenser (c), any solution without supplementary separation has either a violation due to an insufficient ammonia purity in the product stream or due to a double violation of constraints. The solutions that include the condenser are not feasible because of a higher ammonia content in the recycle than 5 %, with more than 91 % of non-feasible solutions being in the range between 5 and 6 %.

Therefore, this allows to conclude that the separation of  $\text{NH}_3$  by membrane filtering is not enough to achieve the specified molar fractions of ammonia in the recycle and product streams, requiring an additional stage of separation by condensation for improvement of these parameters.

#### VI.4.2. Analysis of optimal solutions

For the analysis of the optimal solutions as performed with the results of the previous superstructures, it is necessary to determine the differences between the set of optimal points, to select those that have the most significant variations. As every optimal solution uses two membranes and the additional condenser, the remaining structural variable concerns the choice of the pressure equalization on the permeate streams. Figure VI-6 shows in subplot (a) the distribution of optimal points according to the pressure equalization, while subplots (b) and (c) indicate the membrane temperature and the total length of the membranes, respectively.

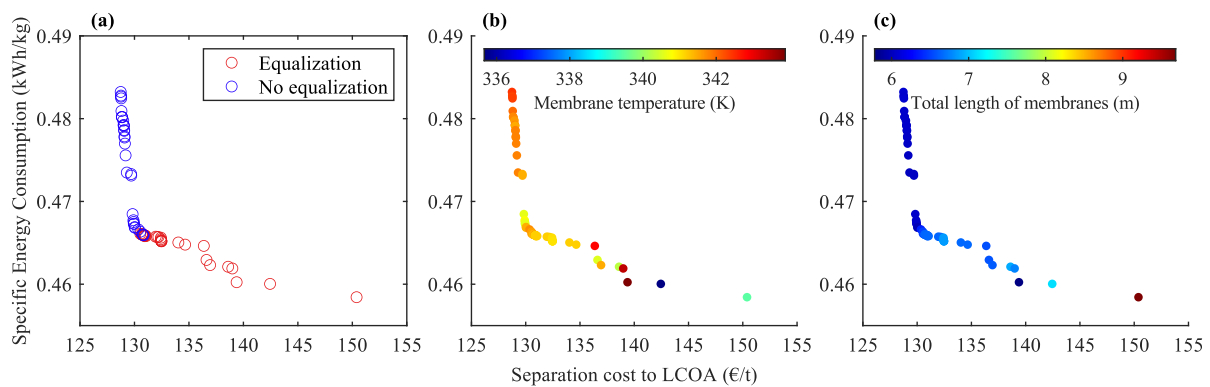


**Figure VI-6.** Distribution of optimal solutions for the membrane superstructure, according to (a) the pressure equalization on the permeate streams, (b) the membrane temperature, and (c) the total length of the membrane.

Regarding the choice of the pressure equalization, there exists two zones on the Pareto Front. The cheapest solutions with higher specific energy consumption, correspond to those solutions that do not include this structural alternative, while points tending to the most expensive cases having the lowest energy consumption, include the pressure equalization. Also, there is a region where both structural alternatives overlap, on the most accentuated change of slope of the Pareto front. In these points, those solutions with reported pressure equalization are in fact at equivalent pressure in the permeate streams, meaning that the pressure difference can be neglected, reason why these points are comparable to those without pressurization.

The impact of this structural alternative on the KPIs is easily deduced. To perform the pressure equalization between the permeate streams of membranes 1 and 2, an additional compressor is required in the permeate stream with the lowest pressure, allowing to increase the pressure up to the same level of pressure than the other permeate stream. This saves compression power as the mixing of permeate streams is performed at equal pressure. On the contrary, if no pressure equalization is carried out, the

mixing of streams would result in the lowest of the pressures, requiring further compression of this final stream to the recycle conditions of the HB process. Therefore, the power savings are reflected in the reduction of the specific energy consumption. On the other hand, including this additional compressor for pressure equalization is what increases the cost of the separation, as seen in subplot (a). This aspect is further detailed in sections VI.4.4 and VI.4.5.

Considering the temperature of the membrane and the total length of the modules, there is a preferential zone of the space search of variables that form the best trade-off between the KPIs. For the temperature, values somewhere between 340 and 343 K are preferred, while the total length of membranes finds an optimal region of solutions between 6 and 7.5 m. These variables, along with the rest of continuous variables are detailed in section VI.4.3.

To analyse the results, it has been decided to select a total of 4 optimal solutions from the Pareto front, reported in Table VI-5. Half of them use the pressure equalization and the remaining do not consider this alternative. The chosen points are well distributed among the set of optimal points, in order to cover the Pareto front from its most extreme points to those centred with the best KPI trade-off. A more exhaustive table containing more of the optimal solutions is available in the Appendix I, in section X.9.

*Table VI-5. Results of the KPI and the optimization variables for the optimal solutions of the membranes case. One point of each optimal configuration is selected. Data for the third membrane is omitted, as no optimal solution concerns this configuration.*

Key Performance Indicator	Units	Point 1	Point 2	Point 3	Point 4
Separation cost to LCOA	€/t	128.34	130.38	130.29	149.95
Specific energy consumption	kWh/kg	0.483	0.466	0.466	0.458
<b>Variables</b>					
Membrane temperature	K	342.44	341.31	341.31	339.48
Length of 1 <sup>st</sup> membrane	m	1.803	2.333	2.283	5.525
Length of 2 <sup>nd</sup> membrane	m	4.271	4.324	4.324	4.161
Pressure of sweep for 1 <sup>st</sup> membrane	bar	14.96	11.79	11.68	14.91
Pressure of sweep for 2 <sup>nd</sup> membrane	bar	10.04	11.69	11.69	11.14
Flowrate of sweep for 1 <sup>st</sup> membrane	kmol/h	0.10	0.10	0.10	0.14
Flowrate of sweep for 2 <sup>nd</sup> membrane	kmol/h	0.11	0.10	0.10	0.20
Condenser temperature	K	273	273	273	272.7
<b>Structural configuration</b>					
Number of membranes	-	2	2	2	2
Pressure equalization	-	No	No	Yes	Yes
Additional condenser	-	Yes	Yes	Yes	Yes
<b>Additional data</b>					
Total length of membranes	m	6.05	6.66	6.61	9.69
Total ammonia recovery	%	65.63	63.06	63.07	63.17
Ammonia mole fraction in recycle	%	4.67	5.00	5.00	4.99

According to the values of the optimization variables reported, some of them tend to the same value as the temperature, which have no more than 3 K of difference, and the pressures on the sweep streams, with not more than 5 bar between the lowest and the highest values. Similarly, the sweep flowrates tend to the lower bound of the variable (0.1 kmol/h), while the condenser temperature reaches its highest level at 273 K.

For every optimal solution of Table VI-5, as well as for the rest of points from the Pareto front, the total ammonia recovery reaches a range between 63.1 and 65.6 %, which is slightly higher than in the

solutions for the condenser separation of Superstructures I and II, where the same parameter achieved values between around 60 %. These results on ammonia separation efficiency are compared with the other separation technologies in section VI.6.

One important aspect that explains the overlapping of solutions for the choice between pressure equalization, as seen in Figure VI-6 (a) is evident with Points 2 and 3 of the previous table. The former solution does not include this structural alternative for the pressures on the permeate streams having a difference of 0.1 bar. On the contrary, the latter point does include this option, even if the pressure difference is 0.01 bar, being almost neglected. This explains why in the Pareto front, solutions appearing as including the pressure equalization have the same KPIs than those without this alternative.

### VI.4.3. Distribution of variables across their boundaries

In what concerns the values for the continuous variables optimized, Figure VI-7 shows the distribution of the variables of each variable according to the number of membranes of the feasible solutions, as well as the optimal points.

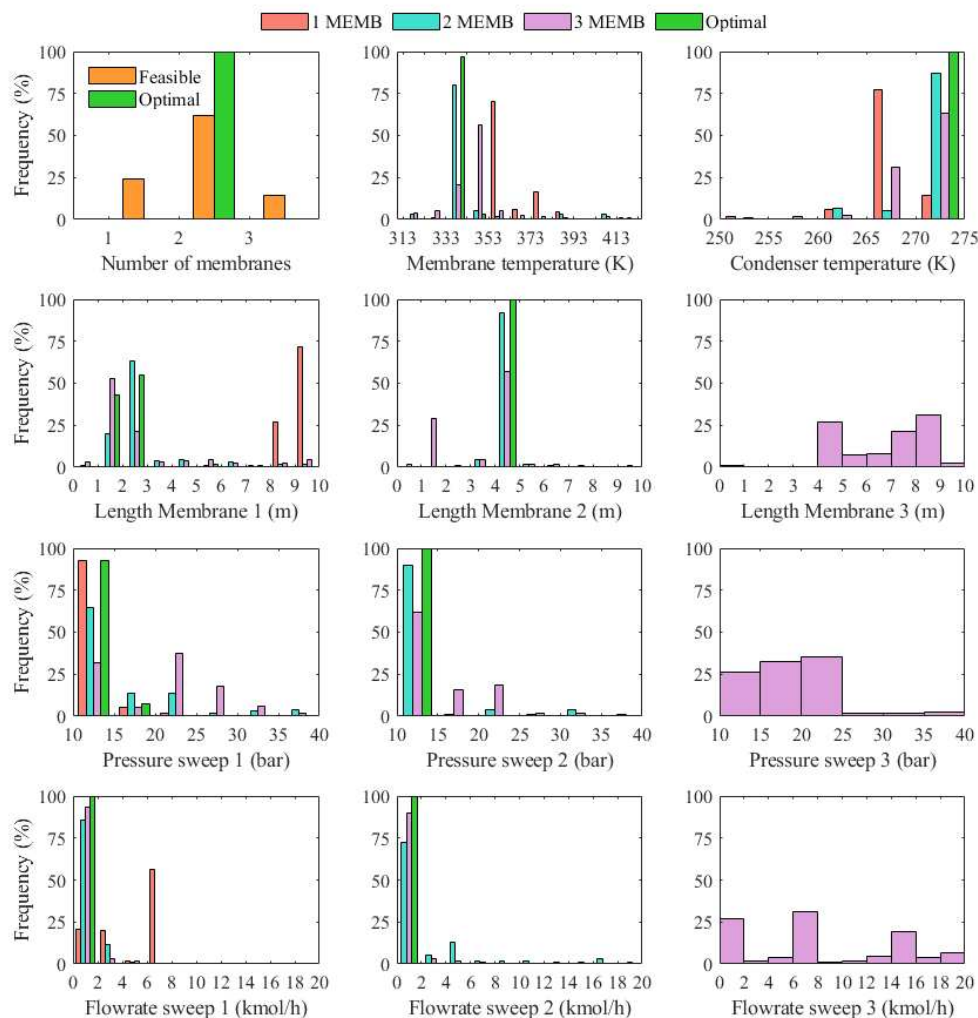


**Figure VI-7.** Histogram representing the incidence frequency for every optimization variable, for the membranes case. Data corresponds to every membrane configuration represented by the optimal solutions. The data considers only the solutions where the variable has an influence due to the structural arrangement. The data for the third membrane has been omitted, as no optimal solution was obtained for this configuration.

Concerning the number of feasible solutions for each configuration of membranes, 1 module is used in 24 % of cases, 2 membranes in 62 %, and 3 membranes in 14 % of the solutions. All the optimal cases use 2 membrane modules.

The operation temperature of the set of membranes has a preferential range for the optimal points between 333 and 343 K, and more precisely in values from 340 to 343 K, as given by the Pareto front observed in Figure VI-6. This preference is highlighted in the figure below, where the selectivities of ammonia over nitrogen and hydrogen are traced as a function of the membrane temperature, indicating the preferential zone of temperature of the Pareto front.

As can be seen, the selectivity of  $\text{NH}_3$  over  $\text{N}_2$  is greater than over  $\text{H}_2$ . On the region between the dashed lines, the selectivity over hydrogen is near its maximum, while its around 20 K lower from the maximum over nitrogen. However, as the selectivity over  $\text{H}_2$  is lower, the optimal temperature tends to maximize this selectivity to avoid more permeance of hydrogen across the ammonia.

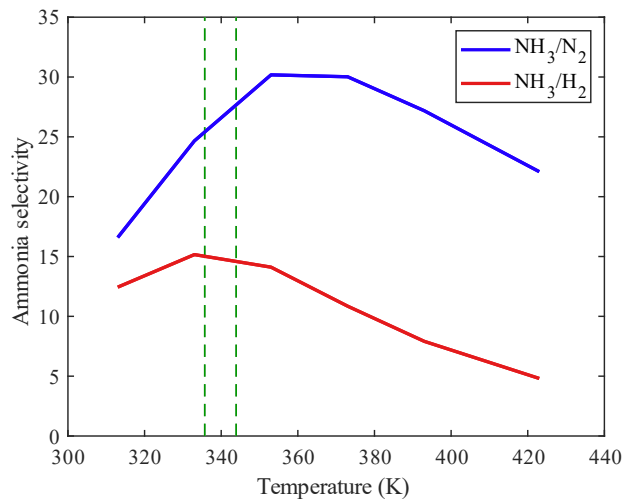


**Figure VI-8.** Mixed selectivities of ammonia over nitrogen and hydrogen as a function of the temperature on the membrane, with the region of temperatures of the optimal solutions highlighted by the dashed green lines - -. Ammonia selectivities are retrieved from [156].

On the other hand, the condensation temperature reaches the higher bound of the range of values, with the optimal solutions being placed between 270 and 273 K. At such temperatures it is possible to guarantee respecting the  $\text{NH}_3$  mole fraction in the recycle without requiring an expensive refrigeration cycle in terms of energy consumption.

Regarding the other parameters of the membranes, the optimal length for the first module is lower than for the second, while the sweep pressures tend to the lower bound of 10 bar. This creates the greatest possible partial pressure difference across the membrane from the retentate to the permeate side, favouring the ammonia permeation through the material. In the same sense goes the low sweep flowrates found for the optimal points, as they reach the lower boundary. This permits to avoid further dilution of ammonia on the permeate side, as the main interest is to recover as much  $\text{NH}_3$  as possible through the membrane, without prejudice of the  $\text{NH}_3$  mole fraction on the permeate due to the permeation of other compounds through the membrane or because of great sweep flowrates.

Concerning the data for the third membrane in the superstructure, there is not a trend in the length nor in the sweep specifications. In any case, using only one membrane or even a third membrane is not

recommended, as these configurations are far from being optimal, when compared to the solutions with 2 separation modules.

#### VI.4.4. Influence of the structure on the economic criteria

In this superstructure, the modules affecting the CAPEX and OPEX are the compressors, the membranes and the separation drum. To study the impact of the structural alternatives on the separation cost, it is necessary to distinguish the different modules of the separation process according to their function and stage.

For instance, the cost of the compressors is divided into the cost in the sweep streams, the pressure equalization step, the recompression before the condensation, the recompression of the recycle stage, and the compressors in the refrigeration cycle. Each group of compressors has a different share on the investment costs, and it is important to distinguish between them in order to determine which one of the stages has more or less impact on the cost.

In Figure VI-9 the share of CAPEX and OPEX for the equipment according to the section of the separation process are represented, as well as the share of electricity.

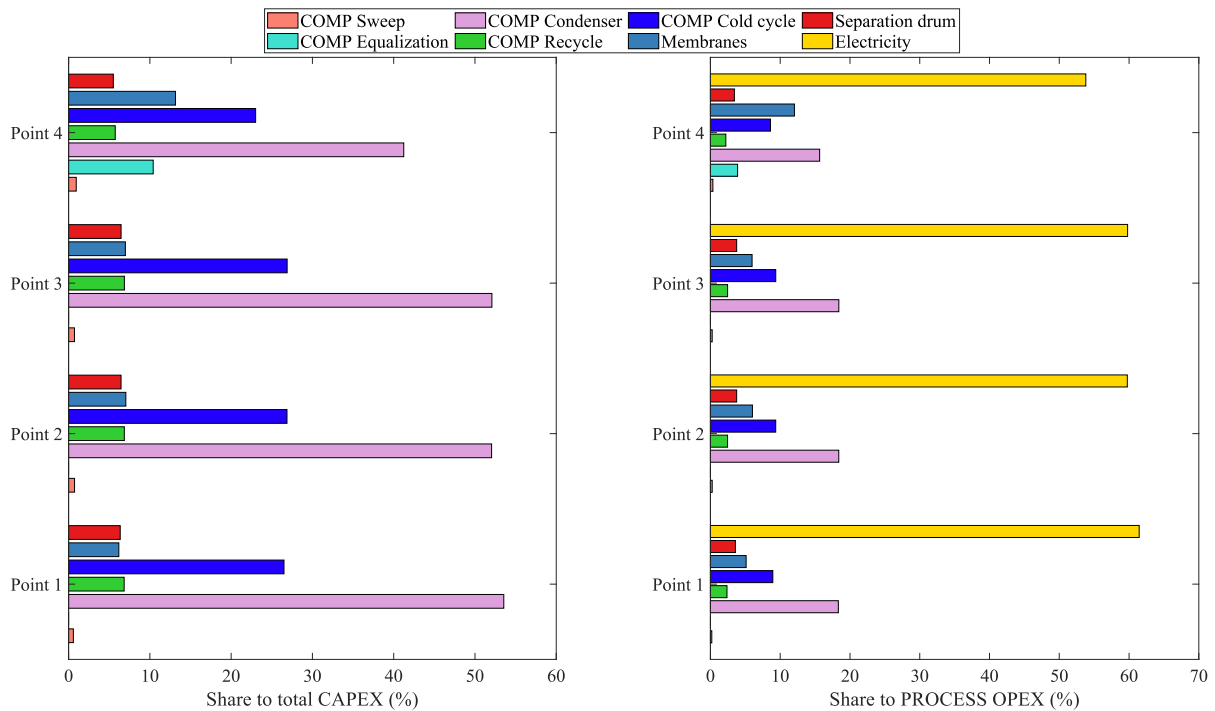


Figure VI-9. Share of CAPEX and OPEX according to the type of equipment and the stages of the separation process, for the optimal solutions of the membrane superstructure.

For a better understanding of the share of costs among the compressors, a recall of the process superstructure is necessary. The reader can refer to the optimal representation of the superstructure, presented in Figure VI-10.

The compressors for the sweep (COMP Sweep) are those responsible for the adjustment of the pressure in the sweep feeds entering to the shell side of the membrane, represented by modules 2, 4 and 6. The equalization compressors (COMP Equalization) are found at the permeate streams coming from the shell side of the membranes, as seen in modules 11, 13 and 16. Then, the condenser compressors (COMP Condenser) adjust the pressure to the required for the recycle on the HB process, as higher pressures

favour the supplementary ammonia separation in the condenser, given by modules 17 and 19. The compressors for recycle (COMP Recycle) are found on the final retentate stream of the membrane, adjusting the pressure to the one required on the recycle stage, which is the module 22. Finally, the modules of the cold cycle (COMP Cold Cycle) are the three units inside the refrigeration loop.

The units responsible for the higher CAPEX, between 40 and 54 %, are the compressors of the condenser preceding the separation drum. These units need a strong power for compression, as the incoming pressure is dictated by the optimization algorithm at the sweep streams pressure. The specified pressure for recycle is 98.4 bar, and the sweep pressures tend to the lower bound of 10 bar, requiring a pressure increase in more than 80 bar. The low pressures on the permeate side favour the ammonia permeation through the membrane but implies more compression power for further separation and recycle.

Following, the cold cycle compressors hold for a quarter of the capital expenditures, as three compressors are needed in the ammonia cold cycle. Reducing the number of compressors is not advisable, as the increase in temperature for small pressure changes is significant due to the properties of the refrigerant.

As it can be observed, the cost of the membranes is considerably low for this separation method. In the worst of cases, it represents 13 % of the CAPEX. Beyond this, the total share of compressors on the capital investment is at least 80 %. The most counterproductive modules are those of the condenser compression, as the low pressure of the permeate streams significantly increase the total cost of separation by the membrane technology. But, if no compression is performed in the permeate streams, further separation in the condenser could not be achieved due to the low-pressure level. At such low pressures (10 – 15 bar), the required cold temperatures could not be achievable by the current refrigeration cycle. In what concerns the OPEX share, the electricity is the main driver of the cost, with more than 50 % for all the selected cases.

Regarding the structural alternatives, the solutions where the pressure equalization are included are Points 3 and 4. Nevertheless, the pressure requirement in Point 3 is equal to 0.01 bar, being insignificant. On the contrary, in Point 4 a pressure increase of 3.8 bar is needed, inducing a share of 11 % on this compressors. At this point, for such a low-pressure difference, the impact on the CAPEX cannot be justified. Nevertheless, the effect on the energy efficiency needs an analysis, as carried out in the next section.

The annual cost of investment and maintenance for each one of the optimal solutions is reflected in the following table:

*Table VI-6. Parameters for the calculation of the economic performance indicator, for the optimal solutions of the membranes case.*

Key Performance Indicator	Units	Point 1	Point 2	Point 3	Point 4
Separation cost to LCOA	€/t	128.34	130.38	130.29	149.95
Specific energy consumption	kWh/kg	0.482	0.466	0.466	0.458
<b>Parameters</b>					
Annualized CAPEX	€/y	322 856.6	317 810.8	317 625.3	372 392.0
Annual OPEX	€/y	114 903.1	109 486.6	109 448.7	119 838.6
Ammonia production	t/y	3 410.77	3 277.12	3 277.66	3 282.70
Ammonia recovery	%	65.63	63.06	63.07	63.17

By comparing these points, it can be suggested that Point 2 and Point 3, which are placed in the same zone of the Pareto front have similar results, even if they are seemingly different in structure. This

follows the fact that the apparent pressure equalization does not have an impact on the economic indicators, due to the similar pressure on both permeate streams. Therefore, overlapping solutions with this specific difference in the structure would suggest a uniqueness in the process structure.

It is known that the alternative separation methods are compared against the condenser regarding the great temperature differences and the important heat duties involved, which in the end impacts on the energy criteria, hereafter analysed.

#### VI.4.5. Influence of the structure on the energy criteria

Following the impact of the process structure and the separation technology on the specific energy consumption, the information in Table VI-7 present the mechanical and thermal power parameters for each one of the sections of the superstructure in study. Again, its comparison with the condenser reference case is further detailed in Superstructure IV, focussing the analysis on this section to the competitive solutions between the membrane case.

Consider the extreme solutions for this case: Point 1 and Point 4, having the lowest separation cost and the lowest specific energy consumption, respectively. Point 1 has a cost 14 % lower than Point 4, but the latter has 5 % less energy consumption than the former.

*Table VI-7. Parameters for the calculation of the energetic performance indicator, for the optimal solutions of the membranes case.*

Key Performance Indicator	Units	Point 1	Point 2	Point 3	Point 4
Separation cost to LCOA	€/t	128.34	130.38	130.29	149.95
Specific energy consumption	kWh/kg	0.482	0.466	0.466	0.458
<b>Requirements</b>		<b>Mechanical energy balance</b>			
Compressors on sweep streams	kW	0.042	0.031	0.030	0.076
Compressors on permeate streams	kW	-	-	0.001	17.657
Compressors before condenser	kW	171.21	156.45	156.50	135.77
Compressor for HB recycle	kW	5.47	5.32	5.33	5.15
Compressors in the cold cycle	kW	28.54	28.38	28.38	28.78
Total mechanical power	kW	205.26	190.18	190.24	187.43
Specific mechanical power	kWh/kg	0.482	0.466	0.466	0.458
<b>Requirements</b>		<b>Thermal energy balance</b>			
Reactor stream cooling duty	kW	1 028.80	1 031.81	1 031.69	1 036.73
Sweep streams heating duty	kW	0.038	0.041	0.042	0.040
Permeate streams cooling duty	kW	13.04	12.26	12.29	28.68
Condenser stream cooling duty	kW	341.74	321.17	321.24	301.33
Recycle streams heating duty	kW	701.09	707.25	707.14	711.47
Ammonia product heating	kW	7.98	7.67	7.67	7.85
Cold cycle cooling duty	kW	118.87	118.19	118.22	119.08
Cold cycle heating duty	kW	91.75	91.23	91.25	91.74
Total thermal power losses	kW	701.58	677.22	677.32	674.72
Specific thermal losses	kWh/kg	1.645	1.653	1.653	1.644

Comparing the values across the solutions, differences are found in the mechanical power consumption of the compressors on the permeate streams and before the condenser. Avoiding this structural alternative of pressure equalization results in higher power requirements. For instance, the two permeate streams of point 1 are at 14.96 and 10.04 bar, while those of point 4 are at 14.91 and 11.14 bar, being the pressure difference somehow similar. The total power of compression before the condenser in Point 1 is 171.2 kW, while the sum of power of the permeate pressure equalization and before the condenser is 155.4 KW for Point 4. The final impact is seen in the specific energy consumption.

Regarding the thermal energy balance there are some differences across the modules of the separation stage, but the effect in the final value of specific thermal losses is not considerably impacted. Even if this indicator is only referred to the separation stage of the HB process, a further analysis including every stage on the  $\text{NH}_3$  synthesis process is required, as detailed in the next chapter.

For this specific superstructure optimization, the solution of Point 3, using 2 membranes, the additional separation by condensation and without pressure equalization on the permeate streams (as dictated by the pressures of the corresponding streams), gives a good trade-off between separation cost and energy consumption. The superstructure representation for this configuration is shown in Figure VI-10, while the complete ProSimPlus flowsheet is shown in Appendix J, in section X.10, including the process mass balances.

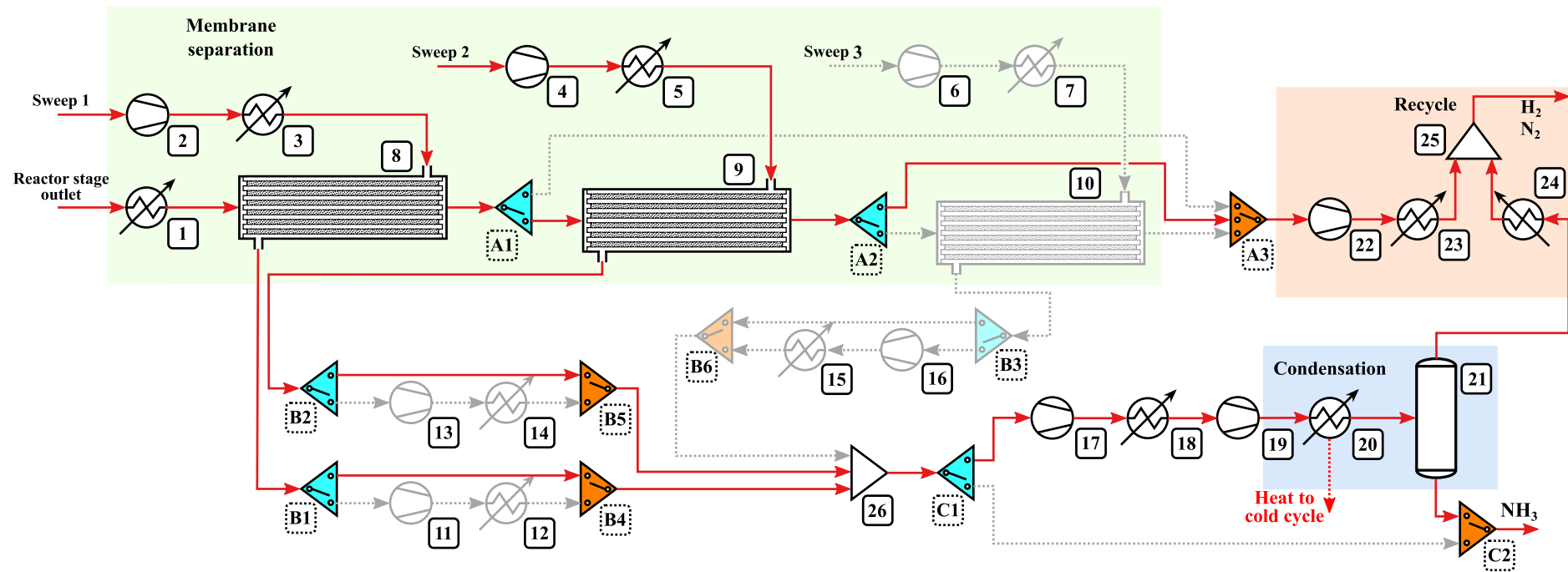


**Figure VI-10.** Superstructure representation of the optimal solution for the membrane separation case. The structure is defined by the red solid process streams  $\color{red}\longrightarrow$ , and the black unit operations. The bypassed streams are the grey dotted streams  $\color{grey}\dashrightarrow$ , while the inactive modules are the grey modules.

## VI.5. Analysis of results for Superstructure IV

For the last superstructure in study, the PSA model is integrated to the Superstructure III to compare its performance with the membrane filters. Here, the condenser is also considered as a unique technology, but can serve as a supplementary separation in case that the alternative methods are not enough to achieve the imposed requirements of purity in the product and composition in the recycle.

This case can be seen as a further development of the Superstructure III, and even it could have been integrated to the results of the previous one, to avoid dividing the cases. Nevertheless, it has been decided to separate them, as for the Superstructures of the reactors, in order to better analyse the results.

### VI.5.1. Analysis of optimal solutions

The optimization of Superstructure IV allowed to achieve a total number of 68 912 evaluations, from which 54 733 (79.4 %) are feasible solutions and 559 are optimal points in the Pareto front, all of them belonging to the condenser separation. For these points, the separation cost to the LCOA varies between 82.0 and 83.5 €/t of NH<sub>3</sub>, while the specific energy consumption of this process stage is found between 0.239 and 0.255 kWh/kg of NH<sub>3</sub>. The feasible solutions are reported in the following figure.

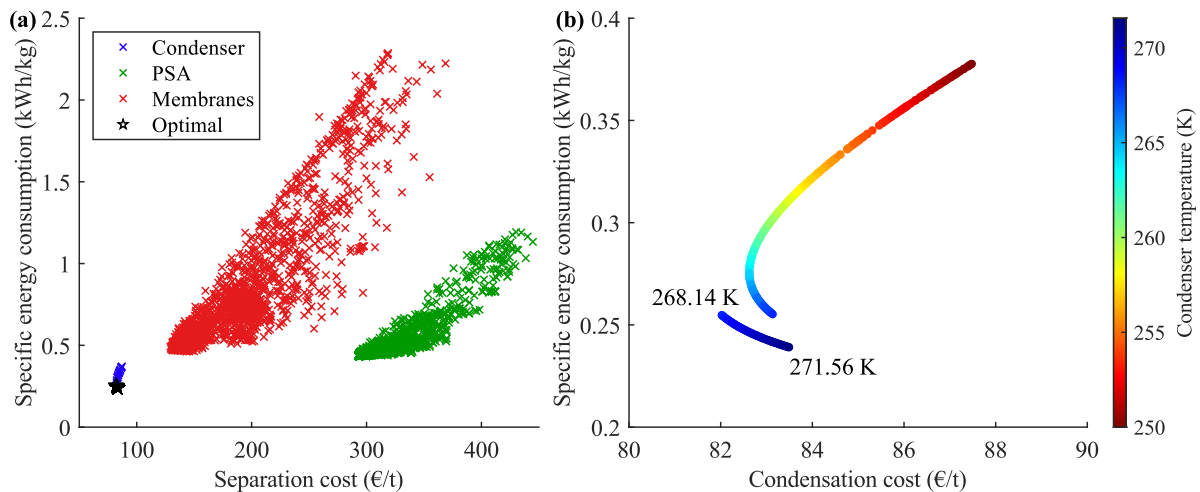


**Figure VI-11.** (a) Distribution of the feasible and optimal solutions according to the separation technology in study for the Superstructure IV. (b) Zoom on the condenser separation case, highlighting the optimal solutions represented by the lower branch with the blueish points.

There is no doubt that the separation by condensation offers the best trade-off between economy and specific energy consumption. Subplot (a), showing the distribution of the feasible solutions according to the separation technology indicates with three clear clusters of points, that each separation technology has an optimum range of solutions, different from the others. In terms of separation costs, from the cheapest to the most expensive, the condenser is placed in first, followed by the membrane separation and last the PSA. Analogously for the energy consumption, the condenser presents the best solutions, while the membranes and the PSA are somehow competitive between them regarding this indicator.

On subplot (b), the feasible solutions for the condenser are shown. This trend has a particular behaviour. For this technology, the unique optimization variable that intervenes is the separation temperature that is fixed in the HEX prior the separation drum. As seen, there is a discontinuity between the optimal points (lower branch) and the rest of feasible solutions (upper branch). Also, every optimal solution has

a temperature between 268.14 and 271.56 K. This discontinuity behaviour is related to the cost of the separation drum and is inspected in section VI.5.2.

Even if only the condenser technology reaches the optimality, it is interesting to study the best trade-off between the points of the other separation methods. With this purpose, the following points are considered for the different analyses that are presented in the subsequent sections. As every optimal solution is represented by the same structural alternative, only some representative points are shown in Appendix K, in section X.11.

For these selected points, the optimal configuration is considered to be the solution with the lowest cost of separation for the condenser, as seen in Figure VI-11 (b), with a separation temperature of 268.14 K. The other point for the condenser corresponds to the first point of the upper branch, with equal energy consumption as the optimal, but slightly higher cost of separation. Point 3, corresponding to the membrane separation technology, and Point 4, using the PSA as method to recover ammonia, are the points best placed among their concurrent solutions.

**Table VI-8.** Results of the KPI and the optimization variables for the optimal solutions of the separation superstructure, showing the values that have an influence on the structure.

Key Performance Indicator	Units	Point 1	Point 2	Point 3	Point 4
Separation cost to LCOA	€/t	81.83	82.96	130.45	293.38
Specific energy consumption	kWh/kg	0.255	0.255	0.466	0.435
<b>Variables</b>					
Adsorbent mass	kg	-	-	-	4000
Temperature of the PSA columns	K	-	-	-	523
Pressure in the low-pressure column	bar	-	-	-	40
Total cycle time	s	-	-	-	1200
Membrane temperature	K	-	-	341.62	-
Length of 1 <sup>st</sup> membrane	m	-	-	2.29	-
Length of 2 <sup>nd</sup> membrane	m	-	-	4.32	-
Sweep pressure for 1 <sup>st</sup> membrane	bar	-	-	11.74	-
Sweep pressure for 2 <sup>nd</sup> membrane	bar	-	-	11.75	-
Sweep flowrate for 1 <sup>st</sup> membrane	kmol/h	-	-	0.11	-
Sweep flowrate for 2 <sup>nd</sup> membrane	kmol/h	-	-	0.13	-
Condenser temperature	K	268.14	268.13	272.83	271.39
<b>Structural configuration</b>					
Separation technology	-	Condenser	Condenser	Membranes	PSA
Number of PSA columns	-	-	-	-	2
Number of membranes	-	-	-	2	-
Additional condenser separation	-	-	-	Yes	Yes
Pressure equalization in permeates	-	-	-	Yes	-

The solution for the membrane configuration is, in fact, reasonably close to the optimal solution obtained in the optimization of Superstructure III, with similar values of the KPIs and the optimization variables. For the considered optimal solution of the PSA separation, there is an interesting behaviour for the values of the variables. The adsorbent mass and the pressure in the low-pressure column reach the upper bound of the space search. On the contrary, the temperature of the columns and the total cycle time get to the lowest available values.

For the three competitive separation technologies, it is necessary to determine the separation efficiency in terms of ammonia production, ammonia purity in the product stream, and ammonia content in the recycle stream. These indicators are discussed in the following section.

### VI.5.2. Separation efficiency and productivity

Depending on the selected separation technology, the amount and purity of the produced ammonia might vary. In Table VI-9 are presented the values allowing to discuss the differences between the separation efficiencies for each one of the points previously selected.

*Table VI-9. Comparison of the separation efficiency for the selected optimal points of each separation technology.*

Parameter	Units	Point 1	Point 2	Point 3	Point 4
Main separation NH <sub>3</sub> recovery	%	60.73	60.72	69.49	71.18
NH <sub>3</sub> molar fraction in main separation	%	99.55	99.55	41.76	53.21
Global separation NH <sub>3</sub> recovery	%	60.73	60.72	63.14	67.23
NH <sub>3</sub> molar fraction in product stream	%	99.55	99.55	99.50	99.51
NH <sub>3</sub> molar fraction in recycle stream	%	4.98	4.99	4.99	4.47

The first two parameters indicate the separation performance of the principal technology being evaluated, meaning that the additional separation by condensation is not considered. This allows to understand how effective the technology is regarding the condenser.

Both the membranes and the PSA methods allow a higher ammonia recovery, defined the percentage of NH<sub>3</sub> in the permeate and low-pressure streams, respectively, regarding the total amount of ammonia fed to the separation stage. However, when comparing the ammonia purity exclusively obtained by these modules, they are far from the required purity of 95 %, with membranes reaching 41.8 % and the PSA a fraction of 53.2 %. This is explained by the fact that a considerable amount of H<sub>2</sub> permeates the membrane, even if the material is around 10 times selective to ammonia over hydrogen. On the PSA separation, a stoichiometric fraction of H<sub>2</sub>:N<sub>2</sub> is also present in the low-pressure stream (both compounds are considered to have the same isotherms and adsorption behaviour), as they are somehow adsorbed in the columns.

With the additional separation by condensation, the total ammonia recovery decreases in 6.3 % for the membranes and in 4 % for the PSA, as the condenser is not able to completely separate the ammonia. However, this additional stage fulfils the purity requirements on the product stream.

The analysis that is hereafter proposed concerns the impact of the separation technologies and the structural choices on the economic and energetic criteria. It is important to understand why these competing technologies give such values for the KPIs, and what is impeding, in the case of the membranes and the PSA, to decrease their separation cost.

### VI.5.3. Influence of the structure on the economic criteria

The optimal case of the condenser (Point 1) is defined as the reference level for comparison with the best results obtained for the other separation technologies. The data presented in Table VI-10 serves as basis for the analysis.

Focussing the attention on the differences between Points 1 and 2, with exactly the same energy consumption, there exists a variation in the separation cost which is explained by the cost of the separation drum. These points represent the trend break seen in Figure VI-11 (b) and is explained from the investment correlation of the separation drum, which is a function of the condenser temperature. The slight temperature change between solutions (0.01 K) crosses a frontier in the correction factors of the drum, affecting the total investment price of the module and provoking this trend rupture in the feasible

solutions. Therefore, the CAPEX and OPEX for the separation drum of Point 2 increase around 17 % regarding Point 1, while the rest of parameters remain similar.

Following, the best solution obtained for the membrane configuration has an increase of 60 % in the separation cost. It is due to the required compressors and the membrane modules, representing a share of 80 % and 20 % in the CAPEX increase, respectively. The same trend is observed on the OPEX.

**Table VI-10.** Parameters for the calculation of the economic performance indicator, for the optimal solutions of the separation superstructure, including the best non-optimal solutions for the membrane and PSA technologies.

Key Performance Indicator	Units	Point 1	Point 2	Point 3	Point 4
Separation cost to LCOA	€/t	81.83	82.96	130.45	293.38
Specific energy consumption	kWh/kg	0.255	0.255	0.466	0.435
Parameters		Capital Expenditures (CAPEX)			
Compressors	€	1 774 101	1 774 477	2 706 216	3 018 952
Separation drum	€	171 552	200 438	201 287	197 347
Membranes	€	-	-	218 105	-
Adsorption columns	€	-	-	-	1 466 755
Adsorbent	€	-	-	-	3 991 523
Parameters		Operational Expenditures (OPEX)			
Compressors	€/y	21 500	21 504	33 443	37 620
Separation drum	€/y	3 474	4 098	4 117	4 112
Membranes	€/y	-	-	6 543	-
Adsorption columns	€/y	-	-	-	32 179
Electricity	€/y	34 397	34 413	65 563	65 171
		Calculation of the separation cost to LCOA			
Total CAPEX	€	1 945 654	1 974 915	3 125 608	8 674 578
Annualized CAPEX	€/y	198 169	201 150	318 350	883 525
Total OPEX	€/y	59 370	60 015	109 667	139 081
Ammonia yearly production	t/y	3 147.4	3 148.2	3 281.2	3 485.4

Regarding the PSA technology, there is a considerable increase of 250 % on the separation cost. Along with the additional investment in compressors, the main driver of the CAPEX is the cost of the adsorbent, followed by the adsorption columns. The sum of these two components represent 63 % of the CAPEX, which is considerably harmful for the competitiveness of the technology, as the final production of ammonia is higher for this method of separation than for the others.

When comparing the ammonia yearly production, an increase of 10.7 % is observed for the PSA separation, while it grows in 4.3 % for the membranes case. However, these technologies remain considerably expensive and their gain in productivity do not justify the economic harm of the investment.

#### VI.5.4. Influence of the structure on the energy criteria

Once analysed the impact of the technologies on the economic criteria, it is necessary to determine if the same effect is seen in the energy criteria. A direct comparison of the specific energy consumption suggests this same trend. However, the purpose of evaluating other separation technologies is also focussed on reducing the amount of thermal energy requirements and losses from the system.

As seen in Table VI-11, the lowest mechanical power consumption is achieved in the separation by condensation, determined by the power consumed by the compressors in the refrigeration cycle. For membranes and PSA separation, the mechanical power is increased to approximately the same value, as

additional compressors are required. This mechanical power parameter has a direct and proportional effect on the specific energy consumption.

In the same trend goes the thermal power requirements, as the condenser technology has the lower specific thermal losses in comparison to the other methods. For the condensation method, the whole of the process stream flowing from the reactor outlet stage is cooled down to the required separation temperature, which is why the thermal power release is the highest, when compared to the membranes and the PSA.

In contrast, the membranes and PSA technology require smaller temperature differences to separate a fraction of the ammonia in their respective modules. Further cooling for the additional separation by condensation incurs in lower cooling duties, as a great part of the incondensable gases have been withdrawn from the process stream.

Nevertheless, when considering the ideal thermal integration and calculating the net thermal power requirements, the condenser system achieves the lowest difference between the cooling and heating requirements, followed by the membranes and the PSA.

*Table VI-11. Parameters for the calculation of the energy performance indicator, for the optimal solutions of the separation superstructure, including the best non-optimal solutions for the membrane and PSA technologies.*

Key Performance Indicator	Units	Point 1	Point 2	Point 3	Point 4
Separation cost to LCOA	€/t	81.83	82.96	130.45	293.38
Specific energy consumption	kWh/kg	0.255	0.255	0.466	0.435
<b>Parameters</b>					
Separation technology	-	Condenser	Condenser	Membranes	PSA
Mechanical power	kW	99.99	100.04	190.59	189.45
Thermal power release	kW	1718.66	1718.83	1483.44	1077.39
Thermal power supply	kW	1145.09	1145.16	806.36	382.83
Net thermal power	kW	573.57	573.67	677.08	694.56
Ammonia hourly production	kg/h	393.43	393.53	410.15	435.67
<b>Results of the thermal balance</b>					
Specific thermal losses	kWh/kg	1.458	1.458	1.651	1.594

For the global balance of thermal energy, the specific thermal losses are calculated from the net thermal balance and the amount of produced ammonia. This parameter shows that, only for the separation stage, the greatest specific energy release to the environment is found for the membrane filtration, with 1.65 kWh/kg of NH<sub>3</sub>, followed by the PSA technology, at 1.59 kWh/kg of NH<sub>3</sub>, and last by the membrane separation, with 1.46 kWh/kg of NH<sub>3</sub>.

Until now, the condenser has been presented as the optimal technology for the recovery of ammonia from the process stream due to its low cost of separation. The flowsheet representation for this solution, including the material balance of the process is depicted in the Appendix L, in section X.12.

The values presented for the energy balance of the different separation methods are only referred to the separation stage and they need to be included in the HB process envelope. This allows to determine potential thermal integration with other stages of the processes. For this purpose, a process thermal balance and integration potential is presented in the next chapter.

## VI.6. Summary of results and discussion

Having studied the Superstructures proposed in this Chapter for application of the superstructure optimization methodology, the analyses of results presented in this chapter were focused on determining how the structural alternatives, related to the separation technologies, affect the KPIs.

This permits to select, among the optimal solutions obtained, the structure that offers the best trade-off between the performance indicators. In this last section, a comparison between the optimal solutions retained for both superstructure cases is presented. The following data allow to compare the optimal solutions obtained for each one of the cases.

*Table VI-12. Summary of optimal solutions for the separation configuration, according to the results of the superstructure optimization of cases III and IV.*

Key Performance Indicator	Units	Case III	Case IV
Process LCOA	€/t	130.68	81.83
Specific energy consumption	kWh/kg	0.466	0.255
Additional data			
Main separation technology	-	Membranes	Condenser
Additional condenser	-	Condenser	-
Main separation NH <sub>3</sub> recovery	%	69.49	60.73
Main separation NH <sub>3</sub> purity	%	41.76	99.55
Global separation NH <sub>3</sub> recovery	%	63.14	60.73
Global separation NH <sub>3</sub> purity	%	99.50	99.55
NH <sub>3</sub> mole fraction in HB recycle stream	%	4.99	4.98
Ammonia yearly production	t/y	3 277.66	3 147.4
Specific mechanical power	kWh/kg	0.466	0.290
Specific thermal losses	kWh/kg	1.653	1.458

The evaluation of the alternative separation technologies, membranes and PSA, have shown that their use as unique separation method is not enough to achieve the required mole fractions of ammonia in the product and the recycle stream. However, they can be used as a preliminary separation method, allowing to avoid such cooling duties in the separation by condensation, as seen when only the condenser is used. These technologies allow to remove part of the non-condensable compounds of the process stream (i.e., H<sub>2</sub> and N<sub>2</sub>), avoiding its cooling and subsequent reheating in the recycle stage.

Cases III and IV were evaluated for a constant flowrate of the reactor outlet stream, under equivalent conditions. While the membrane separation allows the recovery in the permeate streams of more than 69.5 % of the available ammonia, the condenser reaches a recovery of 60.7 % on the product stream. Nevertheless, the ammonia purity on the permeate side is just 41.8 %, as great part of the hydrogen in the process stream permeates the membrane material. On the contrary, the sole separation by condensation permits achieving an ammonia purity higher than 99 %, as required by the process specifications.

Furthermore, more mechanical energy is required when the membrane separation is included, as it is associated with multiple compressors to be included on the sweep and permeate streams, and the thermal losses in this stage follow the same trend. Thus, considering not only the economic parameters but also energy consumption and losses, the separation by condensation is by far the best suitable technology to use in this process. The superstructure representation for this selection is, in conjunction with the autothermal configuration for the reaction stage, presented in the next chapter, where the analysis of the thermal integration potential is presented.

## VI.7. Improvement scenarios for competitiveness

According to the results obtained by the optimization of Superstructure IV, three clusters have been identified in the chart showing the relation between the objective functions, as given in Figure VI-11. As the membrane and PSA performance have a strong dependence on the material used for the separation, in both cases zeolitic materials, the final cost and energy consumption is strongly related to the characteristics of each one of these materials.

Therefore, it is possible to consider hypothetical improvements on the separation performance in order to define how much a material needs to be improved to be competitive with the conventional separation technique, in this case the condenser. In the end, the question to be answered is whether these ideal improvements allow to achieve similar values on the KPIs regarding the condenser.

With this purpose, as the results for the membrane separation are closer to the condenser than those of the PSA, it has been decided to select the best achieved solution for the membrane separation technology, as given in Table VI-8, and to include a multiplicative factor in the permeation correlation of ammonia, to study the influence of the hypothetical improvement of the permeance of this compound, will keeping constant the permeance of  $H_2$  and  $N_2$ . This allows to increase the  $NH_3$  selectivity without creating further permeation of the undesired compounds.

In Figure VI-12, the improvements on the KPIs are reflected as a function of the increase on the permeability of ammonia, by use of the permeability factor, which varies from 1 to 10.

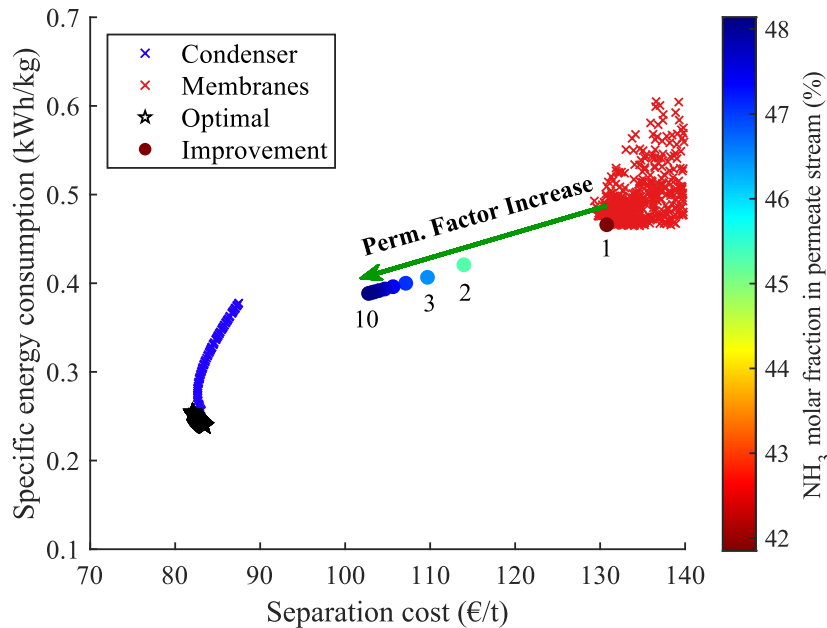


**Figure VI-12.** Improvements on the KPIs according to the hypothetical increase on the  $NH_3$  permeability, keeping constant the  $N_2$  and  $H_2$  permeabilities. The permeability factor corresponds to a multiplicative factor on the ammonia permeability correlation. The selected solution for the analysis is the best achieved solution, given in Table VI-8. The coloured points indicate the final ammonia molar fraction on the permeate stream.

It can be seen from the previous figure that a strong improvement is evident when doubling the permeability factor from the current optimal solution (1). For the maximum improvement of the factor (10), the effect of doubling this factor reaches more than a half of the maximum achievable gain in separation cost and specific energy consumption. Beyond this factor, the gain on the KPIs are gradually reduced until no further improvement.

Consider the best solution achieved by the condenser with a separation cost of 81.82 €/t<sub>NH<sub>3</sub></sub>, and a specific energy consumption of 0.255 kWh/kg<sub>NH<sub>3</sub></sub>, and the optimal solution by the membranes with a separation cost of 130.45 €/t<sub>NH<sub>3</sub></sub>, and a specific energy consumption of 0.466 kWh/kg<sub>NH<sub>3</sub></sub>. The following table allows to compare the results for the hypothetical improvement scenario with these optimal solutions.

*Table VI-13. Results of the KPI for the improvement scenarios with the optimal structure of the membrane as reference case.*

Reference	Separation cost	Spec. energy consumption	NH <sub>3</sub> purity	Condenser cost surplus	Membrane cost reduction	Condenser energy surplus	Membrane energy reduction
	€/t <sub>NH<sub>3</sub></sub>	kWh/kg <sub>NH<sub>3</sub></sub>	%mol				
Condenser	81.83	0.255	99.55	-	-	-	-
Membrane	130.45	0.466	41.76	59.82 %	-	82.73 %	-
<b>PF</b>							
2	113.97	0.421	45.28	39.28 %	- 12.63 %	65.01 %	- 9.70 %
3	109.69	0.407	46.48	34.04 %	- 15.92 %	59.50 %	-12.72 %
4	107.13	0.400	47.08	30.92 %	- 17.88 %	56.86 %	- 14.17 %
5	105.63	0.396	47.43	29.09 %	- 19.02 %	55.31 %	- 15.01 %
6	104.66	0.393	47.67	27.89 %	- 19.77 %	54.31 %	- 15.56 %
7	103.97	0.392	47.84	27.05 %	- 20.30 %	53.60 %	- 15.95 %
8	103.46	0.390	47.96	26.43 %	- 20.69 %	53.08 %	- 16.24 %
9	103.06	0.389	48.06	25.95 %	-20.99 %	52.67 %	- 16.24 %
10	102.75	0.388	48.14	25.57 %	- 21.23 %	52.35 %	- 16.63 %

The use of a membrane material at least twice performant regarding the ammonia permeability could allow to reduce the separation cost in at least 12.6 %, while saving almost 10 % on energy consumption. This represents a surplus on the separation cost of 39.4 % and on the energy consumption of 65 %, regarding the separation by condensation. Further hypothetical improvement on the permeability factor (PF) shows a decrease on the cost and energy savings when compared to the reference case of the optimal membrane solution, until no further evident improvement can be obtained.

Regarding the ammonia purity on the permeate stream, there exists an increase of almost 4 percentual points when doubling the PF value, while it gains around 7 percentual points for a PF of 10. As the process structure remains fixed for this hypothetical scenario, the real improvements on the KPIs and the ammonia purity can be hindered by the use of a suboptimal process structure.

Evidently, if the membrane material to be used had a greater NH<sub>3</sub> permeability while keeping constant the permeabilities of H<sub>2</sub> and N<sub>2</sub>, this would require executing another superstructure optimization, as the operating conditions and the membrane parameters might differ for different performance on the materials. This could lead to new optimal configurations, operating conditions and membrane parameters, different to the current optimal solution. However, to determine the real impact of these scenarios, independent superstructure optimization need to be performed for each one of the hypothetical cases.

Beyond this, the analysis of the ideal PF increase for the given optimal solution of the membrane shows that, for strong increases in the performance of the membrane material, the membrane configuration remains at higher levels of KPI regarding the optimal solutions of the condenser. Nevertheless, this allows to understand how possible improvements on the separation material could be reflected on the KPIs and how they approach towards the conventional separation technique.

## VI.8. Conclusions

The different analyses presented in this Chapter were intended to describe the impacts of the structural alternatives on the KPIs of each superstructure, in order to understand how the selection of an additional operating unit repercussions on the economic and energetic performance indicators.

For sure, further analyses could be proposed to go deeper into the details of the impact of each optimization variable on the KPIs, to identify the possible relationships existing between structural variables and operating conditions, and so on. Nevertheless, it has been found that the proposed methodology has allowed to largely study the process alternatives and to define the most suitable architecture, under the considered hypothesis.

The separation by condensation remains the most favourable technology to include in the HB process for ammonia recovery. For the best of the solutions, its costs represents 81.83 €/t<sub>NH<sub>3</sub></sub>, around 38 % cheaper than the separation by membranes (130.68 €/t<sub>NH<sub>3</sub></sub>) and at least 72 % less expensive than the separation by PSA (293.38 €/t<sub>NH<sub>3</sub></sub>). Furthermore, the specific energy consumption of the condenser equal to 0.255 kWh/kg<sub>NH<sub>3</sub></sub>, is by far better than for the membranes, 0.466 kWh/kg<sub>NH<sub>3</sub></sub>, and for the PSA, equal to 0.435 kWh/kg<sub>NH<sub>3</sub></sub>. Even if the heating and cooling requirements are higher for the condenser, the net thermal balance has the shortest difference.

The main challenge for these alternative separation technologies is to allow achieving ammonia purities in the permeate and low-pressure streams as competitive as the separation by condensation. Otherwise, a supplementary stage by condensation is mandatory. For the data considered in this study (i.e., zeolitic membranes and zeolitic adsorbent), the highest purity values obtained exclusively by these technologies was 41.8 % and 53.2 %, for membranes and PSA, respectively. Thus, there are needs for more selective materials for these alternatives to be competitive with the classic separation by condensation.

# Chapter VII

---

*Energy balance on the process and thermal  
integration potential*

---



## VII. Chapter VII: Energy balance on the process and thermal integration potential

The following chapter will cover subjects related to:

- The description of the thermal balance in the final process superstructure, with the identification of the thermal integration potential, using as basis the Pinch analysis and the proposal of the HEX network.
- Defining the impact that the identified network of HEX has on the investment and operating expenditures, on the process and global LCOA, and on the energy efficiency indicator of the process.
- Performing an energy balance across the process, regarding the scenario defined in Chapter IV, to determine the energy transformation performance from renewable energy to chemical energy contained in  $\text{NH}_3$ .

### VII.1.Introduction

Until now, the work presented has focused its attention in two main subjects: first, the proposal of the methodology for superstructure optimization for its use in a process simulation software, and second, on the construction and evaluation of multiple process superstructures for ammonia synthesis and separation. These points allowed to determine the best suitable structure of the process in terms of the structure of the compression stage, the reactor configuration, the catalytic material, and the separation technology.

For the optimization of these superstructures, the main parts of the process were evaluated and adjusted, according to structural alternatives and operating conditions that allowed to find the best trade-offs between economic and energetic performance indicators.

Beyond this, there is a supplementary step that can be included to give more robustness to the process conception, related to the study on the energy integration potential between the different stages of the process. As it was assumed in Chapter IV, the different heat duties of hot streams can be integrated through HEXs with cold streams to favour the thermal exchange and avoid the requirements of external utilities. This is then part of the heat integration strategy, which intends to give some ideas on the real potential existing for thermal integration across the HB synthesis loop.

This chapter presents the analysis for the thermal integration in the final process superstructure, in section VII.2, with details on the impact of the identified HEX for thermal integration on the economic indicator, while a general balance of the process for energy storage is presented in section VII.3.

### VII.2.Thermal balance and integration potential

To determine the potential thermal integration to propose in the ammonia synthesis process, it is necessary to study the different heat exchanges occurring across the process.

The previous superstructure cases include individual one-stream HEXs, as given by the strategies proposed in Chapter III. These HEXs adjust the outlet temperature according to the pre-specified value or to the algorithm-dictated temperatures. However, no relation exists between the different HEXs

across the process, and therefore, no real thermal exchange is proposed, being impossible to determine the investment costs of these modules.

From the beginning of this thesis, it was decided to avoid defining the full developed HEX network, as optimizing the superstructure and adjusting the thermal integration within the process would require several constraints to be defined, which could extremely complexify its resolution. Still, the approach that has been considered of thermal integration is conservative in such a degree that all the solutions allow a high degree of integration, as described in section IV.4.2.2, in Chapter IV.

Ideally, the thermal integration should be carried out at the same time with the optimization, as it would allow to determine not only the real potential of thermal integration, but also a more precise energy efficiency indicator, and the estimation of the investment and maintenance expenditures of the set of HEX. With this, the impact of the HEX would be reflected on both of the KPIs.

The strategies for the thermal integration analysis, such as the Pinch method and the identification of the HEX network, are then proposed as a supplementary step on the process conception, to be carried out after the superstructure optimization over the selected optimal solution of the superstructure.

With this in mind, the solution retained for this analysis consists of the autothermal optimal configuration, which includes the intermediate and final separation steps using condensers. The following data are obtained from the optimal solution reported for all the HEX present in the process.

**Table VII-1.** Data from heat exchangers for the Pinch analysis for the optimal solution. \*Refer to Figure VII-1 for the identification of the HEX. \*\*HEX19 and HEX20 are added as a further improvement of the process, using two utilities of cooling water.

HEX	ID*	Stream type	Stage	$\dot{Q}$ (kW)	T <sub>in</sub> (K)	T <sub>out</sub> (K)
1	HEX1	Hot stream	Compression	- 75.96	452.83	297.87
4	HEX4	Cold stream	Reaction	122.03	453.50	699.19
5	HEX5	Hot stream	Final separation	- 536.57	703.48	303.15
6	HEX6	Hot stream	Final separation	- 162.51	303.15	250.15
7	HEX7	Cold stream	Recycle	500.65	254.24	699.19
8	HEX8	Cold stream	Final refrigeration cycle	162.51	272.37	273.00
9	HEX9	Hot stream	Final refrigeration cycle	- 7.22	311.02	289.72
10	HEX10	Hot stream	Final refrigeration cycle	- 9.47	329.62	302.61
11	HEX11	Hot stream	Final refrigeration cycle	- 181.41	343.99	308.15
12	HEX12	Cold stream	Reaction	574.45	273.15	691.09
13	HEX13	Hot stream	Intermediate separation	- 639.16	715.91	303.15
14	HEX14	Hot stream	Intermediate separation	- 119.22	303.15	273.15
15	HEX15	Cold stream	Intermediate refrigeration cycle	119.22	272.51	273.15
16	HEX16	Hot stream	Intermediate refrigeration cycle	- 5.26	311.01	289.83
17	HEX17	Hot stream	Intermediate refrigeration cycle	- 6.92	329.55	302.67
18	HEX18	Hot stream	Intermediate refrigeration cycle	- 133.02	343.87	308.15
<b>Additional HEX with cooling water as utility**</b>						
U1	HEX19	Utility	External utility	135.36	288.15	308.15
U2	HEX20	Utility	External utility	135.36	288.15	308.15

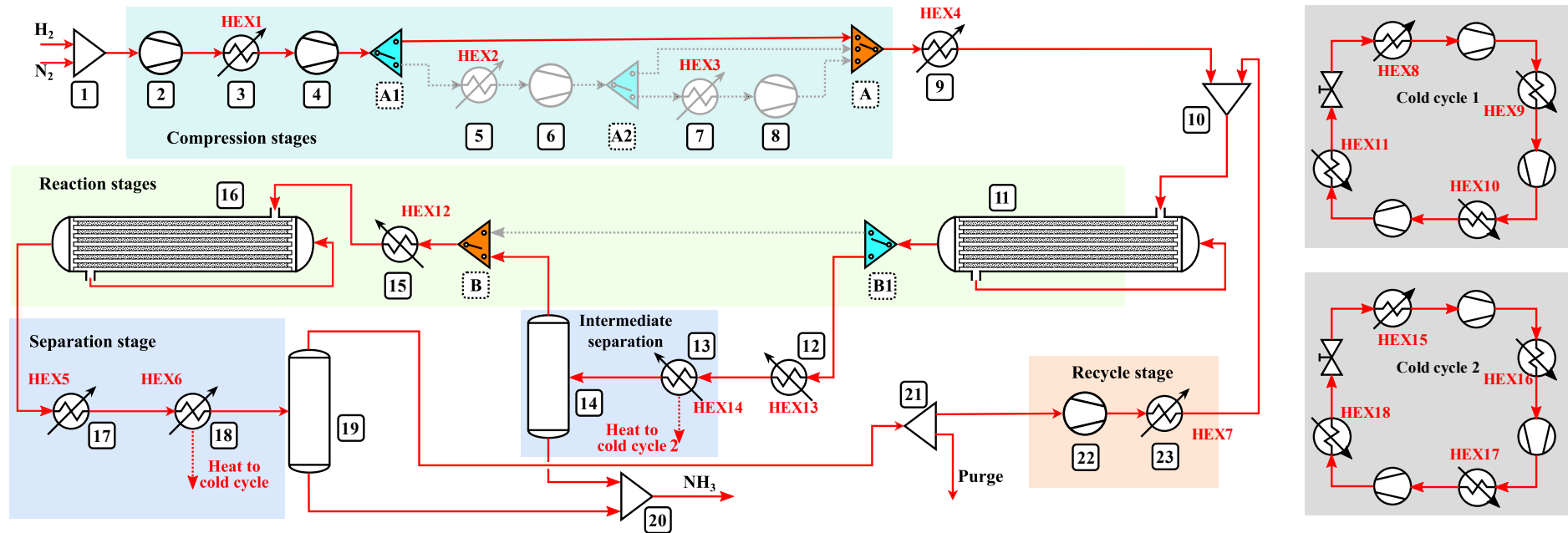


**Figure VII-1.** Superstructure representation of the final optimal solution, indicating the HEX used for the thermal integration analysis and the two refrigeration cycles with their respective HEX indicator. The modules in the main process structure are specified as Mixers (1, 10, 20), Compressors (2, 4, 6, 8, 22), HEX (3, 5, 7, 9, 12, 13, 15, 17, 18, 23), Autothermal reactors (11, 16), Separation drums (14, 19), Splitters (21).

Using the diverse data of heat duties and temperatures at the inlet and outlet streams of each HEX, the hot and cold composite curves shown in Figure VII-2 are constructed, according to the Pinch Design Method, proposed by Linnhoff and Hindmarsh, and detailed in [168].

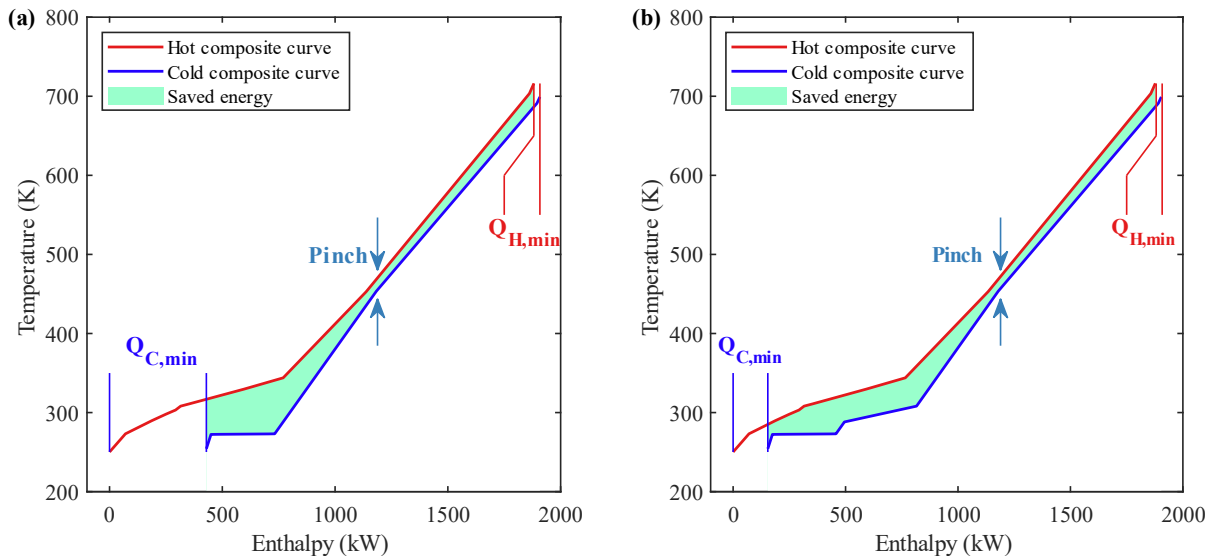


**Figure VII-2.** Hot and cold composite curves for the HEX data in Table VII-1, highlighting the pinch temperature ( $\Delta T_{\min} = 15$  K), the saved energy given by the green surface and the hot and cold utilities, indicated by  $Q_{C,\min}$  and  $Q_{H,\min}$ . In subplot (a) the data for HEX1 to HEX18 are used, while in (b) HEX19 and HEX20 are included, for a better integration of cooling requirements at the lowest temperatures.

In the diagrams shown above, two different representations are available. Subplot (a), showing the potential thermal integration between the process streams obtained from the superstructure optimization, with a minimum attainable temperature (Pinch temperature) of 15 K, and requirements of 26.7 kW of hot utilities and 429.3 kW of cold utilities. The total saved power corresponds to 1452.1 kW, with a thermal integration potential of 76.1 %.

As can be seen in the low-temperature zone of subplot (a), the greatest temperature gradients are found between the composite curves. To better integrate the heat in this zone, cold utilities near ambient temperatures can be included in the process, in order to displace the cold streams with the lowest temperatures further to the left, as achieved in subplot (b).

For the case in (b), two additional HEX were included to the optimal solution, specified as HEX19 and HEX20 in Table VII-1, consisting of cooling water at 15 °C and heated up to 35 °C. Even if this cooling water cannot be exploited to take advantage of its heat content, as is finally rejected to the environment, it favours a better integration of the low-temperature zones of the process. In this final proposition, for the same temperature Pinch, the hot utility requirements remain the same, 26.6 kW, while the cold utilities after inclusion of the cooling water stands for 154.3 kW. The thermal integration potential is equal to 90.5 %.

The HEX network to be proposed for this final configuration intends to describe the thermal energy exchanges across the different HEXs found in the process, for an estimation of the investment costs related to these modules. It is not exhaustive, as the HEX integration in the low temperature range requires more details that are not represented in Figure VII-3, which gives some insights on the integration.

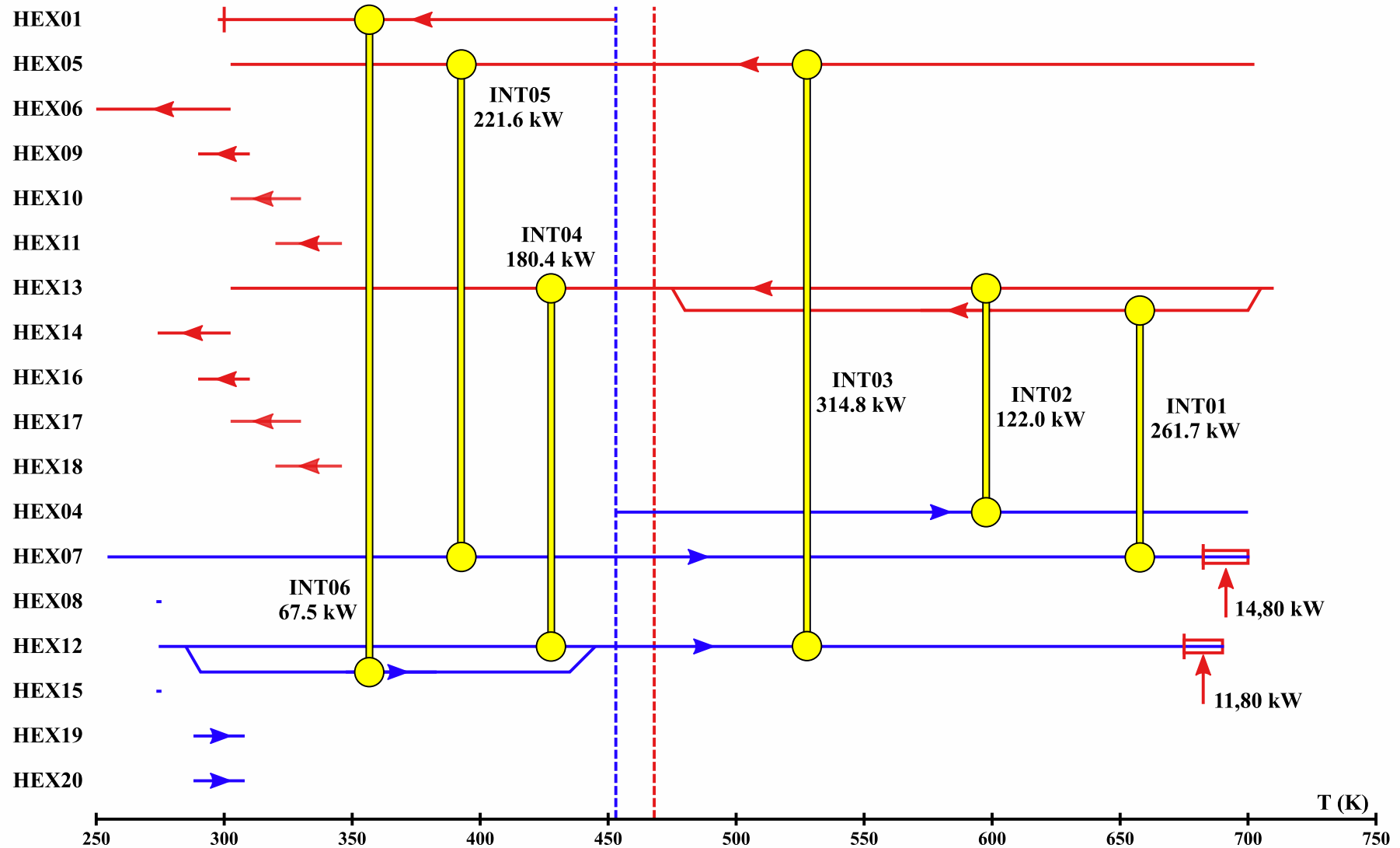


**Figure VII-3.** Representation of the HEX network with potential of being included for thermal integration between the process streams for the optimal autothermal configuration. The HEX network is based on data from Table VII-1. The proposed thermal integration is not exhaustive and includes some of the principal process streams to be integrated.

Consider the HEX network presented in Figure VII-3, where at least six different HEX for thermal integration are highlighted. The integration corresponds mainly to the upper zone of the pinch, which indicates heating requirements in two process streams (HEX07, HEX12) for a total of 26.6 kW, corresponding to the  $Q_{H,min}$  identified in the composite curves of Figure VII-2 (b). For the zone on the lower range of temperatures, the main thermal integration is shown, while the rest of process streams requires a rigorous detailing which is not covered in this analysis. Table VII-2 presents the data of the HEX identified for thermal integration.

**Table VII-2.** Data from the thermal integration between the process streams shown in Figure VII-3.

Module	Hot stream		Cold stream		Exchange data		Expenditures	
	T <sub>in</sub> K	T <sub>out</sub> K	T <sub>in</sub> K	T <sub>out</sub> K	Q̇ kW	Area m <sup>2</sup>	CAPEX €	OPEX €/y
INT01	703.33	468.50	453.50	682.51	314.78	253.3	698 752	15 120
INT02	716.29	468.50	453.50	699.19	122.03	108.8	351 748	7 424
INT03	716.29	468.50	453.50	686.04	261.67	171.9	515 431	11 138
INT04	468.50	352.03	273.15	453.50	180.35	67.0	253 725	5 317
INT05	468.50	303.15	254.25	453.50	221.65	104.1	322 223	6 628
INT06	438.50	300.70	273.15	453.50	67.54	46.7	289 325	6 819

As previously indicated, the thermal integration potential in the scenario of Figure VII-2 (b) is equal to 1723.2 kW. For the identified HEX in the previous table, a total of 1168.1 kW are integrated between the process streams (67.8 %), while the remaining 32.2 % is to be established with further detailing on the low temperature zone.

Recalling the cost of the autothermal configuration retained as the optimal solution, in Chapter V, the process LCOA is equal to 145.7 €/t<sub>NH<sub>3</sub></sub>, while the global LCOA is equal to 790.3 €/t<sub>NH<sub>3</sub></sub>. If the different HEXs identified for thermal integration were to be included in the economic evaluation of the process, it would correspond to a total share of 35.5 % of the CAPEX, increasing the process LCOA in 51 %, from 145.7 to 220.6 €/t<sub>NH<sub>3</sub></sub>, and the final global LCOA in 9.4 %, from 790.3 to 865.3 €/t<sub>NH<sub>3</sub></sub>.

As seen, the HEXs identified have an important impact on the economic indicator, which would, for sure, be greater if further HEXs were included in the analysis to guarantee a full thermal integration on the process. However, the purpose of this work being mainly focused on the superstructure optimization, further details on the HEX network would be interesting for refining the optimal solutions in terms of process cost and the final levelized cost of ammonia production.

Furthermore, as the energetic efficiency indicator is based on the potential thermal integration given by the composite curves, and multiple process structures have similarities in this indicator, the approach that has been used is conservative for the estimation of the energy transformation performance.

### VII.3. Balance of the process for energy storage

The final energy balance for the scenario proposed in Chapter IV is shown in Figure VII-4. It describes the different stages for energy storage in form of ammonia, with the first stage being the electricity production from wind turbines, following with the H<sub>2</sub> and N<sub>2</sub> separation from water and air, respectively, and ending with the HB process for ammonia synthesis, separation, and storage.

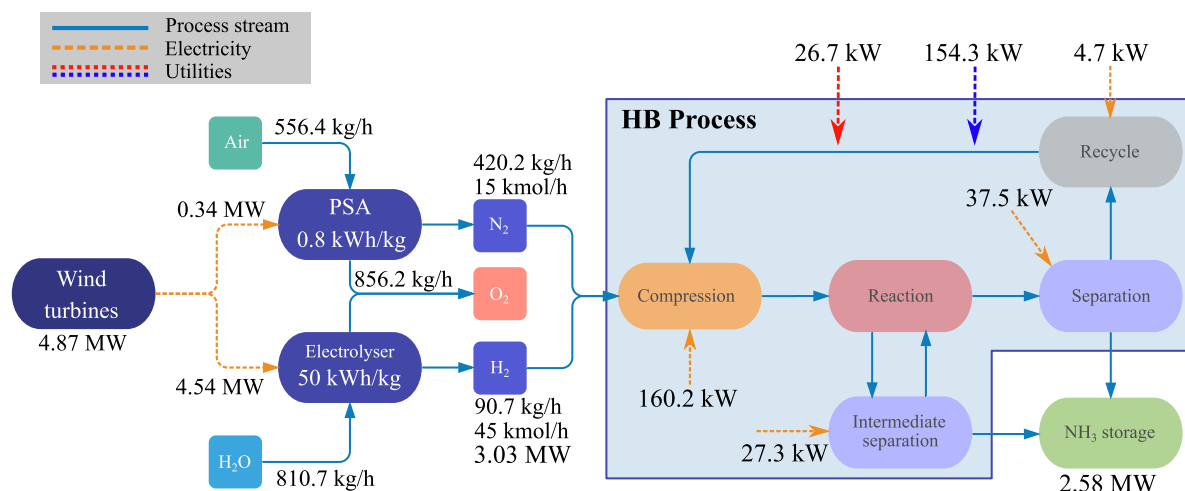


**Figure VII-4.** Final scenario for the production and storage of ammonia from renewable sources of energy, indicating the amount of power contained in the produced ammonia and the supplied as hydrogen to the HB Process.

The autothermal configuration in the HB process, shown in Figure VII-1, including two reactors with Ru-based catalyst under 100 bar of synthesis pressure, as well as an intermediate separation stage by condensation, allows to produce 3994.8 t of NH<sub>3</sub> per year, representing a total power of 2.58 MW and a global hydrogen conversion of 97.76 %.

The total power supply to the energy storage scenario, considering the production of H<sub>2</sub> and N<sub>2</sub> prior to the HB process and the electricity consumption in the synthesis loop is 5.10 MW. A total of 4.87 MW are used to produce the reactive gases (94.9 %), and the remaining is consumed by the HB process. The main driver of electricity consumption is, with no doubt, the electrolysis stage for hydrogen production from water electrolysis, with a power consumption of 4.54 MW.

Regarding the conversion of hydrogen to ammonia, a total supply of 3.03 MW in hydrogen allows to store up to 2.58 MW, which is equal to a ratio of production/supply of 0.853. Theoretically, the highest achievable ratio is 0.872.

In terms of specific energy consumption, the HB process consumes 0.46 kWh/kg of NH<sub>3</sub> (4.50 %), the H<sub>2</sub> electrolysis is responsible for 9.09 kWh/kg of NH<sub>3</sub> (88.85 %), and the nitrogen separation by PSA represents around 0.68 kWh/kg of NH<sub>3</sub> (6.65 %). The total specific energy consumption is then equal to 10.23 kWh/kg of NH<sub>3</sub> or 36.84 GJ/t of NH<sub>3</sub>.

Recalling the data presented in section I.7 of Chapter I, the Best Available Technology (BTA) for ammonia production, based on a methane HB process, is equal to 27.4 GJ/t of NH<sub>3</sub> (7.61 kWh/kg<sub>NH<sub>3</sub></sub>), while the best current electrical HB process accounts for 38.4 GJ/t of NH<sub>3</sub> (10.67 kWh/kg<sub>NH<sub>3</sub></sub>), according to data on the literature [39]. In this study, the final result is 4 % lower, yet it strongly depends on the considered hypothesis used to determine the BTA for the current electrical process, as well as on the assumptions made for the H<sub>2</sub> and N<sub>2</sub> recovery processes, not optimized in this work.

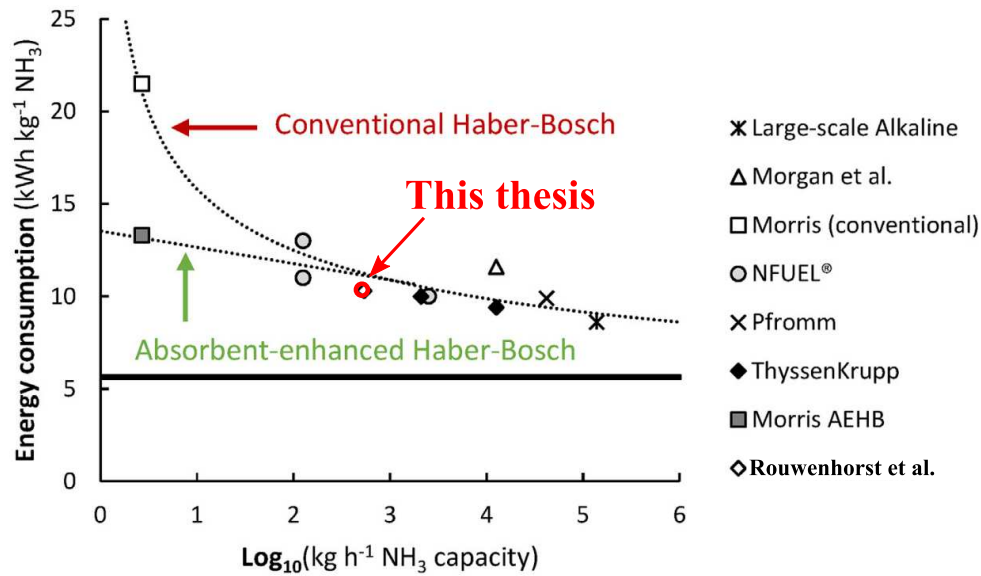


**Figure VII-5.** Placement of the final optimal process structure within the different process scenarios found in literature. The indicators for placement on the diagram are equal to 2.698 on the x-axis (499.35 kg/h) and 10.23 kWh/kg<sub>NH<sub>3</sub></sub> on the y-axis. The diagram has been modified from the one retrieved in works by Rouwenhorst et al., in the next reference [53].

If a comparison of the scenario studied in this thesis is performed with other scenarios found in the literature, the placement of the optimal process retrieved by superstructure optimization solution can be seen in Figure VII-5. The diagram shows the existing relation between the specific energy consumption of the HB process and the ammonia production capacity. For an hourly production of 499.3 kg<sub>NH<sub>3</sub></sub>/h, equivalent to a yearly production of 3994.8 t<sub>NH<sub>3</sub></sub>/y, the value of the x-axis, given in logarithmic value, is 2.698, while the value of the specific energy consumption is 10.23 kWh/kg<sub>NH<sub>3</sub></sub>.

For sure, the specific energy consumption related to the HB synthesis loop, main focus of this thesis, is hidden by the hypothesis made related to the H<sub>2</sub> and N<sub>2</sub> production, which are the main drivers of this indicator. Nevertheless, it allows somehow to compare in a hypothetical scenario the performance of the process for energy storage in ammonia.

## VII.4. Conclusions

In this chapter, a brief description of the thermal integration potential was presented, in order to determine the real thermal integration that can be performed between the streams of the HB process. Using as basis the optimal structure determined after the analysis of the different superstructures covered in Chapters V and VI, consisting of a double autothermal reactor in series, with Ru-based catalyst, including intermediate and final separation by condensation, a thermal balance on the HEX across the process has been presented.

For these modules, the analysis of the composite curves allowed to determine that a potential thermal integration of at least 76.1 % is possible if the HEX network is evaluated and proposed. Heat utilities are required at high temperatures, to fulfil the deficit of 26.7 kW, while cold utilities are needed in higher proportion, to guarantee the thermal exchange of 429.3 kW. Including two additional HEX with cooling water as a possible scenario, allowed to better integrate the cold and hot streams in the lowest range of temperatures, passing to a final requirement of cold utilities equal to 154.3 kW.

Recalling the process performance indicators, a global H<sub>2</sub> conversion of 97.76 % allowed to produce 3994.8 t<sub>NH<sub>3</sub></sub>/y, which in terms of stored power equals 2580 kW, from a hydrogen supply of 3026.5 kW, meaning a power conversion ratio of 0.853.

The complete scenario, considering the H<sub>2</sub> and N<sub>2</sub> production prior the HB process, is responsible for a specific energy consumption of 36.84 GJ/t<sub>NH<sub>3</sub></sub> (i.e., 10.23 kWh/kg<sub>NH<sub>3</sub></sub>) with the best available process in industry, for ammonia production using methane, being placed at 27.4 GJ/t<sub>NH<sub>3</sub></sub>.



# Chapter VIII

---

*General conclusions and perspectives*

---



## VIII. General conclusions and perspectives

### VIII.1. Conclusions

The work presented through the different chapters of this thesis was planned to deal with two main objectives, as described in the introduction. On one side, the main goal has been to propose a methodology for process conception through superstructure optimization. On the other hand, this approach required to be evaluated to determine its advantages and weaknesses, and the ammonia synthesis process has been selected with this purpose in the current context of renewable energy storage. The general findings and contribution of each one of these objectives are hereafter detailed.

**O1: The proposal of a methodology for process conception through superstructure optimization, using a process simulation software as environment and an optimization algorithm as essential feature for its resolution.**

The main contribution of this methodology is the advantage for simultaneously evaluating multiple process alternatives with a common objective, without requiring to manually evaluate each one of them. This finds plenty of potential when numerous structural alternatives are participating in the conception of a process, with multiple competing technologies. It has shown its utility to determine the set of best structural arrangements within a process, allowing to have a good trade-off between the Key Performance Indicators, namely economic and energetic indicators.

The approach has been proposed for its use in ProSimPlus, a software for process simulation under continuous and steady-state regime, and with the addition of MIDACO-Solver, a metaheuristic optimization algorithm able to handle and solve optimization problems of the MINLP type.

Taking advantage of the flexibility of the software in terms of the adaptability of the different process modules via the programming language VBScript, the methodology has been conceived using superstructure switches as the essential module allowing to evaluate a specific processing route within the superstructure. These modules act as flowrate deviators, which bypass certain zones of the process without interest for the current process structure being evaluated. In conjunction with the definition of residual streams and inactive modules, the process simulation software can perform the proper evaluation of a determined structural configuration without prejudice of the remaining processing paths.

At this stage of development of the methodology, the optimality of solutions remains uncertain within the vast, if not infinite, space search of structural possibilities, as the methodology has been tested to a reduced number of process alternatives, integrating some of the common structural configurations found in literature.

Nevertheless, the approach presented in this work has been directed on proposing a method which can be easily learnt and adapted by any process engineer, wishing to propose its own process superstructure in a classical process simulation software.

**O2: Application of the proposed methodology to a scenario of renewable energy storage in chemical compounds, specifically into ammonia, using as reference the conventional Haber-Bosch process.**

In the current context of energy transition and renewable energies increase in the energy market, the energy storage of renewable energy in chemical compounds has been selected to determine the pertinence of such a methodology for process conception.

Considering the conventional Haber-Bosch process, with the ammonia synthesis loop as boundaries of the study, multiple process superstructures have been proposed and evaluated to determine the best structural arrangement.

The structural alternatives were defined to select: (i) the number of compressors in the main compression stage; (ii) the number of catalytic reactors in series; (iii) the catalytic material, common to all the reactors, either Fe-based or Ru-based; (iv) the reactor arrangement, either multibed adiabatic or multitube autothermal; (v) the cooling system for the adiabatic reactors, either indirect (AICR) or direct (AQCR); (vi) the use of intermediate separation between the reactors; (vii) the separation technology, among the condenser, membrane filters, and PSA; (viii) the use of pressure equalization on the permeate streams of the separation by membrane filters; (ix) the use of an additional condenser after the separation by membranes or by PSA.

Superstructures I and II were focused on the structural alternatives (i) to (vi), concerning the optimization of the Haber-Bosch process through the reactor configuration and the catalyst selection, while superstructures III and IV were proposed for the evaluation of the separation technology, according to structural alternatives (vii) to (ix). The ultimate goal for evaluating the methodology should have been a unique superstructure containing every single studied alternative. However, as the different superstructures were conceived and evaluated at different stages of this thesis, they were divided according to the alternatives in study.

The main results found through the optimization of these superstructures, allowed to determine that the best structural arrangement consists of two autothermal reactors in series, using the Ru-based catalyst, with two stages of compression, with intermediate and final separation by condensation. This superstructure is represented in Figure VII-1.

This configuration allows to produce 3 994.8  $t_{\text{NH}_3}/\text{y}$ , representing an LCOA of 790.3 €/t<sub>NH<sub>3</sub></sub>, and an energy efficiency of 67.13 %. When considering the possible thermal integration of the process, the final cost of ammonia production is equal to 865.3 €/t<sub>NH<sub>3</sub></sub>.

For sure, these economic results are not exhaustive and require further detailing for a rigorous economic evaluation of the LCOA. Still, keeping in mind the favourable policies for the integration of renewable energies to the energy market in the next years, the further development of technologies allowing to reduce the cost of renewable energy, and the current unstable context of energy prices, the scenario considered in this work allows to suggest that NH<sub>3</sub> produced from renewable energy can be competitive with conventional routes of production. The latest prices of ammonia produced from natural gas, in the European context were reported above 1 500 €/t<sub>NH<sub>3</sub></sub> in the first trimester of 2022<sup>7</sup>.

Regarding the overall balance of the energy transformation from green H<sub>2</sub> to NH<sub>3</sub> and its energy content, a total of 5.10 MW are to be supplied to the process, to produce 2.58 MW contained in ammonia, according to its LHV. From the total supply, at least 94 % of energy is required for hydrogen and nitrogen production, while the remaining 6 % is consumed by the HB synthesis loop. The global conversion of hydrogen to ammonia represents 97.76 %, which translated into power input and output

---

<sup>7</sup> Report from Standard & Poor's Global (S&P Global), from April 01, 2022. Available online: <https://www.spglobal.com/commodityinsights/en/market-insights/latest-news/energy-transition/040122-higher-ammonia-prices-prompting-european-restarts-but-shortages-remain-traders>

equals to a power supply of 3.03 MW in H<sub>2</sub>, and a power ratio NH<sub>3</sub>/H<sub>2</sub> equal to 0.853. The theoretical power conversion for a complete hydrogen conversion is equal to 0.782.

Finally, the specific power consumption of the complete scenario is equal to 10.23 kWh/kg of NH<sub>3</sub>, with the best available technology for ammonia synthesis, based on hydrogen from natural gas, consuming 27.4 GJ/t of NH<sub>3</sub>. The main driver of the energy consumption is the electrolyser, responsible for 9.09 kWh/kg of NH<sub>3</sub> (88.85 %), while the nitrogen production represents 0.68 kWh/kg of NH<sub>3</sub> (6.65 %), and the HB synthesis loop consumes 0.46 kWh/kg of NH<sub>3</sub> (4.50 %). Evidently, the final energy consumption is the result of the hypothesis considered in the upstream stages of the HB process, for H<sub>2</sub> and N<sub>2</sub> recovery, which were beyond the scope of this work.

## VIII.2. Perspectives

The methodology for superstructure optimization presented in this work has plenty of potential for development. Some hypothesis were considered from the beginning of this work and could be studied to avoid them and propose a more robust methodology. Future lines of research are proposed to handle the following aspects:

- **Support of the superstructure generation on pre-screening methods:** A previous step to the superstructure optimization can be explored, in order to define a more complete process superstructure, including a wider space of alternatives. Methodologies such as P-graph [103] and other graph-oriented approaches, allow to carry out a screening of process structures without needs of a rigorous modelling of the operating units.
- **Development of user-defined operating units for process intensification:** Considering the potential use of user-defined modules within ProSimPlus, engineers can model their own operating units for evaluation in a process superstructure. In fact, the software already has a reaction-separation unit, modelled as a catalytic membrane reactor, but other integrated units can be foreseen for their integration into the software. As it is known, intensified modules benefit from the synergetic effect of multiple phenomena occurring within the same envelope.
- **Implementation of a thermal integration within the optimization strategy:** One of the main drawbacks of the methodology is the hypothesis of considering one-stream HEX, without possibility of defining the corresponding heat exchange surfaces and, therefore, their investment and operating expenditures. This represents an unknown impact of the HEX network on the KPIs, which is established after the superstructure optimization. Considering the thermal integration within the optimization phase would overcome this problem and allow to find a more robust set of optimal solutions, which might lead towards different structural solutions.
- **Definition of environmental indicators:** Within the context of cleaner and carbon-free processes in the future industrial applications for electricity production, there are needs for assessing the environmental impact of processes [159], [160]. Including this type of KPI allows to further improve processes, as it allows to determine the impact of a project during its lifetime, from the construction to the decommissioning, for all the involves fluxes of mass and energy associated not only to the process itself but to the surrounding activities.
- **Definition of exergetic indicators:** A step beyond the energy efficiency evaluation is to perform an exergy balance on the process, in order to identify possible stages on the process

where useful energy is being lost (i.e., process imperfections), to classify the losses under avoidable/unavoidable losses, and to propose process improvements [169]. By performing an assessment of an exergetic balance, energy transformation processes could be adapted to better respond to an efficient use of energy.

- **Defining a systematic approach for results analysis and data exploitation:** The large amount of data obtained from the optimization of superstructures, after several thousands of evaluations of the process flowsheet, can be largely exploited to find any possible relation between operating conditions, structural alternatives, constraints and KPIs. Possibly, the combination of operating conditions over a certain range of values tend towards infeasible zones, or even favour the search of the optimal solutions. However, these possible existing relations remain unknown at this point, and would require robust methods of data analysis.

## IX. References

- [1] IEA, “International Energy Outlook 2021,” 2021. [Online]. Available: <https://www.iea.org/reports/world-energy-outlook-2021>. [Accessed: 11-Jul-2021].
- [2] IRENA, “World energy transitions outlook: 1.5°C Pathway,” *Irena*, 2021. [Online]. Available: <https://irena.org/publications/2021/March/World-Energy-Transitions-Outlook>. [Accessed: 12-Jul-2021].
- [3] IRENA, “Global Renewables Outlook: Energy transformation 2050,” *International Renewable Energy Agency*, 2020. [Online]. Available: <https://www.irena.org/publications/2020/Apr/Global-Renewables-Outlook-2020>. [Accessed: 14-Apr-2021].
- [4] United Nations, “The Sustainable Development Goals Report 2020,” 2020. [Online]. Available: <https://unstats.un.org/sdgs/report/2020/The-Sustainable-Development-Goals-Report-2020.pdf>. [Accessed: 11-Dec-2021].
- [5] S. R. Sinsel, R. L. Riemke, and V. H. Hoffmann, “Challenges and solution technologies for the integration of variable renewable energy sources—a review,” *Renew. Energy*, vol. 145, pp. 2271–2285, 2020.
- [6] O. Ellabban, H. Abu-Rub, and F. Blaabjerg, “Renewable energy resources: Current status, future prospects and their enabling technology,” *Renew. Sustain. Energy Rev.*, vol. 39, pp. 748–764, Nov. 2014.
- [7] IRENA, “Renewable Energy Statistics 2021,” 2021. [Online]. Available: <https://www.irena.org/publications/2021/Aug/Renewable-energy-statistics-2021>. [Accessed: 12-Oct-2021].
- [8] D. Moya, C. Aldás, G. López, and P. Kaparaju, “Municipal solid waste as a valuable renewable energy resource: A worldwide opportunity of energy recovery by using Waste-To-Energy Technologies,” *Energy Procedia*, vol. 134, pp. 286–295, 2017.
- [9] Eurostat, “Annual renewables questionnaire,” 2019. [Online]. Available: <https://ec.europa.eu/eurostat/web/energy/methodology/annual>. [Accessed: 15-Nov-2021].
- [10] S. Impram, S. Varbak Nese, and B. Oral, “Challenges of renewable energy penetration on power system flexibility: A survey,” *Energy Strateg. Rev.*, vol. 31, no. August, p. 100539, 2020.
- [11] A. G. Olabi, C. Onumaegbu, T. Wilberforce, M. Ramadan, M. A. Abdelkareem, and A. H. Al – Alami, “Critical review of energy storage systems,” *Energy*, vol. 214, p. 118987, Jan. 2021.
- [12] A. Z. Al Shaqsi, K. Sopian, and A. Al-Hinai, “Review of energy storage services, applications, limitations, and benefits,” *Energy Reports*, no. xxxx, 2020.
- [13] A. Evans, V. Strezov, and T. J. Evans, “Assessment of utility energy storage options for increased renewable energy penetration,” *Renew. Sustain. Energy Rev.*, vol. 16, no. 6, pp. 4141–4147, 2012.
- [14] K. M. Tan, T. S. Babu, V. K. Ramachandramurthy, P. Kasinathan, S. G. Solanki, and S. K. Raveendran, “Empowering smart grid: A comprehensive review of energy storage technology and application with renewable energy integration,” *J. Energy Storage*, vol. 39, no. April, p. 102591, 2021.
- [15] M. S. Guney and Y. Tepe, “Classification and assessment of energy storage systems,” *Renew. Sustain. Energy Rev.*, vol. 75, no. November 2016, pp. 1187–1197, 2017.
- [16] F. Díaz-González, A. Sumper, O. Gomis-Bellmunt, and R. Villafáfila-Robles, “A review of energy storage technologies for wind power applications,” *Renew. Sustain. Energy Rev.*, vol. 16,

- no. 4, pp. 2154–2171, 2012.
- [17] J. Wu and X. feng Long, “Research progress of solar thermochemical energy storage,” *Int. J. Energy Res.*, vol. 39, no. 7, pp. 869–888, Jun. 2015.
- [18] B. Zakeri and S. Syri, “Electrical energy storage systems: A comparative life cycle cost analysis,” *Renew. Sustain. Energy Rev.*, vol. 42, pp. 569–596, 2015.
- [19] J. A. Faria, “Renaissance of ammonia synthesis for sustainable production of energy and fertilizers,” *Curr. Opin. Green Sustain. Chem.*, vol. 29, p. 100466, Jun. 2021.
- [20] C. K. Das, O. Bass, G. Kothapalli, T. S. Mahmoud, and D. Habibi, “Overview of energy storage systems in distribution networks: Placement, sizing, operation, and power quality,” *Renew. Sustain. Energy Rev.*, vol. 91, no. November 2016, pp. 1205–1230, 2018.
- [21] J. Andersson and S. Grönkvist, “Large-scale storage of hydrogen,” *Int. J. Hydrogen Energy*, vol. 44, no. 23, pp. 11901–11919, May 2019.
- [22] N. Das and J. Kishore Das, “Zeolites: An Emerging Material for Gas Storage and Separation Applications,” in *Zeolites - New Challenges*, IntechOpen, 2020.
- [23] H. W. Langmi, J. Ren, B. North, M. Mathe, and D. Bessarabov, “Hydrogen storage in metal-organic frameworks: A review,” *Electrochim. Acta*, vol. 128, no. 2014, pp. 368–392, 2014.
- [24] P. Ramirez-Vidal *et al.*, “A Step Forward in Understanding the Hydrogen Adsorption and Compression on Activated Carbons,” *ACS Appl. Mater. Interfaces*, vol. 13, no. 10, pp. 12562–12574, Mar. 2021.
- [25] K. M. Thomas, “Hydrogen adsorption and storage on porous materials,” *Catal. Today*, vol. 120, no. 3-4 SPEC. ISS., pp. 389–398, 2007.
- [26] J. W. Leachman, R. T. Jacobsen, S. G. Penoncello, and E. W. Lemmon, “Fundamental Equations of State for Parahydrogen, Normal Hydrogen, and Orthohydrogen,” *J. Phys. Chem. Ref. Data*, vol. 38, no. 3, pp. 721–748, Sep. 2009.
- [27] M. Aziz, A. T. Wijayanta, and A. B. D. Nandiyanto, “Ammonia as Effective Hydrogen Storage: A Review on Production, Storage and Utilization,” *Energies*, vol. 13, no. 12, p. 3062, Jun. 2020.
- [28] V. Dias, M. Pochet, F. Contino, and H. Jeanmart, “Energy and Economic Costs of Chemical Storage,” *Front. Mech. Eng.*, vol. 6, no. May, 2020.
- [29] J.-F. Portha, W. Uribe-Soto, J.-M. Commenge, S. Valentin, and L. Falk, “Techno-Economic and Carbon Footprint Analyses of a Coke Oven Gas Reuse Process for Methanol Production,” *Processes*, vol. 9, no. 6, p. 1042, Jun. 2021.
- [30] W. Uribe-Soto, J. F. Portha, J. M. Commenge, and L. Falk, “A review of thermochemical processes and technologies to use steelworks off-gases,” *Renew. Sustain. Energy Rev.*, vol. 74, no. June 2016, pp. 809–823, 2017.
- [31] A. Valera-Medina, H. Xiao, M. Owen-Jones, W. I. F. David, and P. J. Bowen, “Ammonia for power,” *Prog. Energy Combust. Sci.*, vol. 69, pp. 63–102, Nov. 2018.
- [32] National Center for Biotechnology Information, “PubChem Compound LCSS for CID 222, Ammonia,” 2022. [Online]. Available: <https://pubchem.ncbi.nlm.nih.gov/compound/Ammonia#datasheet=LCSS>. [Accessed: 02-Feb-2022].
- [33] IEA, “Report: Ammonia Technology Roadmap,” 2021. [Online]. Available: <https://www.iea.org/reports/ammonia-technology-roadmap>. [Accessed: 13-Jul-2021].
- [34] F. B. Juangsa, A. R. Irhamna, and M. Aziz, “Production of ammonia as potential hydrogen

- carrier: Review on thermochemical and electrochemical processes,” *Int. J. Hydrogen Energy*, vol. 46, no. 27, pp. 14455–14477, Apr. 2021.
- [35] R. Zhao *et al.*, “Recent progress in the electrochemical ammonia synthesis under ambient conditions,” *EnergyChem*, vol. 1, no. 2, p. 100011, 2019.
- [36] M. E. Gálvez, A. Frei, M. Halmann, and A. Steinfeld, “Ammonia Production via a Two-Step Al<sub>2</sub>O<sub>3</sub>/AlN Thermochemical Cycle. 2. Kinetic Analysis,” *Ind. Eng. Chem. Res.*, vol. 46, no. 7, pp. 2047–2053, 2007.
- [37] F. B. Juangsa and M. Aziz, “Integrated system of thermochemical cycle of ammonia, nitrogen production, and power generation,” *Int. J. Hydrogen Energy*, vol. 44, no. 33, pp. 17525–17534, Jul. 2019.
- [38] K. H. R. Rouwenhorst and L. Lefferts, “Feasibility Study of Plasma-Catalytic Ammonia Synthesis for Energy Storage Applications,” *Catalysts*, vol. 10, no. 9, p. 999, Sep. 2020.
- [39] C. Smith, A. K. Hill, and L. Torrente-Murciano, “Current and future role of Haber–Bosch ammonia in a carbon-free energy landscape,” *Energy Environ. Sci.*, vol. 13, no. 2, pp. 331–344, 2020.
- [40] S. Zhang, Y. Zhao, R. Shi, G. I. N. Waterhouse, and T. Zhang, “Photocatalytic ammonia synthesis: Recent progress and future,” *EnergyChem*, vol. 1, no. 2, p. 100013, Sep. 2019.
- [41] M. Appl, *Ammonia: principles and industrial practice*. Weinheim, New York, Chichester, Brisbane, Singapore, Toronto: Wiley-VCH, 1999.
- [42] American Iron and Steel Institution, “Stainless Steels in Ammonia Production. A Designers’ Handbook Series,” 1978. [Online]. Available: [https://nickelinstitute.org/media/4663/ni\\_aisi\\_9013\\_amoniaproduction.pdf](https://nickelinstitute.org/media/4663/ni_aisi_9013_amoniaproduction.pdf). [Accessed: 27-Jan-2022].
- [43] V. Kaiser, E. Filippi, D. Léger, and P. Lesur, “Calcul des réacteurs catalytiques - Synthèse d’ammoniac,” *Tech. l’ingénieur*, vol. 33, no. 0, p. 19, 1999.
- [44] M. Shimagaki, K. Miyashita, A. Ilyas, and A. Kalyubi, “Ammonia converter operation,” *Plant/Operations Prog.*, vol. 6, no. 2, pp. 118–121, Apr. 1987.
- [45] M. H. Khademi and R. S. Sabbaghi, “Comparison between three types of ammonia synthesis reactor configurations in terms of cooling methods,” *Chem. Eng. Res. Des.*, vol. 128, pp. 306–317, 2017.
- [46] F. Kessler, D. Hoberg, and S. Hruby, “First application of Uhde’s dual pressure ammonia process for revamping of the Duslo ammonia plant,” *Nitrogen 2006 Conference and Exhibition*, 2006. [Online]. Available: <https://www.thyssenkrupp-industrial-solutions.com/en/products-and-services/fertilizer-plants/ammonia-plants-by-uhde/publications>. [Accessed: 12-Dec-2021].
- [47] A. Valera-Medina and A. Roldan, *Sustainable Ammonia Production*. Cham: Springer International Publishing, 2020.
- [48] H. J. Hansen, “Patent: Process and apparatus for performing reactions in the gaseous phase,” 3372988, 1968.
- [49] U. Zardi, “System to improve the efficiency of reactors for exothermic synthesis and more particularly for the reaction of ammonia,” 0287765A2, 1988.
- [50] J. Humphreys, R. Lan, and S. Tao, “Development and Recent Progress on Ammonia Synthesis Catalysts for Haber–Bosch Process,” *Adv. Energy Sustain. Res.*, vol. 2, no. 1, p. 2000043, Jan. 2021.
- [51] H. Liu, *Ammonia Synthesis Catalysts*. WORLD SCIENTIFIC / CHEMICAL INDUSTRY

PRESS, CHINA, 2013.

- [52] M. Malmali, G. Le, J. Hendrickson, J. Prince, A. V. McCormick, and E. L. Cussler, "Better Absorbents for Ammonia Separation," *ACS Sustain. Chem. Eng.*, vol. 6, no. 5, pp. 6536–6546, May 2018.
- [53] K. H. R. Rouwenhorst, A. G. J. Van der Ham, G. Mul, and S. R. A. Kersten, "Islanded ammonia power systems: Technology review & conceptual process design," *Renew. Sustain. Energy Rev.*, vol. 114, no. August 2019, 2019.
- [54] M. Palys, A. McCormick, E. Cussler, and P. Daoutidis, "Modeling and Optimal Design of Absorbent Enhanced Ammonia Synthesis," *Processes*, vol. 6, no. 7, p. 91, Jul. 2018.
- [55] J. D. Beach, J. D. Kintner, and A. W. Welch, "Removal of gaseous NH<sub>3</sub> from an NH<sub>3</sub> reactor product stream," US 2018/0339911 A1, 2018.
- [56] R. Lavie, "Patent: Process for the manufacture of ammonia," 4537760, 1985.
- [57] B. Lin, I. Hsieh, and M. Malmali, "Rapid pressure swing adsorption for small scale ammonia separation: A proof-of-concept," *J. Adv. Manuf. Process.*, vol. 3, no. 2, pp. 1–15, Apr. 2021.
- [58] J. Helminen, J. Helenius, E. Paatero, and I. Turunen, "Comparison of sorbents and isotherm models for NH<sub>3</sub>-gas separation by adsorption," *AIChE J.*, vol. 46, no. 8, pp. 1541–1555, 2000.
- [59] K. H. R. Rouwenhorst, A. G. J. Van der Ham, and L. Lefferts, "Beyond Haber-Bosch: The renaissance of the Claude process," *Int. J. Hydrogen Energy*, no. xxxx, 2021.
- [60] C. Makhloufi, B. Belaissaoui, D. Roizard, and E. Favre, "Interest of poly[bis(trifluoroethoxy)phosphazene] membranes for ammonia recovery - Potential application in Haber process," *Procedia Eng.*, vol. 44, pp. 143–146, 2012.
- [61] O. Camus *et al.*, "Ceramic membranes for ammonia recovery," *AIChE J.*, vol. 52, no. 6, pp. 2055–2065, Jun. 2006.
- [62] Q. Wei, J. M. Lucero, J. M. Crawford, J. D. Way, C. A. Wolden, and M. A. Carreon, "Ammonia separation from N<sub>2</sub> and H<sub>2</sub> over LTA zeolitic imidazolate framework membranes," *J. Memb. Sci.*, vol. 623, no. January, p. 119078, 2021.
- [63] The Parliamentary Office of Science & Technology, "Carbon Footprint of Electricity Generation," 2011. [Online]. Available: <http://researchbriefings.parliament.uk/ResearchBriefing/Summary/POST-PN-383>. [Accessed: 22-Jan-2022].
- [64] I. E. Grossmann and I. Harjunkoski, "Process systems Engineering: Academic and industrial perspectives," *Comput. Chem. Eng.*, vol. 126, pp. 474–484, 2019.
- [65] A. W. Westerberg and I. E. Grossmann, "Research Challenges in Process Systems Engineering," *AIChE J.*, vol. 46, no. 9, pp. 1700–1703, 2000.
- [66] R. W. H. Sargent, "Integrated Design and Optimization of Processes," *Chem. Eng. Prog.*, no. September 1967, pp. 71–78, 1967.
- [67] D. F. Rudd, "The synthesis of system designs: I. Elementary decomposition theory," *AIChE J.*, vol. 14, no. 2, pp. 343–349, 1968.
- [68] N. Nishida, G. Stephanopoulos, and A. W. Westerberg, "A Review of Process Synthesis," *AIChE J.*, vol. 27, no. 3, pp. 321–351, 1981.
- [69] J. A. Caballero and I. E. Grossmann, "Aggregated models for integrated distillation systems," *Ind. Eng. Chem. Res.*, vol. 38, no. 6, pp. 2330–2344, 1999.
- [70] K. P. Papalexandri and E. N. Pistikopoulos, "Generalized modular representation framework for

- process synthesis,” *AIChE J.*, vol. 42, no. 4, pp. 1010–1032, Apr. 1996.
- [71] W. Wu, C. A. Henao, and C. T. Maravelias, “A superstructure representation, generation, and modeling framework for chemical process synthesis,” *AIChE J.*, vol. 62, no. 9, pp. 3199–3214, Sep. 2016.
- [72] A. Aggarwal and C. A. Floudas, “Synthesis of general distillation sequences-nonsharp separations,” *Comput. Chem. Eng.*, vol. 14, no. 6, pp. 631–653, 1990.
- [73] Q. Chen and I. E. Grossmann, *Recent developments and challenges in optimization-based process synthesis*, vol. 8, no. March. 2017.
- [74] R. W. H. Sargent and A. W. Westerberg, “SPEED-UP in Chemical Engineering Design.,” *Trans. Inst. Chem. Eng.*, vol. 42, 1964.
- [75] P. I. Barton and C. C. Pantelides, “Modeling of combined discrete/continuous processes,” *AIChE J.*, vol. 40, no. 6, pp. 966–979, 1994.
- [76] P. I. Barton, “The modelling and simulation of combined discrete/continuous processes,” 1992.
- [77] C. C. Pantelides and P. I. Barton, “Equation-oriented dynamic simulation. Current status and future perspectives,” *Comput. Chem. Eng.*, vol. 17, pp. S263–S285, Jan. 1993.
- [78] L. B. Evans *et al.*, “ASPEN: An Advanced System for Process Engineering,” *Comput. Chem. Eng.*, vol. 3, no. 1–4, pp. 319–327, 1979.
- [79] X. Joulia, B. Koehret, and M. Enjalbert, “Simulateur modulaire séquentiel à convergence simultanée,” *Chem. Eng. J.*, vol. 30, no. 3, pp. 113–127, 1985.
- [80] L. T. Biegler and I. E. Grossmann, “Retrospective on optimization,” *Comput. Chem. Eng.*, vol. 28, no. 8, pp. 1169–1192, 2004.
- [81] J. E. Hendry, D. F. Rudd, and J. D. Seader, “Synthesis in the design of chemical processes,” *AIChE J.*, vol. 19, no. 1, pp. 1–15, 1973.
- [82] S. D. Barnicki and J. J. Siirola, “Process synthesis prospective,” *Comput. Chem. Eng.*, vol. 28, no. 4, pp. 441–446, Apr. 2004.
- [83] S. Cremaschi, “A perspective on process synthesis: Challenges and prospects,” *Comput. Chem. Eng.*, vol. 81, pp. 130–137, Oct. 2015.
- [84] X. Li and A. Kraslawski, “Conceptual process synthesis: Past and current trends,” *Chem. Eng. Process. Process Intensif.*, vol. 43, no. 5, pp. 583–594, 2004.
- [85] L. Mencarelli, Q. Chen, A. Pagot, and I. E. Grossmann, “A review on superstructure optimization approaches in process system engineering,” *Comput. Chem. Eng.*, vol. 136, pp. 1–15, 2020.
- [86] L. T. Biegler, I. E. Grossmann, and A. W. Westerberg, “Issues and trends in the teaching of process and product design,” *AIChE J.*, vol. 59, no. 4, p. NA-NA, 2010.
- [87] A. H. Masso and D. F. Rudd, “The synthesis of system designs. II. Heuristic structuring,” *AIChE J.*, vol. 15, no. 1, pp. 10–17, 1969.
- [88] J. J. Siirola, G. J. Powers, and D. F. Rudd, “Synthesis of System Designs : III. Toward a Process Concept Generator,” *AIChE J.*, vol. 17, no. 3, pp. 677–682, 1971.
- [89] J. M. Douglas, “A Hierarchical Decision Procedure For The Synthesis Of Complex Plants,” *AIChE J.*, vol. 31, no. 3, pp. 353–362, 1985.
- [90] R. M. Smith and B. Linnhoff, “The design of separators in the context of overall processes,” *Chem. Eng. Res. Des.*, vol. 66, pp. 195–228, 1988.
- [91] R. Smith, *Chemical Process Design and Integration*. John Wiley & Sons, 2005.

- [92] J. J. Siirola, "Strategic process synthesis: Advances in the hierarchical approach," *Comput. Chem. Eng.*, vol. 20, no. 96, pp. S1637–S1643, Jan. 1996.
- [93] T. Umeda, A. Shindo, and A. Ichikawa, "Process synthesis by task assignment," *Chem. Eng. Sci.*, vol. 29, pp. 2033–2040, 1974.
- [94] H. Yeomans and I. E. Grossmann, "A systematic modeling framework of superstructure optimization in process synthesis," *Comput. Chem. Eng.*, vol. 23, no. 6, pp. 709–731, 1999.
- [95] T. Umeda, A. Hirai, and A. Ichikawa, "Synthesis of optimal processing system by an integrated approach," *Chem. Eng. Sci.*, vol. 27, pp. 795–804, 1972.
- [96] R. W. H. Sargent and K. Gaminibandara, "Optimum Design of Plate Distillation Columns," *Optim. Action*, pp. 267–314, 1976.
- [97] I. E. Grossmann and R. W. H. Sargent, "Optimum design of heat exchanger networks," *Comput. Chem. Eng.*, vol. 2, no. 1, pp. 1–7, 1978.
- [98] A. C. Kokossis and C. A. Floudas, "Synthesis of isothermal reactor-separator-recycle systems," *Chem. Eng. Sci.*, vol. 46, no. 5–6, pp. 1361–1383, 1991.
- [99] T. Farkas, E. Rev, and Z. Lelkes, "Process flowsheet superstructures: Structural multiplicity and redundancy," *Comput. Chem. Eng.*, vol. 29, no. 10, pp. 2198–2214, Sep. 2005.
- [100] E. Kondili, C. C. Pantelides, and R. W. H. Sargent, "A general algorithm for short-term scheduling of batch operations - I. MILP formulation," *Comput. Chem. Eng.*, vol. 17, no. 2, pp. 211–227, 1993.
- [101] M. Á. Velázquez-Guevara, A. R. Uribe-Ramírez, F. I. Gómez-Castro, J. G. Segovia-Hernández, S. Hernández, and J. M. P. Ortega, "Optimal synthesis of mass exchange networks through a state-task representation superstructure," in *Computer Aided Chemical Engineering*, vol. 43, no. 1989, 2018, pp. 331–336.
- [102] E. M. B. Smith and C. C. Pantelides, "Design of reaction/separation networks using detailed models," *Comput. Chem. Eng.*, vol. 19, no. 95, 1995.
- [103] F. Friedler, K. Tarján, Y. W. Huang, and L. T. Fan, "Graph-theoretic approach to process synthesis: axioms and theorems," *Chem. Eng. Sci.*, vol. 47, no. 8, pp. 1973–1988, 1992.
- [104] F. Friedler, J. B. Varga, E. Fehér, and L. T. Fan, "Combinatorially Accelerated Branch-and-Bound Method for Solving the MIP Model of Process Network Synthesis," 1996, pp. 609–626.
- [105] I. Heckl, F. Friedler, and L. T. Fan, "Solution of separation-network synthesis problems by the P-graph methodology," *Comput. Chem. Eng.*, vol. 34, no. 5, pp. 700–706, 2010.
- [106] K. B. Aviso, J.-Y. Lee, J. C. Dulatre, V. R. Madria, J. Okusa, and R. R. Tan, "A P-graph model for multi-period optimization of sustainable energy systems," *J. Clean. Prod.*, vol. 161, pp. 1338–1351, Sep. 2017.
- [107] L. Vance, H. Cabezas, I. Heckl, B. Bertok, and F. Friedler, "Synthesis of sustainable energy supply chain by the P-graph framework," *Ind. Eng. Chem. Res.*, vol. 52, no. 1, pp. 266–274, 2013.
- [108] P. Varbanov and F. Friedler, "P-graph methodology for cost-effective reduction of carbon emissions involving fuel cell combined cycles," *Appl. Therm. Eng.*, vol. 28, no. 16, pp. 2020–2029, 2008.
- [109] T. Farkas, E. Rev, B. Czuczai, Z. Fonyo, and Z. Lelkes, "R-graph-based distillation column superstructure and MINLP model," *Comput. Aided Chem. Eng.*, vol. 20, no. C, pp. 889–894, 2005.

- [110] Y. Saif, A. Elkamel, and M. Pritzker, "Superstructure optimization for the synthesis of chemical process flowsheets: Application to optimal hybrid membrane systems," *Eng. Optim.*, vol. 41, no. 4, pp. 327–350, 2009.
- [111] G. Liesche, D. Schack, and K. Sundmacher, "The FluxMax approach for simultaneous process synthesis and heat integration: Production of hydrogen cyanide," *AIChE J.*, vol. 65, no. 7, pp. 1–18, 2019.
- [112] P. Pichardo and V. I. Manousiouthakis, "Infinite Dimensional State-space as a systematic process intensification tool: Energetic intensification of hydrogen production," *Chem. Eng. Res. Des.*, vol. 120, pp. 372–395, 2017.
- [113] J. A. Arizmendi-Sánchez and P. N. Sharratt, "Phenomena-based modularisation of chemical process models to approach intensive options," *Chem. Eng. J.*, vol. 135, no. 1–2, pp. 83–94, 2008.
- [114] P. Lutze, D. K. Babi, J. M. Woodley, and R. Gani, "Phenomena based methodology for process synthesis incorporating process intensification," *Ind. Eng. Chem. Res.*, vol. 52, no. 22, pp. 7127–7144, 2013.
- [115] D. K. Babi, J. Holtbruegge, P. Lutze, A. Gorak, J. M. Woodley, and R. Gani, "Sustainable process synthesis–intensification," *Comput. Chem. Eng.*, vol. 81, pp. 218–244, Oct. 2015.
- [116] S. E. Demirel, J. Li, and M. M. F. Hasan, "Systematic process intensification using building blocks," *Comput. Chem. Eng.*, vol. 105, pp. 2–38, Oct. 2017.
- [117] J. Li, S. E. Demirel, and M. M. F. Hasan, "Process Integration Using Block Superstructure," *Ind. Eng. Chem. Res.*, vol. 57, no. 12, pp. 4377–4398, 2018.
- [118] H. Kuhlmann and M. Skiborowski, "Optimization-Based Approach to Process Synthesis for Process Intensification: General Approach and Application to Ethanol Dehydration," *Ind. Eng. Chem. Res.*, vol. 56, no. 45, pp. 13461–13481, 2017.
- [119] S. Sitter, Q. Chen, and I. E. Grossmann, "An overview of process intensification methods," *Curr. Opin. Chem. Eng.*, Jan. 2019.
- [120] M. Emmerich, M. Grötzner, and M. Schütz, "Design of graph-based evolutionary algorithms: a case study for chemical process networks.," *Evol. Comput.*, vol. 9, no. 3, pp. 329–354, 2001.
- [121] S. Boonstra, K. Van Der Blom, H. Hofmeyer, R. Amor, and M. T. M. Emmerich, "Super-Structure and Super-Structure Free Design Search Space Representations for a Building Spatial Design in Multi-Disciplinary Building Optimisation," *23rd Int. Work. Eur. Gr. Intell. Comput. Eng. EG-ICE 2016*, pp. 1–10, 2016.
- [122] P. Voll, M. Lampe, G. Wrobel, and A. Bardow, "Superstructure-free synthesis and optimization of distributed industrial energy supply systems," *Energy*, vol. 45, no. 1, pp. 424–435, 2012.
- [123] P. Voll, C. Klaffke, M. Hennen, and A. Bardow, "Automated superstructure-based synthesis and optimization of distributed energy supply systems," *Energy*, vol. 50, no. 1, pp. 374–388, 2013.
- [124] T. Neveux, "Ab-initio process synthesis using evolutionary programming," *Chem. Eng. Sci.*, vol. 185, pp. 209–221, 2018.
- [125] L. Wang, M. Lampe, P. Voll, Y. Yang, and A. Bardow, "Multi-objective superstructure-free synthesis and optimization of thermal power plants," *Energy*, vol. 116, pp. 1104–1116, Dec. 2016.
- [126] M. A. Duran and I. E. Grossmann, "A mixed-integer nonlinear programming algorithm for process systems synthesis," *AIChE J.*, vol. 32, no. 4, pp. 592–606, 1986.
- [127] M. A. Duran and I. E. Grossmann, "An outer-approximation algorithm for a class of mixed-

- integer nonlinear programs,” *Math. Program.*, vol. 36, no. 3, pp. 307–339, 1986.
- [128] I. E. I. Grossmann, “Review of Nonlinear Mixed-Integer and Disjunctive Programming Techniques,” *Methods*, vol. 3, pp. 227–252, 2002.
- [129] F. Trespalacios and I. E. Grossmann, “Review of mixed-integer nonlinear and generalized disjunctive programming methods,” *Chemie-Ingenieur-Technik*, vol. 86, no. 7, pp. 991–1012, 2014.
- [130] I. E. Grossmann, J. A. Caballero, and H. Yeomans, “Mathematical Programming Approaches to the Synthesis of Chemical Process Systems,” *Korean J. Chem. Eng.*, vol. 17, no. SUPPL., pp. 407–426, 2000.
- [131] P. Belotti, C. Kirches, S. Leyffer, J. Linderoth, J. Luedtke, and A. Mahajan, “Mixed-integer nonlinear optimization,” *Acta Numer.*, vol. 22, pp. 1–131, 2013.
- [132] P. P. Oteiza, D. A. Rodríguez, and N. B. Brignole, *Parallel cooperative optimization through hyperheuristics*, vol. 44. Elsevier Masson SAS, 2018.
- [133] J. Valadi and P. Siarry, *Applications of metaheuristics in process engineering*, vol. 9783319065. 2014.
- [134] W. B. Dolan, P. T. Cummings, and M. D. LeVan, “Process optimization via simulated annealing: Application to network design,” *AIChE J.*, vol. 35, no. 5, pp. 725–736, 1989.
- [135] I. P. Androulakis and V. Venkatasubramanian, “A genetic algorithmic framework for process design and optimization,” *Comput. Chem. Eng.*, vol. 15, no. 4, pp. 217–228, 1991.
- [136] P. S. Shelokar, V. K. Jayaraman, and B. D. Kulkarni, “Multiobjective optimization of reactor-regenerator system using ant algorithm,” *Pet. Sci. Technol.*, vol. 21, no. 7–8, pp. 1167–1184, 2003.
- [137] A. Dimian, C. Bildea, and A. Kiss, *Integrated Design and Simulation of Chemical Processes*. Elsevier Science, 2014.
- [138] J.-W. Qian, J.-N. Jaubert, and R. Privat, “Phase equilibria in hydrogen-containing binary systems modeled with the Peng–Robinson equation of state and temperature-dependent binary interaction parameters calculated through a group-contribution method,” *J. Supercrit. Fluids*, vol. 75, pp. 58–71, Mar. 2013.
- [139] J.-N. Jaubert, R. Privat, and F. Mutelet, “Predicting the phase equilibria of synthetic petroleum fluids with the PPR78 approach,” *AIChE J.*, vol. 56, no. 12, pp. 3225–3235, Dec. 2010.
- [140] J.-N. Jaubert and F. Mutelet, “VLE predictions with the Peng–Robinson equation of state and temperature dependent kij calculated through a group contribution method,” *Fluid Phase Equilib.*, vol. 224, no. 2, pp. 285–304, Oct. 2004.
- [141] A. Chauvel, G. Fournier, and C. Raimbault, *Manual of Process Economic Evaluation*. Paris: Editions Technip, 2003.
- [142] M. Schlüter, J. A. Egea, and J. R. Banga, “Extended ant colony optimization for non-convex mixed integer nonlinear programming,” *Comput. Oper. Res.*, vol. 36, no. 7, pp. 2217–2229, 2009.
- [143] M. Schlüter and M. Gerdt, “The oracle penalty method,” *J. Glob. Optim.*, vol. 47, no. 2, pp. 293–325, 2010.
- [144] M. Schlüter, C. H. Yam, T. Watanabe, and A. Oyama, “Parallelization Impact on Many-Objective Optimization for Space Trajectory Design,” *Int. J. Mach. Learn. Comput.*, vol. 6, no. 1, pp. 1–6, 2016.

- [145] M. Schlüter, “MIDACO Solver, User Manual,” 2018. [Online]. Available: [http://www.midaco-solver.com/data/other/MIDACO\\_User\\_Manual.pdf](http://www.midaco-solver.com/data/other/MIDACO_User_Manual.pdf). [Accessed: 04-Feb-2021].
- [146] Q. Zhao, “Conception and optimization of supercritical CO<sub>2</sub> Brayton cycles for coal-fired power plant application,” 2018. [Online]. Available: <https://hal.univ-lorraine.fr/tel-01920767>. [Accessed: 14-Apr-2021].
- [147] M. J. Palys, A. Kuznetsov, J. Tallaksen, M. Reese, and P. Daoutidis, “A novel system for ammonia-based sustainable energy and agriculture: Concept and design optimization,” *Chem. Eng. Process. - Process Intensif.*, vol. 140, no. November 2018, pp. 11–21, 2019.
- [148] Y. A. Katsigiannis, G. S. Stavrakakis, and C. Pharconides, “Effect of Wind Turbine Classes on the Electricity Production of Wind Farms in Cyprus Island,” *Conf. Pap. Energy*, vol. 2013, pp. 1–6, May 2013.
- [149] W. D. Seider, D. R. Lewin, J. D. Seader, S. Widagdo, R. Gani, and K. M. Ng, *Product and Process Design Principles: Synthesis, Analysis and Evaluation*. Wiley, 2016.
- [150] D. W. Green and R. H. Perry, *Perry’s Chemical Engineers’ Handbook*, 8th editio. McGrawHill, 2008.
- [151] I. López-Paniagua, J. Rodríguez-Martín, S. Sánchez-Orgaz, and J. J. Roncal-Casano, “Step by step derivation of the optimum multistage compression ratio and an application case,” *Entropy*, vol. 22, no. 6, pp. 1–13, 2020.
- [152] G. F. Froment, K. B. Bischoff, and J. De Wilde, *Chemical Reactor Analysis and Design*, 3rd editio. John Wiley & Sons, 210AD.
- [153] A. Nielsen, J. Kjaer, and B. Hansen, “Rate equation and mechanism of ammonia synthesis at industrial conditions,” *J. Catal.*, vol. 3, no. 1, pp. 68–79, 1964.
- [154] I. Rossetti, N. Pernicone, F. Ferrero, and L. Forni, “Kinetic study of ammonia synthesis on a promoted Ru/C catalyst,” *Ind. Eng. Chem. Res.*, vol. 45, no. 12, pp. 4150–4155, 2006.
- [155] M. Yoshida, T. Ogawa, Y. Imamura, and K. N. Ishihara, “Economies of scale in ammonia synthesis loops embedded with iron- and ruthenium-based catalysts,” *Int. J. Hydrogen Energy*, no. xxxx, 2021.
- [156] C. Pengilly, “Membranes for gas separation,” University of Bath, 2016.
- [157] K. S. Knaebel and E. L. Cussler, “A Novel Pressure Swing Adsorption System for Ammonia Synthesis,” 1996, pp. 457–464.
- [158] M. D. Sees, T. Kirkes, and C. C. Chen, “A simple and practical process modeling methodology for pressure swing adsorption,” *Comput. Chem. Eng.*, vol. 147, p. 107235, 2021.
- [159] J. F. Portha, J. N. Jaubert, S. Louret, and M. N. Pons, “Definition of a thermodynamic parameter to calculate carbon dioxide emissions in a catalytic reforming process,” *Int. J. Thermodyn.*, vol. 11, no. 2, pp. 81–89, 2008.
- [160] J. F. Portha, S. Louret, M. N. Pons, and J. N. Jaubert, “Estimation of the environmental impact of a petrochemical process using coupled LCA and exergy analysis,” *Resour. Conserv. Recycl.*, vol. 54, no. 5, pp. 291–298, 2010.
- [161] S. Gourmelon, R. Théry-Hétreux, and P. Floquet, “A systematic approach: Combining process optimisation exergy analysis and energy recovery for a better efficiency of industrial processes,” *Int. J. Exergy*, vol. 23, no. 4, pp. 298–329, 2017.
- [162] A. Ghannadzadeh, R. Thery-Hetreux, O. Baudouin, P. Baudet, P. Floquet, and X. Joulia, “General methodology for exergy balance in ProSimPlus® process simulator,” *Energy*, vol. 44, no. 1, pp. 38–59, 2012.

- [163] International Energy Agency (IEA), “The future of hydrogen fuel,” 2019. [Online]. Available: <https://www.iea.org/reports/the-future-of-hydrogen>. [Accessed: 25-Mar-2021].
- [164] O. Osman, S. Sgouridis, and A. Sleptchenko, “Scaling the production of renewable ammonia: A techno-economic optimization applied in regions with high insolation,” *J. Clean. Prod.*, vol. 271, p. 121627, 2020.
- [165] H. Zhang, L. Wang, J. Van herle, F. Maréchal, and U. Desideri, “Techno-economic comparison of green ammonia production processes,” *Appl. Energy*, vol. 259, no. November 2019, p. 114135, 2020.
- [166] E. Peduzzi, G. Boissonnet, G. Haarlemmer, and F. Maréchal, “Thermo-economic analysis and multi-objective optimisation of lignocellulosic biomass conversion to Fischer-Tropsch fuels,” *Sustain. Energy Fuels*, vol. 2, no. 5, pp. 1069–1084, 2018.
- [167] C. Quintero-Masselski, J.-F. Portha, and L. Falk, “Conception and optimization of an ammonia synthesis superstructure for energy storage,” *Chem. Eng. Res. Des.*, vol. 177, pp. 826–842, Jan. 2022.
- [168] J. J. Klemes, P. S. Varbanov, S. R. W. Wan Alwi, and Z. A. Manan, *Process Integration and Intensification*. DE GRUYTER, 2014.
- [169] J. Szargut, *Exergy Method. Technical and Ecological Applications*. WIT Press, 2005.
- [170] ProSim S.A., “ProSimPlus - Continuous steady-state process simulator,” 2020. [Online]. Available: <https://www.prosim.net/en/>. [Accessed: 04-Apr-2021].

# Appendix



## X. Appendix

### X.1. Appendix A – Hypothesis and correlations for economic calculations

#### X.1.1. Data and correlations for economic calculations

The calculations based on the *Pré-Estime* method consists of the estimation of the base price of an equipment, and the adjustment of the price with factors related to operating condition limits, material type, and size factors. These concepts are described by the following equations:

$$URP = BP * \prod F_C \quad \text{Eq. X-1}$$

$$ARP = BP * F_A * F_S + (URP - BP) \quad \text{Eq. X-2}$$

$$F_S = f \left( \sum_{i=1}^{n_C} URP_C \right) \forall i \in C \quad \text{Eq. X-3}$$

Where  $BP$  is the base price of the equipment,  $URP$  is the unassembled real price,  $ARP$  is the assembled real price,  $F_C$ ,  $F_A$  and  $F_S$  are the correction, assembly and sizing factors,  $URP_C$  is the  $URP$  of a specific category  $C$  of equipment and  $n_C$  is the total amount of equipment of the category  $C$ . Correction and assembly factors are specific to each type of equipment, while the sizing factor allows to consider the effect of scale when purchasing similar units.

On the other hand, the cost estimation for the *Functional Modules Method* is based on determining the base price of the equipment, considering correlations with logarithmic values of the operating conditions of the module, and applying corrective factor to calculate the assembled real price.

While the assembled real prices are calculated by different methods, the final price of the module has prices which differ among them according to the reference year of evaluation. The PEM values are calculated in euros of year 2000, while the FMM is calculated in French francs of year 1985. Then, conversion factors to euros of year 2021 are applied.

The relation between 1985-FF and 2000-€ is 0.2105<sup>8</sup>. To convert from 2000-€ to 2021-€, the Chemical Engineering Plant Cost Index (CEPCI) values are implemented. The index for year 2000 corresponds to 394.1, while it is equal to 686.7 for the month of May 2021.

#### X.1.2. Base price correlations and parameters

The equipment considered for the economic calculations are compressors, reactors and the condenser, and their corresponding correlations for the estimation of the base price are as follows:

$$BP_{Compressor} = \exp(A_1 + A_2 * \ln(\dot{W})) * P_C \quad \text{Eq. X-4}$$

$$BP_{Reactor} = \exp(B_1 + B_2 * \ln(\dot{n}) + B_3 * \ln(\tau) + B_4 * \ln(P)) * B_5 * P_C \quad \text{Eq. X-5}$$

---

<sup>8</sup> According to prices reported in INSEE (Institut national de la statistique et des études économiques), on the website <https://www.insee.fr/fr/accueil>

$$BP_{Condenser} = BP_{Shell} + BP_{Bottoms} + BP_{Accessories} \quad \text{Eq. X-6}$$

$$BP_{Shell} = (C_1 + C_2 * \exp(C_3 * D_{Cond})) * W_{Shell} * P_C \quad \text{Eq. X-7}$$

$$BP_{Bottoms} = (D_1 + D_2 * \exp(D_3 * D_{Cond})) * W_{Bottoms} * P_C \quad \text{Eq. X-8}$$

$$BP_{Accessories} = \exp(E_1 + E_2 + \ln(W_{Condenser})) * P_C \quad \text{Eq. X-9}$$

The base price correlations are dependent of operating conditions and equipment parameters. For the compressors,  $\dot{W}$  is the power of compression in kW. For the reactors,  $\dot{n}$  is the total molar flowrate in kmol/h,  $\tau$  is the residence time in s, and  $P$  is the pressure in bar at the inlet stream. For the condenser, as it is considered to be a column, it is composed of shell, bottoms, and accessories, with  $W$  being the weight in kg. The parameter  $P_C$  is related to a currency conversion from dollar to euro. Parameters  $K_1$  to  $K_j$ , specific to each equipment, were directly recovered from ProSimPlus economic evaluation module, and are shown in Table X-1.

**Table X-1.** Values of parameters for base price correlations [170]

	1	2	3	4	5
<b>A</b>	9.6276	0.5	-	-	-
<b>B</b>	2.9386	0.2908	0.2426	0.2789	210.3651
<b>C</b>	2.7376	2.7319	-7.603*10 <sup>-4</sup>	-	-
<b>D</b>	2.7376	2.7319	-7.603*10 <sup>-4</sup>	-	-
<b>E</b>	6.0794	0.3867	-	-	-

### X.1.3. Unassembled real price and correction factors

Once the base price is determined, correction factors are used to calculate the unassembled real price. In the case of compressors these factors depend on the type of driver used, the maximum pressure allowed and the material of the equipment, with values shown in Table X-2.

**Table X-2.** Correction factor of compressors [170]

Compressor driver		Maximum pressure		Compressor material	
Type	Factor	Pressure (bar)	Factor	Type	Factor
Electric	1.00	$P \leq 75$	1.00	Cast steel	1.00
Turbine < 100 kW	1.50	$75 < P \leq 100$	1.05	304 Stainless steel	1.40
Turbine 100 – 1000 kW	1.15	$100 < P \leq 150$	1.10	316 Stainless steel	1.70
Turbine > 1000 kW	1.07	$150 < P \leq 200$	1.18	Other	1.00

For the reactors, it depends only on the material, as shown in Table X-3.

**Table X-3.** Correction factor of reactors [170]

Reactor material	
Type	Factor
Carbon steel	1.00
SA203	1.30
304 Stainless steel	2.80
316 Stainless steel	3.30
Other	1.00

Finally, for the condenser, correction factors apply for each part of the equipment. The shell correction factors are function of the wall thickness and the material designation. For the bottoms, same factors apply, as well as a shell diameter factor. For the accessories, only the material type is considered. The wall thickness correction factor is calculated using Eq. X-10.

$$F_{\epsilon} = \exp\left(\sum_{i=0}^9 F_i * (\ln(\epsilon))^i\right) \quad \text{Eq. X-10}$$

In Eq. X-10,  $\epsilon$  is the wall thickness in mm and  $F_i$  are constant parameters, shown in Table X-4.

**Table X-4.** Wall thickness correction factor parameters for shell and bottoms [170]

F0	2.8709	F5	- 0.2016
F1	- 2.0128	F6	0.0807
F2	0	F7	- 0.012
F3	0.6651	F8	6.232*10 <sup>-3</sup>
F4	0	F9	1.001*10 <sup>-5</sup>

To determine the thickness of the wall, Eq. X-11 is used.

$$\epsilon = \frac{P * R}{\alpha * t - 0.6 * P} + s_e \quad \text{Eq. X-11}$$

Where  $P$  is the pressure in bar,  $R$  is the radius of the vessel in mm,  $\alpha$  is the welding factor equal to 1,  $t$  is the maximum allowable pressure in bar, which depends on the material and the operating temperature, and  $s_e$  denotes the thickness for corrosion, usually 3 mm.

The shell diameter factor for the bottoms of the condenser is given in Table X-5.

**Table X-5.** Shell diameter correction factor [170]

Diameter (m)	Factor
D ≤ 1.0	2.8
1.0 < D ≤ 1.5	2.5
1.5 < D ≤ 2.0	2.0
D > 2.0	1.5

Lastly, the material correction factor for shell, bottoms and accessories are the following:

**Table X-6.** Material correction factor for Shell (S), Bottoms (B) and Accessories (A) of the condenser. [141]

ASTM Code	AISI Code	Other	S-B	A
SA 285 C	-	-	1.0	1.0
SA 203 A-D	-	-	1.3	1.2
SA 357	-	-	1.8	1.6
SA 240	304	-	2.3	2.5
SA 240	304 L	-	2.3	-
SA 240	310 S	-	3.8	3.5
SA 240	316	-	3.0	3.0
SA 240	316 L	-	3.2	-
SA 240	316 (Ti)	-	3.1	-
SA 240	321	-	2.6	2.5
SA 240	347	-	2.9	3.0
SA 240	410	-	2.4	-
-	-	Uranus 50	3.6	-
-	-	Uranus B6	4.8	-
-	-	Monel 400	6.5	7.0
-	-	Inconel 600	10.0	8.5
-	-	Inconel 625	16.0	-
-	-	Hastelloy G	12.5	-

#### X.1.4. Assembled real price, assembly, and sizing factors

To calculate the assembled real price, a unique assembly factor is used for each type of equipment. The values are 2.72 for compressors, 9 for reactors and 2.98 for the condenser. For the sizing factors, a correlation is used as given in Eq. X-12, which depends on the category of the equipment and the sum of the URP of every equipment of a common category, as dictated by Eq. X-3.

$$F_S = S_1 + S_2 * \sum URP_C + S_3 * \left( \sum URP_C \right)^2 + S_4 * \left( \sum URP_C \right)^3 \quad \text{Eq. X-12}$$

$$URP_C = \sum_{i=1}^{N_C} URP_i / (P_C * 10^6) \quad \forall i \in C \quad \text{Eq. X-13}$$

For Eq. X-13 in case that the  $URP_C$  is greater than 8, the value of 8 should be used as  $URP_C$ . Compressors are included in the category of “Tubular heat exchangers and diverse equipment”, while the condenser corresponds to the “Drums” category. Reactors are not included, as they are calculated with the Functional Modules method, that does not consider sizing factors. Parameters of Eq. X-12 for compressors and the condenser are shown in Table X-7.

*Table X-7. Parameters for sizing factor [170]*

Parameter	Compressor	Condenser
$S_1$	1.1629	1.1826
$S_2$	- 7.986*10 <sup>-2</sup>	- 8.821*10 <sup>-2</sup>
$S_3$	1.115*10 <sup>-2</sup>	1.215*10 <sup>-2</sup>
$S_4$	- 5.762*10 <sup>-4</sup>	- 6.071*10 <sup>-4</sup>

Regarding the price of the membranes, not described until now, internal prices from the research groups of the laboratory have been implemented, which are based on the permanent membrane frame cost, and the cost of the membrane material that needs replacement. It is calculated by the following equation.

$$ARP_{MEMB} = aK_{mf} \left( \frac{A}{2000} \right)^{0.7} + a_m K_m A \quad \text{Eq. X-14}$$

Where  $a$  and  $a_m$  are the annuity coefficient for the module and for the membrane material, equal to 20 and 5 years, respectively. The parameters  $K_{mf}$  and  $K_m$  are the base frame cost and the unit cost of the membrane material, equal to 250 000 € and 50 €/m<sup>2</sup>, likewise.  $A$  is the area of the membrane.

## X.2. Appendix B – PSA pseudo-continuous model

The PSA pseudo-continuous model is based on the virtual moving bed approach. It is described by the hypothesis that the adsorbent included in the columns is continuously regenerated at a constant rate. The model can be easily explained according to the black-box representation seen in Figure X-1.

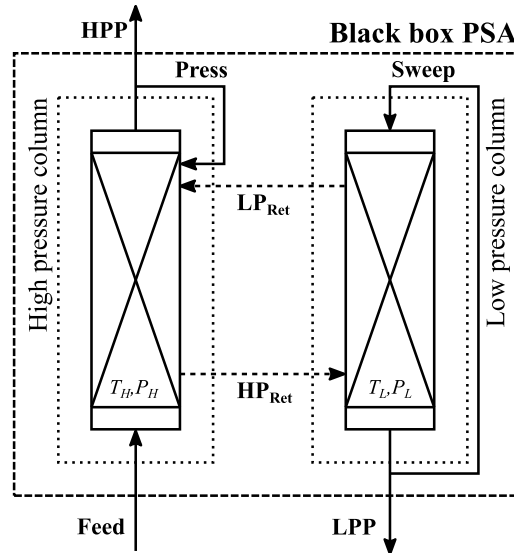


**Figure X-1.** Representation of the black-box model for the virtual moving bed PSA. The HPP stream (High Pressure Product) is mainly hydrogen and nitrogen, not adsorbed in the column. The LPP stream (Low Pressure Product) is mostly ammonia. The pressurization of the HP column is made with a fraction of the HPP stream (Press), while the purging of the LP column is made with a fraction of the LPP stream (Sweep). Streams  $LP_{Ret}$  and  $HP_{Ret}$ , linking the two columns, are referred to the moving bed of adsorbent continuously regenerated. Adapted from [158].

The process stream to separate is supplied to the High-Pressure (HP) column, which is later divided into two process streams as a result of the separation: the High-Pressure Product (HPP), consisting mostly of hydrogen and nitrogen (i.e., the least adsorbent compounds), and the Low-Pressure Product (LPP), with the most adsorbent component, which is ammonia.

There exist four main steps in the PSA cycle: feed, rinse, blowdown and pressurization. The ammonia contained in the feed is preferentially adsorbed by the zeolite material (H-Y zeolite) until the bed saturation, which is considered fully saturated with a **bed-state efficiency** equal to 1. This efficiency indicates how much of the adsorbent bed is saturated before the blowdown. Next, a HP rinse is carried out with a fraction of the LPP stream, consisting mainly of ammonia. This residual stream from the rinse contains some residual hydrogen and nitrogen removed from the bulk phase of the bed.

Following, the blowdown allows to desorb and remove most of the adsorbed ammonia, by pressure change from the HP to the LP conditions. Finally, the bed is pressurized using a fraction of the HPP stream, containing mainly hydrogen and nitrogen, before proceeding to the feed step again.

Inside the black box, multiple hypotheses are considered. For simplicity, the columns are isothermal on their operation and no pressure losses are supposed across the adsorbent. The main pressure driver is the LPP recompression for the HP rinse stage. The adsorption efficiency is equal to 1. The selectivity of a compound  $i$  is defined as follows:

$$S_{i,j} = \frac{z_{i,j}\dot{n}_j}{\sum_{k=1}^{inlets} z_{i,k}\dot{n}_k} \quad \text{Eq. X-15}$$

Where  $S_{i,j}$  indicates the selectivity of compound  $i$  in stream  $j$ ,  $z$  is the molar fraction,  $\dot{n}$  is the molar flowrate and  $k$  is the number of inlet streams. The mass-specific total molar hold-up of compound  $i$  at equilibrium conditions ( $H_i^{eq}$ ) can be defined as follows:

$$H_i^{eq} = q_i^*(T, C_{i,F}) + \frac{\varepsilon C_{i,F}}{\rho_B} \quad \text{Eq. X-16}$$

Where the first term indicates the adsorbate hold-up, which depends on the temperature  $T$  and the feed concentration  $C_{i,F}$ , and the second term is referred to the bulk-phase hold-up, depending on the bed void fraction  $\varepsilon$  and the bed density  $\rho_B$ .

Under steady-state conditions, the flowrate of saturated solid and entrained fluid in the retentate (c.f. LP<sub>ret</sub> and HP<sub>ret</sub> fictive streams in Figure X-1) is defined as:

$$z_{i,R} \dot{n}_R = H_i^{eq} \dot{m}_{ads} \quad \text{Eq. X-17}$$

Where  $\dot{m}_{ads}$  is the flowrate of adsorbent. By rearranging Eq. X-15 and Eq. X-17, it is possible to obtain the following relations.

$$S_{i,R} = \frac{H_i^{eq} \dot{m}_{ads}}{\sum_{k=1}^{inlets} z_{i,k} \dot{n}_k} \quad \text{Eq. X-18}$$

$$S_{i,R} = \frac{\Phi_i \left[ \eta_i q_i^*(T, C_{i,F}) + \frac{\varepsilon C_{i,F}}{\rho_B} \right] \dot{m}_{ads}}{\sum_{k=1}^{inlets} z_{i,k} \dot{n}_k} \quad \text{Eq. X-19}$$

Where  $\Phi_i$  is the bed-state efficiency and  $\eta_i$  is the adsorption efficiency, both parameters supposed equal to 1. Eq. X-19 represents the **two-efficiency model** (TEM). To define the HP and LP streams retentate selectivities, the diagram shown in Figure X-1 allows to propose the following equations:

$$S_{i,HR} = \frac{\Phi_i^H H_i^H \bar{m}_{ads}}{y_{i,F} \bar{n}_F + y_{i,HPP} \bar{n}_P + \Phi_i^L H_i^L \bar{m}_{ads}} \quad \text{Eq. X-20}$$

$$S_{i,LR} = \frac{\Phi_i^L H_i^L \bar{m}_{ads}}{y_{i,LPP} \bar{n}_R + \Phi_i^H H_i^H \bar{m}_{ads}} \quad \text{Eq. X-21}$$

Where subindexes HR and LR are referred to the HP column retentate and LP column retentate streams, respectively, indexes H and L are related to HP and LP columns,  $y_{i,j}$  is the molar fraction of compound  $i$  in stream  $j$ , and subindexes F, P and R describe the feed, pressurization, and rinse streams, respectively. The  $\bar{m}$  and  $\bar{n}$  are normalized mass and molar flowrates of the corresponding streams given by the subindexes. They are calculated as follows:

$$\bar{m}_{ads} = \frac{N m_{ads}}{t_{cycle}} \quad \text{Eq. X-22}$$

$$\bar{n}_k = \frac{N \dot{n}_k t_k}{t_{cycle}} \quad \text{Eq. X-23}$$

Where  $N$  is the number of columns in the black-box system,  $m_{ads}$  is the total mass of adsorbent considering all the columns,  $\dot{n}_k$  is the molar flowrate of stream  $k$ ,  $t_k$  is the time of stage  $k$  in the cycle, and  $t_{cycle}$  is the total time of a complete cycle. The time of each step of the cycle, considering the total time as the sum of each stage, is defined as 60 % for the feed, 10 % for the rinse, 10 % for the blowdown and 20 % for the pressurization.

This model is then based on proper adsorption isotherms, calculated as function of the temperature of the column, on the HP and LP levels, and on normalized flowrates involved in the black-box system.

### X.3. Appendix C – Results for the Fe-based adiabatic reactor configuration

**Table X-8.** Results for the optimization of Superstructure I, for the Fe-based catalyst, including the values of the objective functions and the optimization variables with direct influence on the process structure. The split ratios for the AQCR splitters are omitted, as no optimal solutions were obtained for this cooling configuration.

KPI	Units	P1	P2	P3	P4	P5	P6	P7	P8	P9	P10	P11	P12	P13	P14	P15	P16	P17
Global LCOA	€/t	751,6	752,4	756,9	756,9	761,5	761,6	776,1	776,3	785,5	785,8	805,0	805,9	813,5	815,5	815,5	815,5	815,5
Energy efficiency	%	54,46	54,57	55,21	55,20	55,40	55,50	55,62	55,94	56,16	56,29	56,35	56,39	56,41	56,43	56,43	56,42	56,42
<b>Variables</b>																		
Pressure	bar	154,48	151,74	151,79	151,79	151,00	151,79	169,19	156,76	150,00	150,37	156,80	151,30	151,44	150,00	150,07	150,06	150,12
Temperature 1 <sup>st</sup> reactor	K	637,55	636,04	636,00	636,00	636,43	636,00	651,84	636,28	638,26	672,62	636,10	712,23	647,83	642,43	642,40	642,35	642,32
Temperature 2 <sup>nd</sup> reactor	K	-	-	-	-	-	-	688,08	688,57	650,28	676,51	673,05	696,32	637,74	639,85	639,72	640,15	640,01
Temperature 3 <sup>rd</sup> reactor	K	-	-	-	-	-	-	-	-	-	-	735,14	675,19	671,86	663,21	663,29	664,75	663,28
Length of 1 <sup>st</sup> reactor	m	3,08	3,63	3,64	3,64	3,07	3,64	1,53	2,85	2,59	2,61	2,89	0,53	3,29	3,49	3,51	3,45	3,49
Length of 2 <sup>nd</sup> reactor	m	-	-	-	-	-	-	5,90	5,61	6,21	6,54	6,92	3,46	4,56	5,35	5,35	5,38	5,34
Length of 3 <sup>rd</sup> reactor	m	-	-	-	-	-	-	-	-	-	-	1,21	5,05	6,98	6,67	6,56	6,61	6,66
Separation temperature	K	253,05	254,49	254,48	254,48	253,08	254,48	253,17	253,14	257,71	265,42	258,94	261,10	258,70	261,16	261,13	261,19	261,06
<b>Structure</b>																		
Number of compressors	-	2	2	3	3	4	4	3	3	4	4	4	4	4	4	4	4	4
Number of reactors	-	1	1	1	1	1	1	2	2	2	2	3	3	3	3	3	3	3
Cooling configuration	-	Absent	Absent	Absent	Absent	Absent	Absent	AICR										



## X.4. Appendix D – Results for the Ru-based adiabatic reactor configuration

**Table X-9** Results for the optimization of Superstructure I, for the Ru-based catalyst, including the values of the objective functions and the optimization variables with direct influence on the process structure. The split ratios for the AQCR splitters are omitted, as no optimal solutions were obtained for this cooling configuration.

KPI	Units	P1	P2	P3	P4	P5	P6	P7	P8	P9	P10	P11	P12	P13	P14	P15	P16	P17	
Global LCOA	€/t	753,9	756,7	758,9	759,5	760,6	760,9	761,5	761,6	761,7	762,1	762,8	762,9	763,0	763,0	763,1	763,3	763,9	
Energy efficiency	%	55,32	55,49	55,80	56,44	56,74	56,93	56,97	57,17	57,18	57,19	57,22	57,23	57,25	57,27	57,28	57,32	57,38	
<b>Variables</b>																			
Pressure	bar	97,98	89,39	80,43	97,86	99,66	94,19	89,11	83,38	83,38	83,38	79,83	76,66	76,91	76,87	77,38	75,88	71,80	
Temperature 1 <sup>st</sup> reactor	K	655,18	646,66	636,00	688,56	677,40	661,14	668,02	665,10	665,10	665,10	665,93	665,68	665,50	666,29	665,64	665,10	660,30	
Temperature 2 <sup>nd</sup> reactor	K	-	-	-	688,72	657,21	658,26	653,87	655,22	655,22	655,22	651,57	655,28	655,21	653,09	652,54	654,92	653,66	
Temperature 3 <sup>rd</sup> reactor	K	-	-	-	-	-	-	-	-	-	-	-	-	-	-	-	-	-	
Length of 1 <sup>st</sup> reactor	m	2,84	3,54	4,90	1,13	1,40	2,15	1,62	1,86	1,98	1,98	1,86	1,77	1,84	1,83	1,88	1,88	2,11	
Length of 2 <sup>nd</sup> reactor	m	-	-	-	2,24	5,21	4,53	5,06	4,98	4,98	5,23	5,25	4,64	4,77	5,01	5,27	5,23	4,68	
Length of 3 <sup>rd</sup> reactor	m	-	-	-	-	-	-	-	-	-	-	-	-	-	-	-	-	-	
Separation temperature	K	253,08	253,87	253,27	253,11	253,26	253,12	253,40	253,06	253,06	253,06	253,01	253,15	253,04	253,03	253,00	253,00	253,11	
<b>Structure</b>																			
Number of compressors	-	2	2	2	2	2	2	2	2	2	2	2	2	2	2	2	2	2	
Number of reactors	-	1	1	1	2	2	2	2	2	2	2	2	2	2	2	2	2	2	
Cooling configuration	-	Absent	Absent	Absent	AICR														
KPI	Units	P18	P19	P20	P21	P22	P23	P24	P25	P26	P27	P28	P29	P30	P31	P32	P33	P34	
Global LCOA	€/t	765,4	765,6	766,0	766,3	766,3	767,9	768,3	768,5	768,8	769,2	770,7	772,6	785,8	786,6	786,9	789,8	803,6	
Energy efficiency	%	57,39	57,41	57,42	57,55	57,55	57,59	57,64	57,64	57,64	57,66	57,72	57,80	57,84	57,85	57,85	58,02	58,14	
<b>Variables</b>																			
Pressure	bar	68,68	86,33	87,48	83,38	83,38	77,76	75,88	75,54	75,09	71,80	83,38	75,88	72,17	94,90	93,92	72,36	65,81	
Temperature 1 <sup>st</sup> reactor	K	660,30	674,78	671,90	664,92	664,92	666,10	665,10	664,61	665,60	660,30	664,92	665,11	710,32	691,85	691,85	710,43	655,28	
Temperature 2 <sup>nd</sup> reactor	K	653,66	654,30	656,10	655,20	655,20	653,96	654,92	651,21	654,37	653,66	655,20	654,92	678,00	689,85	689,95	677,04	641,93	
Temperature 3 <sup>rd</sup> reactor	K	-	-	-	-	-	-	-	-	-	-	-	-	664,99	669,67	669,67	664,90	641,30	
Length of 1 <sup>st</sup> reactor	m	2,11	1,38	1,61	1,86	1,86	1,82	1,88	1,97	1,95	2,11	1,86	1,88	0,60	1,10	1,10	0,83	3,94	
Length of 2 <sup>nd</sup> reactor	m	4,68	5,05	5,14	4,98	4,98	5,20	5,23	5,16	5,23	4,68	4,98	5,23	1,97	2,23	2,23	1,94	3,40	
Length of 3 <sup>rd</sup> reactor	m	-	-	-	-	-	-	-	-	-	-	-	-	3,59	5,01	5,01	3,62	6,12	
Separation temperature	K	253,11	253,00	253,01	253,06	253,06	253,06	253,00	253,14	253,03	253,11	253,06	253,00	256,29	253,06	253,06	256,42	253,33	
<b>Structure</b>																			
Number of compressors	-	2	3	3	3	3	3	3	3	3	3	4	4	3	4	4	4	4	
Number of reactors	-	2	2	2	2	2	2	2	2	2	2	2	2	3	3	3	3	3	
Cooling configuration	-	AICR																	



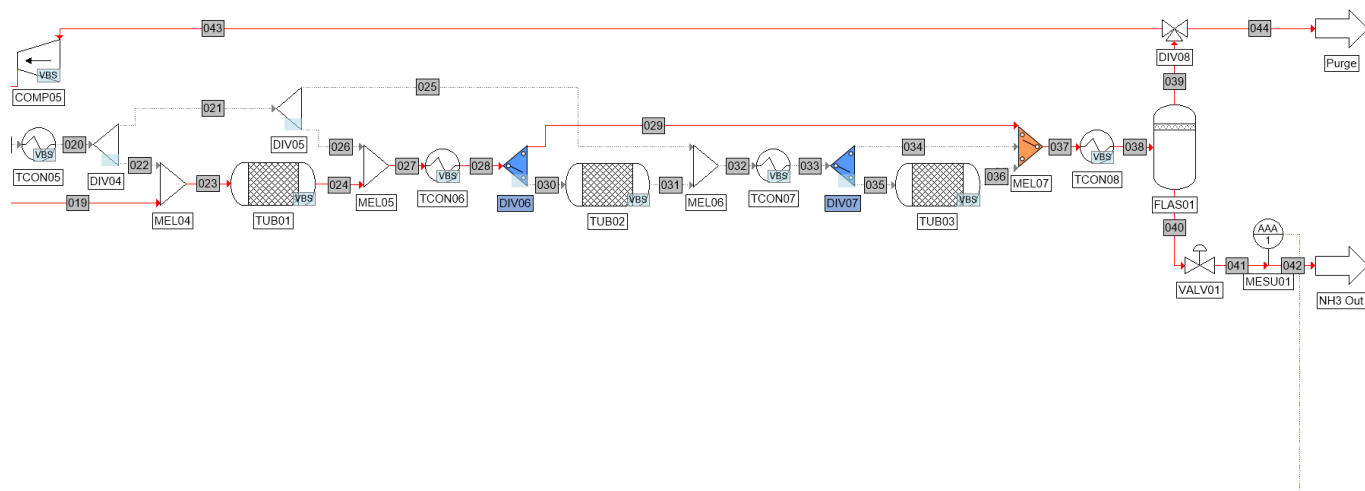


**Table X-10. Continuation**

<b>Stream</b>	<b>025</b>	<b>026</b>	<b>027</b>	<b>028</b>	<b>029</b>	<b>030</b>	<b>031</b>	<b>032</b>
Mass flowrate (kg/h)	0.00	0.00	2866.45	2866.45	2866.45	0.00	0.00	0.00
Molar flowrate (kmol/h)	0.00	0.00	300.76	300.76	300.76	0.00	0.00	0.00
Nitrogen molar fraction	0.00	0.00	0.22	0.22	0.22	0.22	0.22	0.22
Hydrogen molar fraction	0.00	0.00	0.66	0.66	0.66	0.66	0.66	0.66
Ammonia molar fraction	0.00	0.00	0.12	0.12	0.12	0.12	0.12	0.12
Temperature (°C)	362.84	362.84	517.36	517.36	517.36	517.36	517.36	517.36
Pressure (bar)	153.8	153.8	151.7	151.7	151.7	151.7	151.7	151.7
<b>Stream</b>	<b>033</b>	<b>034</b>	<b>035</b>	<b>036</b>	<b>037</b>	<b>038</b>	<b>039</b>	<b>040</b>
Mass flowrate (kg/h)	0.00	0.00	0.00	0.00	2866.45	2866.45	2379.01	487.44
Molar flowrate (kmol/h)	0.00	0.00	0.00	0.00	300.76	300.76	272.06	28.69
Nitrogen molar fraction	0.22	0.22	0.22	0.22	0.22	0.22	0.24	0.00
Hydrogen molar fraction	0.66	0.66	0.66	0.66	0.66	0.66	0.73	0.00
Ammonia molar fraction	0.12	0.12	0.12	0.12	0.12	0.12	0.02	1.00
Temperature (°C)	517.36	517.36	517.36	517.36	517.36	-18.67	-18.67	-18.67
Pressure (bar)	151.7	151.7	151.7	151.7	151.7	151.7	151.7	151.7
<b>Stream</b>	<b>041</b>	<b>042</b>	<b>043</b>	<b>044</b>	<b>045</b>	<b>046</b>		
Mass flowrate (kg/h)	487.44	487.44	2355.22	23.79	2355.22	2355.07		
Molar flowrate (kmol/h)	28.69	28.69	269.34	2.72	269.34	269.33		
Nitrogen molar fraction	0.00	0.00	0.24	0.24	0.24	0.24		
Hydrogen molar fraction	0.00	0.00	0.73	0.73	0.73	0.73		
Ammonia molar fraction	1.00	1.00	0.02	0.02	0.02	0.02		
Temperature (°C)	-15.34	-15.34	-18.67	-18.67	-17.34	362.85		
Pressure (bar)	10.0	10.0	151.7	151.7	153.8	153.8		

## X.6. Appendix F - Flowsheet representation and material balance data for the Ru-based adiabatic reactor configuration

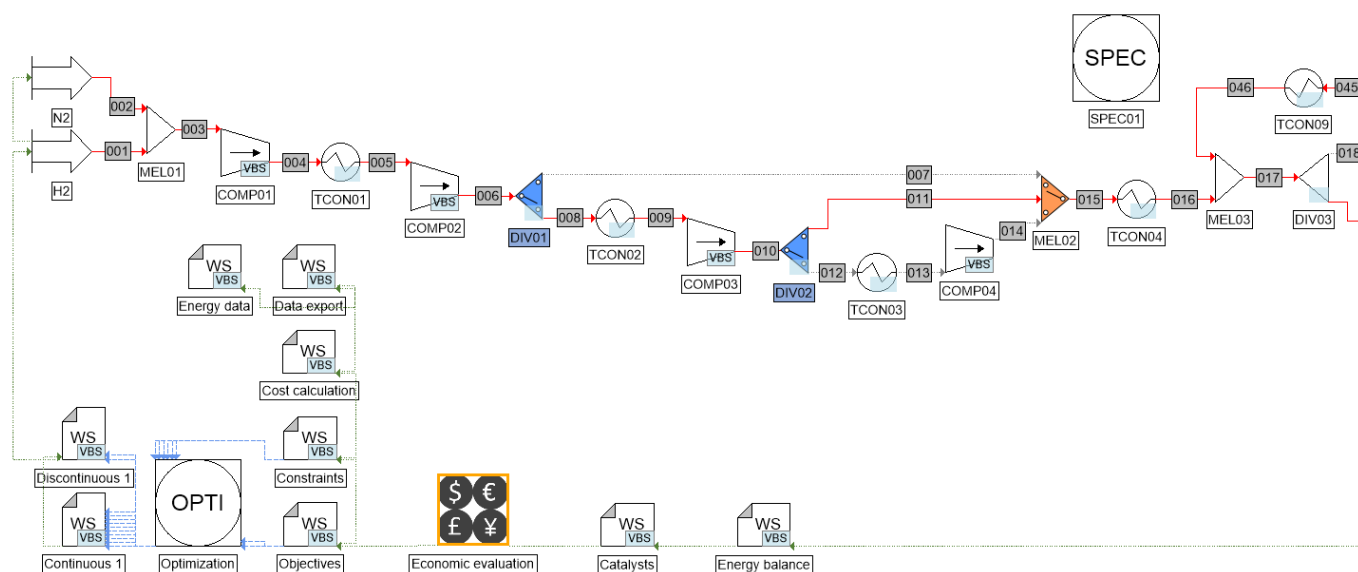


**Table X-11.** Information of streams on the process for the Ru-based adiabatic optimal solution.

Stream	001	002	003	004	005	006	007	008
Mass flowrate (kg/h)	90.71	420.20	510.92	510.92	510.92	510.92	0	510.92
Molar flowrate (kmol/h)	45.00	15.00	60.00	60.00	60.00	60.00	0	60.00
Nitrogen molar fraction	0.00	1.00	0.25	0.25	0.25	0.25	0	0.25
Hydrogen molar fraction	1.00	0.00	0.75	0.75	0.75	0.75	0	0.75
Ammonia molar fraction	0.00	0.00	0.00	0.00	0.00	0.00	0	0.00
Temperature (°C)	30.00	30.00	29.72	117.78	29.72	117.92	-	117.92
Pressure (bar)	10.0	10.0	10.0	19.9	19.9	39.6	-	39.6
Stream	009	010	011	012	013	014	015	016
Mass flowrate (kg/h)	510.92	510.92	510.92	0	0	0	510.92	510.92
Molar flowrate (kmol/h)	60.00	60.00	60.00	0	0	0	60.00	60.00
Nitrogen molar fraction	0.25	0.25	0.25	0	0	0	0.25	0.25
Hydrogen molar fraction	0.75	0.75	0.75	0	0	0	0.75	0.75
Ammonia molar fraction	0.00	0.00	0.00	0	0	0	0.00	0.00
Temperature (°C)	29.72	118.16	118.16	-	-	-	118.16	392.95
Pressure (bar)	39.6	78.8	78.8	-	-	-	78.8	78.8
Stream	017	018	019	020	021	022	023	024
Mass flowrate (kg/h)	2729.82	0	2729.82	0	0	0	2729.82	2729.91
Molar flowrate (kmol/h)	311.73	0	311.73	0	0	0	311.73	294.54
Nitrogen molar fraction	0.24	0	0.24	0	0	0	0.24	0.23
Hydrogen molar fraction	0.73	0	0.73	0	0	0	0.73	0.68
Ammonia molar fraction	0.03	0	0.03	0	0	0	0.03	0.09
Temperature (°C)	392.94	-	392.94	-	-	-	392.94	489.98
Pressure (bar)	78.8	-	78.8	-	-	-	78.8	78.3

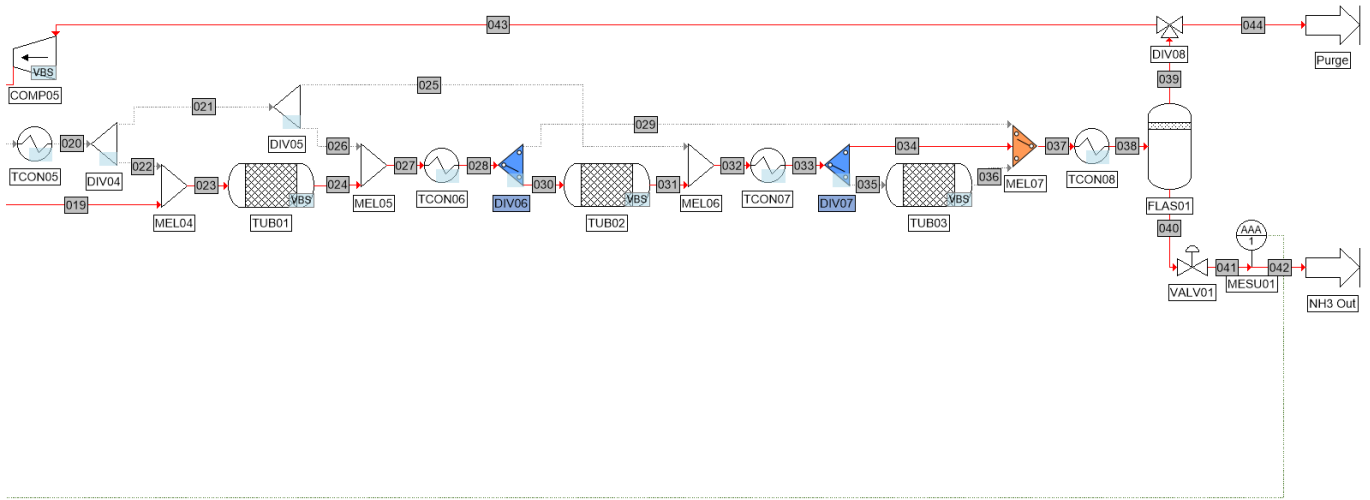


Table X-11. Continuation

Stream	025	026	027	028	029	030	031	032
Mass flowrate (kg/h)	0	0	2729.91	2729.91	0	2729.91	2729.95	2729.95
Molar flowrate (kmol/h)	0	0	294.54	294.54	0	294.54	283.00	283.00
Nitrogen molar fraction	0	0	0.23	0.23	0	0.23	0.22	0.22
Hydrogen molar fraction	0	0	0.68	0.68	0	0.68	0.65	0.65
Ammonia molar fraction	0	0	0.09	0.09	0	0.09	0.13	0.13
Temperature (°C)	-	-	489.98	380.81	-	380.81	446.99	446.99
Pressure (bar)	-	-	78.3	78.3	-	78.3	76.7	76.7
Stream	033	034	035	036	037	038	039	040
Mass flowrate (kg/h)	2729.95	2729.95	0	0	2729.95	2729.95	2241.34	488.61
Molar flowrate (kmol/h)	283.00	283.00	0	0	283.00	283.00	254.28	28.73
Nitrogen molar fraction	0.22	0.22	0	0	0.22	0.22	0.24	0.00
Hydrogen molar fraction	0.65	0.65	0	0	0.65	0.65	0.72	0.00
Ammonia molar fraction	0.13	0.13	0	0	0.13	0.13	0.03	1.00
Temperature (°C)	446.99	446.99	-	-	446.99	-20.09	-20.09	-20.09
Pressure (bar)	76.7	76.7	-	-	76.7	76.7	76.7	76.7
Stream	041	042	043	044	045	046		
Mass flowrate (kg/h)	488.61	488.61	2218.92	22.41	2218.92	2218.91		
Molar flowrate (kmol/h)	28.73	28.73	251.73	2.54	251.73	251.73		
Nitrogen molar fraction	0.00	0.00	0.24	0.24	0.24	0.24		
Hydrogen molar fraction	0.00	0.00	0.72	0.72	0.72	0.72		
Ammonia molar fraction	1.00	1.00	0.03	0.03	0.03	0.03		
Temperature (°C)	-18.48	-18.48	-20.09	-20.09	-17.45	392.95		
Pressure (bar)	10.0	10.0	76.7	76.7	78.8	78.8		

## X.7. Appendix G – Results for the autothermal reactor configuration

*Table X-12 Results for the optimization of Superstructure II, for the Ru-based catalyst, including the values of the objective functions and the optimization variables with direct influence on the process structure.*

KPI	Units	P1	P2	P3	P4	P5	P6	P7	P8	P9	P10	P11	P12	P13
Global LCOA	€/t	129,7	130,7	134,2	134,2	130,2	134,0	133,7	132,7	141,8	145,7	141,4	141,1	130,3
Energy efficiency	%	64,00	65,64	66,17	66,16	65,46	66,09	66,05	65,98	66,59	67,13	66,45	66,40	65,60
<b>Variables</b>														
Pressure	bar	99,36	99,99	100,00	100,00	100,00	100,00	100,00	100,00	100,00	100,00	100,00	100,00	99,82
Temperature 1 <sup>st</sup> reactor	K	703,24	699,16	699,19	699,19	687,41	690,84	699,19	699,19	699,19	699,19	702,63	700,14	699,72
Temperature 2 <sup>nd</sup> reactor	K	695,27	643,15	691,09	691,09	691,09	691,09	691,09	691,09	691,09	691,09	698,89	701,77	696,21
Length of 1 <sup>st</sup> reactor	m	3,70	7,00	7,00	7,00	7,00	6,95	7,00	6,95	7,00	7,00	7,00	7,00	7,00
Length of 2 <sup>nd</sup> reactor	m	2,28	1,00	6,23	6,23	1,00	6,23	5,45	4,28	6,23	6,23	5,16	4,85	1,00
Inter. separation temperature	K	250,46	250,15	273,15	273,15	273,15	273,15	273,15	273,15	273,15	273,15	262,02	260,93	260,61
Final separation temperature	K	251,81	250,15	250,15	250,15	250,15	250,15	250,15	250,15	250,15	250,15	250,15	250,15	250,15
<b>Structure</b>														
Number of compressors	-	2	2	2	2	2	2	2	2	3	2	3	3	2
Additional separation	-	No	Yes	No	No	No								



## X.8. Appendix H - Flowsheet representation and material balance data for the autothermal reactor configuration

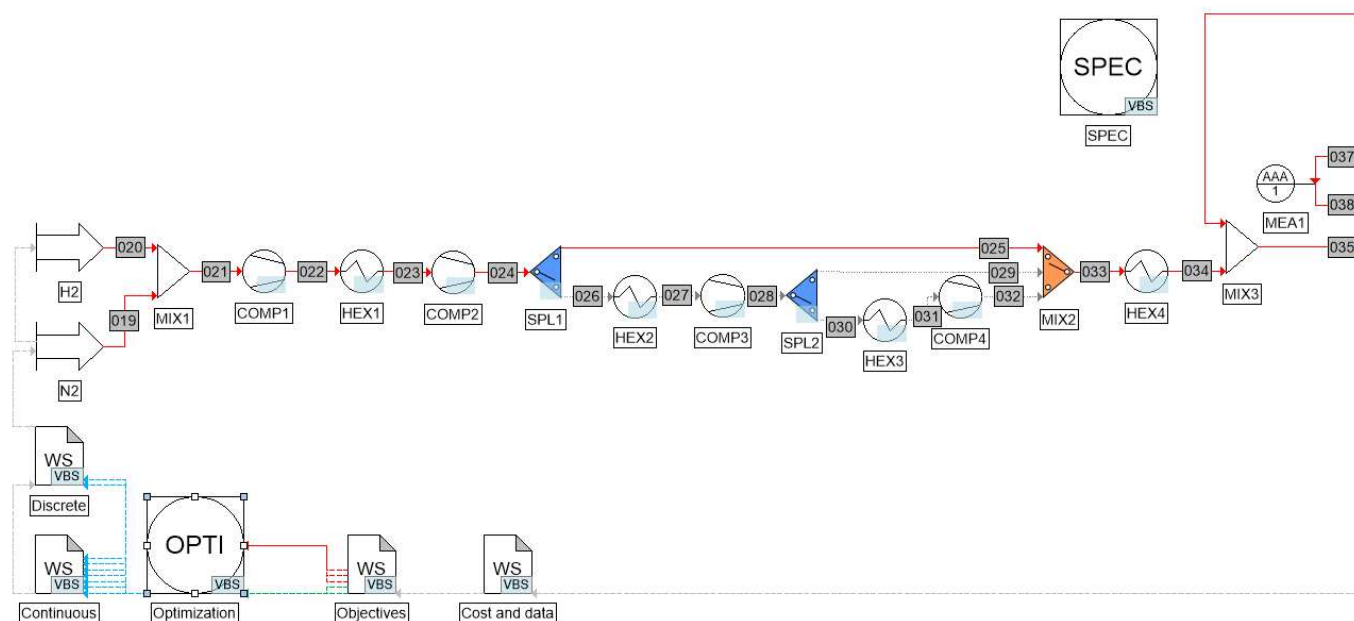


**Table X-13.** Information of streams on the process for the Ru-based autothermal optimal solution.

Stream	001	002	003	004	005	006	007	008	009	010
Mass flowrate (kg/h)	403.63	403.63	403.63	403.63	403.63	403.63	403.63	403.63	403.63	550.79
Molar flowrate (kmol/h)	23.76	23.76	23.76	23.76	23.76	23.76	23.76	23.76	23.76	32.42
Nitrogen molar fraction	0.001	0.001	0.001	0.001	0.001	0.001	0.001	0.001	0.001	0.001
Hydrogen molar fraction	0.004	0.004	0.004	0.004	0.004	0.004	0.004	0.004	0.004	0.004
Ammonia molar fraction	0.995	0.995	0.995	0.995	0.995	0.995	0.995	0.995	0.995	0.995
Temperature (°C)	308.15	272.51	273.15	311.01	289.83	329.55	302.67	343.87	308.15	308.15
Pressure (bar)	15.0	4.3	4.3	6.5	6.5	9.9	9.9	15.0	15.0	15.0
Stream	011	012	013	014	015	016	017	018	019	020
Mass flowrate (kg/h)	550.79	550.79	550.79	550.79	550.79	550.79	550.79	550.79	420.18	90.71
Molar flowrate (kmol/h)	32.42	32.42	32.42	32.42	32.42	32.42	32.42	32.42	15.00	45.00
Nitrogen molar fraction	0.001	0.001	0.001	0.001	0.001	0.001	0.001	0.001	1.000	0.000
Hydrogen molar fraction	0.004	0.004	0.004	0.004	0.004	0.004	0.004	0.004	0.000	1.000
Ammonia molar fraction	0.995	0.995	0.995	0.995	0.995	0.995	0.995	0.995	0.000	0.000
Temperature (°C)	272.36	273.00	311.02	289.72	329.62	302.61	343.99	308.15	298.15	298.15
Pressure (bar)	4.3	4.3	6.5	6.5	9.9	9.9	15.0	15.0	10.0	10.0
Stream	021	022	023	024	025	026	027	028	029	030
Mass flowrate (kg/h)	510.90	510.90	510.90	510.90	510.90	0.00	0.00	0.00	0.00	0.00
Molar flowrate (kmol/h)	60.00	60.00	60.00	60.00	60.00	0.00	0.00	0.00	0.00	0.00
Nitrogen molar fraction	0.25	0.25	0.25	0.25	0.25	0.25	0.25	0.25	0.00	0.25
Hydrogen molar fraction	0.75	0.75	0.75	0.75	0.75	0.75	0.75	0.75	0.00	0.75
Ammonia molar fraction	0.00	0.00	0.00	0.00	0.00	0.00	0.00	0.00	0.00	0.00
Temperature (°C)	297.87	452.83	297.87	453.50	453.50	453.50	453.50	453.50	453.50	453.50
Pressure (bar)	10.0	31.6	31.6	100.0	100.0	100.0	100.0	100.0	100.0	100.0

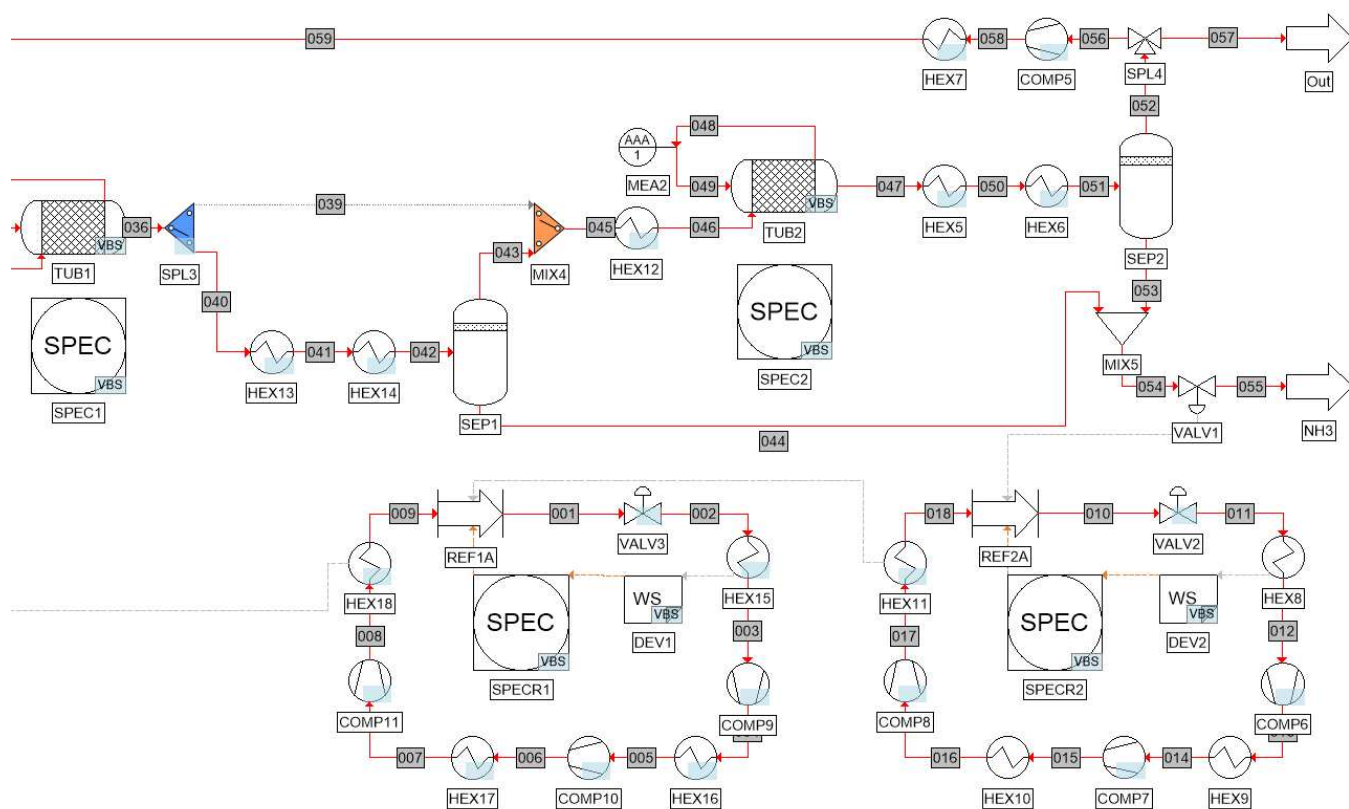


Table XI-13. Continuation

Stream	031	032	033	034	035	036	037	038	039	040
Mass flowrate (kg/h)	0.00	0.00	510.90	510.90	1680.34	1680.41	1680.35	1680.35	0.00	1680.41
Molar flowrate (kmol/h)	0.00	0.00	60.00	60.00	193.81	173.84	193.81	193.81	0.00	173.84
Nitrogen molar fraction	0.25	0.25	0.25	0.25	0.25	0.22	0.25	0.25	0.00	0.22
Hydrogen molar fraction	0.75	0.75	0.75	0.75	0.74	0.65	0.74	0.74	0.00	0.65
Ammonia molar fraction	0.00	0.00	0.00	0.00	0.02	0.14	0.02	0.02	0.00	0.14
Temperature (°C)	453.50	453.50	453.50	699.19	699.18	716.01	711.07	711.07	716.01	716.01
Pressure (bar)	100.0	100.0	100.0	100.0	100.0	97.9	100.0	100.0	97.9	97.9
Stream	041	042	043	044	045	046	047	048	049	050
Mass flowrate (kg/h)	1680.41	1680.41	1453.28	227.13	1453.28	1453.28	1453.22	1453.17	1453.17	1453.22
Molar flowrate (kmol/h)	173.84	173.84	160.47	13.37	160.47	160.47	151.15	160.45	160.45	151.15
Nitrogen molar fraction	0.22	0.22	0.23	0.00	0.23	0.23	0.22	0.23	0.23	0.22
Hydrogen molar fraction	0.65	0.65	0.70	0.00	0.70	0.70	0.65	0.70	0.70	0.65
Ammonia molar fraction	0.14	0.14	0.06	0.99	0.06	0.06	0.13	0.06	0.06	0.13
Temperature (°C)	303.15	273.15	273.15	273.15	273.15	691.09	703.40	697.54	697.54	303.15
Pressure (bar)	97.9	97.9	97.9	97.9	97.9	97.9	95.9	97.9	97.9	95.9
Stream	051	052	053	054	055	056	057	058	059	
Mass flowrate (kg/h)	1453.22	1181.21	272.01	499.14	499.14	1169.40	11.81	1169.40	1169.45	
Molar flowrate (kmol/h)	151.15	135.15	16.00	29.37	29.37	133.80	1.35	133.80	133.81	
Nitrogen molar fraction	0.22	0.24	0.00	0.00	0.00	0.24	0.24	0.24	0.24	
Hydrogen molar fraction	0.65	0.73	0.00	0.00	0.00	0.73	0.73	0.73	0.73	
Ammonia molar fraction	0.13	0.03	1.00	1.00	1.00	0.03	0.03	0.03	0.03	
Temperature (°C)	250.15	250.15	250.15	260.75	262.64	250.15	250.15	254.24	699.19	
Pressure (bar)	95.9	95.9	95.9	95.9	15.0	95.9	95.9	100.0	100.0	

## X.9. Appendix I – Results for the membrane separation configuration

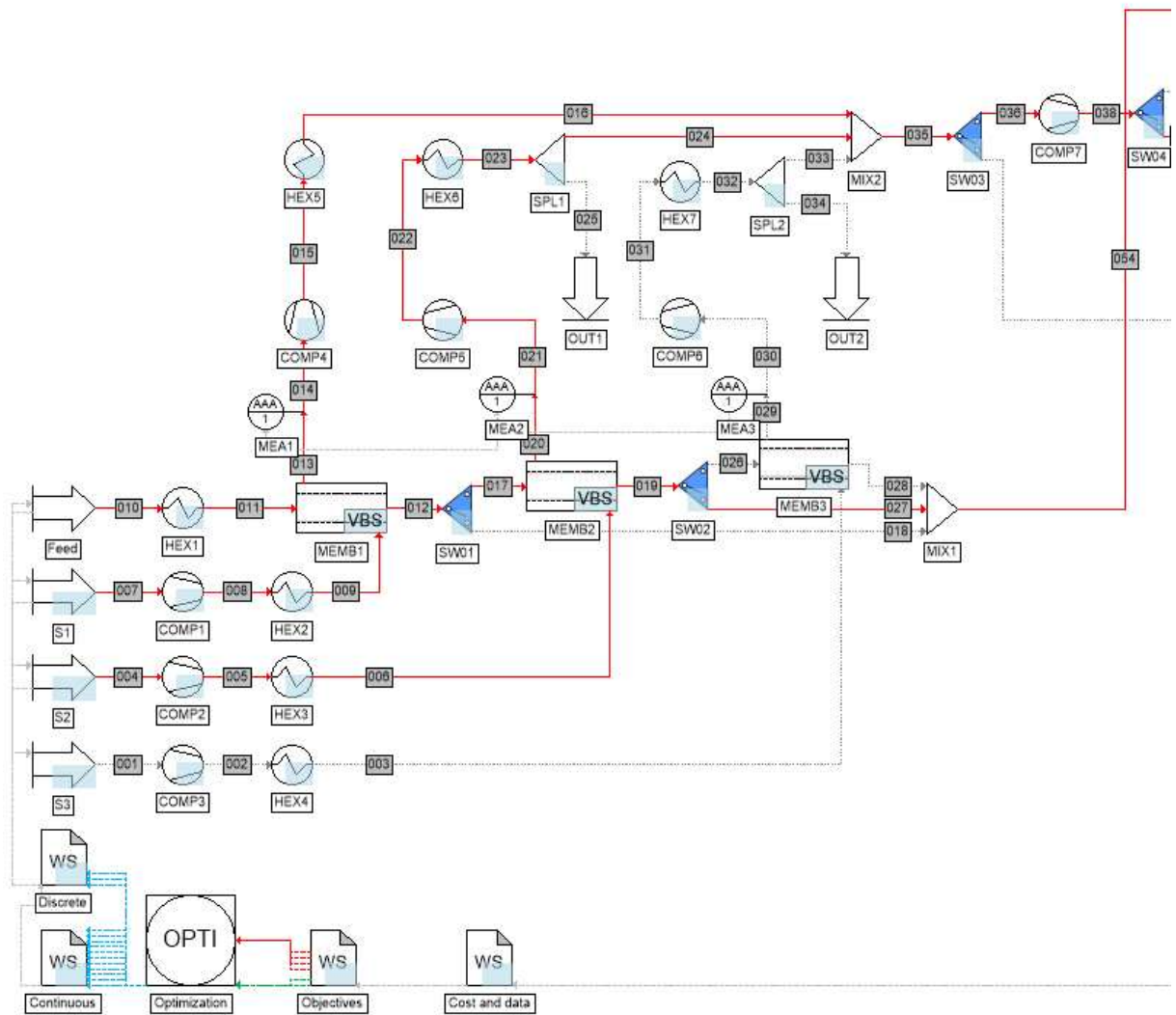
*Table X-14 Results for the optimization of Superstructure III, including the values of the objective functions and the optimization variables with direct influence on the process structure.*

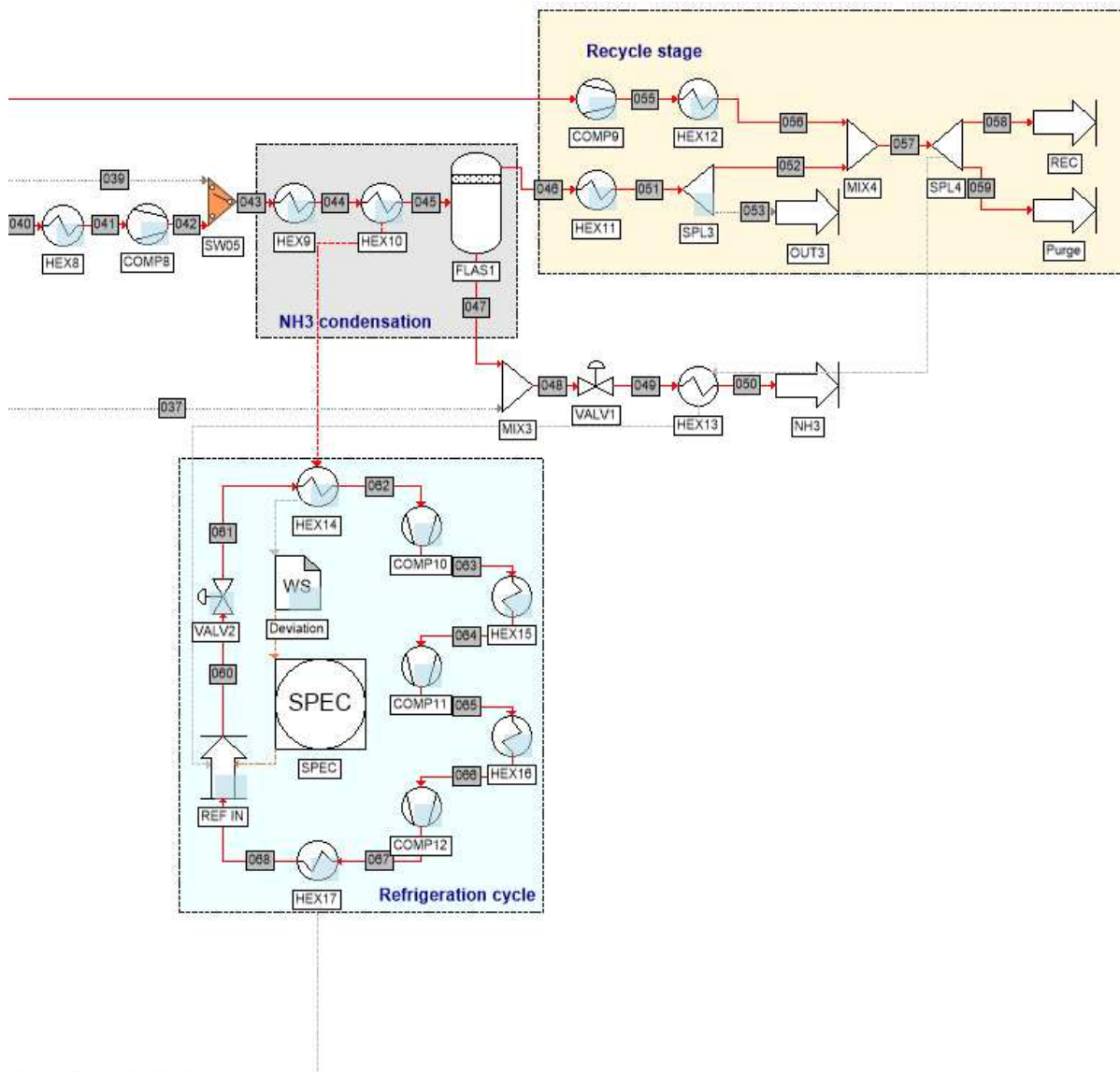
KPI	Units	P1	P2	P3	P4	P5	P6	P7	P8	P9	P10	P11	P12	P13	P14	P15	P16	P17
Separation cost	€/t	128.7	128.8	128.8	128.8	128.8	128.8	128.9	128.9	129.0	129.0	129.0	129.0	129.1	129.1	129.1	129.1	129.1
Specific energy cons.	kWh/kg	0.483	0.483	0.483	0.482	0.481	0.480	0.480	0.480	0.480	0.479	0.479	0.479	0.479	0.479	0.478	0.478	0.477
<b>Variables</b>																		
Membrane temperature	K	342.44	342.35	342.30	342.33	341.98	341.70	341.71	341.76	341.60	341.80	341.65	341.45	341.80	341.80	341.80	341.80	341.80
Length of 1 <sup>st</sup> membrane	m	1.80	1.80	1.80	1.80	1.79	1.80	1.80	1.80	1.80	1.76	1.79	1.79	1.80	1.80	1.80	1.80	1.80
Length of 2 <sup>nd</sup> membrane	m	4.27	4.27	4.27	4.27	4.27	4.27	4.27	4.27	4.27	4.27	4.27	4.27	4.26	4.26	4.25	4.25	4.25
Pressure of 1 <sup>st</sup> sweep	bar	14.96	15.08	15.15	15.08	14.66	14.64	14.76	14.76	14.69	14.86	14.71	14.82	14.86	14.86	14.86	14.86	14.86
Pressure of 2 <sup>nd</sup> sweep	bar	10.04	10.06	10.04	10.09	10.08	10.08	10.09	10.10	10.11	10.17	10.15	10.13	10.17	10.17	10.17	10.17	10.17
Flowrate of 1 <sup>st</sup> sweep	kmol/h	0.10	0.10	0.10	0.10	0.10	0.10	0.10	0.10	0.10	0.10	0.10	0.10	0.10	0.10	0.10	0.10	0.10
Flowrate of 2 <sup>nd</sup> sweep	kmol/h	0.11	0.11	0.12	0.12	0.10	0.10	0.10	0.10	0.10	0.10	0.12	0.11	0.10	0.10	0.10	0.10	0.10
Condenser temperature	K	273.00	273.00	273.00	273.00	272.99	273.00	273.00	273.00	273.00	273.00	273.00	273.00	273.00	273.00	273.00	273.00	273.00
<b>Structure</b>																		
Number of membranes	-	2	2	2	2	2	2	2	2	2	2	2	2	2	2	2	2	2
Additional condenser	-	Yes																
Pressure equalization	-	No																
KPI	Units	P18	P19	P20	P21	P22	P23	P24	P25	P26	P27	P28	P29	P30	P31	P32	P33	P34
Separation cost	€/t	129.2	129.3	129.7	129.7	129.8	129.9	129.9	129.9	129.9	130.0	130.0	130.4	130.5	130.5	130.7	130.7	130.7
Specific energy cons.	kWh/kg	0.476	0.473	0.473	0.473	0.468	0.468	0.468	0.467	0.467	0.467	0.467	0.467	0.466	0.466	0.466	0.466	0.466
<b>Variables</b>																		
Membrane temperature	K	341.80	341.78	341.42	341.42	340.60	340.80	340.70	340.60	340.60	341.41	341.41	341.72	341.56	341.51	341.36	341.36	341.36
Length of 1 <sup>st</sup> membrane	m	1.80	1.80	1.66	1.66	1.75	1.75	1.75	1.75	1.75	1.66	1.66	2.06	2.18	2.17	2.28	2.28	2.29
Length of 2 <sup>nd</sup> membrane	m	4.23	4.22	4.38	4.38	4.31	4.31	4.31	4.31	4.31	4.32	4.32	4.32	4.32	4.32	4.32	4.32	4.32
Pressure of 1 <sup>st</sup> sweep	bar	14.86	14.86	11.67	11.67	11.90	11.90	11.90	11.90	11.90	11.67	11.67	11.67	11.69	11.68	11.68	11.68	11.68
Pressure of 2 <sup>nd</sup> sweep	bar	10.17	10.19	11.51	11.51	11.18	11.28	11.28	11.28	11.28	11.59	11.59	11.67	11.69	11.70	11.69	11.69	11.69
Flowrate of 1 <sup>st</sup> sweep	kmol/h	0.10	0.10	0.10	0.10	0.10	0.10	0.10	0.10	0.10	0.10	0.10	0.10	0.10	0.10	0.10	0.10	0.10
Flowrate of 2 <sup>nd</sup> sweep	kmol/h	0.10	0.10	0.12	0.12	0.10	0.10	0.10	0.10	0.10	0.11	0.11	0.10	0.10	0.10	0.10	0.10	0.10
Condenser temperature	K	273.00	273.00	273.00	273.00	272.98	272.98	272.98	273.00	272.98	273.00	273.00	273.00	273.00	273.00	273.00	273.00	273.00
<b>Structure</b>																		
Number of membranes	-	2	2	2	2	2	2	2	2	2	2	2	2	2	2	2	2	2
Additional condenser	-	Yes																
Pressure equalization	-	No	Yes	Yes	Yes	Yes												

Table X-14. Continuation

<b>KPI</b>	<b>Units</b>	<b>P35</b>	<b>P36</b>	<b>P37</b>	<b>P38</b>	<b>P39</b>	<b>P40</b>	<b>P41</b>	<b>P42</b>	<b>P43</b>	<b>P44</b>	<b>P45</b>	<b>P46</b>	<b>P47</b>	<b>P48</b>	<b>P49</b>	<b>P50</b>	<b>P51</b>	
Separation cost	€/t	130.7	130.7	130.8	130.8	130.8	130.8	130.9	130.9	130.9	130.9	130.9	130.9	131.1	131.9	132.1	132.2	132.4	
Specific energy cons.	kWh/kg	0.466	0.466	0.466	0.466	0.466	0.466	0.466	0.466	0.466	0.466	0.466	0.466	0.466	0.466	0.466	0.466	0.465	
<b>Variables</b>																			
Membrane temperature	K	341.36	341.36	341.36	341.31	341.67	341.18	341.10	341.10	341.16	341.16	341.16	341.16	341.16	341.16	341.16	341.16	341.16	341.03
Length of 1 <sup>st</sup> membrane	m	2.29	2.31	2.33	2.33	2.32	2.33	2.31	2.31	2.31	2.32	2.31	2.32	2.32	2.32	2.32	2.31	2.32	2.45
Length of 2 <sup>nd</sup> membrane	m	4.32	4.32	4.32	4.32	4.32	4.33	4.34	4.34	4.34	4.34	4.34	4.34	4.34	4.34	4.34	4.34	4.34	4.40
Pressure of 1 <sup>st</sup> sweep	bar	11.68	11.68	11.79	11.79	11.85	11.77	11.79	11.79	11.80	11.80	11.81	11.80	11.80	11.83	11.84	11.85	11.85	12.18
Pressure of 2 <sup>nd</sup> sweep	bar	11.69	11.69	11.69	11.69	11.76	11.73	11.80	11.80	11.81	11.81	11.81	11.81	11.81	11.81	11.81	11.81	11.81	12.49
Flowrate of 1 <sup>st</sup> sweep	kmol/h	0.10	0.10	0.10	0.10	0.10	0.10	0.10	0.10	0.10	0.10	0.10	0.10	0.10	0.10	0.10	0.10	0.10	0.10
Flowrate of 2 <sup>nd</sup> sweep	kmol/h	0.10	0.10	0.10	0.10	0.10	0.10	0.10	0.10	0.10	0.10	0.10	0.10	0.10	0.10	0.10	0.10	0.10	0.22
Condenser temperature	K	273.00	273.00	273.00	273.00	272.90	272.88	272.71	272.71	272.62	272.62	272.62	272.62	272.62	272.62	272.62	272.62	272.62	272.62
<b>Structure</b>																			
Number of membranes	-	2	2	2	2	2	2	2	2	2	2	2	2	2	2	2	2	2	2
Additional condenser	-	Yes	Yes																
Pressure equalization	-	Yes	Yes	No	No	No	No	Yes	Yes										
<b>KPI</b>	<b>Units</b>	<b>P52</b>	<b>P53</b>	<b>P54</b>	<b>P55</b>	<b>P56</b>	<b>P57</b>	<b>P58</b>	<b>P59</b>	<b>P60</b>	<b>P61</b>	<b>P62</b>	<b>P63</b>	<b>P64</b>	<b>P65</b>	<b>P66</b>	<b>P67</b>		
Separation cost	€/t	132.4	132.5	132.5	132.5	132.5	132.5	134.0	134.7	136.4	136.6	136.9	138.6	139.0	139.4	142.4	150.4		
Specific energy cons.	kWh/kg	0.466	0.465	0.465	0.465	0.465	0.465	0.465	0.465	0.465	0.463	0.462	0.462	0.462	0.460	0.460	0.458		
<b>Variables</b>																			
Membrane temperature	K	341.03	341.03	341.02	341.03	341.04	341.03	341.16	341.18	342.80	340.53	341.46	340.26	343.37	343.89	335.67	339.48		
Length of 1 <sup>st</sup> membrane	m	2.45	2.45	2.45	2.45	2.45	2.45	2.32	2.32	2.26	2.25	2.29	2.60	2.48	1.64	2.72	5.53		
Length of 2 <sup>nd</sup> membrane	m	4.40	4.40	4.40	4.40	4.40	4.40	4.34	4.34	4.31	4.33	4.33	4.32	4.29	4.14	4.39	4.16		
Pressure of 1 <sup>st</sup> sweep	bar	12.18	12.19	12.20	12.20	12.18	12.18	12.02	12.12	12.61	12.55	12.84	13.22	13.80	16.56	16.94	14.91		
Pressure of 2 <sup>nd</sup> sweep	bar	12.49	12.50	12.50	12.50	12.51	12.51	11.81	11.81	11.77	11.56	11.74	11.34	11.78	10.05	11.18	11.14		
Flowrate of 1 <sup>st</sup> sweep	kmol/h	0.10	0.10	0.10	0.10	0.10	0.10	0.10	0.11	0.10	0.10	0.10	0.14	0.11	0.13	0.13	0.14		
Flowrate of 2 <sup>nd</sup> sweep	kmol/h	0.23	0.23	0.23	0.23	0.22	0.22	0.10	0.10	0.18	0.11	0.10	0.10	0.32	0.18	0.32	0.20		
Condenser temperature	K	272.64	272.62	272.62	272.62	272.62	272.62	272.62	272.62	272.93	272.99	272.99	272.95	272.92	272.52	270.58	272.68		
<b>Structure</b>																			
Number of membranes	-	2	2	2	2	2	2	2	2	2	2	2	2	2	2	2	2		
Additional condenser	-	Yes																	
Pressure equalization	-	Yes																	

## X.10. Appendix J - Flowsheet representation and material balance data for the membrane separation configuration





**Table X-15.** Information of streams on the process for the membrane separation optimal solution.

<b>Stream</b>	<b>001</b>	<b>002</b>	<b>003</b>	<b>004</b>	<b>005</b>	<b>006</b>	<b>007</b>	<b>008</b>	<b>009</b>	<b>010</b>
Mass flowrate (kg/h)	0	0	0	2.80	2.80	2.80	2.80	2.80	2.80	2912.24
Molar flowrate (kmol/h)	0	0	0	0.10	0.10	0.10	0.10	0.10	0.10	304.05
Nitrogen molar fraction	0	0	0	1.000	1.000	1.000	1.000	1.000	1.000	0.219
Hydrogen molar fraction	0	0	0	0.000	0.000	0.000	0.000	0.000	0.000	0.656
Ammonia molar fraction	0	0	0	0.000	0.000	0.000	0.000	0.000	0.000	0.125
Temperature (°C)	-	-	-	25.00	43.15	68.21	25.00	43.06	68.21	451.15
Pressure (bar)	-	-	-	10.0	11.7	11.7	10.0	11.7	11.7	96.6
<b>Stream</b>	<b>011</b>	<b>012</b>	<b>013</b>	<b>014</b>	<b>015</b>	<b>016</b>	<b>017</b>	<b>018</b>	<b>019</b>	<b>020</b>
Mass flowrate (kg/h)	2912.24	2901.77	13.28	13.28	13.28	13.28	2901.77	0	2233.43	671.18
Molar flowrate (kmol/h)	304.05	303.20	0.95	0.95	0.95	0.95	303.20	0	241.28	62.02
Nitrogen molar fraction	0.219	0.219	0.157	0.157	0.157	0.157	0.219	0	0.251	0.098
Hydrogen molar fraction	0.656	0.657	0.318	0.318	0.318	0.318	0.657	0	0.701	0.485
Ammonia molar fraction	0.125	0.124	0.525	0.525	0.525	0.525	0.124	0	0.048	0.417
Temperature (°C)	68.21	68.21	68.21	68.21	68.30	46.85	68.21	-	68.21	68.21
Pressure (bar)	96.6	96.5	11.7	11.7	11.7	11.7	96.5	-	96.5	11.7
<b>Stream</b>	<b>021</b>	<b>022</b>	<b>023</b>	<b>024</b>	<b>025</b>	<b>026</b>	<b>027</b>	<b>028</b>	<b>029</b>	<b>030</b>
Mass flowrate (kg/h)	671.18	671.18	671.18	671.18	0	0	2233.43	0	0	0
Molar flowrate (kmol/h)	62.02	62.02	62.02	62.02	0	0	241.28	0	0	0
Nitrogen molar fraction	0.098	0.098	0.098	0.098	0	0	0.251	0	0	0
Hydrogen molar fraction	0.485	0.485	0.485	0.485	0	0	0.701	0	0	0
Ammonia molar fraction	0.417	0.417	0.417	0.417	0	0	0.048	0	0	0
Temperature (°C)	68.21	68.21	46.85	46.85	-	-	68.21	-	-	-
Pressure (bar)	11.7	11.7	11.7	11.7	-	-	96.5	-	-	-
<b>Stream</b>	<b>031</b>	<b>032</b>	<b>033</b>	<b>034</b>	<b>035</b>	<b>036</b>	<b>037</b>	<b>038</b>	<b>039</b>	<b>040</b>
Mass flowrate (kg/h)	0	0	0	0	684.46	684.46	0	684.46	0	684.46
Molar flowrate (kmol/h)	0	0	0	0	62.97	62.97	0	62.97	0	62.97
Nitrogen molar fraction	0	0	0	0	0.099	0.099	0	0.099	0	0.099
Hydrogen molar fraction	0	0	0	0	0.483	0.483	0	0.483	0	0.483
Ammonia molar fraction	0	0	0	0	0.419	0.419	0	0.419	0	0.419
Temperature (°C)	-	-	-	-	46.85	46.85	-	179.12	-	179.12
Pressure (bar)	-	-	-	-	11.7	11.7	-	33.9	-	33.9
<b>Stream</b>	<b>041</b>	<b>042</b>	<b>043</b>	<b>044</b>	<b>045</b>	<b>046</b>	<b>047</b>	<b>048</b>	<b>049</b>	<b>050</b>
Mass flowrate (kg/h)	684.46	684.46	684.46	684.46	684.46	275.97	408.49	408.49	408.49	408.49
Molar flowrate (kmol/h)	62.97	62.97	62.97	62.97	62.97	38.91	24.06	24.06	24.06	24.06
Nitrogen molar fraction	0.099	0.099	0.099	0.099	0.099	0.159	0.001	0.001	0.001	0.001
Hydrogen molar fraction	0.483	0.483	0.483	0.483	0.483	0.779	0.004	0.004	0.004	0.004
Ammonia molar fraction	0.419	0.419	0.419	0.419	0.419	0.062	0.995	0.995	0.995	0.995
Temperature (°C)	46.85	179.78	179.78	46.85	-0.15	-0.15	-0.15	-0.15	1.42	15.00
Pressure (bar)	33.9	98.4	98.4	98.4	98.4	98.4	98.4	98.4	15.0	15.0
<b>Stream</b>	<b>051</b>	<b>052</b>	<b>053</b>	<b>054</b>	<b>055</b>	<b>056</b>	<b>057</b>	<b>058</b>	<b>059</b>	<b>060</b>
Mass flowrate (kg/h)	275.97	275.97	0.00	2233.43	2233.43	2233.43	2509.40	2484.30	25.09	313.82
Molar flowrate (kmol/h)	38.91	38.91	0.00	241.28	241.28	241.28	280.19	277.39	2.80	18.47
Nitrogen molar fraction	0.159	0.159	0.000	0.251	0.251	0.251	0.238	0.238	0.238	0.001
Hydrogen molar fraction	0.779	0.779	0.000	0.701	0.701	0.701	0.712	0.712	0.712	0.004
Ammonia molar fraction	0.062	0.062	0.000	0.048	0.048	0.048	0.050	0.050	0.050	0.995
Temperature (°C)	358.04	358.04	358.04	68.21	70.73	358.04	358.04	358.04	358.04	35.00
Pressure (bar)	98.4	98.4	98.4	96.5	98.4	98.4	98.4	98.4	98.4	15.0
<b>Stream</b>	<b>061</b>	<b>062</b>	<b>063</b>	<b>064</b>	<b>065</b>	<b>066</b>	<b>067</b>	<b>068</b>		
Mass flowrate (kg/h)	313.82	313.82	313.82	313.82	313.82	313.82	313.82	313.82		
Molar flowrate (kmol/h)	18.47	18.47	18.47	18.47	18.47	18.47	18.47	18.47		
Nitrogen molar fraction	0.001	0.001	0.001	0.001	0.001	0.001	0.001	0.001		
Hydrogen molar fraction	0.004	0.004	0.004	0.004	0.004	0.004	0.004	0.004		
Ammonia molar fraction	0.995	0.995	0.995	0.995	0.995	0.995	0.995	0.995		
Temperature (°C)	-10.63	-10.15	38.72	14.16	66.57	30.32	85.15	35.00		
Pressure (bar)	2.9	2.9	5.0	5.0	8.7	8.7	15.0	15.0		

## X.11. Appendix K – Results for the membrane-PSA-condenser separation configuration

**Table X-16.** Results for the optimization of Superstructure IV, including the values of the objective functions and the optimization variables with direct influence on the process structure. As only the condenser technology achieves the optimality, and it depends exclusively on the condenser temperature, the total number of optimal solutions (559) is not reported, with only 34 points being shown. In the end, the difference between optimal points is a slight variation on the condenser temperature.

<b>KPI</b>	<b>Units</b>	<b>P1</b>	<b>P2</b>	<b>P3</b>	<b>P4</b>	<b>P5</b>	<b>P6</b>	<b>P7</b>	<b>P8</b>	<b>P9</b>	<b>P10</b>	<b>P11</b>	<b>P12</b>	<b>P13</b>	<b>P14</b>	<b>P15</b>	<b>P16</b>	<b>P17</b>
Separation cost	€/t	82.02	82.06	82.11	82.16	82.20	82.24	82.27	82.31	82.35	82.38	82.42	82.46	82.49	82.53	82.56	82.60	82.63
Specific energy cons.	kWh/kg	0.255	0.254	0.253	0.252	0.252	0.251	0.251	0.250	0.250	0.249	0.249	0.248	0.248	0.247	0.247	0.247	0.246
<b>Variables</b>																		
Condenser temperature	K	268.14	268.31	268.47	268.63	268.78	268.88	268.98	269.09	269.20	269.29	269.40	269.50	269.58	269.66	269.75	269.84	269.92
<b>Structure</b>																		
Separation technology	-	Cond.																
<b>KPI</b>	<b>Units</b>	<b>P18</b>	<b>P19</b>	<b>P20</b>	<b>P21</b>	<b>P22</b>	<b>P23</b>	<b>P24</b>	<b>P25</b>	<b>P26</b>	<b>P27</b>	<b>P28</b>	<b>P29</b>	<b>P30</b>	<b>P31</b>	<b>P32</b>	<b>P33</b>	<b>P34</b>
Separation cost	€/t	82.67	82.70	82.73	82.77	82.81	82.86	82.91	82.96	83.00	83.05	83.11	83.17	83.23	83.30	83.37	83.45	83.50
Specific energy cons.	kWh/kg	0.246	0.246	0.245	0.245	0.244	0.244	0.244	0.243	0.243	0.242	0.242	0.241	0.241	0.240	0.240	0.239	0.239
<b>Variables</b>																		
Condenser temperature	K	270.00	270.07	270.15	270.23	270.31	270.41	270.51	270.61	270.69	270.78	270.90	271.01	271.12	271.23	271.35	271.48	271.56
<b>Structure</b>																		
Separation technology	-	Cond.																





**Table X-17.** Information of streams on the process for the PSA-Membrane-Condenser separation optimal solution. Only the data for the relevant streams is shown, avoiding streams from the PSA and membrane separation technologies.

<b>Stream</b>	<b>016</b>	<b>019</b>	<b>051</b>	<b>052</b>	<b>053</b>	<b>054</b>	<b>055</b>	<b>056</b>	<b>057</b>
Mass flowrate (kg/h)	2912.24	2912.24	2912.24	2912.24	0.00	2912.24	2912.24	2912.24	0.00
Molar flowrate (kmol/h)	304.05	304.05	304.05	304.05	0.00	304.05	304.05	304.05	0.00
Nitrogen molar fraction	0.219	0.219	0.219	0.219	0.000	0.219	0.219	0.219	0.219
Hydrogen molar fraction	0.656	0.656	0.656	0.656	0.000	0.656	0.656	0.656	0.656
Ammonia molar fraction	0.125	0.125	0.125	0.125	0.000	0.125	0.125	0.125	0.125
Temperature (°C)	451.15	451.15	451.15	451.15	451.15	46.85	49.09	49.09	49.09
Pressure (bar)	96.6	96.6	96.6	96.6	96.6	96.6	98.4	98.4	98.4
<b>Stream</b>	<b>058</b>	<b>059</b>	<b>060</b>	<b>061</b>	<b>062</b>	<b>063</b>	<b>064</b>	<b>065</b>	<b>066</b>
Mass flowrate (kg/h)	0.00	0.00	2912.24	2912.24	2912.24	2518.85	393.39	393.39	393.39
Molar flowrate (kmol/h)	0.00	0.00	304.05	304.05	304.05	280.90	23.15	23.15	23.15
Nitrogen molar fraction	0.219	0.219	0.219	0.219	0.219	0.237	0.001	0.001	0.001
Hydrogen molar fraction	0.656	0.656	0.656	0.656	0.656	0.710	0.003	0.003	0.003
Ammonia molar fraction	0.125	0.125	0.125	0.125	0.125	0.053	0.995	0.995	0.995
Temperature (°C)	49.09	49.09	49.09	46.85	-5.01	-5.01	-5.01	-5.01	-3.25
Pressure (bar)	98.4	98.4	98.4	98.4	98.4	98.4	98.4	98.4	15.0
<b>Stream</b>	<b>067</b>	<b>068</b>	<b>069</b>	<b>070</b>	<b>078</b>	<b>079</b>	<b>080</b>	<b>081</b>	<b>082</b>
Mass flowrate (kg/h)	393.39	2518.85	2518.85	0.00	2518.85	2493.66	25.19	925.81	925.81
Molar flowrate (kmol/h)	23.15	280.90	280.90	0.00	280.90	278.09	2.81	54.50	54.50
Nitrogen molar fraction	0.001	0.237	0.237	0.000	0.237	0.237	0.237	0.001	0.001
Hydrogen molar fraction	0.003	0.710	0.710	0.000	0.710	0.710	0.710	0.004	0.004
Ammonia molar fraction	0.995	0.053	0.053	0.000	0.053	0.053	0.053	0.995	0.995
Temperature (°C)	15.00	358.04	358.04	358.04	358.04	358.04	358.04	35.00	-15.43
Pressure (bar)	15.0	98.4	98.4	98.4	98.4	98.4	98.4	15.0	2.4
<b>Stream</b>	<b>083</b>	<b>084</b>	<b>085</b>	<b>086</b>	<b>087</b>	<b>088</b>	<b>089</b>		
Mass flowrate (kg/h)	925.81	925.81	925.81	925.81	925.81	925.81	925.81		
Molar flowrate (kmol/h)	54.50	54.50	54.50	54.50	54.50	54.50	54.50		
Nitrogen molar fraction	0.001	0.001	0.001	0.001	0.001	0.001	0.001		
Hydrogen molar fraction	0.004	0.004	0.004	0.004	0.004	0.004	0.004		
Ammonia molar fraction	0.995	0.995	0.995	0.995	0.995	0.995	0.995		
Temperature (°C)	-15.01	39.34	10.49	69.04	28.23	89.77	343.15		
Pressure (bar)	2.4	4.4	4.4	8.1	8.1	15.0	15.0		

---

**Résumé en français des travaux menés  
et des résultats obtenus**

---



# XI. Résumé en français des travaux menés et des résultats obtenus

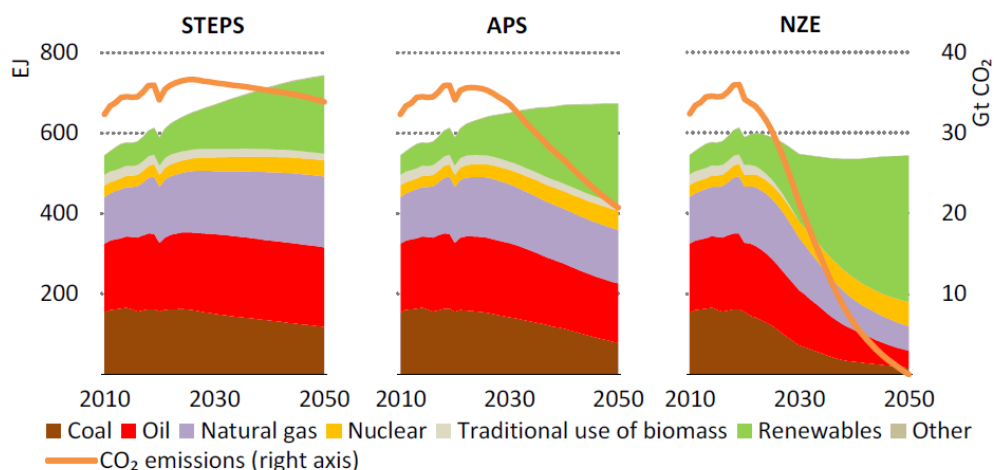
## XI.1. Introduction générale

### XI.1.1. Contexte

Le dernier rapport du *World Energy Outlook* (WEO) de l'Agence internationale de l'énergie (AIE), préparé pour la dernière Conférence des Parties (COP26), décrit trois principaux scénarios possibles résultant des politiques et des engagements des gouvernements sur l'évolution du système énergétique, donnant des résultats différents dans la recherche d'une limitation de l'augmentation de la température mondiale. Le scénario des politiques déclarées (STEPS) est le plus prudent, car il ne tient pas compte de la réalisation complète des objectifs actuels, atteignant une augmentation de 2.5 °C d'ici 2100. Le scénario des engagements annoncés (APS) prend en compte la réalisation complète des engagements proposés, même si les projections indiquent une augmentation de la température de 2.0 °C. Le scénario d'émissions nettes nulles (NZE) considère que chaque pays atteint des émissions nettes nulles d'ici 2050, limitant l'augmentation de la température mondiale à 1.5 °C, avec une probabilité de 50 % [1].

Comme le montre la Figure XI-1, avec la progression prévue de la part des sources d'énergie dans l'approvisionnement total en énergie primaire, ainsi que les émissions mondiales de CO<sub>2</sub>, la plus grande différence entre les scénarios est la forte réduction des sources à base de combustibles fossiles (c'est-à-dire le charbon, le pétrole et le gaz naturel), et la forte augmentation de la contribution des sources d'énergie renouvelables.

Dans le scénario STEPS les combustibles fossiles maintiennent en 2050 un approvisionnement énergétique équivalent à la situation actuelle, avec un léger transfert entre le charbon et le gaz naturel, ce qui signifie une quantité d'émissions similaire à la situation actuelle, soit près de 33 Gt CO<sub>2</sub>. Néanmoins, le scénario le plus ambitieux, le NZE, exige une part finale de sources renouvelables d'environ 60 %, avec une forte transition à partir de 2030 et au-delà, permettant d'atteindre des émissions nettes nulles.



IEA. All rights reserved.

**Figure XI-1.** Projection de 2010 à 2050 de la part de marché et de la consommation d'énergie (EJ) et des émissions mondiales de CO<sub>2</sub>, selon les scénarios STEPS : Stated Policies Scenario, APS : Announced Pledges Scenario et NZE : Net Zero Emissions Scenario. [1]

Le point commun de ces trois scénarios est la recherche de solutions durables, avec des technologies électrifiées, efficaces, interconnectées et décarbonées [1]. Selon les projections de l'Agence

internationale pour les énergies renouvelables (IRENA), d'ici à 2050 l'électricité sera le principal vecteur énergétique avec 50 % de la part de marché des énergies renouvelables. [2].

En fait, en 2019 la production d'énergie renouvelable a augmenté plus que la demande d'électricité, avec une diminution de l'électricité produite à partir de combustibles fossiles. C'est la première fois depuis des décennies que la demande d'énergie et l'électricité produite à partir de combustibles fossiles ont un comportement inverse [3]. Parmi les solutions prévues pour réduire les émissions de carbone dans le scénario NZE, la production d'électricité à partir de sources renouvelables partage la première place avec les économies d'énergie et l'efficacité énergétique, avec une part de 25 % chacune. Les autres solutions sont l'électrification des secteurs d'utilisation finale (20 %), l'utilisation de l'hydrogène et de ses dérivés (10 %), et la capture, le stockage et l'utilisation du carbone (CCSU) (20 %). [2].

Les données de la dernière décennie permettent d'affirmer que les mesures politiques et économiques favorisent l'investissement dans le développement de technologies plus vertes et leur intégration sur le marché de l'énergie. Sur de nombreux marchés, les sources d'énergie renouvelables dans les projets nouvellement mis en service ont atteint le coût minimum par rapport aux autres sources. Par exemple, le coût nivelé de l'électricité (LCOE) solaire photovoltaïque (PV) est passé de 0.381 \$/kWh en 2010 à 0.057 \$/kWh en 2020, soit une baisse de 85 %. De même, pour les projets éoliens terrestres, le passage de 0.089 \$/kWh en 2010 à 0.039 \$/kWh en 2020 représente une réduction de 56 %. À titre de comparaison, la production d'électricité à partir de combustibles fossiles varie entre 0.055 et 0.148 \$/kWh en fonction du lieu et de la source de combustible. [2].

Les années à venir seront cruciales pour l'aplatissement de la courbe d'augmentation de la température mondiale vers une limite maximale de 1.5 °C d'ici 2100 et la forte diminution des émissions mondiales de carbone. Le déploiement de la production d'énergie propre et son intégration au marché de l'énergie joueront un rôle clé dans la réalisation de ces objectifs, ce qui va dans le sens des objectifs proposés dans ce travail.

### **XI.1.2. Objectifs**

La recherche de procédés efficaces, durables et économiques est un défi important auquel les ingénieurs des procédés sont constamment confrontés dans la recherche et l'industrie. Plus les procédés sont contraints par des critères restrictifs, plus l'ingénieur doit déterminer des procédés optimaux en utilisant les différentes technologies disponibles pour la transformation de la masse et de l'énergie.

Pour faire face à ces restrictions, les ingénieurs doivent déterminer la meilleure configuration structurelle d'un procédé, conduisant à la disposition optimale des unités de traitement, avec la mise en place respective des conditions d'exploitation. Telle qu'elle est présentée, cette tâche pourrait nécessiter l'évaluation de plusieurs schémas de procédé pour trouver la meilleure configuration, ce qui est une approche épuisante et chronophage à exécuter manuellement.

Il est donc prévu que ce travail permette aux ingénieurs de procédés d'évaluer plusieurs alternatives de procédé dans une superstructure de procédé unique, afin de déterminer la meilleure disposition structurelle, l'ensemble des conditions d'opération et/ou des paramètres de design, menant à la configuration optimale du procédé en ce qui concerne certains critères économiques, énergétiques et/ou environnementaux.

En résumé, les travaux présentés ci-après visent à couvrir deux objectifs principaux dans la recherche de procédés de transformation plus efficaces et dans le contexte des sources d'énergie renouvelables :

**O1** : La proposition d'une méthodologie pour la conception de procédés par l'optimisation des superstructures, en utilisant un logiciel de simulation de procédés comme environnement et un algorithme d'optimisation MINLP comme caractéristique essentielle pour sa résolution.

**O2** : L'application de la méthodologie proposée à un scénario de stockage d'énergie renouvelable dans des composés chimiques, plus précisément dans l'ammoniac, en utilisant comme référence le procédé conventionnel Haber-Bosch.

### **XI.1.3. Plan de la thèse**

Ce manuscrit est divisé en huit chapitres qui présentent les différentes étapes réalisées dans cette thèse pour la proposition de la méthodologie de superstructure et l'évaluation du procédé Haber-Bosch pour la synthèse de l'ammoniac. Le contenu de chaque chapitre est résumé comme suit :

- Chapitre I** Présente le contexte actuel des énergies renouvelables et les technologies de stockage de l'énergie, en décrivant le stockage chimique de l'énergie comme une solution potentielle pour permettre leur intégration sur le marché de l'énergie. Il couvre également les généralités sur les procédés de synthèse de l'ammoniac que l'on trouve dans l'industrie et les voies non conventionnelles pour sa production.
- Chapitre II** Couvre les différentes stratégies de synthèse des procédés disponibles dans la littérature, à savoir les techniques de décomposition hiérarchique et l'optimisation basée sur les mathématiques. Des détails sur les méthodes d'optimisation des superstructures sont présentés.
- Chapitre III** Décrit les généralités du logiciel de simulation et l'algorithme d'optimisation utilisé pour mettre en œuvre la méthodologie. Il présente également les principes de conception de la superstructure, la méthodologie de sa conception et les stratégies envisagées permettant de réduire le temps de calcul de l'optimisation.
- Chapitre IV** Présente le cadre du problème et le scénario hypothétique du stockage des énergies renouvelables dans l'ammoniac, avec la définition des limites du système pour l'étude. Il présente également les données préliminaires nécessaires à la modélisation de chaque étape du procédé HB, ainsi que les indicateurs clés de performance à minimiser.
- Chapitre V** Décrit les deux premiers cas de superstructure de l'étude liés à l'optimisation du procédé Haber-Bosch par la sélection des configurations du réacteur et du matériau catalytique.
- Chapitre VI** Couvre les troisième et quatrième cas de superstructure de l'étude, liés à l'optimisation du procédé HB par la sélection de la technologie de séparation pour la récupération de  $\text{NH}_3$ .
- Chapitre VII** Détaille l'analyse de l'intégration thermique potentielle entre les différents courants du procédé, avec une brève description du réseau HEX et de son impact sur le KPI économique.
- Chapitre VIII** Présente les conclusions générales et les perspectives de recherches futures, en soulignant les principales contributions de ce travail, les inconvénients qui nécessitent une attention particulière et qui doivent être traités, ainsi que certains domaines identifiés pour l'amélioration de la méthodologie présentée.

## XI.2. Principaux résultats obtenus

Le travail présenté à travers les différents chapitres de cette thèse a été planifié pour répondre à deux objectifs principaux comme décrit dans l'introduction. D'une part, l'objectif principal a été de proposer une méthodologie de conception de procédés par l'optimisation des superstructures. D'autre part, cette approche devait être évaluée pour déterminer ses avantages et ses faiblesses, et le procédé de synthèse de l'ammoniac a été sélectionné dans ce but dans le contexte actuel du stockage des énergies renouvelables. Les résultats généraux et la contribution de chacun de ces objectifs sont détaillés ci-après.

**O1 : La proposition d'une méthodologie pour la conception de procédés par l'optimisation des superstructures, en utilisant un logiciel de simulation de procédés comme environnement et un algorithme d'optimisation MINLP comme caractéristique essentielle pour sa résolution.**

La principale contribution de cette méthodologie, présentée avec ses différentes étapes dans la Figure XI-2, est l'avantage d'évaluer simultanément plusieurs alternatives de processus avec un objectif commun, sans avoir à évaluer manuellement chacune d'entre elles. Cette méthode présente un grand potentiel lorsque de nombreuses alternatives structurales participent à la conception d'un procédé avec de multiples technologies concurrentes. Elle a montré son utilité pour déterminer l'ensemble des meilleurs arrangements structurels au sein d'un procédé, permettant d'obtenir un bon compromis entre les indicateurs clés de performance, à savoir les indicateurs économiques et énergétiques.

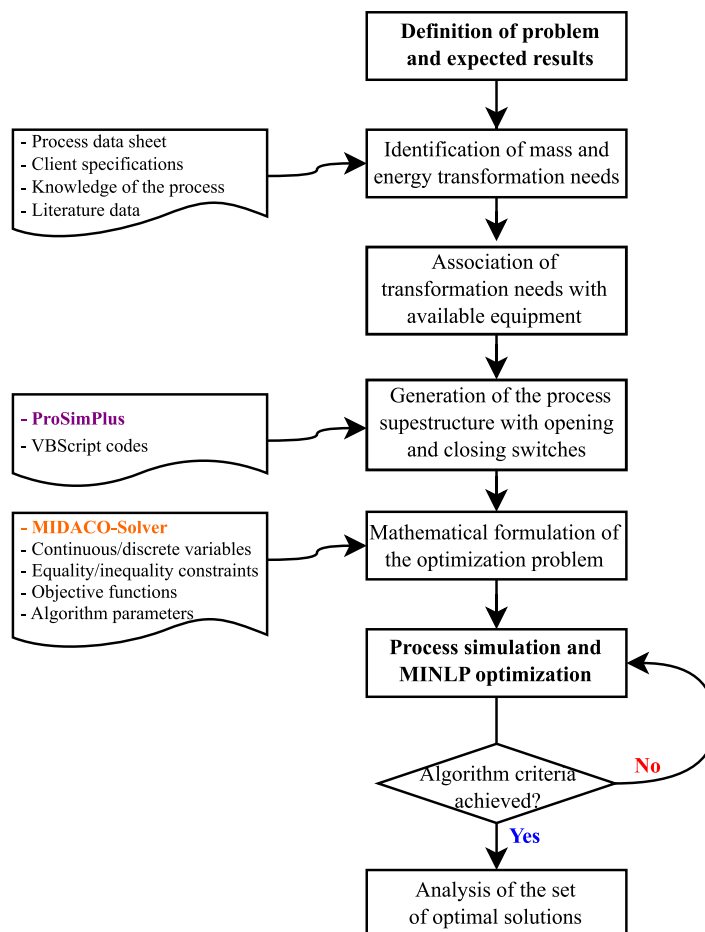


Figure XI-2. Procédure de conception et d'optimisation des superstructures.

L'approche a été proposée pour son utilisation dans ProSimPlus, un logiciel de simulation de procédés en régime continu et en régime permanent, et avec l'ajout de MIDACO-Solver, un algorithme d'optimisation métaheuristique capable de traiter et de résoudre des problèmes d'optimisation de type MINLP.

En profitant de la flexibilité du logiciel en termes d'adaptabilité des différents modules du procédé via le langage de programmation VBScript, la méthodologie a été conçue en utilisant les commutateurs de superstructure comme module essentiel permettant d'évaluer une structure de procédé spécifique au sein de la superstructure. Ces modules agissent comme des déviateurs des courants, qui contournent certaines zones du procédé sans intérêt pour la structure en cours d'évaluation. En conjonction avec la définition des flux résiduels et des modules inactifs, le logiciel de simulation peut effectuer l'évaluation correcte d'une configuration structurelle déterminée sans préjudice des voies de traitement restantes.

A ce stade du développement de la méthodologie, l'optimalité des solutions reste incertaine dans le vaste, voire infini, espace de recherche des possibilités structurelles, car la méthodologie a été testée sur un nombre réduit d'alternatives de procédé, intégrant certaines des configurations structurelles courantes trouvées dans la littérature.

Néanmoins, l'approche présentée dans ce travail a été orientée vers la proposition d'une méthode qui peut être facilement apprise et adaptée par tout ingénieur de procédés souhaitant proposer sa propre superstructure dans un logiciel classique de simulation de procédés.

## **O2 : Application de la méthodologie proposée à un scénario de stockage d'énergie renouvelable dans des composés chimiques, plus précisément dans l'ammoniac, en utilisant comme référence le procédé conventionnel Haber-Bosch.**

Dans le contexte actuel de transition énergétique et d'augmentation des énergies renouvelables sur le marché de l'énergie, le stockage de l'énergie renouvelable dans des composés chimiques a été choisi pour déterminer la pertinence d'une telle méthodologie pour la conception de procédés.

En considérant le procédé Haber-Bosch conventionnel, avec la boucle de synthèse de l'ammoniac comme limites de l'étude, multiples superstructures de procédé ont été proposées et évaluées pour déterminer la meilleure disposition structurelle.

Les alternatives structurelles ont été définies pour choisir : (i) le nombre de compresseurs dans l'étage de compression principal ; (ii) le nombre de réacteurs catalytiques en série ; (iii) le matériau catalytique commun à tous les réacteurs à base de Fe ou de Ru ; (iv) la disposition des réacteurs, soit adiabatique multi-lits, soit autothermique multitubes ; (v) le système de refroidissement des réacteurs adiabatiques, soit indirect (AICR), soit direct (AQCR) ; (vi) l'utilisation d'une séparation intermédiaire entre les réacteurs ; (vii) la technologie de séparation, parmi le condenseur, les filtres à membrane et le PSA ; (viii) l'utilisation d'une égalisation de pression sur les flux de perméat de la séparation par filtres à membrane ; (ix) l'utilisation d'un condenseur supplémentaire après la séparation par membranes ou par PSA.

Les superstructures I et II étaient axées sur les alternatives structurelles (i) à (vi), concernant l'optimisation du procédé Haber-Bosch par la configuration du réacteur et la sélection du catalyseur, tandis que les superstructures III et IV étaient proposées pour l'évaluation de la technologie de séparation, selon les alternatives structurelles (vii) à (ix). L'objectif ultime de l'évaluation de la méthodologie aurait dû être une superstructure unique contenant chaque alternative étudiée. Cependant,

comme les différentes superstructures ont été conçues et évaluées à différentes étapes de cette thèse, elles ont été divisées en fonction des alternatives à l'étude.

Les principaux résultats trouvés par l'optimisation de ces superstructures ont permis de déterminer que le meilleur arrangement structurel consiste en deux réacteurs autothermiques en série, utilisant le catalyseur à base de Ru, avec deux étapes de compression, et avec séparation intermédiaire et finale par condensation. Cette superstructure est représentée sur la Figure XI-4.

Cette configuration permet de produire 3 994.8 t<sub>NH<sub>3</sub></sub> /an, qui se traduit en un LCOA de 790.3 €/t<sub>NH<sub>3</sub></sub>, et une efficacité énergétique de 67.13 %. Si l'on considère l'éventuelle intégration thermique du procédé, le coût final de la production d'ammoniac est égal à 865.3 €/t<sub>NH<sub>3</sub></sub>.

Il est certain que ces résultats économiques ne sont pas exhaustifs et nécessitent d'être détaillés davantage pour une évaluation économique rigoureuse de l'LCOA. Néanmoins, en gardant à l'esprit les politiques favorables à l'intégration des énergies renouvelables au marché de l'énergie dans les prochaines années, le développement des technologies permettant de réduire le coût des énergies renouvelables, et le contexte actuel d'instabilité des prix de l'énergie, le scénario envisagé dans ce travail permet de suggérer que le NH<sub>3</sub> produit à partir d'énergies renouvelables peut être compétitif par rapport aux voies de production conventionnelles. Les derniers prix de l'NH<sub>3</sub> produit à partir de gaz naturel, dans le contexte européen, étaient supérieurs à 1 500 €/t<sub>NH<sub>3</sub></sub> au cours du premier trimestre de 2022<sup>9</sup>.

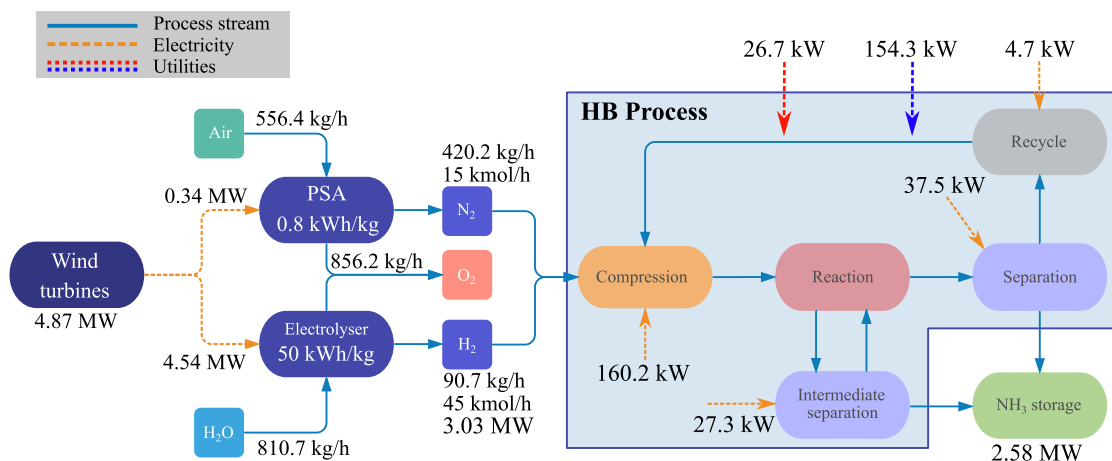


**Figure XI-3.** Scénario final pour la production et le stockage d'ammoniac à partir de sources d'énergie renouvelables, indiquant la quantité d'énergie contenue dans l'ammoniac produit et celle fournie sous forme d'hydrogène au procédé HB.

En ce qui concerne le bilan global montrée dans la Figure XI-3 sur la transformation énergétique de l'H<sub>2</sub> vert en NH<sub>3</sub> et son contenu énergétique, un total de 5.10 MW doit être fourni au procédé pour produire 2.58 MW contenus dans l'ammoniac, en fonction de son PCI. Sur l'approvisionnement total, au moins 94 % de l'énergie est nécessaire pour la production d'hydrogène et d'azote, tandis que les 6 % restants sont consommés par la boucle de synthèse HB. La conversion globale de l'hydrogène en ammoniac représente 97.76 %, ce qui, traduit en puissance d'entrée et de sortie, équivaut à une fourniture de puissance de 3.03 MW en H<sub>2</sub> et à un rapport de puissance NH<sub>3</sub> /H<sub>2</sub> égal à 0.853. La puissance théorique de conversion pour une conversion complète de l'hydrogène est égale à 0.782.

<sup>9</sup> Rapport de Standard & Poor's Global (S&P Global), du 01 avril 2022. Disponible en ligne : <https://www.spglobal.com/commodityinsights/en/market-insights/latest-news/energy-transition/040122-higher-ammonia-prices-prompting-european-restarts-but-shortages-remain-traders>

Enfin, la consommation d'énergie spécifique du scénario complet est égale à 10.23 kWh/kg de NH<sub>3</sub>, et la meilleure technologie disponible pour la synthèse de l'ammoniac, basée sur l'hydrogène du gaz naturel, consommant 27.4 GJ/t de NH<sub>3</sub>, soit 7.61 kWh/kg<sub>NH<sub>3</sub></sub>. Le principal responsable de la consommation d'énergie est l'électrolyseur, avec 9.09 kWh/kg<sub>NH<sub>3</sub></sub> (88.85 %), tandis que la production d'azote représente 0.68 kWh/kg<sub>NH<sub>3</sub></sub> (6.65 %) et que la boucle de synthèse HB consomme 0.46 kWh/kg<sub>NH<sub>3</sub></sub> (4.50 %). De toute évidence, la consommation d'énergie finale est le résultat des hypothèses envisagées dans les étapes amont du procédé HB pour la récupération de H<sub>2</sub> et de N<sub>2</sub>, qui dépassaient le cadre de ce travail.

### XI.3. Perspectives

La méthodologie d'optimisation des superstructures présentée dans ce travail a un fort potentiel de développement. Certaines hypothèses ont été envisagées dès le début de ce travail et pourraient être étudiées pour les éviter et proposer une méthodologie plus robuste. De futurs axes de recherche sont proposés pour traiter les aspects suivants :

- **Soutenir la génération des superstructures sur des méthodes de présélection** : Une étape préalable à l'optimisation de la superstructure peut être explorée, afin de définir une superstructure de processus plus complète, incluant un espace plus large d'alternatives. Des méthodologies telles que P-graph [103] et d'autres approches orientées graphe, permettent d'effectuer une présélection des structures de processus sans avoir besoin d'une modélisation rigoureuse des unités opérationnelles.
- **Développement d'unités opérationnelles définies par l'utilisateur pour l'intensification du procédé** : Compte tenu de l'utilisation potentielle de modules définis par l'utilisateur dans ProSimPlus, les ingénieurs peuvent modéliser leurs propres unités opératoires pour les évaluer dans une superstructure. À titre d'exemple, le logiciel dispose déjà d'un module intensifié réacteur-séparateur, modélisée comme un réacteur membranaire, mais d'autres unités intégrées peuvent être prévues pour leur intégration dans le logiciel. Comme on le sait, les modules intensifiés bénéficient de l'effet synergique de plusieurs phénomènes se produisant dans la même enveloppe.
- **Mise en œuvre d'une intégration thermique au sein de la stratégie d'optimisation** : L'un des principaux inconvénients de la méthodologie est l'hypothèse de considérer un seul courant dans l'échangeur de chaleur, sans possibilité de définir les surfaces d'échange thermique correspondantes et, par conséquent, leurs dépenses d'investissement et d'exploitation. Cela représente un impact inconnu du réseau HEX sur les KPI, qui est établi après l'optimisation de la superstructure. La prise en compte de l'intégration thermique dans la phase d'optimisation permettrait de surmonter ce problème et de trouver un ensemble plus robuste de solutions optimales, qui pourraient conduire à des solutions structurelles différentes.
- **Définition des indicateurs environnementaux** : Dans le cadre de procédés plus propres et sans carbone dans les futures applications industrielles de production d'électricité, il est nécessaire d'évaluer l'impact environnemental des processus [159], [160]. L'inclusion de ce type de KPI permet d'améliorer davantage les procédés, car elle permet de déterminer l'impact d'un projet pendant sa durée de vie, de la construction au démantèlement, pour tous les flux de masse et d'énergie associés non seulement au processus lui-même mais aussi aux activités avoisinantes.

- **Définition d'indicateurs exergetiques** : Une étape au-delà de l'évaluation de l'efficacité énergétique consiste à réaliser un bilan exergetique du procédé, afin d'identifier les étapes possibles du procédé où de l'énergie utile est perdue (c'est-à-dire les imperfections du procédé), de classer les pertes en pertes évitables/incontournables, et de proposer des améliorations du procédé [169]. En effectuant une évaluation d'un bilan énergétique, les procédés de transformation de l'énergie pourraient être adaptés pour mieux répondre à une utilisation efficace de l'énergie.
- **Définir une approche systématique pour l'analyse des résultats et l'exploitation des données** : La grande quantité de données obtenues par l'optimisation des superstructures après plusieurs milliers d'évaluations du schéma de procédé, peut être largement exploitée pour trouver toute relation possible entre les conditions de fonctionnement, les alternatives structurales, les contraintes et les KPI. Il est possible que la combinaison des conditions d'exploitation sur une certaine plage de valeurs tende vers des zones infaisables, ou même favorise la recherche des solutions optimales. Cependant, ces éventuelles relations existantes restent inconnues à ce stade. et nécessiteraient des méthodes robustes d'analyse des données.

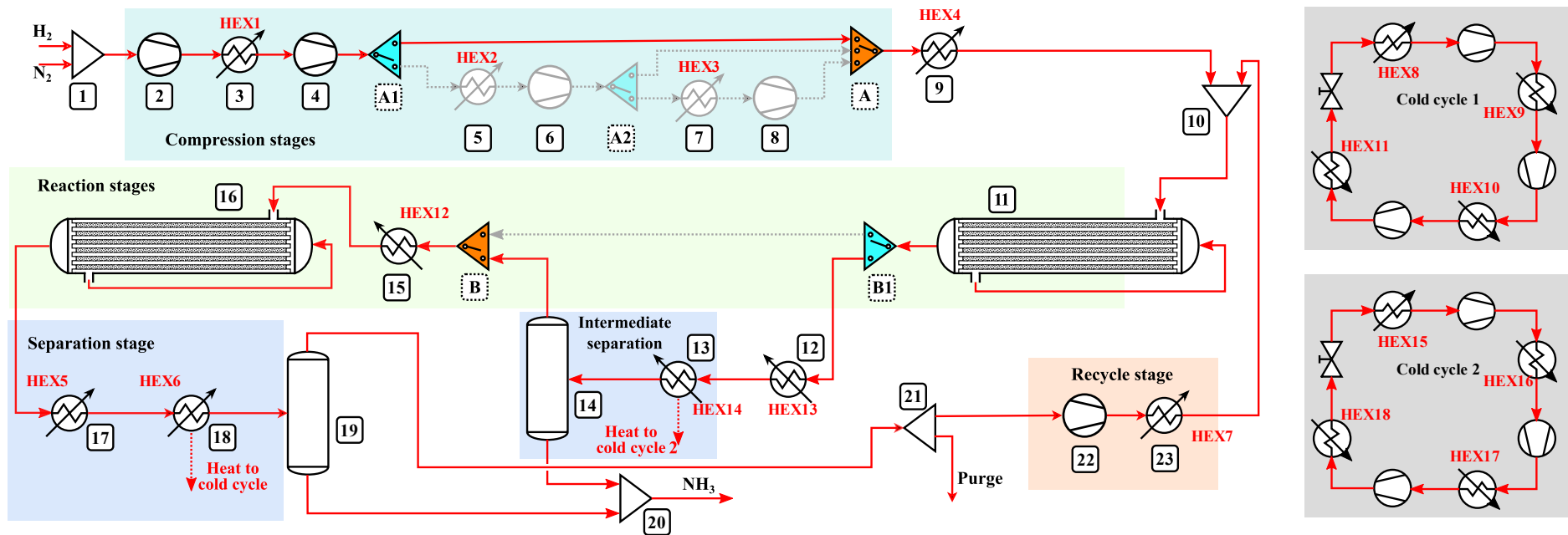


**Figure XI-4.** Représentation de la superstructure de la solution optimale finale, indiquant les échangeurs de chaleur utilisés pour l'analyse d'intégration thermique et les deux cycles de réfrigération avec leur HEX respectif. Les modules de la structure principale du processus sont spécifiés comme suit : Mélangeurs (1, 10, 20). Compresseurs (2, 4, 6, 8, 22). HEX (3, 5, 7, 9, 12, 13, 15, 17, 18, 23). Réacteurs autothermiques (11, 16). Séparateur (14, 19). Diviseur de courant (21).

## Abstract

Projections from the International Renewable Energy Agency (IRENA) support that by the year 2050 electricity will be the main energy carrier with 50 % of the share of the energy market. The deployment of clean energy production and its integration to the energy market will play a key role towards this objective. Also, the quest for more efficient, sustainable, and economic processes is one important challenge that process engineers are constantly facing in research and industry, which commonly needs to determine the best structural configuration of a process, leading to the optimal interconnection of the processing units, with the respective set up of the operating conditions. This task would require evaluating several process designs to find the best configuration, which is a tedious and time-consuming approach to execute manually. Therefore, this work is foreseen to enable a practical methodology for process engineers to evaluate multiple process alternatives within a unique superstructure, to determine the best structural arrangement, the set of operating conditions and/or design parameters, leading towards the optimal process configuration regarding some economic, energetic and/or environmental criteria. The methodology is applied to a scenario of energy storage in ammonia, using as reference the conventional Haber-Bosch process. Four process superstructures have been proposed and evaluated to determine the best process structure, which include the selection of: (i) the number of compressors in the main compression stage; (ii) the number of catalytic reactors; (iii) the catalytic material, either Fe-based or Ru-based; (iv) the reactor arrangement, either multibed adiabatic or multitube autothermal; (v) the cooling system for the adiabatic reactors, either indirect (AICR) or direct (AQCR); (vi) the use of intermediate separation; (vii) the separation technology, among the condenser, membrane filters, and PSA; (viii) the use of pressure equalization on the permeate streams of the membrane filters; (ix) the use of an additional condenser after the separation by membranes or by PSA. The main results found through the optimization of these superstructures allowed to determine that the best structural arrangement consists of two autothermal reactors in series, using the Ru-based catalyst, with two stages of compression, with intermediate and final separation by condensation. This configuration allows to produce 3 994.8 t<sub>NH<sub>3</sub></sub>/y, representing an LCOA of 790.3 €/t<sub>NH<sub>3</sub></sub>, and an energy efficiency of 67.13 %. The specific power consumption of the complete scenario is equal to 10.23 kWh/kg<sub>NH<sub>3</sub></sub>, with the best available technology for ammonia synthesis, based on hydrogen from natural gas, consuming 27.4 GJ/t<sub>NH<sub>3</sub></sub>. The main driver of the energy consumption is the electrolyser, responsible for 9.09 kWh/kg<sub>NH<sub>3</sub></sub> (88.85 %), while the nitrogen production represents 0.68 kWh/kg<sub>NH<sub>3</sub></sub> (6.65 %), and the HB synthesis loop consumes 0.46 kWh/kg<sub>NH<sub>3</sub></sub> (4.50 %).

## Résumé

Selon les projections de l'Agence internationale pour les énergies renouvelables (IRENA), d'ici 2050 l'électricité sera le principal vecteur énergétique avec une part de 50 % du marché de l'énergie. Le déploiement de la production d'énergie propre et son intégration au marché de l'énergie joueront un rôle clé dans la réalisation de cet objectif. De même, la recherche de procédés plus efficaces, durables et économiques est un défi important auquel les ingénieurs des procédés sont constamment confrontés dans la recherche et l'industrie, qui doivent généralement déterminer la meilleure configuration structurelle d'un procédé, conduisant à l'interconnexion optimale des unités opératoires, avec la mise en place respective des conditions opératoires. Cette tâche nécessite l'évaluation de plusieurs schémas de procédé pour trouver la meilleure configuration, ce qui est une approche épuisante et chronophage à exécuter manuellement. Par conséquent, ce travail a pour objectif de proposer une méthodologie pratique aux ingénieurs de processus afin qu'ils puissent évaluer multiples alternatives d'un procédé dans une superstructure unique, afin de déterminer la meilleure disposition structurelle, l'ensemble des conditions opératoires et/ou les paramètres de design, menant à la configuration de procédé optimale en ce qui concerne certains critères économiques, énergétiques et/ou environnementaux. La méthodologie est appliquée à un scénario de stockage d'énergie dans l'ammoniac, en utilisant comme référence le procédé conventionnel de production Haber-Bosch. Quatre superstructures de procédé ont été proposées et évaluées afin de déterminer la meilleure structure de procédé, qui inclut la sélection de : (i) le nombre de compresseurs dans l'étage de compression principal ; (ii) le nombre de réacteurs catalytiques ; (iii) le matériau catalytique, soit à base de Fe, soit à base de Ru ; (iv) la disposition des réacteurs, soit adiabatiques multi-lits, soit autothermiques multitubes ; (v) le système de refroidissement des réacteurs adiabatiques, soit indirect (AICR), soit direct (AQCR) ; (vi) l'utilisation d'une séparation intermédiaire ; (vii) la technologie de séparation, parmi le condenseur, les filtres à membrane et le PSA ; (viii) l'utilisation d'une égalisation de pression sur les flux de perméat des filtres à membrane ; (ix) l'utilisation d'un condenseur supplémentaire après la séparation par membranes ou par PSA. Les principaux résultats trouvés à travers l'optimisation de ces superstructures ont permis de déterminer que le meilleur arrangement structurel consiste en deux réacteurs autothermiques en série, utilisant le catalyseur à base de Ru, avec deux étapes de compression, avec séparation intermédiaire et finale par condensation. Cette configuration permet de produire 3 994.8 t<sub>NH<sub>3</sub></sub>/an, qui se traduit en un coût de production (LCOA) de 790.3 €/t<sub>NH<sub>3</sub></sub>, et une efficacité énergétique de 67.13 %. La consommation spécifique d'énergie du scénario complet est égale à 10.23 kWh/kg<sub>NH<sub>3</sub></sub>, alors que la meilleure technologie disponible pour la synthèse de l'ammoniac, basée sur l'hydrogène issu du gaz naturel, consomme 27.6 kWh/kg<sub>NH<sub>3</sub></sub>. Le principal responsable de la consommation d'énergie est l'électrolyseur, avec 9.09 kWh/kg<sub>NH<sub>3</sub></sub> (88.85 %), tandis que la production d'azote représente 0.68 kWh/kg<sub>NH<sub>3</sub></sub> (6.65 %) et le procédé HB consomme 0.46 kWh/kg<sub>NH<sub>3</sub></sub> (4.50 %).